LIÈGE université
GIGA

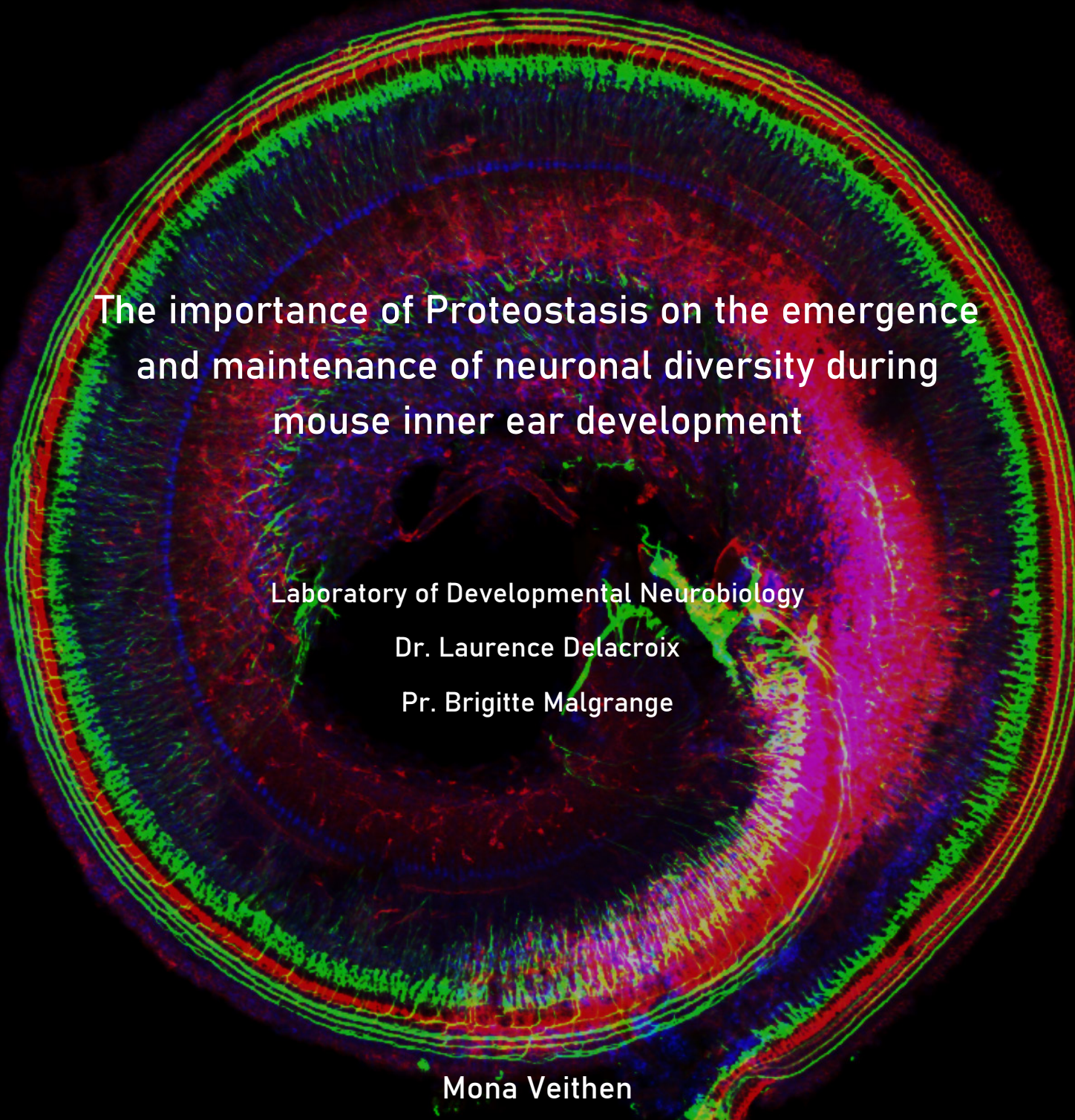

The importance of Proteostasis on the emergence and maintenance of neuronal diversity during mouse inner ear development

Laboratory of Developmental Neurobiology

Dr. Laurence Delacroix

Pr. Brigitte Malgrange

Mona Veithen

A thesis presented for the degree of PhD in Biomedical and Pharmaceutical Sciences

Academic year 2024-2025

Abstract

Transcriptomic studies from the last years could show that spiral ganglions neurons not only differ at the physiological and morphological level but also at the molecular level, leading to the nowadays well-characterized 3 neuronal subtypes: Ia, Ib and Ic. Growing evidence suggests a preferential vulnerability of the Ic subtype during age and noise trauma, strongly affecting the ability of patients to understand speech in a noisy background and thus highlighting the importance of the normal functioning of each SGN subtype. As well, transcriptomic studies could show that neuronal differentiation and diversification already starts during mouse embryonic development. Protein aggregation as a result of a disrupted protein homeostasis has already been linked to sensorineural hearing loss, especially in case of age-related and drug-induced HL. In our proteotoxic model of Elp3-deficient mice, our lab could show that there is an ER-stress induced neuronal cell death during development resulting in complete deafness. Thus, we planned to unravel the importance of proteostasis during development on the emergence and maintenance of the spiral ganglion neurons, as well as the vestibular counterpart, the vestibular ganglion neurons (VGNs).

In this study, we first determined the identity of the remaining neurons in Elp3-deficient cochlea and discovered that Elp3 loss impacts correct subtype specification. More precisely, Elp3 depletion resulted in a predominance of neurons showing molecular Ia characteristics whereas they resemble Ic subtypes regarding the topological features of their paired Ribbons. This diversity failure became evident around birth, first in the basal and middle turn of the cochlea hinting for a subtype identity switch in a base-to-apex gradient towards molecular Ia subtypes. Additionally, we showed that the embryonic neuronal cell death solely arises from the neuronal compartment. Besides this, we could show that Elp3KO animals present vestibular behavioral defects together with huge innervation defects in the vestibular organs including the Cristae and the Utricle. We showed that Elp3 depletion was associated with a pronounced loss of Calyx-only synapses and a moderate loss of Dimorphic Calyces in the utricle, whereas in the Cristae the initial absence of Calyx synapses has come back to normal levels during the first two postnatal weeks, hinting for either a delayed synaptic innervation or for a potential synaptic restoration process.

Together, we deciphered an important role of Elp3 in target innervation of both the cochlear hearing organ and the vestibules responsible for balance sensation. These results open the door for future investigations to unravel the discrepancies discovered at the cochlear level and to shed light on the molecular and cellular processes involved in the innervation defects at the vestibular level.

Résumé

Les études transcriptomiques des dernières années ont montré que les neurones des ganglions spirales (NGSs) diffèrent non seulement au niveau physiologique et morphologique, mais aussi au niveau moléculaire, ce qui a conduit à la caractérisation bien établie de trois sous-types neuronaux : Ia, Ib et Ic. De plus en plus de preuves suggèrent une vulnérabilité préférentielle du sous-type Ic lors du vieillissement et du trauma accoustique, ce qui affecte fortement la capacité des patients à comprendre la parole dans un environnement bruyant, mettant ainsi en évidence l'importance du bon fonctionnement de chaque sous-type de NGS. Par ailleurs, les études transcriptomiques ont montré que la différenciation et la diversification neuronales commencent déjà pendant le développement embryonnaire de la souris. L'agrégation de protéines due à une homéostasie protéique perturbée a déjà été liée à la perte auditive neurosensorielle (SNHL), en particulier dans le cas de la perte auditive liée à l'âge et induite par des médicaments. Dans notre modèle protéotoxique de souris déficientes en Elp3, notre laboratoire a démontré que la mort cellulaire neuronale induite par le stress du réticulum endoplasmique (RE) pendant le développement entraîne une perte auditive totale. Par conséquent, nous avons cherché à explorer l'importance de l'homéostasie protéique durant le développement pour l'émergence et le maintien des neurones des ganglions spirales ainsi que des neurones des ganglions vestibulaires (NGVs), les homologues vestibulaires.

Dans cette étude, nous avons d'abord déterminé l'identité des neurones restants dans la cochlée déficiente en Elp3 et découvert que la perte d'Elp3 perturbe la spécification correcte des sous-types, entraînant une prédominance de neurones présentant des caractéristiques moléculaires de type Ia, tout en ressemblant aux sous-types Ic concernant les caractéristiques topologiques de leurs synapses appariées. Ce problème de diversité est devenu évident autour de la naissance, d'abord dans les tours basale et moyenne de la cochlée, suggérant un changement d'identité de sous-type dans un gradient de la base vers l'apex vers les sous-types moléculaires Ia. De plus, nous avons montré que la mort cellulaire neuronale embryonnaire provient exclusivement du compartiment neuronal. En outre, nous avons démontré que les animaux Elp3KO présentent des défauts comportementaux vestibulaires, ainsi que d'importants défauts d'innervation dans les organes vestibulaires, y compris les crêtes et l'utricule. Nous avons observé que la déplétion d'Elp3 était associée à une réduction prononcée de la présence de synapses « Calyx-only » et une perte plus modérée des synapses « Dimorphiques » dans l'utricule, tandis que dans les crêtes, l'absence initiale de synapses de Calice est retourné à un niveau normal au cours des deux premières semaines postnatales, suggérant soit une innervation synaptique retardée, soit un processus de restauration synaptique.

En conclusion, nous avons élucidé le rôle crucial d'Elp3 dans l'innervation des cibles de l'organe auditif cochléaire ainsi que des organes vestibulaires responsables de la sensation d'équilibre. Ces résultats ouvrent la voie à de futures investigations pour explorer les divergences observées au niveau cochléaire et éclairer les processus moléculaires et cellulaires impliqués dans les défauts d'innervation au niveau vestibulaire.

Acknowledgements

Tout d'abord, merci aux membres de jurys d'avoir pris le temps de lire et d'évaluer le manuscrit. Merci pour votre critique toujours constructif et pour les discussions intéressantes durant les 4 dernières années. J'espère que vous apprécier la lecture.

Ensuite, je tiens à remercier Professeur Brigitte Malgrange de m'avoir accueilli dans le labo et dans l'équipe. Merci de m'avoir préparé pour le FRIA de la meilleure manière possible avec toutes tes forces d'encouragement et d'avoir continué à croire en moi quand moi-même je ne le faisais plus. Cette aventure a aussi été possible grâce à ta confiance en moi, merci mille fois.

Mes remerciements les plus profondes vont à Dr Laurence Delacroix qui était là du début jusqu'à la fin de cette aventure. Merci de m'avoir donné la possibilité de travailler sur ton projet de cœur et de m'avoir donné toute ma liberté sur le projet. Merci pour ta patience, ton enthousiasme, ton temps précieux malgré tes trois agendas de ministre et nos nombreux échanges scientifiques. Merci pour tous ce que tu m'as appris durant les 6 dernières années, j'espère que je suis devenu une meilleure scientifique grâce à toi. Tu as seulement rendu tout ça possible, merci pour tout.

Ensuite, le plus grand merci à mes collèges du labo Malgrange, sans qui cette aventure n'aurait pas été la même chose.

Seb, je n'ai jamais rencontré une personne si perfectionniste, franche et drôle et un ami si loyal comme toi tu l'es. Merci pour tous les moments qu'on a passés ensemble, tous les fous rires, et s'il te plait, ne change jamais la personne qui tu es. (Et j'espère que tu me pardonnes que j'avais quitté l'aquarium, mais tu étais juste trop insupportable)

Camille, quel plaisir d'avoir fait ta rencontre, merci pour tous les chouettes moments qu'on a passé ensemble soit au bureau ou hors du labo, pour ton soutien au quotidien et ton avis scientifique que j'ai apprécié énormément, c'était un véritable plaisir d'avoir partagé le bureau avec toi.

Sali, the one and only Marie-Thérèse, t'es un véritable exemple avec ta gentillesse, ta bienveillance, et ta capacité de toujours voir le meilleur dans chaque personne. Tu nous montre tous les jours ce que l'humanité vaut, merci pour tout.

Mary, on avait partagé le bureau dès le premier jour, merci pour toutes les discussions scientifiques ou non-scientifiques au labo et hors du labo, ton soutien indéfectible et ton avis toujours très bien placé. Le temps qu'on eût ensemble au labo était beaucoup trop court,

mais j'ai pu apprendre énormément de chose durant ce temps grâce à ton esprit critique, merci pour tout.

Yamina, j'en suis énormément chanceuse et reconnaissante d'avoir pu faire ta connaissance, merci pour ta cordialité, ta bienveillance et ton amabilité. Tu as laissé un plus grand trou dans le labo que ce que tu penses.

Tine, we never had the occasion to really get to know each other perfectly, but I always admired your perseverance, your "diplomatic" view on things, your high skills of showing empathy, and your endless kindness. Never change who you are, you're the perfect example of the person everyone aims to be.

Merci PB pour ton aide technique d'ici et là, ton humour et ta sérénité, qui ont rendu ces 4 années plus réjouissantes.

Merci aussi à Enes, Auriane, Ilyas, Erwan, Timothée, … même si on s'est seulement croisé à la fin, c'était un plaisir d'avoir pu faire votre connaissance.

Nath, on a commencé cette aventure ensemble et on l'a (presque) fini ensemble. Merci pour ces 9 ans que j'avais le plaisir de faire ta connaissance, tu as toujours été un exemple avec ta professionnalité, ton intelligence et avec ta vue scientifique, mais aussi avec ton aptitude de toujours voir le positif dans tout. Merci mille fois.

Merci aussi à Ron, Fanny, Julie, Romain et Silvia, merci pour tous les aventures en vélos en montant la montagne du Sart-Tilmant, nos sessions de squash et toutes les chouettes conversations d'ici et là.

Merci aussi à tous les autres membres du GIGA Neuroscience et ceux que j'ai pu croiser sur le chemin, vous avez rendu ces années inoubliables.

Pour terminer, merci à Céline, la plus belle rencontre au cours de ma thèse. Merci pour être mon pilier au quotidien, ton soutien indéfectible et tes encouragements sans cesse. Cette thèse a seulement pu trouver sa fin grâce à toi car ta jamais arrêter de croire en moi. Merci de faire en moi une meilleure version de moi-même. J'ai hâte de notre futur qu'on va construire ensemble (avec Micheline).

Zuallerletzt, ein Riesen Dank an meine Familie und insbesondere meine Eltern, ohne die das alles erst gar nicht möglich gewesen wäre. Danke für eure bedingungslose Unterstützung und dass ihr nie aufgehört habt an mich zu glauben. Ich hoffe, dass ich euch stolz gemacht habe.

List of Abbreviations

4-PBA	Sodium phenylbutyrate
ABR	Auditory Brainstem Response
AD	Alzheimer's disease
ALS	Amyotrophic lateral sclerosis
AMPA	α-Amino-3-hydroxy-5-methyl-4-isoxazol-Propionsäure
AP	Apical progenitors
ARHL	Age-related hearing loss
ATP	Adenosine Triphosphate
BiP	Binding Immunoglobulin Protein
cCasp3	cleaved Caspase 3
CHOP	C/EBP homologous protein
CreERT	Cre recombinase Estrogen receptor T
CVG	Cochleo-vestibular ganglion
DAPI	4',6-Diamidin-2-phenylindol
dB	decibel
ENaC	Epithelial Sodium channel
EPSP	Excitatory postsynaptic potential
ER	Endoplasmic Reticulum
ERAD	Endoplasmic Reticulum associated degradation
ES	Endolymphatic sac
GLAST(=EAAT1)	Excitatory amino acid transporter 1
GRP94	Heat shock protein 90B1
Gαi	Gi-protein alpha subunit
HC	Hair cell
HD	Huntington disease
HDAC	Histone Deacetylase
Hes	Hairy and enhancer of split
Hey	Hairy Ears, Y-Linked
Id	Inhibitor Of DNA Binding
HIFIA	Hypoxia Inducible Factor 1 Subunit Alpha
HL	Hearing loss
HSP	Heat shock protein

HuD (=ELAVL4)	ELAV-like protein 4
IHC	Inner Hair cell
IP	Intermediate progenitors
IRE1	endoribonuclease inositol-requiring enzyme 1
IRES	Internal Ribosome entry side
Kcc4	Potassium Chloride Cotransporter 4
LES	Lateral Extrastriolar region
LGN (=GPSM2)	G-protein-signaling modulator 2
LOC	Lateral olivocochlear
LPR	Line of Polarity reversal
MANF	Mesencephalic Astrocyte Derived Neurotrophic Factor
MES	Medial extrastriolar region
MET	Mechanoelectrical transduction
MOC	Medial olivocochlear
Ngn1	Neurogenin-1
NIHL	Noise-induced hearing loss
OHC	Outer Hair cell
OoC	Organ of Corti
PCP	Planar cell polarity
PD	Parkinson disease
PDI	Protein disulfide-isomerase
PERK	protein kinase R (PKR)-like endoplasmic reticulum kinase
RFP	Red Fluorescent protein
ROS	Reactive oxygen species
SC	Supporting cell
SGN	Spiral ganglion neuron
SOD1	Superoxide Dismutase 1
Sox	(SRY-related HMG box protein)
SR	Spontaneous discharge rate
Tuj1	Tubulin beta-3
UPR	Unfolded Protein Response
UPS	Ubiquitin Proteasome System
VGN	Vestibular ganglion neuron
Wnt	Wingless-related Integration Site

Table of contents

Introduction

PART I – HEARING AND COCHLEA

The inner ear is a highly specialized organ responsible for both hearing and balance, relying on intricate structures and finely-tuned physiological and molecular processes for proper function. To understand its development and maintenance, it is important to explore the cochlea, the auditory component of the inner ear (part I), and the vestibular system that governs balance and spatial orientation (part II). Both structures depend on precise cellular identities and organization, and on protein homeostasis to maintain cellular health and function (part III). Loss or alterations in the proteostasis network paves the way to a myriad of diseases, such as metabolic and neurodegenerative disorders or cancer. The inner ear is no exception as proteostasis disruption can lead to hearing impairments and potentially to vestibular dysfunctions.

According to the World Health Organization (WHO), more than 430 million people suffer from disabling hearing loss today and this number is likely to increase to no less than 700 million by 2050.

A normal hearing threshold in humans is generally considered to be around 20 decibels (dB), which is a sound pression level corresponding to a quiet whisper or a ticking watch. Hearing loss is diagnosed when a person's hearing threshold is higher than this, meaning sounds need to be louder for them to be heard. As the decibel scale is logarithmic, a 10 dB increase represents a tenfold increase in sound intensity. Hearing loss can be mild (auditory threshold around 20-40 dB), moderate (41-70 dB), severe (71-90 dB) or profound (over 91 dB). Disabling hearing loss defines presenting a hearing threshold of more than 35 dB. In general, people with severe to profound hearing loss need devices to improve their hearing such as hearing aids, cochlear implants etc. whereas profound hearing loss can rarely be cured or restored.

Hearing loss can have many consequences on the quality of life of individuals affected if not treated. It can lead to social isolation and further depressions, problems of communication and speech, have an impact on education and employment. In addition, hearing impairments also represent an economical burden to the society, as it induces both direct medical costs to provide patients with hearing devices or specific treatments, and indirect costs related to specific education programs or trainings as well as loss of productivity and social service expenses.

Depending on the ear structure that is affected in patients, there are three types of hearing loss: sensorineural, conductive and mixed. Sensorineural hearing loss is the most common type and it originates from defects in the inner ear. In the majority of these cases, the auditory sensory cells or neurons are lost or dysfunctional and this deafness form is rarely treatable. In contrast, conductive hearing loss arises from abnormalities within the middle and external ear, hampering mechanical sound wave transmission rather than signal detection. Upon therapeutical or surgical interventions

(against ear infections or malformations, respectively), many of these cases can be cured. Mixed hearing loss represents a combination of both sensorineural and conductive forms.

Hearing loss can be congenital, affecting 1.33 babies out of 1000 in developed countries or acquired, hence appearing later during life. Hearing loss prevalence increases with age: whereas it affects 2.83 children out of 1000 and 3.5 teenagers out of 1000, already 1 out of 3 people aged 65 or more are affected. While congenital cases are predominantly of genetic or viral infection origins, acquired forms are most often due to sound overexposure, ototoxic drugs or ageing.

Until today, there are no treatments available to prevent or restore hearing loss. New strategies are currently being explored to replace damaged sensory cells or neurons. Promoting cell regeneration within the tissue or using stem cells to generate auditory cells for transplantation opens new avenues to treat certain types of hearing loss. However, translation to humans is complex and still under investigation (Lee & Waldhaus, 2022). Gene therapy is the most promising strategy to date, as recent clinical studies showed pioneering results in children suffering from profound deafness caused by mutations in the otoferlin gene. Indeed, the use of viral vectors reintroducing the normal gene in the otic cells leads to a rapid and complete restoration of their hearing ability (Lv et al., 2024; Qi et al., 2024).

2. Anatomy of the human ear

The whole ear comprises 3 parts that ensure the correct transmission, amplification and detection of sound waves, respectively: the external ear, middle ear and inner ear. The external or outer ear consists of the auricle and the auditory canal. The middle ear is separated from the ear canal by the tympanic membrane (or eardrum) and comprises the three ossicles (Malleus, Incus, Stapes) and the eustachian tube. Together, they are crucial for the propagation of the sound wave from the outside through the ear canal to reach the eardrum, whose vibration induces the movement of the ossicles. These ossicles amplify and propagate the sound wave to the inner ear, as the stapes hit its ventral portion, the cochlea, which is essential to sound signal detection (Figure 1). In addition to its auditory part, the inner ear is also made of a dorsal vestibule, comprising semicircular canals, which is responsible for balance sensation, In this first part of the introduction, the focus will be on the cochlea, while part II is dedicated to the vestibular structure and function.

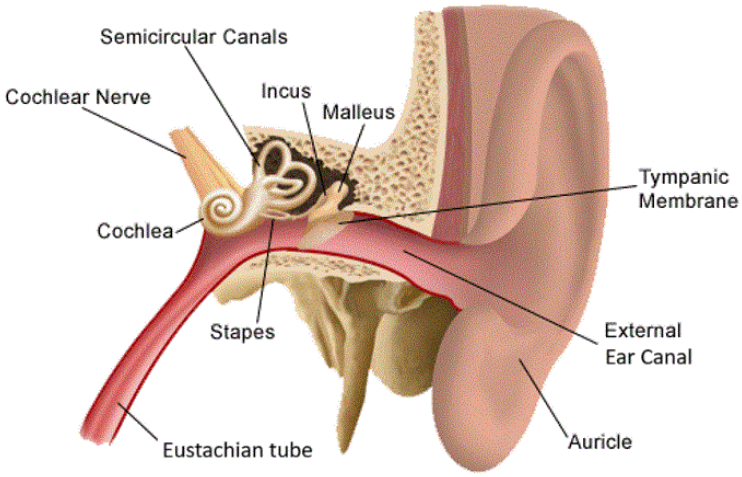

Figure 1. Anatomy of the ear. The ear is composed of three parts: the outer, middle and inner ear. The outer ear comprises the auricle and the external ear canal. The middle ear comprises the malleus, incus, stapes and the eustachian tube. The inner consists of the cochlea and the vestibule (e.g. semicircular canals). *From standfordchildrens.org*

3. The cochlea

The cochlea is a coiled organ made of three cavities filled with fluid. Two cavities, the scala vestibuli and scala tympani are filled with perilymph, having a low concentration of potassium (K+) and whose composition is close to plasma or cerebrospinal fluid. The scala media, lying in between the latter and separated by the Reissner's and the basilar membranes, is filled with the endolymph, an exquisite biological fluid displaying a high concentration of K+. This scala media houses a sensory epithelium, called the Organ of Corti (OoC), that ensures the detection and transmission of the sound signal to the brain (Lim, 1986) (Figure 2). The various cell types composing this highly specialized epithelium, namely the sensory Hair cells (HCs) and the Supporting cells (SCs), as well as the spiral ganglion neurons (SGNs) contacting the sensory HCs, are further developed in the following paragraphs.

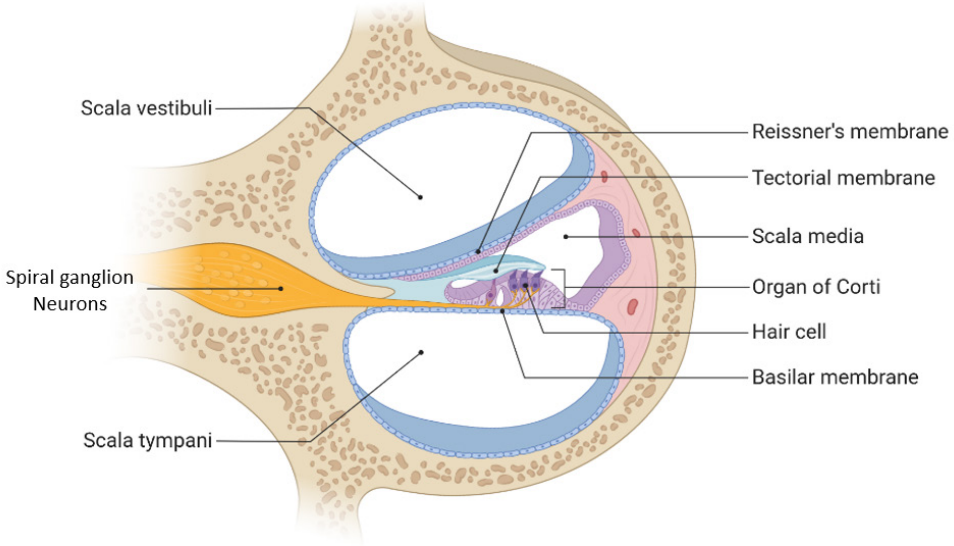

Figure 2 (previous page). Cross-section of the cochlear duct. The cochlear duct with the three cavities (scala vestibuli, scala tympani, scala media). The Reissner's membrane separates the scala vestibuli from the scala media and the basilar membrane separates the scala media from the scala tympani. The scala media in the middle houses the organ of Corti (OoC), the sensory epithelium, with the sound-detecting Hair cells (HCs). The mechanical stimuli, converted by the HCs into an electrical signal, is transmitted to the spiral ganglion neurons (SGNs) that will convey the sound information via the cochlear nerve to the brain.

3.1 The HCs

The HCs are known to be the main mechanosensory cells responsible for sound detection. Their role is to transduce the mechanical stimuli into an electrical signal that is transmitted to peripheral neurons within the cochlea, the SGNs, and further relayed up to the brain. This is possible due to their very specific structure, physiology and function. They hold their name from the hairy bundle, made of stereocilia, which is present at their apical pole. These actin-based apical protrusions are arranged in a V shape and organized in staircase rows with the shortest lying in medial position while the highest reside more laterally, next to the kinocilium (the only true cilium, enriched in microtubule) present at the vertex of the V. These stereocilia are connected to those of the neighboring rows via tip links and the whole bundle makes up the mechanosensory organelle of HCs. (Figure 3)

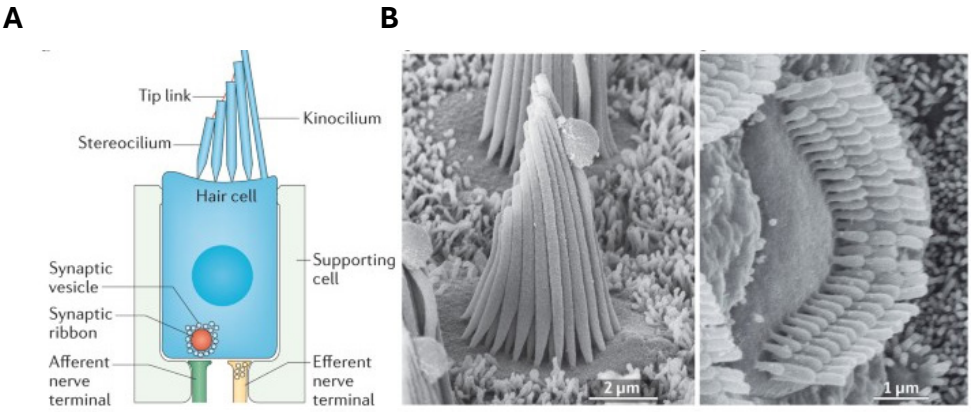

Figure 3. Cochlear Hair cells and microscopic structure of their stereociliary bundles. A) Inner Hair cells present a hair bundle in a W-shape whereas the Outer Hair cells have a V-shaped hair bundle. The longest stereocilia, the kinocilium, is a specialized primary cilium with a classical 9 + 2 axoneme but lacking the inner dynein arms, making them different from classical "motile" cilia and thus immobile. *(D. Wang & Zhou, 2021)* B) the stereocilia are connected with each other via the tip-links, and, in case of deflections towards the kinocilium, leads to the opening of the MET channels and ultimately to the release of neurotransmitters from the synaptic vesicles. C) electron microscopic images of the hair bundles showing the step-like structure of the stereocilia. *From Hudspeth, 2014.*

When a sound wave reaches the cochlea, the fluidic movement and the subsequent displacement of cochlear membranes induces the deflection of the stereocilia bundles towards the highest row. This bending of stereocilia leads to the opening of the mechanoelectrical transduction (MET) channels,

which are located at the base of tip link connectors. Once opened, these channels allow the entry of K+ ions from the endolymph to the HC, causing its depolarization. This depolarization induces the opening of voltage-dependent Calcium channels at the basolateral pole of the HC and the entry of calcium ions, which in turn enable the fusion of synaptic vesicles at the so called "active zone". This highly specialized region houses the Ribbon synapses that are electron-dense structures tethering several 100 synaptic vesicles ready to be released upon sound stimulation (Figure 4). This enables a fast, dynamic and precise transmission of the sound signal. This presynaptic machinery is essentially made of Ribeye protein (encoded by Ctbp2 gene) and the main neurotransmitter of IHCs is Glutamate. Upon its release into the synaptic cleft, it binds to the postsynaptic glutamate receptors present in the SGN peripheral processes to induce an excitatory postsynaptic potential, which in turn triggers an action potential further transmitted to the brain.

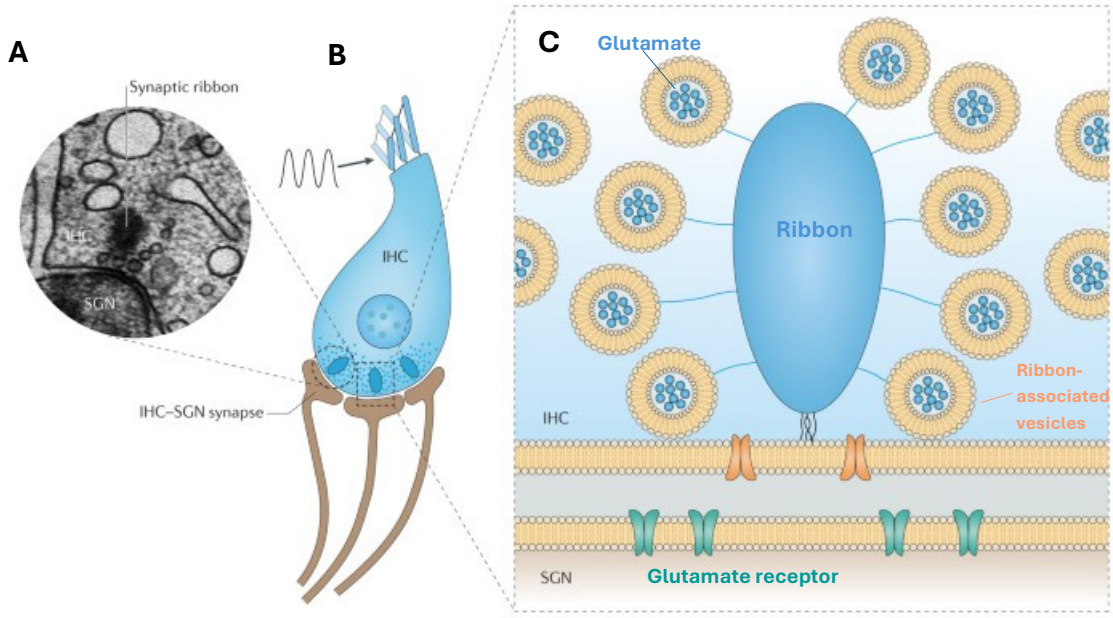

Figure 4. the HC "Active Zone". A) electron microscopic image shows the electron dense structure, termed Ribbon, with the tethered Glutamate-filled synaptic vesicles. B) the deflection of the stereociliary bundle induces a depolarization of the inner HC. C) zoom on the "active zone" comprising the Ribbons. *From Moser and Starr, 2016.*

All along the cochlear duct, we can find 3 rows of outer HCs (OHCs) and 1 row of inner HCs (IHCs). The IHCs are the main decoders of the sound signal, whereas the OHCs are implicated in amplifying the sound signal. This happens through a process called electromotility and is possible thanks to the electromotile motor protein Prestin which is localized at the basolateral membrane of the OHC (J. Zheng et al., 2000). Prestin enables the contraction and elongation upon depolarization and hyperpolarization of the OHC, respectively. This cellular contraction and elongation enhance the displacement of cochlear membranes in response to sound waves which is further detected by the IHC. A complete loss of the OHCs is generally associated with a hearing threshold of 40-50 dB.

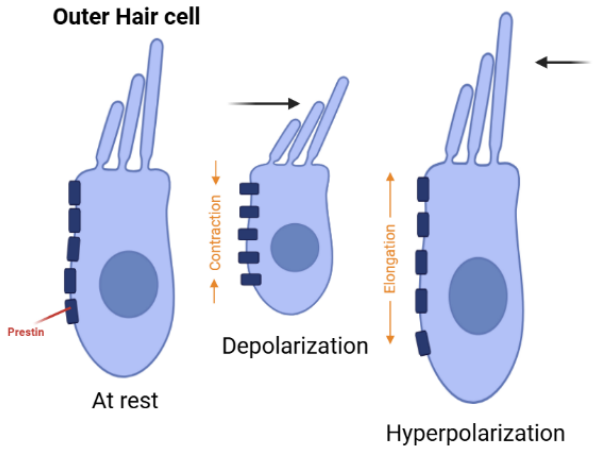

Figure 5. Electromotility of OHCs. The deflection of the hair bundle leading to a depolarization of the membrane potential induces the contraction of the OHC thanks to Prestin. In case of hyperpolarization, the OHC elongates. Together, this enables the coordinated movement of the basilar membrane underlying the HCs thus enhancing the sound signal.

3.2 The supporting cells

Within the organ of Corti, the sensory HCs are surrounded by supporting cells (SCs). Based on their location within the epithelium as well as their expression signatures and functions (Kelley 2020), many different types of SCs have been identified: inner border, inner phalangeal (both surrounding the IHCs), inner Pillar, outer Pillar, Deiters' cells (the last two supporting the OHCs) and Hensen's cells. Together, Inner and outer Pillar cells form the extracellular space called the tunnel of Corti (Figure 6A).

In the cochlea, the supporting cells mainly serve as a scaffold to the overlying HCs. Beside this, they regulate ion homeostasis in the organ of Corti by recycling K^+ from the HCs back to the endolymph. This recycling process, which is essential to guarantee fluid homeostasis and prevent cochlear toxicity, is due to the expression of the K^+/Cl^- cotransporter Kcc4 (Boettger et al., 2002). Moreover, SCs absorb Na^+ from the scala media to reduce its concentration in the endolymph through ENaC channels, present at their apical side (Gründer et al., 2001). They are also implicated in the clearance of Glutamate that is released by Inner HCs into the synaptic cleft to avoid excitotoxicity thanks to the expression of GLAST transporter at their basolateral side (Glowatzki et al., 2006).

Noteworthy, supporting cells present many more roles than the ones described above. For instance, SCs were shown to play a role in the generation of IHC spontaneous activity during the early postnatal period in rodents (Tritsch et al., 2007; Tritsch & Bergles, 2010). To do so, they release ATP that activates the purinergic receptors present on HCs, and on SCs themselves, leading to a release of intracellular Calcium depolarizing the IHCs (Figure 6C). This spontaneous activity, disappearing after the onset of hearing at P12 (Tritsch et al., 2007), is known to be crucial for synaptic maturation and refinement of the auditory circuit, but also for the identity consolidation of cochlear neuronal subtypes (Shrestha et al., 2018).

In birds and reptiles, supporting cells have a unique role in replacing HCs after damage and thus restoring hearing and balance function (Warchol 2011). In the avian inner ear, HC replacement can

occur by two distinct mechanisms: mitotic regeneration implies that a SC first divides before differentiating into either a supporting cell or a HC, or by direct transdifferentiation into a HC. In contrast, this ability to replace injured HCs in mammals is very limited and is restricted to the early postnatal period. In adult mammalian ears, more precisely in the inner ears of guinea pigs, spontaneous HC regeneration by direct transdifferentiation has only been observed at a very low level in the vestibular epithelium after HC damage (Forge et al., 1993) (Figure 6B). Forcing the expression of Atoh1 or inhibition of the Notch pathway could result in HC regeneration in adult utricle (Lin et al., 2011) but is still limited in the cochlea, likely because of epigenetic barriers. Combined strategies targeting multiple signaling pathways known to be crucial to HC development are currently the main focus of HC regeneration studies (reviewed in Smith-Cortinez et al., 2023).

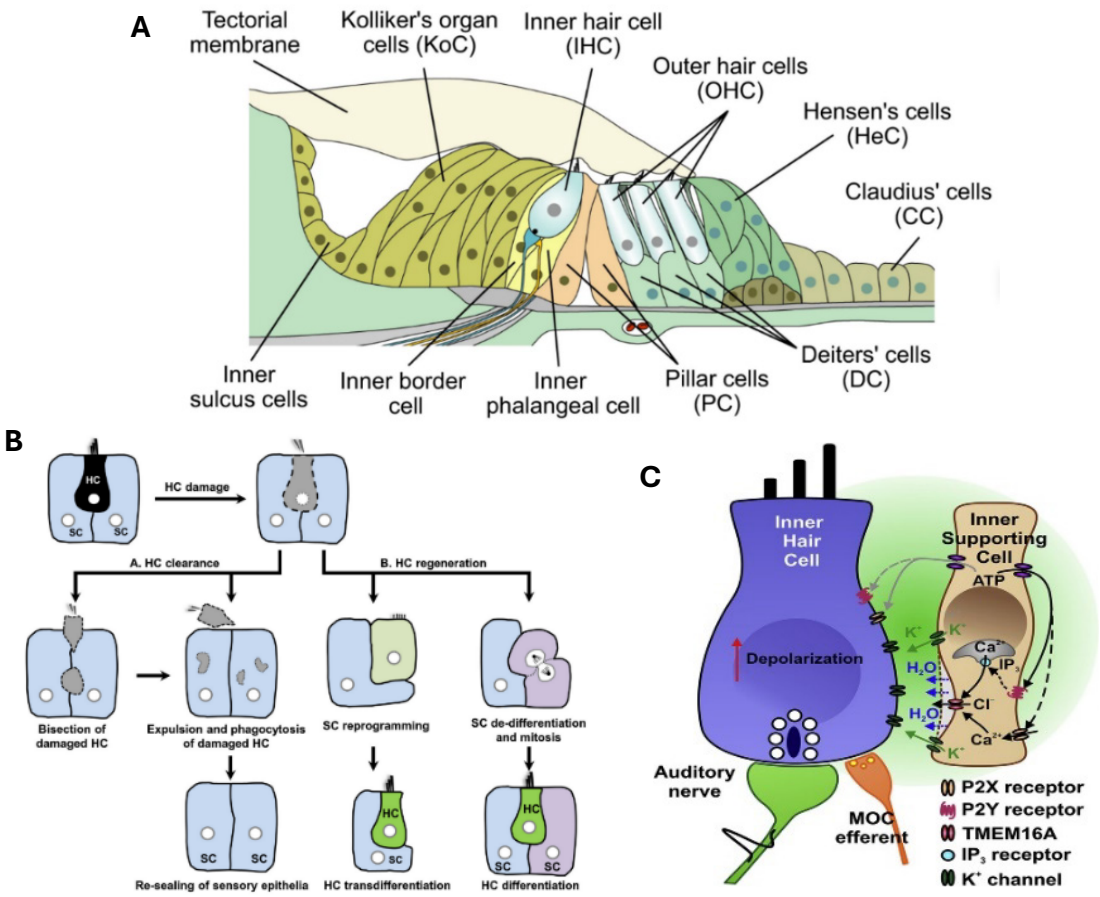

Figure 6. The supporting cells and their main functions. A) the supporting cells within the sensory epithelium, from left to right: Inner sulcus cells, Kölliker's organ cells (KoC), inner border cells, inner phalangeal cells, inner Pillar cells (PC), Deiters' cells (DC), Hensen's cells (HeC), Claudius' cells (CC). *From Velez-Ortega et al. 2023.* B) the role of SCs during HC regeneration. They participate to clearance and/or regeneration of HCs through either direct transdifferentiation or mitotic proliferation. *From Wan et al. 2013.* C) Supporting cells generate a spontaneous activation of the inner HCs by the release of ATP and thus an activation of purinergic receptors present on HCs and SCs. *From Wang et al. 2015*

3.3 Innervation of the Organ of Corti

2.3.1 Afferent and efferent systems

The HCs within the Organ of Corti are innervated by auditory afferent and efferent neurons. The auditory afferences, or spiral ganglion neurons (SGNs), ensure the correct transmission of the sound-evoked stimuli from the HCs and consist in the first neuronal relay up to the auditory brain cortex.

The SGNs can be divided into two main classes: type I and type II. Type I SGNs are myelinated and directly innervate the Inner HCs and make out 95% of all neurons whereas the unmyelinated Type II neurons innervate the Outer HCs and make out 5% of the neuronal population. A single type I neuron makes a contact with a single IHC whereas a type II neurons innervates first an OHC and branches towards the basal end of the cochlea to form *en passant* synapses with multiple OHCs. In parallel, each single IHC is innervated by 5-30 SGNs I, with the highest number of synaptic contacts in the region with the greatest sound sensitivity, whereas a single OHC is contacted by merely 1-3 SGN II. Type I SGNs are known to participate directly in the encoding of the auditory information whereas Type II SGNs seem to be implicated in nociception (Flores et al., 2015). Both types of neurons are activated by Glutamate release from the corresponding HC at the so-called *Active zone* housing a specialized Ribbon synapse, which is crucial for a fast and precise encoding of the sound information.

The efferent system, playing a crucial role in providing positive and negative feedback from the brainstem (Guinan, 2010), consists of two pathways: the medial and the lateral olivocochlear pathway (MOC and LOC, respectively). The **MOC** neurons are myelinated and, when activated in response to sound, they provide a negative feedback loop through cholinergic signaling (M. C. Liberman & Brown, 1986). They can directly innervate the OHCs and reduce their amplification potential by decreasing their electromotility capacity (Russell & Murugasu, 1997). Recently, electron microscopic reconstructions showed that OHCs are not the only targets of MOC efferences, as these also innervate the dendrites of the auditory afferences with a preference for the neurons innervating the Inner HC on the pillar side (Hua et al., 2021). Altogether, by regulating the cochlear amplification and signal transmission through the primary afferences, they allow for a better signal-to-noise ratio (Kawase et al., 1993). The **LOCs** pathway consists of unmyelinated neurons that innervate the projections of SGNs close to their synaptic contacts with the IHC (M. C. Liberman, 1980), thereby modulating their excitability (Groff & Liberman, 2003). LOC neurons preferentially innervate the multi-ribbon forming SGNs at the modiolar side of the Inner HC (Hua et al., 2020) (Figure 7). Interestingly, another study could demonstrate that the efferent innervation is essential for the normal modiolar-pillar gradient of Ribbon size (Yin et al., 2014). Together, the LOC and MOC neurons protect against acoustic trauma and subsequent cochlear damage, as they partially prevent the temporary threshold shift in response to noise overexposure (Kujawa & Liberman, 1997; Rajan, 1988).

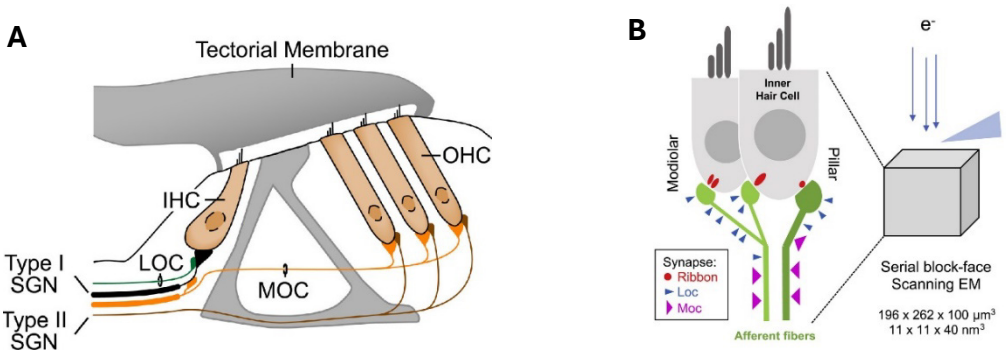

Figure 7. the efferent system. A) the efferent system is made of the lateral and medial olivocochlear pathway, LOC and MOC, respectively. The LOC efferents make synaptic contacts with the type I SGNs whereas the MOC can either make contacts with the type I dendrites or directly with the OHCs. *From Romero and Trussel 2022.* B) the unmyelinated LOCs preferentially contact the multi-Ribbon-forming type I SGNs on the modiolar side whereas the MOCs make more contacts with single Ribbons type I SGNs on the pillar side. *From Hua et al. 2020*

2.3.2 Type I SGN diversity

Within the spiral ganglion, type I neurons can be further subdivided into three subtypes: Type Ia, Ib and Ic. For several decades, it has been known that those three subtypes differ at the morphological and electrophysiological level. Kiang *et al.* performed the first electrophysiological recordings on auditory nerve fibers in the cat and found that they differ regarding their sensitivity to sound (activation threshold) and their spontaneous firing rate (SR). In 1978, Liberman was the first to classify them into 3 classes: low threshold/high SR (>18 spikes/s), medium threshold/medium SR (0.5-18 spikes/s) and high threshold/low SR (<0.5 spikes/s) (Figure 8B). Four years later, he could prove a correlation between their electrophysiological properties and the basal innervation side of the Inner HC: high SR fibers preferentially innervate the pillar side whereas low SR fibers rather make synaptic contacts with the IHC at the modiolar side (M. C. Liberman, 1982) (Figure 8A). He described their contribution to a wide dynamic range of sound intensity encoding and the necessity of low SR fibers for understanding speech in a noisy background (Costalupes et al., 1984; M. C. Liberman, 1982). Later, electrophysiological studies on rat cochlear preparations proved for the first time the presence of a heterogenous population of fibers with different SRs in rodents (Wu et al., 2016), and confocal high-resolution imaging on mouse cochlear samples showed that there is also a gradient of Ribbon synapse size and AMPA receptor patch size at the pre- and postsynaptic level, respectively. Interestingly, this gradient of presynaptic components is opposite to the postsynaptic ones and likely contributes to the differences of fiber activation threshold and spontaneous firing rate (L. D. Liberman et al., 2011) (Figure 8A).

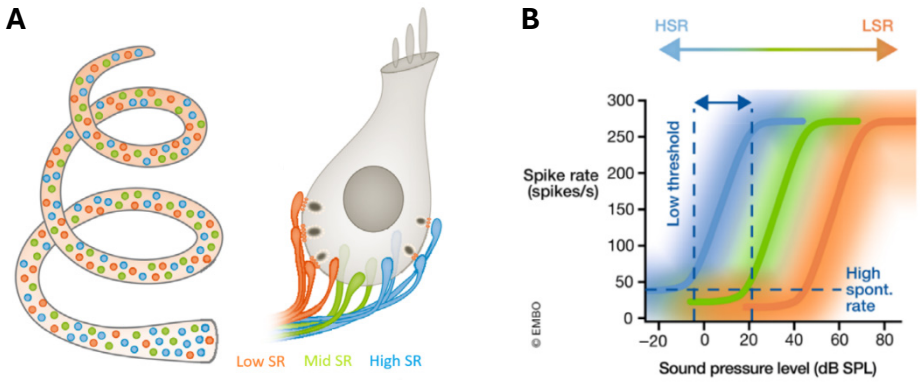

Figure 8. the afferent system in the cochlea. **A)** the inner HC is innervated by the three neuronal subtypes, Ia, Ib and Ic, showing a specific modiolar-to-pillar gradient along the basal side of the IHC. There is an equal distribution of Ia/Ib/Ic neurons at the Apex and the Mid turn, and slightly higher proportions of Ia neurons at the Basal turn. B) the three subtypes present specific electrophysiological properties regarding the activation threshold and the high spontaneous discharge rate. Ia subtypes (blue) are activated in presence of low intensity sounds and present a high spontaneous firing rate (in absence of sound), whereas the Ic subtypes (orange) are only activated in presence of high intensity sounds and present a low spontaneous firing rate in absence of sound. *Adapted from Moser et al. 2023.*

This physiological heterogeneity of the neuronal population raised questions about their origin: are the neurons basically very similar but respond differently to the input they receive from the presynaptic components (that differs in a modiolar-pillar direction at the level of the Inner HC) or is this pool of neurons molecularly different and expresses different types of receptors, ion channels, etc. that account for their differences in activation threshold and SR? Answering this question seemed more and more important as understanding their biology and individual functions is crucial for better adapting therapeutic strategies to the increasing prevalence of hearing loss. Noteworthy, specific vulnerabilities of the low SR fibers could already be demonstrated in case of age-related hearing loss (Schmiedt et al., 1996) and acoustic trauma (Furman et al., 2013). The predominant loss of low SR/High threshold fibers during aging or following noise overexposure explains the difficulties of patients understanding speech in a noisy background.

To tackle this question, researchers performed single-cell RNA sequencing (scRNAseq) studies on SGNs of adult mice to see if there could be different neuronal clusters based on their transcriptome or if it's impossible to demonstrate a molecular diversity (Petitpré, 2018; Shrestha et al., 2018; S. Sun et al., 2018).

In all of these three studies, 2 different clusters could be found: one expressing specific markers of type II neurons (Th, NGFR) and one expressing specific markers for type I neurons (Epha4, Tuj1) (Petitpré, 2018; Shrestha et al., 2018; S. Sun et al., 2018). Interestingly, differences in gene expression of specific Glutamate receptor subunits, K+ channels subunits and presynaptic vesicle-associated proteins could be found (Petitpré, 2018; Shrestha et al., 2018). These distinctive expression patterns explain the well-known differences between type I and II SGNs regarding Glutamate responsiveness,

neuronal excitability and presynaptic release properties ion of HCs at all (Bermingham et al., 1999)(Glowatzki & Fuchs, 2002; Weisz et al., 2014).

Type I SGNs could be further clustered into 3 subgroups: Ia, Ib and Ic (Figure 9A) *(Note that in Petitpré et al. 2018, "Ic" refers to Ia, "Ib" refers to Ic and "Ia" refers to Ib)*. Those 3 subtypes are present in similar proportions with a slightly higher abundance of Ib subtypes (Figure 9B). Several genes are specifically expressed by each of the 3 subtypes, making them good molecular markers. For instance, Ia SGNs are enriched in *Calretinin (Calb2)*, and exclusively express *Cacna1b*. Subtype Ib neurons specifically express *Calbindin (Calb1),* whereas Ic neurons are characterized by the expression of *Lypd1* and *Grm8*. (Shrestha et al., 2018) (Figure 9C). The differential expression levels of *Calb1* and *Calb2* between the three subtypes could explain their different firing properties as they play an important role in Ca^{2+} binding and regulation of its availability. Besides this, Ia SGNs show a higher expression of genes implicated in mitochondrial function, which correlates with their higher mitochondrial content (M. C. Liberman, 1980), and express higher levels of Neurofilament-H, in good accordance with their larger fiber diameter (Elder et al., 1998). The physiological diversity of type I SGNs is also underlined by different sets of ion channels expressed in each of the subtypes, particularly for the K+ channels, which are major contributors to the firing pattern and excitability of neurons (Petitpré, 2018) (Figure 9D).

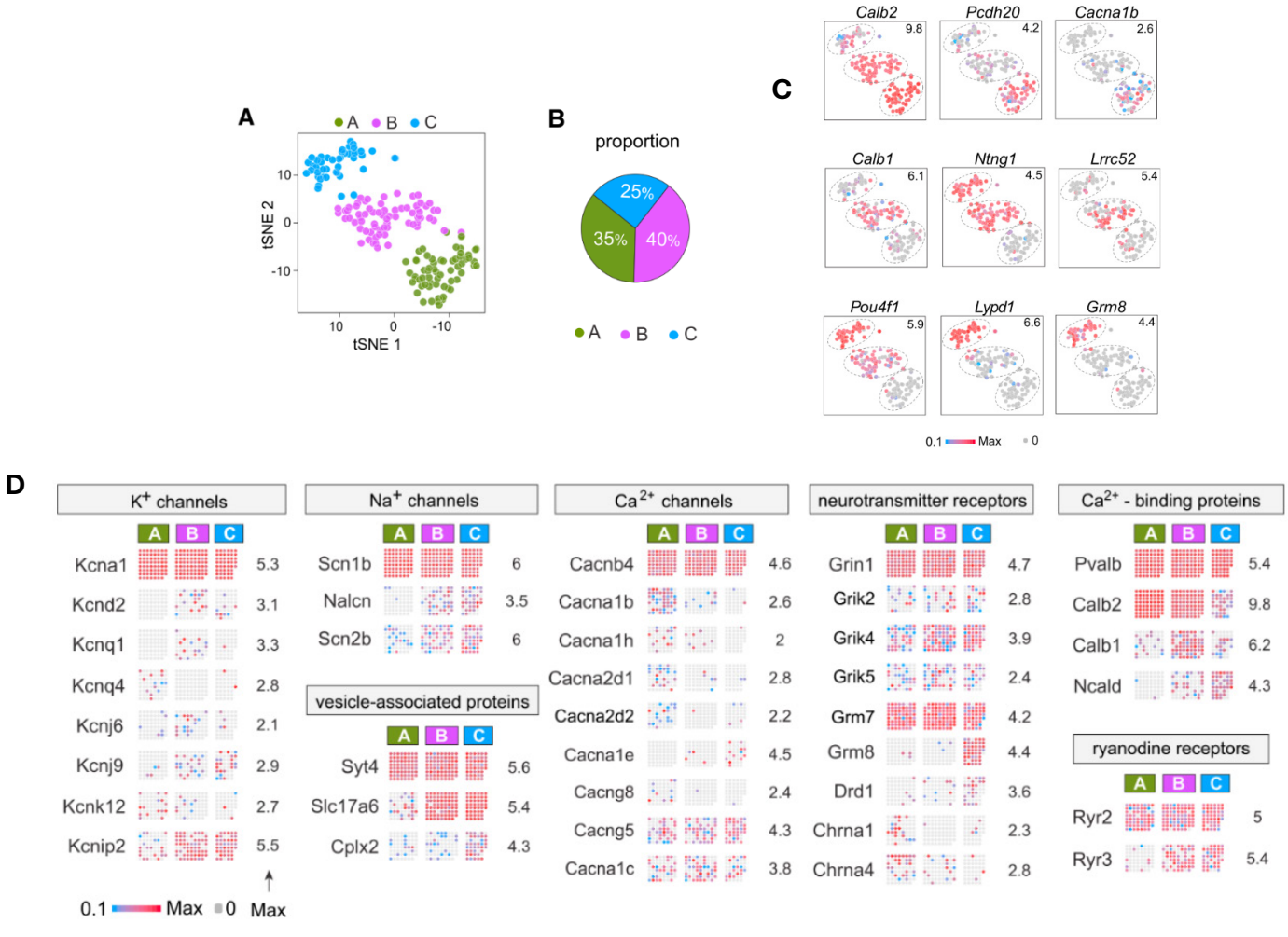

Figure 9 (previous page). the three neuronal clusters and their molecular signatures. A-B) t-SNE showing the three clusters with their respective proportions. C) Genes that are differentially expressed in one or two clusters making them subtype- or subgroup-specific markers. D) Differential expression pattern of ion channels (potassium, sodium, calcium), neurotransmitter receptors, vesicle-associated proteins, calcium-binding proteins and ryanodine receptors. *From Shrestha et al. 2018.*

In addition, Shrestha *et al.* reported tonotopic differences, as some transcripts are enriched in the Apex, Mid or in the Base. However, the classical set of markers (Calb2, Lypd1, Cacna1b and Ntng1) are not differentially expressed between the three turns. In addition, the proportions of Ia, Ib and Ic were very similar between Apex and Mid with a slightly higher proportion of Ia neurons at the Base at the expense of Ib neurons (Shrestha et al., 2018).

After having identified the three molecularly different clusters, transgenic mouse lines combined with Immunostainings for Calb2 have been used to trace individual fibers up to the Inner Hair Cell (IHC) to match the molecular properties with the morphological ones. For instance, Calb2 Immunostaining in combination with Neurofilament staining, used to label all the SGN fibers, revealed that the fibers with a low Calb2 staining intensity preferentially innervated the modiolar side and faced larger Ribbons, whereas fibers with high Calb2 staining intensity predominantly innervated the pillar side to face smaller Ribbon synapses (Figure 10). These findings support the hypothesis that the 3 clusters defined based on their molecular signature can be linked to the previously described subtypes, classified according to their morphological characteristics (Shrestha et al., 2018).

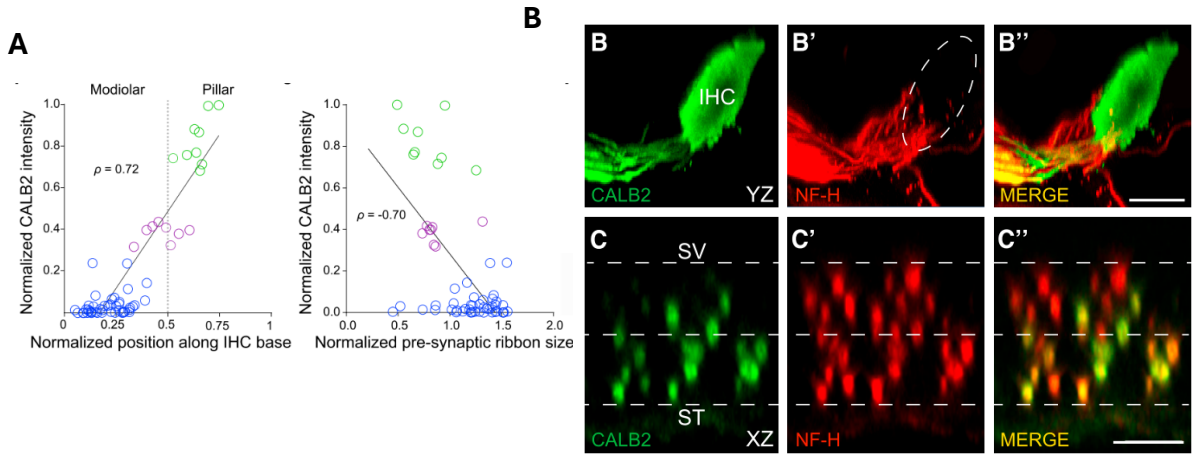

Figure 10. Correlation between Calb2 staining intensity and position along the IHC base. A) cochlear whole mount stainings showing the distribution of Calb2+ fibers along the basolateral side of the IHC. Neurofilament (NF-H) labels all the fibers. The Merge shows that CALB2+ fibers are rather found on the IHC pillar side. B) quantifications show a significant positive correlation between the normalized CALB2 intensity and the position along the Inner HC. In parallel, there is a negative correlation between the CALB2 intensity and the presynaptic Ribbon size. *From Shrestha et al. 2018.*

Recently, another group provided more insights into the correlation between molecular and morphological characteristics of auditory neurons. Siebald *et al.* performed lineage tracing studies by using Lypd1CreERT and Calb2CreERT mouse lines and showed that neurons expressing Lypd1 (Ic subtype) preferentially innervate the IHC on the modiolar side and present a homogeneous group of neurons with low SRs. In contrast, the neurons that express Calb2 innervate the IHC at the pillar side but exhibit a larger range of SRs, likely due to a heterogenous population of Ia/Ib neurons that are labelled with the Calb2-CreERT construct (Siebald et al., 2023). These results showed that the molecularly and physiologically defined subgroups only correlate in part and that there exists a postnatal consolidation regarding their gene expression and specific innervation pattern.

By performing current-clamp recordings on isolated neurons at the whole cell level, Petitpré *et al.* revealed two groups of SGNs based on their accommodation rate to increased current injections. One group of neurons presents unitary spike accommodation (UA), meaning that they do not fire more than one action potential (AP) in response to a depolarization step, while the other group displays multiple spikes accommodation (MA) as they fire multiple APs with a frequency increasing with current intensity. Post-Immunostainings of the recorded neurons with Calb2 revealed that the Ia and Ib SGNs correspond to UA type, whereas the Ic SGNs display both UA and MA characteristics, with a 50-50% distribution hinting that they can be further subdivided into two groups (Figure 11). Interestingly, by looking at the expression profile of *Kcnc2*, a K+ channel known to be responsible for sustained repetitive firing in neurons (Rudy & McBain, 2001), two populations of Ic SGNs could be distinguished. The *Kcnc2+* population could correspond to the Ic-MA neurons whereas the *Kcnc2-* population would relate to the Ic-UA neurons, however further experiments would be necessary to confirm this. Altogether, these findings validate that there is physiological heterogeneity among the molecularly distinct type I SGNs (Petitpré, 2018).

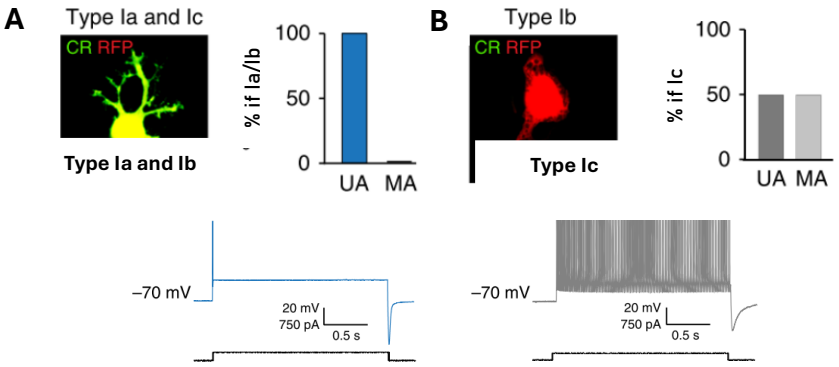

Figure 11. electrophysiological diversity within the neuronal population. A) Calb2(CR)+ SGNs, that can be either Ia or Ib subtypes show always unitary spike accommodation (UA), characterized by the production of one single Action Potential in response to a current injection. B) Calb(CR)- SGNs which present the type Ic SGNs, show a 50/50 division into UA and MA neurons, characterized by the formation of multiple Action Potentials in presence of a current. *Adapted from Petitpré et al. 2018.*

4. Development of the cochlea

The development of the inner ears starts with the formation of the otic placode, an ectodermal region near the hindbrain, at Embryonic day 8 (E8). This otic placode invaginates between E8.5-E9 to build the otic cup and further closes to form the otic vesicle (Morsli et al., 1998) at E9.5. At this stage, neuroblasts delaminate from a neurosensory domain located in the ventral region of the otocyst. They migrate short distances to form the cochleo-vestibular ganglion (CVG).

From E10.5 onwards, the spherical otic vesicle undergoes massive morphogenetic changes, resulting in the formation of distinct dorsal and ventral parts that will further develop into the vestibular and the cochlear portions, respectively (Figure 12). The cochlear duct progressively extends and coils, meanwhile a subset of cells specified as prosensory expand to form a narrow stripe all along the elongated cochlea. This prosensory domain houses progenitor cells that will differentiate, from E14.5 onwards along a base-to-apex gradient, into either HCs or SCs. At birth, the inner ear has reached its gross morphology, HCs are formed all along the tonotopic axis of the cochlea, and SGNs are already contacting their target cells. However, further maturation steps are needed during the first postnatal weeks to attain functional maturity, as hearing onset is around P15 in mouse.

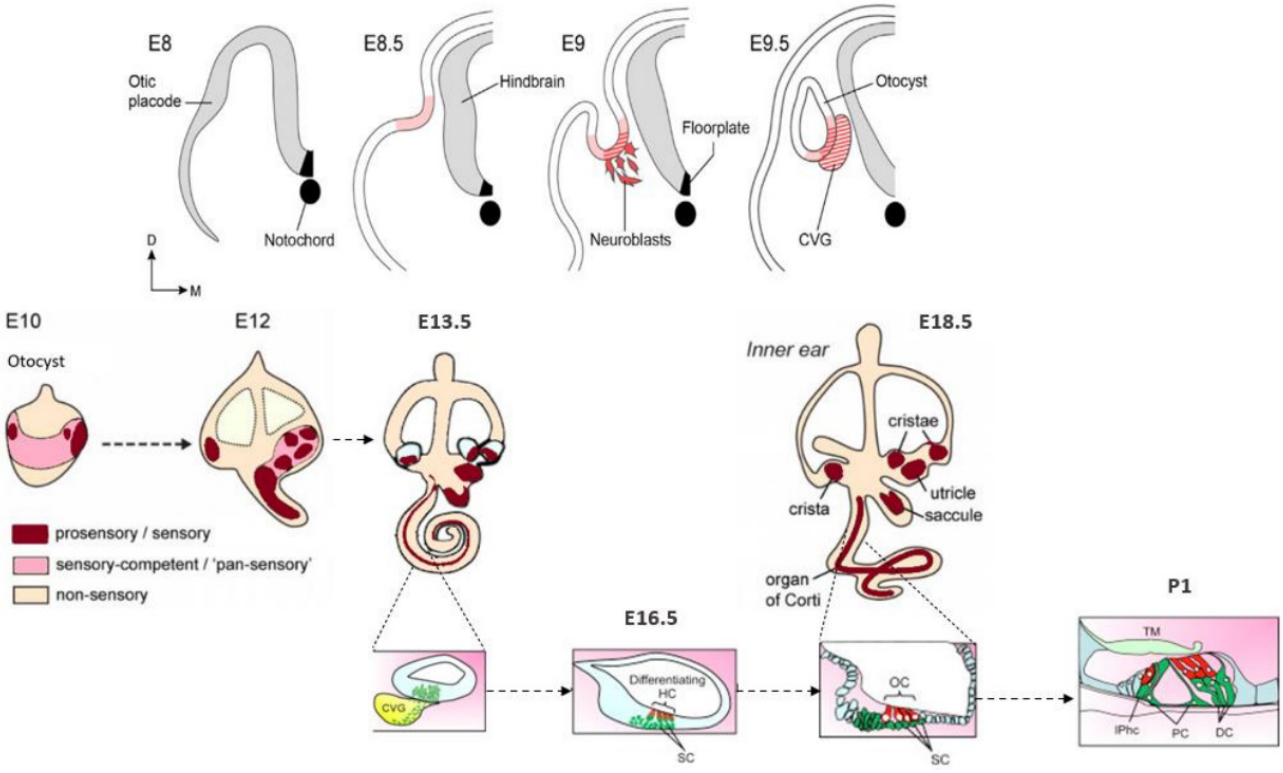

Figure 12 (previous page). Inner ear development. A) the inner ear development starts with the formation of the otic placode next to the neuronal tube at E8. The otic placode invaginates to form the otic cup at E8.5-9. At the anteroventral portion of the otic cup the neuronal progenitors start to delaminate from a neurosensory domain and form the cochleo-vestibular ganglion in parallel to the formation of the otocyst. B) the cochlear part will develop from the ventral part of the otocyst whereas the vestibule will develop from the dorsal part. The prosensory domain contains the prosensory progenitors that will differentiate into SCs and HCs between E13.5 and E16.5 in a Base-to-Apex gradient. At P1, the organ of Corti contains shows the final structure with the main cell types, but functional maturity will only be reached around P15, which is the hearing onset in mice. *Adapted from Wu et al. 2016.*

4.1 Focus on HC development and its molecular players

As mentioned above, the sensory and non-sensory cells composing the organ of Corti derive from the prosensory domain that is specified early during development. Prosensory domain expansion as well as cell fate determination are both under the control of Notch pathway, which thus plays a crucial role in HC development.

The Notch system is made of different receptors (Notch1, -2, -3, -4) and two classes of transmembrane ligands (Jagged, Delta like), which are expressed on neighboring cells. Two distinct mechanisms of action have been reported for Notch signaling: lateral induction, which promotes similar cell fates through positive feedback between Notch receptors and Jagged ligands, and lateral inhibition, which drives opposite cell fates via negative feedback between Notch and Delta ligands (Figure 13).

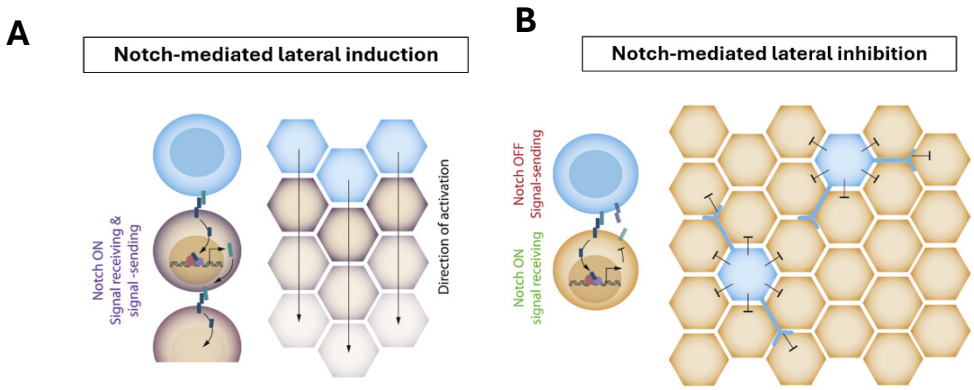

Figure 13. Notch system. Notch-mediated lateral induction and inhibition. A) illustration showing the interaction between a signal-sending cell (bearing a Notch ligand) and a signal-receiving cell (bearing a Notch receptor). The interaction induces the cleavage of the intracellular receptor domain (NICD) by a gamma-secretase which is translocated to the nucleus and leads to the expression of Notch-specific target genes. B) Notch-mediated lateral inhibition consists in a Notch OFF signal-sending cell that activates Notch in a neighbor cell (Notch ON signal receiving cell) but preventing it from expressing a Notch ligand and thus from becoming itself a signal sending cell. Notch-mediated lateral induction consists in a signal sending cell that activates Notch in neighbor cells and inducing the expression of Notch ligands in these cells, thus every cell becoming a Notch ON signal receiving and sending cell. *Adapted from Sjöqvist and Andersson, 2019.*

4.1.1 Prosensory domain formation

During mouse embryonic development, Notch mediated-lateral induction is known to be essential for the formation and maintenance of the prosensory domain of the inner ear. Several experiments in chicken, including ectopic expression of Notch pathway components or inhibition of Notch by pharmacological inhibitors, showed that there is a positive feedback loop: Notch activation leads to Jag1 expression, which in turn activates neighboring cells to promote pro-sensory cell specification (Daudet et al., 2007; Hartman et al., 2010; Neves et al., 2011). How Notch receptor activation leads to pro-sensory cell specification depends on Sox2 (SRY-related HMG box protein 2) upregulation (Figure 14). Indeed, the Sox2 transcription factor is both necessary and sufficient to induce the formation of the prosensory domain as the complete knock out in mice leads to the absence of sensory development including deafness and the ectopic expression enables the ectopic formation of prosensory patches (Dabdoub et al., 2008; Kiernan et al., 2005; Puligilla & Kelley, 2017).

4.1.2 Terminal differentiation of HCs and SCs

The progenitors present in the prosensory domain undergo several rounds of proliferation before starting to express p27kip to exit the cell cycle around E12.5-13.5 in an Apex-to-Base gradient. Once post-mitotic, they start to differentiate around E14.5 in a Base-to-Apex gradient, with IHCs differentiating before OHCs. This cell differentiation is induced by Atoh1 transcription factor, the major inducer of HC fate (Bermingham et al., 1999). Studies showed that when Atoh1 expression is prevented, there is no generation of HCs at all (Bermingham et al., 1999), whereas forced expression of Atoh1 leads to supernumerary as well as ectopic HCs in the inner ear (J. L. Zheng & Gao, 2000). This proves that Atoh1 is both necessary and sufficient to induce HC development.

Atoh1 activity and HC differentiation is regulated by Notch-mediated lateral inhibition. More precisely, the cells expressing the Notch ligands Dll1 and Jag2 activate Notch1 receptor expressed on neighboring cells. This leads to the upregulation of Notch target genes of the Hes (e.g. Hes1 and Hes5), Hey and Id families, which are well known antagonists of Atoh1, and therefore prevent the activated cells from adopting HC fate. The cells that express the Notch ligands will become HCs and block the surrounding cells from adopting the same cell fate (Figure 14). As such, these cells become SCs, which is thought to be the default mode of differentiation.

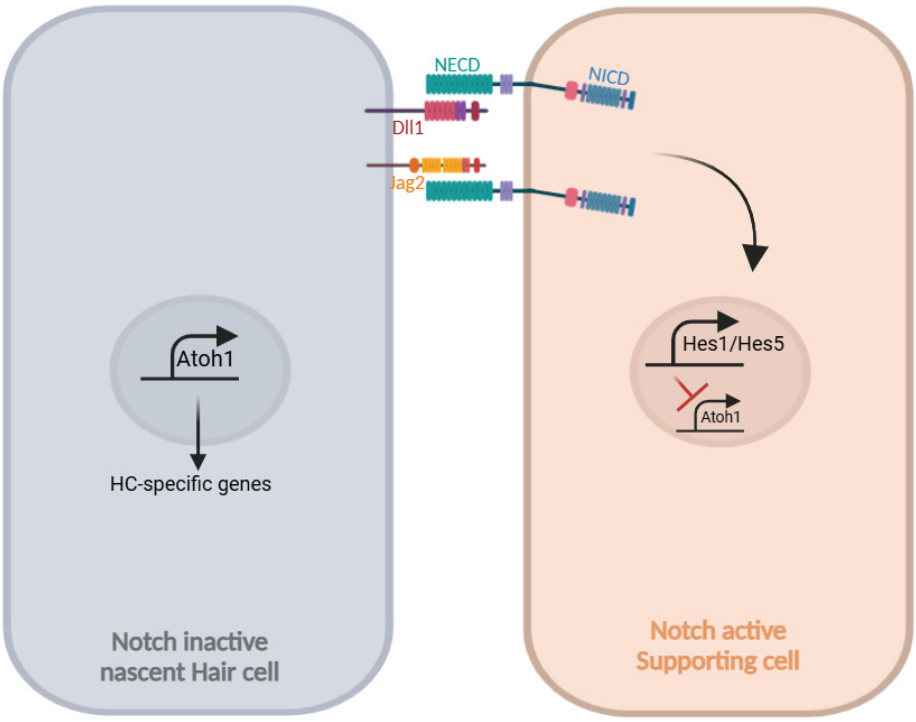

Figure 14. Notch-mediated lateral inhibition promotes terminal differentiation of HCs. The signal sending cell expresses the Notch ligands Jag2 and Delta-like-ligand 2 (Dll2) and interacts with Notch1 receptor of the signal-receiving cell. This leads to the upregulation of the Notch-target genes Hes1 and Hes5 that are known antagonists of Atoh1 which prevents the cell from adopting a HC fate and thus develops as a SC. In contrast in the signal-sending cell, the inactivation of the Notch pathway and hence the absence of Hes1/5 expression permits the expression of Atoh1 which promotes the differentiation into a mature HC.

The Sox2 transcription factor plays a complex role during HC differentiation by exerting both inductive and antagonistic effects on Atoh1. It has been shown to act as an activator of Atoh1 transcription and is thus required for Atoh1 to be expressed at high levels in cells adopting a HC fate (Kempfle et al., 2016; Neves et al., 2013). More precisely, in vivo experiments in mouse have shown that the depletion of Sox2 from E13.5 onwards abolishes HC development (Kempfle et al., 2016). Following this role as an inducer of Atoh1 expression, Sox2 is rapidly downregulated in differentiating HCs while its expression is maintained in the nucleus of surrounding SCs. This loss of Sox2 from nascent HCs is crucial for cells to adopt their fate, as it was shown to antagonize Atoh1 by blocking its activity. This hypothesis is underlined by experiments showing that a forced sustained expression of Sox2 prevents Atoh1-induced HC differentiation. In contrast, a hypomorphic mutation of Sox2, leading to a decreased Sox2 expression level during development, is accompanied with ectopic expression of Atoh1 in the developing SCs causing an overproduction of HCs (Dabdoub et al., 2008). In this case, Sox2 level is sufficient to induce Atoh1 expression in epithelial cells, but insufficient to antagonize its activity. As Atoh1 upregulates its own expression, high levels of Atoh1 are found in sensory and non-sensory cells expressing low amounts of Sox2, all of which differentiate into HCs. Altogether, these findings suggest that Sox2 is instrumental to Atoh1 induction in epithelial cells destined to become future HCs, but that

it needs to be switched off at later stages to allow proper Atoh1-driven transcriptional program of HC differentiation.

4.1.3 Role of Sox9 during HC development

In our laboratory, we uncovered that Sox9, another member of Sox transcription factors family, also plays a role during HC emergence in the organ of Corti. It is part of the SoxE family comprising Sox8, Sox9 and Sox10 (Koopman et al., 1989). The different regions characterizing Sox9 are a self-dimerization domain, transactivation domain and a DNA binding domain (=HMG domain) (Gubbay et al., 1990). Sox9 can act as a transcriptional activator or as a repressor depending on the binding partner, co-factors and the binding sites (Bernard et al., 2003; Kamachi et al., 2000). Indeed, without binding to other factors (Sox members or others), Sox9 is unable to regulate expression of a target gene.

In the developing inner ear, Sox9 is expressed in the otic placode at E8.5. Later, Sox9 protein is present in the otic epithelium and the periotic mesenchyme from E9.5 to E12.5 (Barrionuevo et al., 2008) and in the whole prosensory domain until E14.5 (Figure 15). At P0, it is solely expressed in SCs. Although Sox9 has a similar expression profile than Sox2 during these developmental stages, we found that Sox9 is downregulated more quickly than Sox2 in nascent HCs, hinting for different roles in the terminal cell differentiation process (Mak et al., 2009) (Figure 15). This expression pattern has been confirmed in the human inner ear, with Sox9 being rapidly downregulated in nascent HCs while Sox2 persists for a longer period (Locher et al., 2013).

By performing ex vivo electroporations, we showed that maintained expression of Sox9 in E13.5-14.5 progenitors blocks HC differentiation. Indeed, no Sox9 transfected cells were able to adopt a HC fate, even when co-expressed with the HC inducer Atoh1. This prompted us to suggest that Sox9 strongly antagonizes Atoh1 factor, which was confirmed by demonstrating a reduced Atoh1 transcriptional activity in the presence of Sox9. Our study revealed that, in cochlear cells, Sox9 upregulates Hey1 and HeyL, which are well-known inhibitors of Atoh1 function. Upon Sox9 transfection, Atoh1 activity could indeed be restored by knocking down Hey1 and HeyL, as evidenced by the elevated expression of an Atoh1-responsive reporter gene. Overexpressing Hey1 and HeyL in sensory progenitors, through electroporation experiments, prevented HC differentiation and genetic ablation of both transcription factors resulted in supernumerary HCs in vivo. Altogether, our results showed that in the developing sensory epithelium Sox9 needs to be downregulated from nascent HCs to allow them to adopt HC fate. The results of this study have been published in Cells and can be viewed in the Annex of this manuscript (Veithen et al., 2023). It is not included in the main text (results section), as I contributed to this work before conducting my thesis research project.

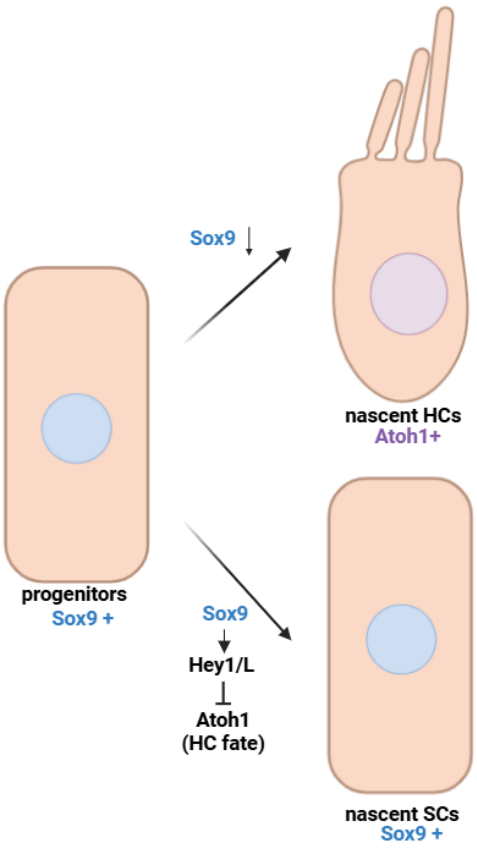

Figure 15. Role of Sox9 during inner ear development. Sox9 is expressed in the cochlear sensory progenitors and rapidly downregulated in nascent HCs. In progenitors committed to SC fate, Sox9 upregulates Hey1 and HeyL that are known antagonists of Atoh1 function, thereby preventing the progenitors from adopting HC fate *(Veithen et al., 2023).*

Of note, mutations of Sox9 are responsible for a disease called campomelic dysplasia, characterized by skeletal malformation, cartilage dysplasia and sex reversal. Patients present a very low survival rate of 5-10% in the first year of life (Mansour et al., 2002; Savarirayan et al., 2003). As well, they show misdeveloped outer ears (Tokita et al., 1979) and sensorineural hearing loss (Savarirayan et al., 2003), hinting for an important role of Sox9 during inner ear development.

4.1.4 Establishment of HC polarity

The planar polarity of HCs is reflected by the structure, position, and organization of the hair bundles at their apical surface. It is crucial for the auditory function as it underlies the mechanosensory mechanisms. In the mammalian cochlea, there are two levels of planar polarity: the **intrinsic polarity**, which refers to the polarity at the level of an individual HC (e.g. the hair bundle angle and position), and the **planar cell polarity**, which lies at the tissular level and corresponds to the coordinated orientation of hair bundles between neighboring HCs (e.g. all V-shaped bundles pointing to the same direction, towards the lateral side of the tissue). These planar polarity mechanisms are orchestrated by different signaling pathways and genes. The two principal pathways that guide the intrinsic polarity within individual HCs are the Par3-Rac1-PAK and the Gαi/LGN pathways. The Par3-Rac1-PAK pathway is one of the first to be discovered being linked to intrinsic polarity. Mutants of the small GTPase Rac1

present stereocilia bundles that are dissociated from the lateral kinocilia and aberrantly formed. Its downstream effector PAK in its phosphorylated and thus activated form is localized at the lateral cell border. Further, the activation of PAK by Rac1 is regulated by the polarity protein Par3 to guide the pattern of the apical area of the HCs (Grimsley + Myers 2009). The Gαi/LGN pathway is responsible for the patterning of the apical HC surface and more specifically the lateral region behind the stereocilia that is devoid of actin microvilli. Indeed, the restricted enrichment of Gαi and LGN at the lateral pole of the HC apical surface defines the "bare zone" and together they govern the restricted distribution of αPKC to the opposite "medial zone" (Figure 16) (Tarchini et al., 2013). In addition, Gαi and LGN have been shown to be required for the elongation for the longest row of stereocilia during development (Tadenev et al., 2019) and recently to be crucial for the maintenance of a steady stereocilia height in adult mice (Hartig et al., 2024). Moser *et al.* showed that Gαi and LGN are both indispensable for the correct modiolar-pillar gradient of Ribbon size (see paragraph 2.3.2 on SGN diversity) and thus described a new role of intrinsic polarity proteins that are present at the apical HC surface in defining a spatial gradient of synapses present at the baso-lateral side of the IHC (Jean et al., 2019).

The planar cell polarity pathway is guided by intercellular signaling complexes that coordinate the polarity between neighboring HCs. The PCP core proteins are the transmembrane *Vangl1/2* protein (Van Gogh-like protein), the transmembrane receptor *Celsr1* and the Wnt receptor *Frizzled* that are conserved between vertebrates and invertebrates. As they are responsible for the coordinated hair bundle orientation between neighboring HCs, PCP mutants show mainly misorientated hair bundles (Figure 16). Interestingly, the polarity defect in Vangl2 mutants is quite prominent in mice at birth but refines during the 2 first postnatal weeks so that a polarity defect is no longer obvious at P10-P15(Copley et al., 2013). However, it is not clear if Vangl1 compensates for the loss of Vangl2. It seems that the PCP and the intrinsic polarity pathways act in parallel in an independent manner as Gαi mutants do not show impaired PCP protein distribution (Grimsley-Myers et al., 2009) and PCP mutants show normal bundle polarization and normal intrinsic polarity protein distribution (Grimsley-Myers et al., 2009; Tarchini et al., 2013). Nevertheless, in Rac1 KO the Frizzled3 protein shows a modest abnormal distribution, suggesting that the two pathways could sometimes crosstalk with each other (Grimsley-Myers et al., 2009).

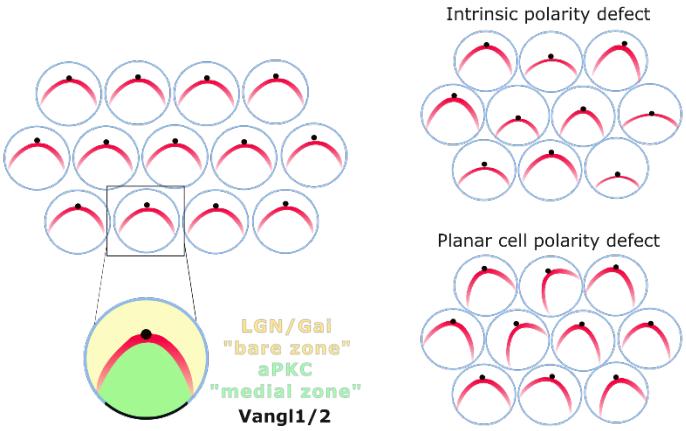

Figure 16 Planar polarity in cochlear sensory epithelium. Illustration on the left showing the normal HC polarity at cellular and tissular level with the classical distribution of the intrinsic polarity proteins Gαi/LGN/aPKC and the PCP proteins Vangl1 and 2. In case of intrinsic polarity defects, the position of the kinocilium, the bare zone area, the medial zone area and the hair bundle angle can be impaired. In case of PCP defect, the coordinated orientation of neighboring HCs is disturbed.

4.2 Focus on otic neuron development

4.2.1 Otic neuron specification

The otic neuronal progenitors, also called neuroblasts, derive from the neurosensory domain, located in the antero-ventral part of the otic cup and vesicle between E9 and E11 (see Figure 13). Critical players during the early neuronal development are the proneural basic Helix-Loop-Helix factors. Neurogenin1 (Ngn1) has been reported to be expressed as early as E9 in the neuroblasts, as soon as they delaminate, to regulate neuronal specification but is switched off once they have formed the CVG (Ma et al., 1998, 2000). From this moment on, NeuroD1 is being upregulated to regulate neuronal progenitor survival and differentiation (Jahan et al., 2010; Kim et al., 2001; M. Liu et al., 2000; Raft et al., 2007). Interestingly, Sox2 would be required for early steps of otic neurogenesis, including for Ngn1 expression, however it is thought to be a competence factor rather than a direct initiator of the neural fate (Steevens et al., 2017).

4.2.2 Otic neuron differentiation

After several rounds of proliferation, neuroblasts become post-mitotic to differentiate into bipolar neurons in a base-to-apex gradient between E9.5 and E13.5. Following this, they start forming peripheral projections to reach the sensory epithelium (Koundakjian et al., 2007). As the first HCs only appear in the cochlear base at E14.5, the early formation of neuronal projections and innervation is thought to be a process that is independent of the presence of mature target cells. Accordingly, Atoh1 knock out mice still present normal projection patterns despite missing HCs in the otic epithelia (Fritzsch et al., 2005; Pan et al., 2011).

During the formation of neuronal projections, Gata3, a zinc finger transcription factor has been described as crucial not only for regulating neuronal cell fate but also for correct neurite outgrowth and cochlear wiring as the loss of Gata3 leads to premature SGN differentiation and excessive neurite formation as well as impaired pathfinding (Appler et al., 2013).

4.2.3 Emergence of VGNs and SGNs

Differentiated neurons can be subdivided into 2 populations, one innervating the HCs in the vestibule (vestibular ganglion neurons, VGNs) on the dorsal side of the developing inner ear and one innervating the cochlear HCs (spiral ganglion neurons, SGNs) located on the ventral side of the inner ear. It was known for long that the VGNs and SGNs arise respectively from early born-Ngn1+ or late born-Ngn1+ neuronal progenitors (Koundakjian et al., 2007), but the exact time point at which they start presenting distinct molecular signatures was unclear. Recently, by performing scRNAseq studies on otic vesicles at E9.5, E11.5 and 13.5, Sun and colleagues showed that VGNs and SGNs arise from a common population of undifferentiated CVG cells, then subdivide at E11.5 into distinct clusters (Y. Sun et al., 2022) (Figure 17). Later on, VGNs further subdivide into 2 subclusters at E13.5 (Gata3+/Sall3- and Gata3-/Sall3+). However, if these two VGN populations innervate different vestibular end organs or if they are maintained until adulthood and correspond to distinct VGN subtypes is still elusive and needs to be elucidated.

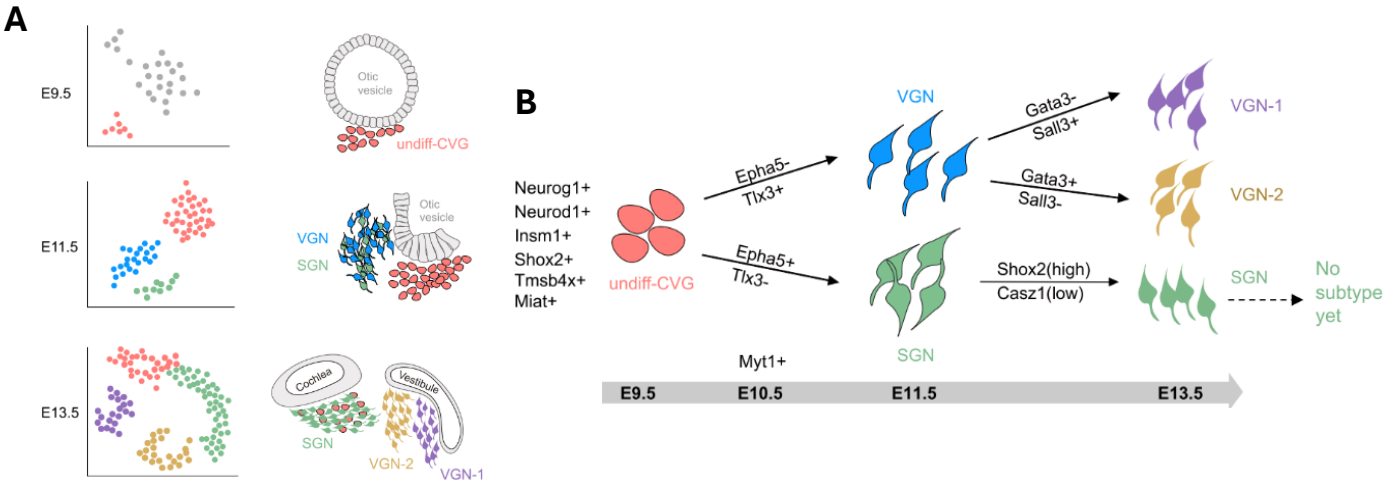

Figure 17. Inner ear neuronal development. A) scRNAseq studies discovered a single cluster of undifferentiated cells at E9.5, a cluster of SGN and VGN at E11.5 and 2 clusters of VGN and 1 SGN at E13.5. B) Illustration showing the temporal development of the undifferentiated CVGs into 2 VGN subpopulations and 1 SGN cluster. The first homogeneous VGN population can be distinguished from the SGN population by the expression of Tlx3+ and the absence of Epha5. Later, when the VGNs divide into two subcluster, this split is characterized by the opposing expression of Gata3 and Sall3, whereas SGNs differs from the VGNs through the expression of Shox2 and Casz1. *From Sun et al., 2022.*

4.2.4 Emergence of SGN subtypes

To further elucidate how the SGNs diversify into their final 4 subtypes, Petitpré et al. performed scRNAseq on neurons isolated from FACS sorted Tomato+ cells coming from Ntrk3^{Cre} or PV^{Cre} mice at embryonic stages E14.5, E15.5, E16.5, E17.5 and E18.5. SMART-Seq2 analyses show that unspecialized neurons first diverge into a Ic- and an intermediate Ia/Ib/II-branch of neurons around E15-16. During this first branching, there is an upregulation of Runx1 and Meis2 factors, with the latter being lost in the final Ic-subtypes. The transcription factor Pou4f1 shows an increased expression in the Ic-trajectory and a decreased expression in the Ia/Ib/II intermediate cells (Figure 18). As this first split parallels the innervation of the HCs, the cell-cell communication between HCs and SGNs (which does not yet include synaptic release or HC spontaneous activity) could contribute to the emergence of subtypes. Thus, the release of specific extrinsic signals, in a HC subcellular manner (pillar vs modiolar), still makes them a strong candidate for driving SGN diversification, but it cannot fully be excluded that other cell types surrounding the IHC such as the SCs or non-sensory cells are implicated in this process of neuronal embryonic specification as well.

Interestingly, the well-known transcription factor Neurod1 has been identified as a regulator of Ic cell fate as it is active in the first specification period of the unspecialized SGNs and specifically expressed at the beginning of the Ic branch. More importantly, the depletion of Neurod1 from E8.5 onwards in the developing neurons led to a loss of Ic subtypes at E16.5 and P0, which is not correlated to an apoptotic cell death of the Ic cluster (Petitpré et al., 2022).

During the next branching step, the separation of the intermediate cell population into Ia/Ib and II neurons is characterized by a reduced expression of Runx1 and Shox2 and an increase of Sox9 and Tshz3 in the type II neurons, whereas Prox1 is elevated in the Ia/Ib intermediate cells. The final split leading to differentiated Ia and Ib subtypes is paralleled by an upregulation of Runx1 and Pou4f1 in the Ib neurons and a decreased expression of Runx1 in the Ia subtype (Figure 18).

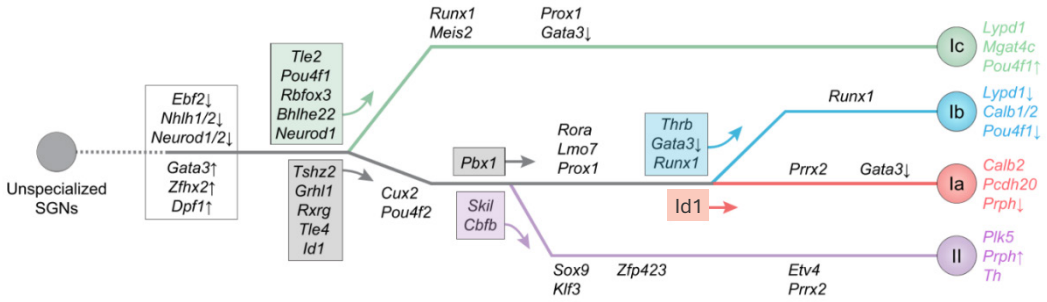

Figure 18. Developmental pathway of the SGNs proposed by Petitpré et al. Pseudotime analysis described a developmental trajectory in which unspecialized SGNs first split into the future Ic subtypes and intermediate Ia/Ib/II SGNs through an upregulation of NeuroD1. The Ia/Ib/II intermediate branch will further split into to the future type II subtypes (characterized by an upregulation of Sox9) and intermediate Ia/Ib neurons (characterized by an increase of Prox1 expression). Lastly, the separation of the intermediate Ia/Ib branch into the final Ia and Ib neurons parallels an increase of Runx1 in the Ib branch and a steady expression of Id1 in the Ia branch. *Adapted from Petitpré et al., 2022.*

Sanders and Kelley showed similar results with scRNAseq analyses performed on neuronal samples dissected at E14, E16, E18 and P1, even if the sample collection method (FACS sorted >< dissection) and the sequencing method (SMART-Seq2 >< 10X Chromium) were different in the 2 studies. Their results indicate that during the first split the Ic subtypes do not directly form a unique group, but their precursors are the same as for the Ib subtypes that develop in a next split. In parallel, Ia and II neurons develop from a common cluster of precursors (Figure 19A and B). They identified **Lypd1**/Runx1/Ntng1 as markers expressed at the beginning of the Ib/Ic and Ia/II branches but then progressively restricted to the Ib/Ic branch, whereas **Tle4**/Id1/Gata3 upregulation occurs in the Ia/II branch. These expression patterns suggest that the Ia/II specification happens in an inductive manner whereas the Ib/Ic specification happens in a default mode. During the second split of the Ib/Ic precursors into immature Ib and Ic cells, Mafb expression is maintained in the Ib branch while it decreases in the Ic branch. Conversely, Tgfb2/Igfbp2/Runx1t1 expression decreases in the Ib branch but remains high in the Ic branch. In the third and last split from Ia/II precursors into immature Ia and II neurons, Efna5 and Sox9 are significantly upregulated in the type II branch whereas expression of Fgf10 and Shox2 is sustained only in the Ia branch.(Sanders & Kelley, 2022)

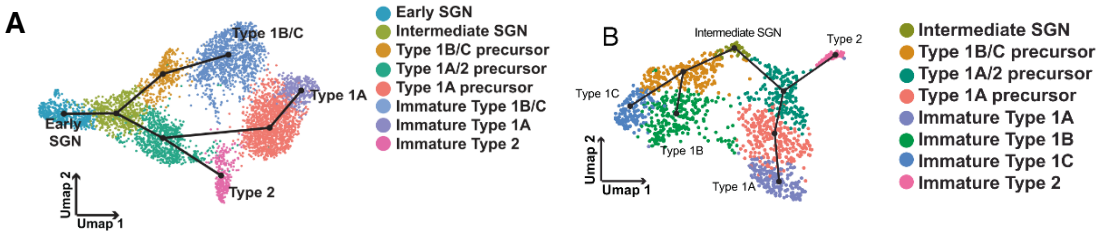

Figure 19. Developmental trajectory described by Sanders and Kelley. A) UMAP containing slingshot trajectory of the combined dataset of E14-16-18-P1 shows a first split of early SGNs into Ib/Ic precursors and Ia/II precursors followed by a second split into immature type II and Ia neurons. The absence of two separate Ib and Ic clusters is likely due to the transcriptional similarity between those neurons compared to the other neurons coming from more immature time points. B) Slingshot trajectory analysis performed on E18.5 and P1 dataset show a first diversification of intermediate into Ib/Ic precursors and Ia/II precursors around E14 and a next split into the final Ia, Ib, Ic and II neurons at E16. *From Sanders and Kelley, 2022.*

Overall, the major difference consists in the specification of the Ib subtypes: whereas Petitpré et al. suggests that it develops from a common branch with the Ia/II subtypes, Kelley describes an initial cluster of progenitors common to Ib and Ic subtypes. Further in vivo studies using lineage tracing experiments will be necessary to clarify these discrepancies.

On top, it could be demonstrated that the 4 SGN subtypes are already present at P3 (Petitpré et al., 2018), and undergo a refinement period over the first 4 weeks. More precisely, the markers expressed in mature SGNs, Calb2 and Lypd1, first show a high degree of co-expression shortly after birth but start to be expressed more exclusively until 4 weeks of age, and this at the transcript level (Shrestha et al., 2018) (Figure 20) as well as at the protein level (S. Sun et al., 2018).

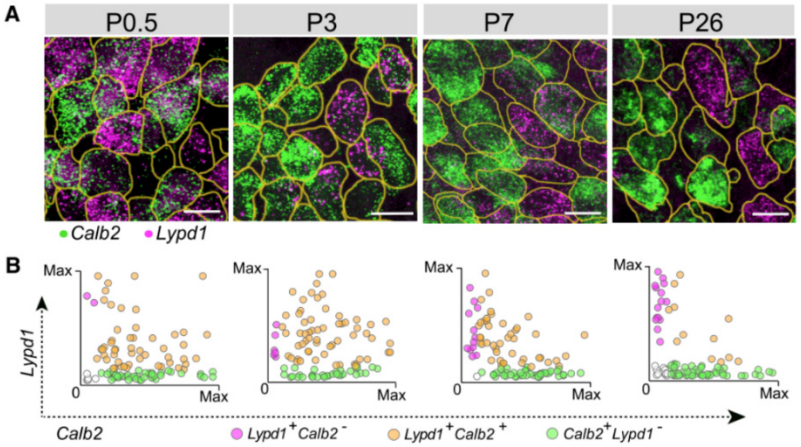

Figure 20. Signature refinement during the first postnatal week. A+B) the subtype specific markers Calb2 and Lypd1 show a largely overlapping expression pattern shortly after birth, but then gradually start to be exclusively expressed so that at P26, SGNs express either one or the other marker and are rarely double-positive. F*rom Shrestha et al. 2018.*

Interestingly, it could be shown that synaptic transmission during the early pre-hearing period (and so the IHC-driven activity) is crucial for the SGN identity consolidation as VGlut3KO animals (with no Glutamate release) present an increased proportion of Calb2+ Ia subtypes and a decreased proportion of the Lypd1+ Ic subtypes, and this only visible from P8 onwards proving that the onset of subtype specification is independent of the activity driven by the IHC and the synaptic transmission (Shrestha et al., 2018). Additionally, mice with disrupted mechano-transduction (as in TmieKO, Pcdh15KO and Lhfpl5KO mice) showed affected specification of type I and II neurons as well as type Ia, Ib and Ic as shown by the increased co-expression of subtype specific markers at the protein level at P28. This phenotype is already present at P14 thus indicating an onset during the pre-hearing period too (Sun et al., 2018).

PART II – BALANCE AND VESTIBULE

5. Vestibule

The vestibule is the part of the inner ear that is responsible for balance sensation. This dorsal otic structure contains 5 sensory organs: 2 maculae comprising the utricle and saccule, and 3 cristae located at the base of each semicircular canal, the horizontal, anterior and posterior cristae (Figure 21A). The utricle and saccule are responsible for the perception of lateral head movements in a horizontal (acceleration in a car e.g.) and vertical manner (moving up in an elevator e.g.), respectively. Both these epithelia are embedded in a membrane, which is covered by a layer of calcium crystals, called otoliths or otoconia. The 3 cristae allow us to perceive angular head movements and our position in a 3-dimensional space due to their inclined position within the inner ear. They are also embedded in a gelatinous structure, called cupula, but they are devoid of solid crystals.

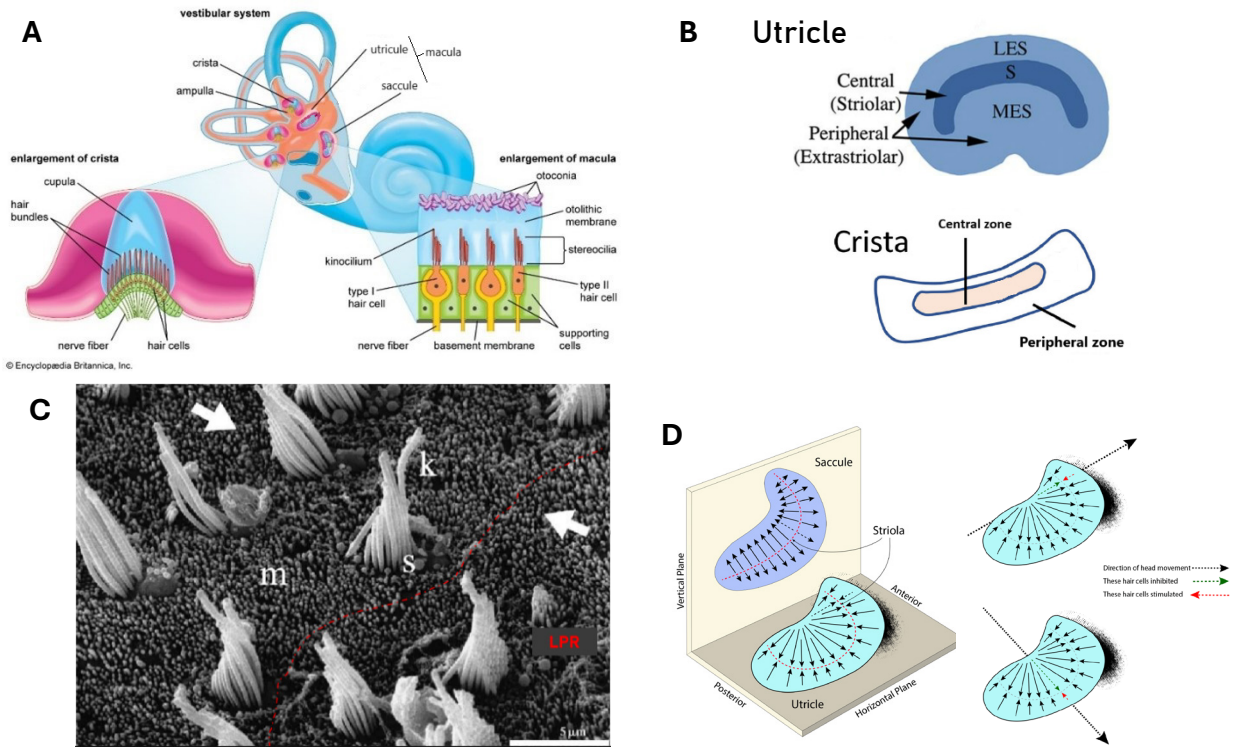

Figure 21. The vestibular system. A) the inner ear comprising the vestibular system with the 5 sensory organs: the 3 cristae ampullaris and the 2 maculae. The cristae (left) is the sensory epithelium located in the Ampulla, an enlarged region at the end of each semicircular canal. All of the five sensory organs contain specialized HCs, nerve fibers and supporting cells. B) The utricle with the striolar region and the lateral and medial extrastriolar region (LES + MES). The Cristae containing the central and peripheral zone. *Adapted from Stone et al. 2021 and Maroto et al. 2021.* C) Electron microscopic image of a turtle's utricle showing the Line of Polarity Reversal in red with the HCs orientated in opposing directions (indicated by arrows). *k: kinocilium; m: microvilli; s: sterovilli. Adapted from Severinsen et al. 2003.* D) the horizontal and vertical orientation of the utricle and saccule within the inner ear to perceive horizontal and vertical linear accelerations, respectively. The LPR is located at the level of the striola, dividing the maculae in two distinct anatomical zones with the hair bundles pointing in opposing directions. Acceleration in one direction stimulates the HCs on one side of the LPR whereas the other side remains inhibited. *Adapted from https://www.enteducationswansea.org/vestibular-physiology.*

All sensory organs in the vestibule are made of epithelial Hair cells and Supporting cells. In the Cristae, the stereociliary bundles of Hair cells protrude into the "cupula", which is gelatinous mass laying on top of the sensory epithelium (Figure 21A). Upon rotational movements, the endolymph pushes the cupula against the hair cell bundles causing their deflection and thus inducing a depolarizing signal within the Hair cell. This information will be transmitted by the afferent neurons forming the VIIIth cranial nerve towards the central nervous system. The process within maculae happens in the same manner with the particularity that the hair bundles protrude into a gelatinous mass and are topped with crystal-like structures, so-called otoconia (Figure 21A). In presence of linear motions, this causes the shift of the endolymph and the otoconia and so the deflection of the hair cell bundles to induce a mechanoelectrical signal that is further transmitted to the brain.

The sensory epithelia of the 2 maculae and 3 cristae comprise two anatomical zones. In maculae a central *striolar* zone is surrounded by the *extrastriolar* zone (lateral and medial, LES and MES), whereas these regions are simply termed *central* and *peripheral* zones in cristae (Figure 21B). The striolar region can be distinguished from the extrastriolar region by a higher HC density and the presence of larger otoconial crystals (reviewed I in Eatock & Songer, 2011). In the utricle and saccule, these two regions are separated by a Line of Polarity Reversal (LPR) because the hair bundles present on the HCs located on either side are oriented in opposite directions. Interestingly, the relative orientation of hair bundles across LPR differs between utricle and saccule. While the kinocilia point towards each other within the utricle (towards LPR), they point away from each other (towards the periphery of the epithelium) within the saccule. This allows the detection of linear acceleration in opposing directions as only the HCs on the same side of the LPR are activated whereas the ones at the other side remain inactivated. In contrast, within the cristae the hair bundles all point in the same direction within the whole epithelia hence there is no LPR (Figure 21C+D).

5.1 HCs in the semicircular canals and the maculae

When the head moves, the deflection of the stereociliary bundles towards the kinocilium allows the opening of mechanically-gated ion channels and the entry of potassium causing a depolarization of the hair cell (Figure 22). This depolarization enables the opening of voltage-gated Ca2+ channels and so the entering of calcium ions into the Hair cell that leads to the fusion of synaptic vesicles with the basolateral membrane. The synaptic vesicles release the neurotransmitter Glutamate into the synaptic cleft to induce a EPSP at the post-synapse to results in an Action Potential within the axon of the afferent fiber which transmits the signal to the brain. The stronger the movement of the head, the stronger the deflections of the hair bundles and the greater the release of Glutamate and thus the higher the rate of Action potentials at the nerve fiber. Bending of the stereocilia in the opposite direction, away from the kinocilium, results in a hyperpolarization of the hair cell and thus in an inhibitory signal.

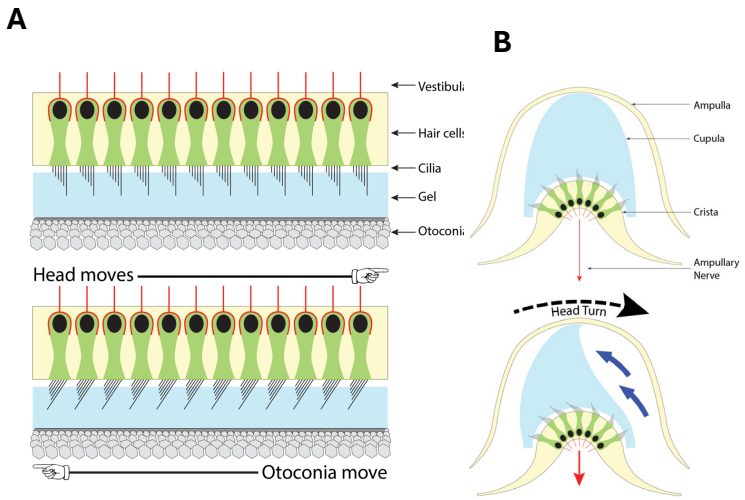

Figure 22. Movement detection and transmission in vestibular maculae and cristae. A) In the maculae (utricle and saccule), the head movement displaces the otoconia and the gelatinous mass in the opposite direction that induces the deflection of the hair bundles leading to the opening of the mechanosensory channels. B) in the cristae, when the head turns in an angular direction, the cupula is displaced in the opposite direction which deflects the hair bundles and opens the mechanosensory channels. *From https://www.enteducationswansea.org/vestibular-physiology.*

Each of the 5 sensory epithelia comprises two types of HCs: type I and type II (Mackowetzky et al., 2021). These two types of HCs differ morphologically, physiologically and molecularly. Type I HCs are known to be more Calice shaped with a narrow neck and long stereocilia and are innervated by cup-like afferent terminals called calyx synapses. Type II HCs have a cylindrical shape with short stereocilia and present basolateral cytoplasmic extensions (Pujol et al., 2014) and are innervated by several small bouton synapses (Figure 23). Type I HCs are slightly more concentrated in the central area of Cristae and the striolar area of maculae but the ratio of type I and II is roughly 50/50 in peripheral/extrastriolar regions. Recent scRNAseq studies have revealed specific markers of adult HCs: Spp1 is a pan marker for adult HC I and Mapt and Calb2 constitute markers for adult/mature type II HCs. Interestingly, differences between regions within each group of HCs could be demonstrated, for instance striolar HCs type I specifically express Oncomoduline (Ocm). (McInturff et al., 2018)

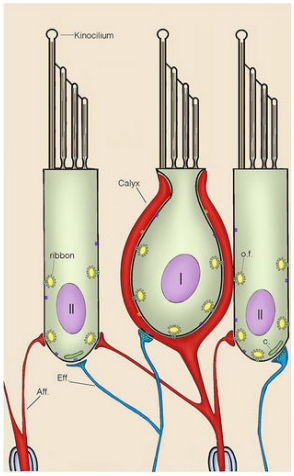

Figure 23. Type I and II HCs in the vestibular organs. The type I HCs differ from the type II HCs by a more calyceal shape, a narrow neck and a Calyx-innervation. Type II HCs have a cylindrical shape and are contacted by small bouton synapses. *From intechopen.com.*

Physiologically, type I HCs have low-voltage-activated outward-rectifying, K+ conductance, termed gK,L that produces smaller and faster voltage responses enabling the detection of high frequency head movements (specifically the central HC I). The type II HCs present rather high voltage-activated K+ conductance and are thus more adapted to detect maintained heads tilts (more specifically the extrastriolar/peripheral afferents) (reviewed in Eatock & Songer, 2011).

5.2 Vestibular supporting cells and their implication in HC regeneration

The vestibular supporting cells are epithelial cells that are morphologically more homogeneous than the cochlear ones. In the vestibular epithelium they provide structural and metabolic support to the neighboring Hair cells, but they also play a role in tissue homeostasis and cell regeneration. First, they serve as progenitors to renew HCs during natural cellular turnover in adulthood (Jørgensen & Mathiesen, 1988). This was longtime thought to be restricted to birds and reptiles, until a study from 2017 that showed it was possible in adult mice utricles. In this study, the authors showed that in normal non-damage conditions, a small number of HCs I and II are cleared by phagocytosis and only HCs II are replaced by SCs (Bucks et al., 2017). Secondly, SCs are able to spontaneously regenerate HCs after ototoxin-induced HC death in birds (Tsue et al., 1994) and mammals (Bucks et al., 2017; Lin et al., 2011). Whereas in birds the regeneration of HCs parallels with a complete functional recovery (Carey et al., 1996; Jones & Nelson, 1992), in mammals the number of regenerated HCs, the HC diversity and the functional recovery is incomplete and very limited (Forge et al., 1993; Golub et al., 2012; González-Garrido et al., 2021; Kawamoto et al., 2009; Zeng et al., 2020). Third, they have a phagocytotic capacity to clear HC debris after ototoxic damage in birds (Bird et al., 2010) and mammals (Monzack et al., 2015).

In humans, a recent study suggests that an induced regeneration of HCs after Gentamicin-induced HC death could also be possible but in a limited manner. In this study, human vestibular epithelia were treated ex-vivo with Gentamicin to induce HC death. The viral transduction of supporting cells with *ATOH1* resulted in generation of HC-like Myo7A+ cells presenting an upregulation of 335 putative HC markers and the formation of hair bundles. Nevertheless, some expected HC markers were not expressed, and the hair bundles were less organized, suggesting an incomplete differentiation. (R. R. Taylor et al., 2018)

5.3 Vestibular afferents

The afferent fibers of the vestibular system can be divided into 3 morphologically distinct subtypes: those that form Calyx synapses on type I HCs and called *Calyx-only neurons*, those that form bouton contacts on type II HCs, called *Bouton-only neurons,* and those that form both Calyx and bouton

contacts with type I and II HCs, respectively, termed *Dimorphic neurons*. Dimorphic neurons are the most common type, they are found both in the striolar/central and extrastriolar/peripheral regions. The Calyx-only neurons innervate HCs only in the striolar/central region. (Fernandez et al., 1990) (Figure 24). Some Calyces in the striolar/central region englobe several neighboring HCs at the same time, these are called *complex Calyces,* and they can originate from a Calyx-only or a Dimorphic afferent, whereas the calyces found in the peripheral region necessarily originating from a dimorphic afferent always encapsulate a single HC I. The bouton-only neurons, also able to branch up to 20 times, are the rarest kind of afferences and nearly exclusively found in the extrastriolar/peripheral region.

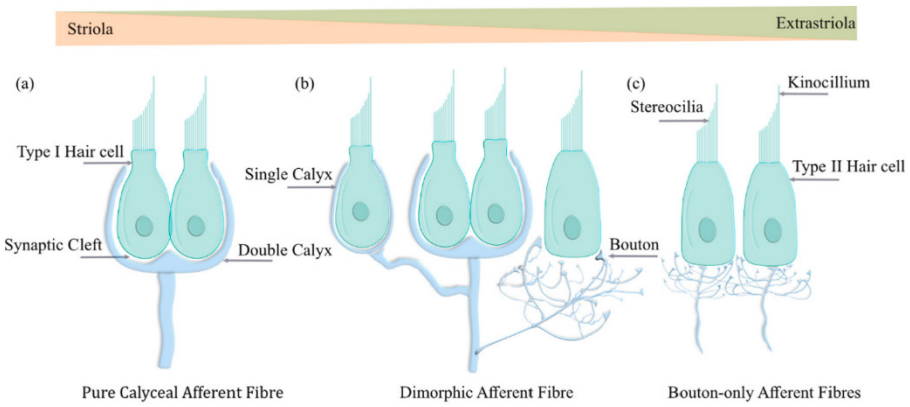

Figure 24. The vestibular innervation pattern in the maculae. Vestibular HCs are innervated by three different types of neurons: the Calyx-only neurons (Pure Calyceal afferents), Bouton-only neurons and dimorphic neurons. Calyx-only neurons (a) innervate type I HCs only in the striolar region, Bouton-only (c) neurons innervate type II HCs exclusively in the extrastriolar region and Dimorphic neurons (b) innervate both type I and type II HCs in the striola and extrastriolar region. Complex Calyces, innervating 2-5 neighboring HCs at the same time, are only found in the striolar region. Dimorphic neurons are the most common type of afferent fibers whereas Bouton-only are the rarest kind of fibers. *From Mukhopadhyay and Pangrisic, 2022.*

Molecularly, the 3 neuronal subtypes can be distinguished based on the expression of some specific markers. For instance, the Calyx-only afferents specifically express Calretinin (Calb2) whereas the Calyces of Dimorphic afferents are Calb2-negative (Dechesne et al., 1994; Desmadryl & Dechesne, 1992). The HCs I innervated by Calb2-positive Calyces are lying medial to the Line of Polarity Reversal and thus define visually the striolar region (A. Li et al., 2008). Whereas it was thought that all striolar HCs type I, surrounded by Calyces, always express Oncomodulin (Simmons et al., 2010), a more recent study revealed a more complex situation, with the presence of a few type I HCs (presence of Calyces) that do not express Ocm and the presence of some type II HCs (absence of a Calyx) that express Ocm (Hoffman et al., 2018).

Beside Calb2, Calbindin (Calb1) also labels specifically the Calyces of Calyx-only afferents and is absent in dimorphic afferents. Additionally, Calb1 is expressed by the type I HCs (Dechesne et al., 1988), and its expression pattern is quite similar to the one of Ocm, whereas at the level of the Calyx

synapses, its expression colocalizes with Calb2, making them good candidates for identifying and quantifying the presence of Calyx-only and Dimorphic neurons (Prins et al., 2020).

Further scRNAseq studies will be necessary to define molecular signatures and to link the 3 morphological subtypes to 3 putative molecular subtypes. It is likely that transcriptomic profiles will even reveal more VGN subclasses and provide deeper insight into their respective functions. To date, it rather seems that functional differences are region-dependent, as calyx-only and dimorphic neurons that reside in the central/striolar region show an irregular and phasic firing pattern whereas the extrastriolar/peripheral neurons (bouton-only and dimorphic neurons) exhibit a more regular and tonic firing pattern. The irregular firing neurons have larger diameters with faster conductance (Fernandez et al., 1990; Goldberg, 2000), a lower threshold for high frequency stimulus (Curthoys et al., 2017) and more adapting response dynamics. While they seem better adapted to detect transient movements and the onset of rapid movements, the regular spiking afferents seem to be better adapted to detect sustained motions as well as gravity (Curthoys et al., 2017; Hullar et al., 2005; Sadeghi et al., 2007).

5.4 Development

The vestibule starts to develop in parallel to the cochlea: it originates from the otic placode that invaginates to form the otocyst. Then, the neuroblasts start to delaminate at E9.5 from the ventral part of the otocyst to migrate towards the ventro-medial side before starting to differentiate into vestibular ganglion neurons. Between E11.5-12.5 in mouse dorsal part of the otocyst, the HCs emerge from neuroepithelial progenitors within the 5 different patches to give rise to future maculae and cristae.

5.4.1 HC development

The sensory progenitors exit the cell cycle between E13.5-14.5 and this occurs in a central to peripheral gradient (reviewed in Burns and Stone, 2017). In mouse cristae the hair cell differentiation parallels the cell cycle exit. Experimental studies in the mouse utricle showed that HC production and differentiation continues until 2 weeks after birth. First, the medial side of the LPR develops around E13.5, to continue the expansion of the lateral side of the LPR during late embryonic and early postnatal stages. Half of the final number of the utricular HCs develop during the first two postnatal weeks (Burns et al., 2012). About 30% of those HCs added postnatally arise from cell divisions between P0-P2, whereas the others likely originate from HC precursors that exited the cell cycle just before birth. The cells are mostly added in the peripheral region of the maculae or close to the striola (Bucks et al., 2017; Burns et al., 2012). Interestingly, fate-mapping experiments in the utricle revealed that most of

the postnatally generated hair cells become type II HCs, which are localized in the extrastriolar region (Warchol et al., 2019). The HCs undergo a period of morphological and electrophysiological maturation, independent of the region, during the late embryonic and early postnatal phases. Importantly, all this relates to the development of rodent vestibular systems, whereas in human the whole development and maturation happens during embryonic stages (Severinsen et al., 2010).

The newly formed Hair cells start to express Atoh1 mRNA at E11.5 (Raft et al., 2007) and present their first hair bundles at E13.5 in the utricle (reviewed in Burns and Stone, 2017) and E14.5 in the cristae.

Recent scRNAseq studies confirmed the spatio-temporal development of vestibular hair cells (McInturff et al., 2018). Transcriptomic analysis on utricular tissues from P1, P12 and P100 revealed 3 distinct clusters (immature, HC I, HC II) and confirmed Atoh1 as a marker of immature HCs (P. Chen et al., 2002). Of note, a higher diversity of HCs may exist in the utricle but due to the small sample size more subclusters could not be found. At P1, the majority of HCs have a signature different from the ones present in P12 and P100 samples and correspond to immature HCs, while only a small number of HCs present mature type I features. This is consistent with previous findings that discovered the presence of striolar HCs type I in the neonatal utricle (Burns et al., 2015; Eatock et al., 1998; Géléoc et al., 2004). Furthermore, Sox2 and Calb2 have been confirmed to be expressed first in immature HCs, but are then downregulated in mature type I HCs to be restricted in mature type II HCs. Additionally, Mapt and Spp1 show an increased expression in P12 samples and they relate to mature type II and type I HCs, respectively. Overall, type I HCs develop from the posterior-medial region towards the anterior-lateral region of the utricle whereas the HCs type II develop from the central striola uniformly towards the periphery. Additionally, fate mapping experiments using Atoh1CreERT and Plp1CreERT mouse lines revealed that around 98% of all type I HCs develop prior to birth whereas 98% of future type II HCs develop after birth (Burns et al., 2012) (Figure 25).

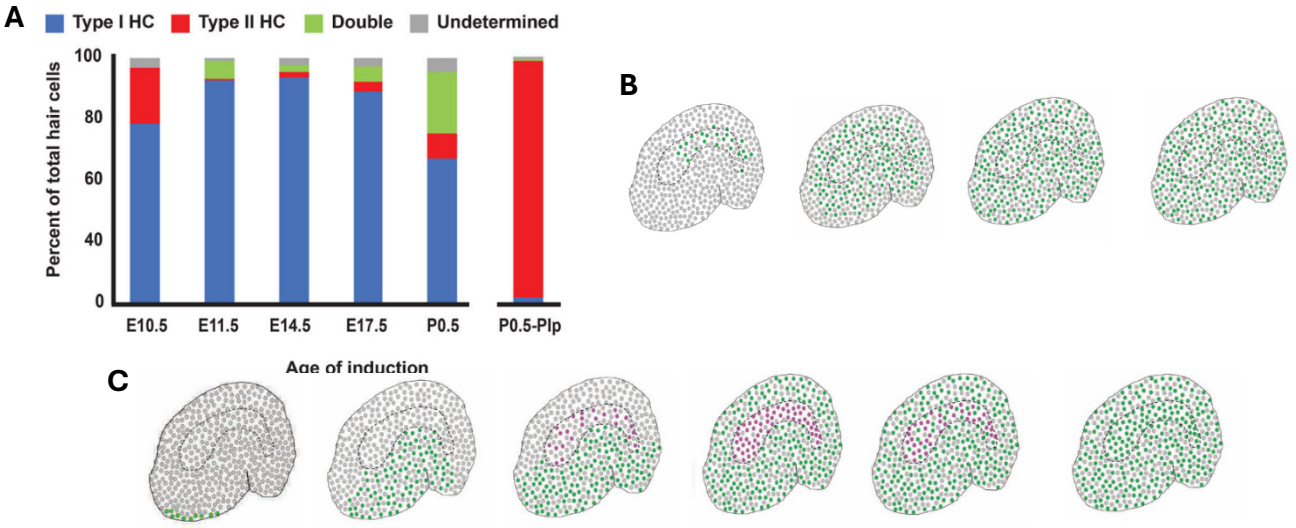

Figure 25 (previous page). Development of type I and type II HCs. A) Graph showing the timepoint of Tamoxifen treatment (age of induction) of Atoh1CreERT (E10.5-P0.5) and Plp1CreERT (P0.5) mice. Type I HCs (blue) are mostly generated before birth with a peak at E14.5, whereas type II HCs (red) are principally generated after birth. B) spatiotemporal development of type II HCs (green) in a striolar-to-extrastriolar direction. C) spatiotemporal development of type I HCs (green) in a posterior/medial-to-anterior/lateral direction with striolar HCs type I becoming Oncomodulin-positive (purple). *From Burns et al., 2012.*

5.4.2 Neuronal development

The vestibular ganglion neurons originate from the same population of delaminating neurons as the cochlear ones. These delaminating neurons downregulate Sox2 (Evsen et al., 2013) to express both NeuroD1 (a neural differentiation gene) and its regulator Neurogenin1 (Ma et al., 1998). It has been known for a long time that vestibular ganglion neurons (VGNs) are born before spiral ganglion neurons (SGNs) (Ruben, 1967), but whether they emerge from a common Ngn1+ population or from 2 different domains in the otocyst remained longtime elusive. Fate-mapping studies using a Tamoxifen-inducible Ngn1CreERT2 mouse line showed that a single Tamoxifen injection at E8.5 uniquely labels the VGNs; Tamoxifen injections at E12.5 only labels SGNs and if Tamoxifen is injected at E13.5 no neurons are labelled. This underlies the hypothesis that there is an early Ngn1-expressing subpopulation of progenitors that gives rise to VGNs whereas the late Ngn1-expressing subpopulation will give rise to spiral ganglion neurons, and from E13.5 onwards the neurogenesis is finished (Koundakjian et al., 2007). Interestingly, a similar study showed the presence of Ngn1-derived HCs and SCs in the utricle and the saccule suggesting that the macular sensory epithelium derives from the neurogenic region of the otocyst, which is not the case for the cochlear sensory epithelium. This is possible due to a reciprocal regulation of sensory fates by a negative autoregulation of Ngn1 and a positive autoregulation of Atoh1 (Raft et al., 2007).

As already described in a previous section, a scRNAseq study performed on inner ear tissues from E9.5, E11.5 and E13.5 showed that VGNs and SGNs emerge at E11.5 from an undifferentiated population of cochlear-vestibular ganglion neurons to further split into 2 different clusters of VGNs (VGN-1 and VGN-2) with still one single SGN cluster (Y. Sun et al., 2022).

5.4.3 Development of vestibular innervation

Regarding the innervation of vestibular HCs in the mouse utricle, a few sporadic bouton synapses could be detected at E15 and some partial Calyces at E18, but the presence of fully developed bouton and Calyx-synapses could not be observed until 2 weeks after birth. Warchol et al. performed a detailed analysis of how Calyx innervation develops in mouse utricles (Warchol et al., 2019). Notably,

between P0 and P14 there is a 25-fold increase in the density of complete Calyx-synapses within the whole utricular epithelium and in parallel an increase in the number of Sox2-negative HCs. These HCs are considered putative type I HCs as Sox2 is first expressed in immature HCs before being downregulated in type I HCs to remain expressed in HCs type II (Hume et al., 2007; McInturff et al., 2018; Oesterle et al., 2008). More precisely, at P0 most HCs are Sox2-positive (representing immature HCs), and only a small number of HCs has already lost Sox2 expression and this only in the striola. At P5, additional cells become Sox2-negative, exclusively in the striolar region again. At P14 finally, half of the HCs in the striolar and extrastriolar region are Sox2-negative, thus representing maturing type I HCs. This maturation process seems to start in the striola and later extend to the extrastriolar region. Regarding the development of Calyx synapses, full Calyces (the presence of a full circle around the HC) are rare in the utricle at P0 but increase in number at P14. Interestingly, the formation of Calyx synapses happens in a different manner in the striola compared to the extrastriola. For instance, within the P0-P5 striola there are very few Sox2-negative cells (developing HC I) at the earliest postnatal stages (P0-5) that lack a full Calyx at the same time. But after P5, there is a significant loss of Sox2 expression in the HCs with the appearance of Calyces at the same time. In contrast, in the extrastriolar region the Calyces start to form even before Sox2 disappears from HCs leading to the presence of some Sox2+ HCs with immature Calyces. This demonstrates that the downregulation of Sox2 from developing type I HCs and the formation of Calyx synapses are two independent processes (Figure 26).

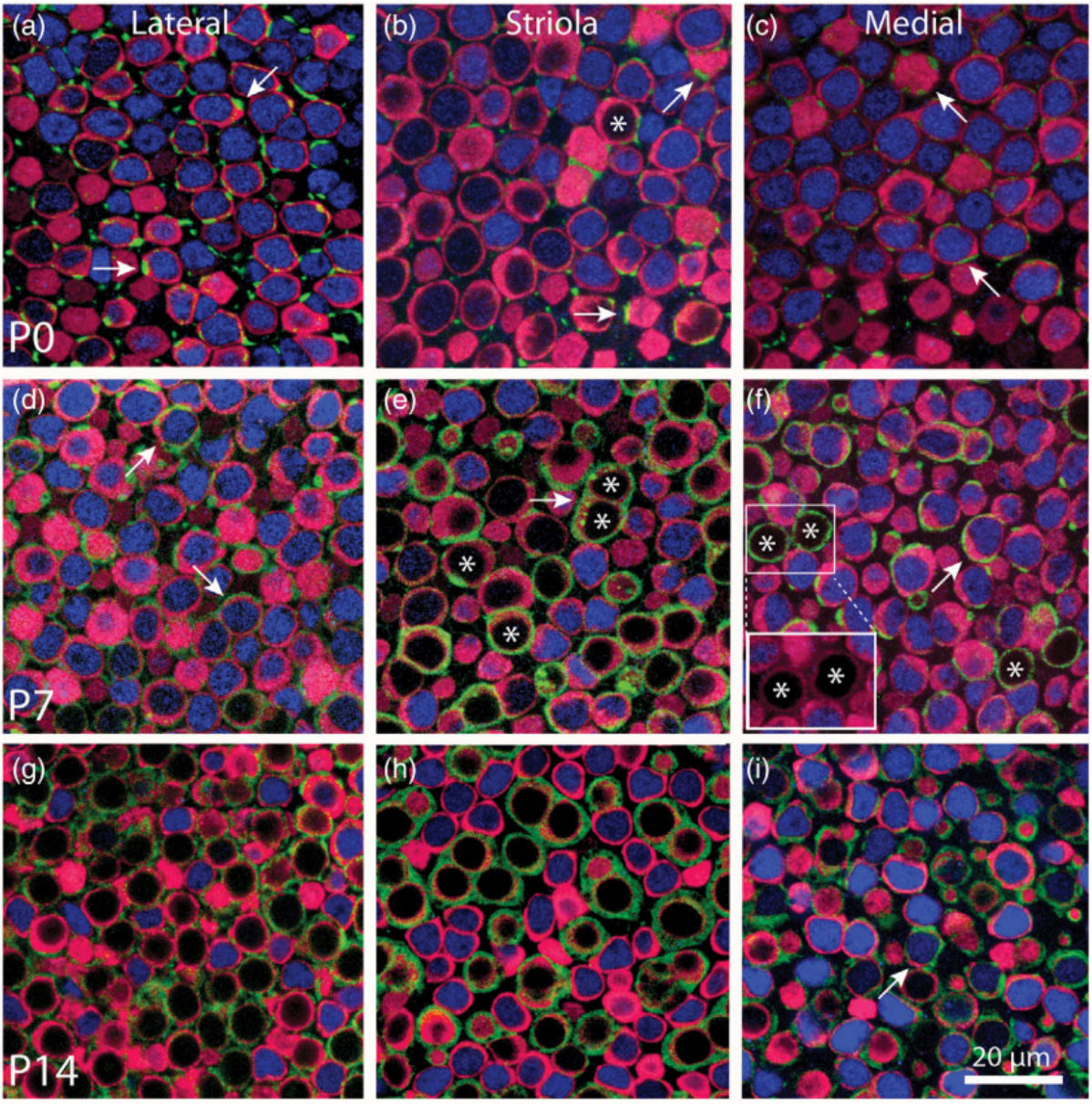

Figure 26 Calyx development in the early postnatal utricle. a,b,c) At P0, there are only very few full Calyces in both the striolar and the extrastriolar region, but some immature incomplete Calyces can already be observed. At the same time, most HCs are still Sox2-positive representing immature HCs. d,e,f) At P7, a loss of Sox2 immunoreactivity can already be observed in the HCs of the striolar region with full Calyceal innervation at the same time (stars). This is in contrast to the extrastriolar region, where only very few HCs have lost Sox2 immunoreactivity (stars) and full Calyces can be observed around Sox2-positive HCs (arrows). g,h,i) Finally at P14, in both the striolar and extrastriolar region, Sox2-negative HCs are surrounded by full Calyces (mature type I HCs) and Sox2-positive HCs show small bouton-like synaptic contacts (mature type II HCs). *From Warchol et al., 2019.*

PART III – PROTEIN HOMEOSTASIS

6. Importance of a balanced and healthy proteome

Most proteins that are synthesized within a cell need to be folded to adopt a specific 3D conformation to exert their normal function until they are degraded or recycled. The term *Proteostasis* refers to protein homeostasis, which requires the balance between protein synthesis, protein folding and degradation to keep a steady level of functioning proteins and to get rid of excessive, misfolded or non-functional proteins as soon as possible. To ensure the maintenance of proteostasis, the *Proteostasis network* comprises protein biogenesis and folding machineries, the protein degradation systems, factors regulating conformational maintenance and safeguard systems to control protein quality and induce adaptive cellular responses in case of abnormalities (Figure 27). The dysfunction of proteostasis occurs when the balanced coordination of these cellular processes is disrupted, leading to an accumulation of misfolded proteins that are either non-functional or mis-functional, thereby affecting the normal biological cellular functions. Furthermore, misfolded proteins often display the ability to form large protein aggregates that threaten cell viability.

The reason why protein aggregates are toxic to a cell is not yet clear but in vitro studies suggest that there are two major mechanisms. First, soluble oligomers form pore-like structures and fibrillar aggregates that may be able to deform or pierce membranes (Lashuel et al., 2002; Milanesi et al., 2012). Secondly, aggregated proteins interact with other functional proteins and sequester them into the aggregate (Olzscha et al., 2011). This can be key proteins such as nucleocytoplasmic factors or ribonucleoproteins (Chou et al., 2018; Woerner et al., 2016; Zhang et al., 2016), but also components of the proteostasis network like chaperones, which will further impair the capacity of the cell to solve the proteotoxic stress, increase the formation of further protein aggregates and finally lead to proteostasis collapse and cell death (Park et al., 2013; Yu et al., 2014).

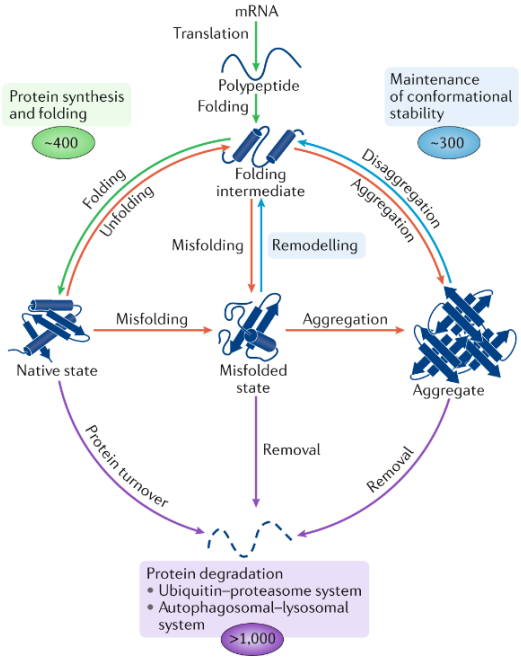

Figure 27. The Proteostasis system. The proteostasis system and its components regulate: 1) the correct folding of newly synthesized proteins to help them acquire their native state (green), 2) the maintenance of a conformational stability by remodeling misfolded proteins and disaggregating aggregates (blue), and 3) the degradation and removal of misfolded and aggregated proteins, by the Ubiquitin-Proteasome system and the Autophagosome-lysosome system, respectively (purple). *From Hipp et al., 2019.*

Notably, the cell capacity to maintain homeostasis declines with age due to the accumulation of external stress factors and oxidative damage leading to an increased risk of developing degenerative disorders. This includes, in particular, neurodegenerative disorders, as neurons (being postmitotic cells) have no possibility to dilute aggregates through cell division and are hence more susceptible to a dysfunctional proteostasis system. Some neurodegenerative disorders are characterized by the aggregation and inclusion of very specific proteins that are toxic to the neuron (Ross and Poirier, 2004). For instance, Parkinson disease is hallmarked by the aggregation of the α-synuclein protein in the substantia nigra, Alzheimer's Disease is characterized by the deposition of extracellular amyloid-beta plaques and intracellular tau-tangles in the cortex, and Huntington's disease by the accumulation of huntingtin. Even if these disorders are marked by the aggregation of very specific disease-related proteins, other types of proteins are also present in the aggregates reflecting a general dysfunction of the proteostasis network. Those proteins with a high vulnerability to aggregate have been shown to be present at higher concentrations compared to their solubility, thus being "super-saturated" proteins (Ciryam et al., 2013).

6.1 Components of the Proteostasis network

6.1.1 Protein translation: ribosomes and tRNAs

The first step of proteostasis regulation happens during protein translation. As nascent peptide chains form and exit the ribosome, they are subjected to co-translational folding, therefore translation dynamics is crucial to ensure protein integrity (Pechmann & Frydman, 2013). Elongation rate is influenced by the codon content of mRNAs, as ribosomes are subjected to pausing and even stalling when encountering a rare codon (Fedyukina & Cavagnero, 2011). This slowdown in protein synthesis is directly linked to the availability of the cognate tRNA molecules and how efficiently it may be selected by the ribosome. The relative abundance of cognate, near-cognate (accommodating for non-canonical "wobble" base pairing with the third nucleotide of the codon) and non-cognate tRNAs, as well as the cellular demand for particular tRNAs, all impact with the speed of decoding. Hence, in addition to mRNA sequence, the composition of the tRNA pool importantly controls translation velocity.

Chemical modifications of RNAs also regulate protein synthesis rate. While mRNA modifications generally affect translation initiation, rRNA and tRNA modifications are important regulators of ribosomal elongation process. Amongst all ribonucleic acids, tRNAs are the most decorated by post-transcriptional modifications, ranging from simple methylation to complex hypermodified species (see Figure 25). On average, tRNAs contain 13 modifications per molecule (reviewed in Suzuki, 2021) Depending on their type and position, these chemical changes can affect tRNA structure, stability, localization, amino acid charging level, ribosome binding, as well as translational kinetics and fidelity.

When located in the anticodon loop or in its close vicinity, modifications of tRNAs affect base pairing and thereby influence mRNA decoding capacity. For instance, 2-thiolation of U_{34}, the wobble uridine present in the anticodon loop of multiple tRNAs, increases codon binding affinity and reduces tRNA rejection, accelerating translation process but also limiting the risk of mistranslation and misfolding (Ranjan & Rodnina, 2017). Various enzymes and protein complexes, some of which are conserved from yeast to mammals, are involved in tRNA modifications and thus contribute to the proteostasis network. The Elongator protein 3 (Elp3), a tRNA modifying enzyme that importantly contributes to proteome integrity and neurodegenerative disorders, is further developed in a following paragraph (cf. section 6).

6.1.2 Chaperones

Chaperones, such as heat shock proteins HSP70 and HSP90, are crucial to proteostasis by assisting the folding process of a polypeptide during its translation as well as ensuring misfolded proteins to refold in order to reverse aggregation (Hartl et al., 2011). They act through binding to the unfolded or misfolded non-native protein, however they are never part of its final structure (Cortez & Sim, 2014; Perlmutter, 2002). Interestingly, it could be shown that chaperones, especially ATP-dependent chaperones, decrease in level with age and in neurodegenerative disorders such as AD, PD and HD patients and thus likely contribute to the progression of neurodegeneration (Brehme et al., 2014).

Small molecules acting as chaperones have been developed for clinical use. Pharmacological chaperones are used to treat diseases that are caused by mutant proteins that are intrinsically active but unstable and, therefore, cleared out from the cell. Through specific binding to their targets, these drugs stabilize the mutant protein and limit their degradation, restoring functional protein level (Liguori et al., 2020). Chemical chaperones are small molecules that need to be present in high concentration to be effective as they act non-specifically to prevent protein interaction (Cortez & Sim, 2014). Sodium phenylbutyrate, also known as 4-PBA, is a hydrophobic chemical chaperone that delayed functional decline of patients affected by Amyotrophic Lateral Sclerosis (ALS) (Paganoni et al., 2020). It has two major mechanisms of action: first, it acts as a HDAC inhibitor and promotes the transcription of several genes including the ones encoding heat shock proteins (Iannitti & Palmieri, 2011; Kaur et al., 2018). Second, it inhibits the aggregation of aberrant proteins by binding to exposed hydrophobic residues and promotes their transport from the ER via COPII vesicles leading to an amelioration of ER stress (Kubota et al., 2006) (Figure 28).

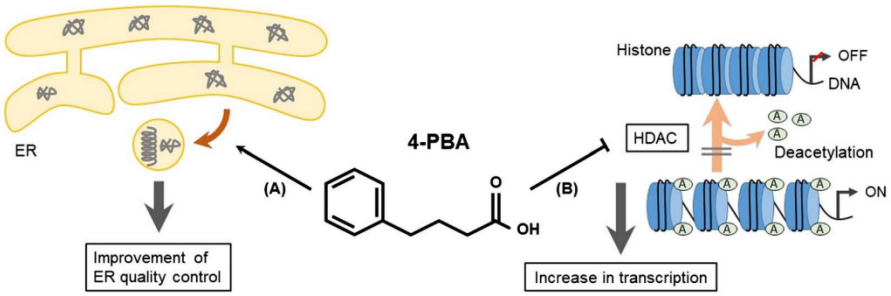

Figure 28. The mechanism of action of 4-PBA. 4-PBA has two major mechanisms of action, which is 1) binding to exposed hydrophobic residues, thus preventing protein aggregation, and promoting the transport from the endoplasmic reticulum away to ameliorate ER quality control. 2) it inhibits the histone-deacetylase and so favorizes the transcription of ER stress-related genes, such as chaperones. *From Sugiyama and Nishitoh, 2024.*

6.1.3 Protein degradation systems

Another essential process to sustain protein homeostasis is the degradation of misfolded proteins and whole protein aggregates. Removal of those toxic molecules may be achieved by two major mechanisms, the Ubiquitin-Proteasome system (UPS) and the Autophagy system, respectively. Single proteins that are degraded by the Ubiquitin-Proteasome system first require to be unfolded whereas the autophagy-lysosome pathway degrades whole protein aggregates, each time supported by the help of chaperones. Those systems cooperate to regulate and control the accumulation of misfolded or aberrant proteins.

Aggresomes, which are structures thought to play a cytoprotective function, are formed when the UPS system is overwhelmed. The polyubiquitinated misfolded and aggregated proteins that fail to be degraded are transported retrogradely along microtubules to the centrosome, where they gather to form the perinuclear Aggresome. This allows the sequestration of toxic aggregates into a subcellular compartment s, as Aggresomes are ensheathed by intermediate filaments. In non-neuronal cells these are vimentin filaments whereas in neuronal cells these are neurofilaments (Johnston et al., 1998; J. P. Taylor et al., 2003). The role of the intermediate filament capsules is not totally clear, but it is expected to promote the stability of the Aggresome or to prevent aberrant non-specific interactions with other proteins. In addition, the formation of Aggresomes generally facilitates the elimination of larger aggregates by the autophagy pathway, which in this context can be termed aggrephagy (reviewed in Chin et al., 2008).

6.1.4 Unfolded Protein Response

Cells are naturally equipped with protein quality control systems that detect misfolded or aggregated proteins and trigger adaptive cellular responses to alleviate proteotoxic stress. Surveillance

mechanisms have been described in the cytoplasmic and mitochondrial compartments, however the best described stress response pathway relates to the endoplasmic reticulum (ER), where proteins that are dedicated to be secreted or integrated into the plasma membrane are assembled. The Unfolded Protein Response (UPR) is activated in the presence of misfolded proteins in ER lumen. In general, the induction of UPR system in response to ER-stress leads to the upregulation of chaperones, increased efficiency of proteasomal and autophagic clearance and reduced global protein synthesis rate. If the capacity of the cell to cope with the stress becomes inefficient despite those adaptations, the outcome of the UPR system becomes cell death as apoptosis is specifically induced.

The UPR system is composed of three major branches: the ATF6, PERK and IRE1 branch, which may act in parallel. The first branch is dependent on the ATF6 factor, which is initially a transmembrane protein with a large ER-luminal domain acting in first line as a sensor of misfolded proteins. Upon binding with misfolded proteins in the ER, it is transported to the Golgi apparatus and its luminal and cytosolic domains are cleaved by two proteases, S1P and S2P. The cytosolic N-terminal domain is translocated to the nucleus and acts as a transcription factor to induce the expression of specific UPR target genes such as BiP (a HSP70 chaperone), PDI and GRP94 (HSP90 chaperone) to alleviate the ER stress. The second branch is reliant on PERK, a transmembrane kinase located at the level of the ER membrane. In case of ER stress, PERK is activated following dimerization and auto-phosphorylation and it phosphorylates the translation initiation factor eIF2a to inactivate it. This decreases global mRNA translation rates (which further reduces the global protein folding load) but in parallel leads to a preferential translation of the ATF4 transcription factor that is implicated in the upregulation of the pro-apoptotic factor CHOP and others. This indicates that the PERK pathway is implicated in regulating cell death when the system is overwhelmed and cannot cope with persistent ER stress. The last branch is regulated by IRE1, a transmembrane kinase that also exerts an endoribonuclease activity and thus presents mRNA splicing capacity. In the presence of unfolded proteins, IRE1 oligomerizes and is subjected to conformational changes that activate its RNase activity. Activated IRE1 induces the excision of an exon within the XBP1 mRNA, giving rise to the XBP1 transcription factor form that is responsible for the enhanced expression of chaperones, lipid biosynthesis enzymes and ERAD-associated proteins (Figure 29).

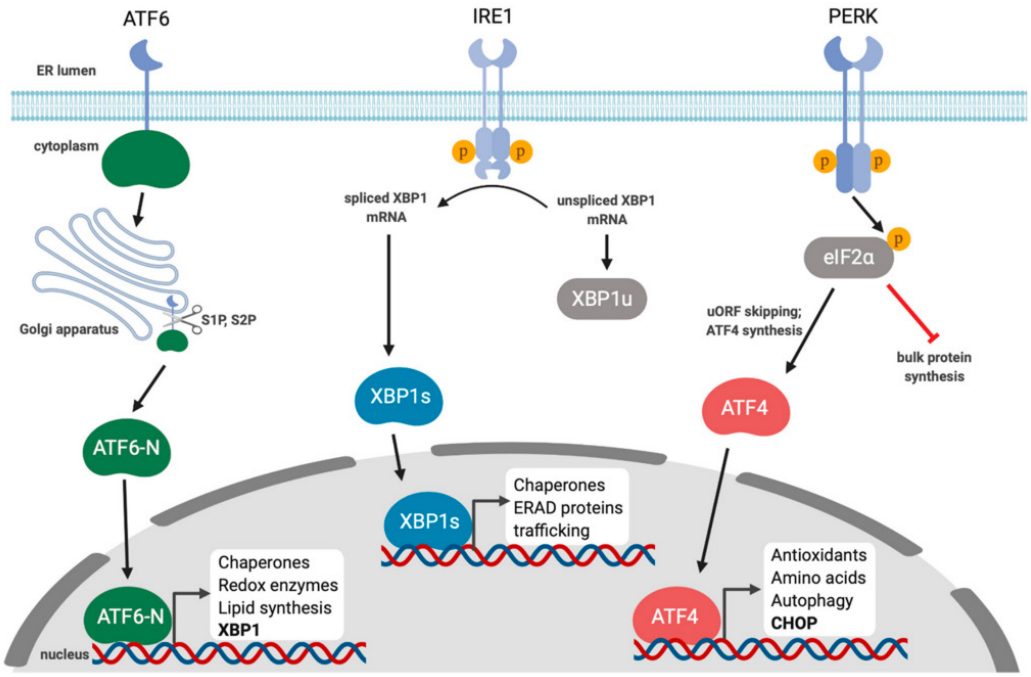

Figure 29. The Unfolded Protein Response. The UPR system is made of three arms: the ATF6 arm, the IRE1 arm and the PERK arm. The ATF6 branch is activated in case of the presence of misfolded proteins in the ER lumen and leads overall to the expression of genes coding for Chaperones, quality control proteins as well as redox pathway components. After the activation of the IRE1 pathway, XBP1spliced (XBPs) translocates to the nucleus and regulates the expression of genes coding for Chaperones and ERAD proteins. ATF4 translation, which is promoted in case of eIF2a phosphorylation, leads to the transactivation of genes implicated in amino acid biosynthesis, antioxidant response, autophagy and apoptosis (CHOP). *From Johnston and McCormick, 2020.*

6.2 Proteotoxicity and hearing loss

There are evidences that proteostasis disruption is related to hearing loss (HL), at least in the context of drug-induced and age-related hearing loss. Some papers show a link with noise-induced and hereditary hearing loss, however these conditions are less well studied.

6.2.1 Drug-induced HL

ER stress was shown to be induced upon treatment with the anticancer drug Cisplatin, which is well known to display adverse effects on the hearing function of patients. Indeed, Li *et al.* showed that Cisplatin-induced HC death correlates with an upregulation of UPR target genes in cochlear explants. Treatment with Stress response inhibitor targeting the pro-apoptotic CHOP pathway was able to rescue hearing loss and reduce HC loss following Cisplatin treatment in vivo. This demonstrates that protein misfolding and aggregation might be one possible mechanism of Cisplatin ototoxicity and that UPR could be modulated to alleviate Cisplatin-induced hearing loss in cancer patients (J. Li et al., 2024). Besides, aminoglycosides, belonging to a class of antibiotics that exert ribotoxic functions on a

broad range of bacteria, could also induce hearing loss by impairing cellular proteostasis in treated patients. In a mouse model of aminoglycoside-induced cochlear damage, haploinsufficient XBP1 mice showed an increased susceptibility towards high frequency hearing loss, neuronal loss and synaptic loss due to a compromised UPR activity. This correlated with an increased positive staining for the pro-apoptotic factor CHOP within the spiral ganglion suggesting the accumulation of misfolded proteins in SGNs and ER stress-induced neuronal apoptosis. Moreover, treatment with a chemical chaperone was able to reduce the aminoglycoside-induced hearing loss in $XBP1^{+/-}$ mice further emphasizing the link between aminoglycoside-induced hearing loss and proteostasis disruption (Oishi et al., 2015). In addition, Kanamycin-induced deafness in mice could be associated with an ER-stress induced upregulation of CHOP and Casp12 resulting in apoptotic neuronal cell death (Tu et al., 2019). Lastly, perilymphatic perfusions of the ER stress inducer Tunicamycin induces progressive hearing loss together with degeneration of OHCs and SGN nerve endings in rats. Moreover, ER stress associated genes (e.g. Chop, ATF4) were shown to be upregulated at the whole cochlear level (Fujinami et al., 2012).

6.2.2 Age-induced HL

Studies in mice gave hints that age-related hearing loss (ARHL) can be linked to proteostasis disruption: In a mouse model of ARHL, the pharmacological upregulation of Heat shock proteins could attenuate the auditory threshold shift (Mikuriya et al., 2008) and the age-related reduced UPR capacity leads to an activation of the pro-apoptotic branch (CHOP) due to ER-stress and thus results in apoptosis within cochlea of aged mice (Wang et al., 2015).

6.2.3 Noise-induced HL

Noise-induced hearing loss (NIHL) is one of the most common acquired forms of hearing loss and several different biological processes, such as oxidative stress and inflammation, are implicated in this pathology. Recent studies start to point out the contribution of ER stress and UPR to NIHL. For instance, acoustic trauma studies in guinea pigs have been shown to be associated with increased protein levels of BiP, Chop and Casp12 (Xue et al., 2016; Xue et al., 2009). The ER-resident chaperones Sig-1R have been shown to be upregulated by the ATF4 pathway with a protective function in ER stress (Mitsuda et al., 2011). Hence, treatments with agonist of Sig-1R alleviates threshold shifts and cell death in a mouse model of noise trauma (Yamashita et al., 2015). In addition, application of a stress response inhibitor prior to acoustic trauma was able to prevent synaptic loss as well as the reduction of the ABR peak I amplitude, in a sex-dependent manner, indicating that UPR contributes to the noise-induced synaptopathy (Rouse et al., 2020).

6.2.4 Hereditary HL

There are some genetic mutations associated with increased ER stress and hearing loss, the most common are Connexin-31 (Cx31), Usher (Cdh23) and Wolframin.

Connexin-31

Mutations in the gap junction protein Connexin 31 have been shown to be associated with hearing loss. In line with this, mutant Cx31-transfected HeLa cells show a reduced Cx31 trafficking, increase in BiP expression and increased association between BiP and Cx31, giving signs of ER stress (Xia et al., 2010).

Cdh23

Usher syndrome is the most frequent form of hereditary deafness. Until now, more than 10 genes have been discovered to be associated with Usher syndrome, one of them being Cdh23. In a mouse model of Cdh23 mutation-associated hearing loss, Cdh23 colocalized with BiP in OHCs away from its usual localization. Further, the PERK pathway of the UPR was activated. Interestingly, disruption of Chop gene expression protected against Cdh23-related hearing loss and OHC death, and treatment with an ER stress inhibitor was sufficient to alleviate the hearing loss progression and OHC death in mutant mice (Hu et al., 2016).

Wolframin

Wolframin is an ER-transmembrane protein and a negative regulator of the UPR (Fonseca et al., 2005). Mutations in the Wolframin gene are associated with the Wolfram syndrome (WS), a disease characterized by diabetes, blindness and deafness. Mutations generally cause loss-of-function of Wolframin, therefore leading to an increased ER stress and UPR activation in cultured cells or mouse models of WS (Bonnet Wersinger et al., 2014; Ishihara et al., 2004; Yamada et al., 2006). In the inner ear, it has been shown to be expressed in several cell types such as HCs, SGNs, SCs and fibrocytes (Bonnet Wersinger et al., 2014), however a direct link between WS-associated hearing loss and ER stress has not yet been studied.

6.2.5 Regulators of Proteostasis and HL

Many genes regulating the proteostasis network could thus represent deafness-modifying genes, meaning that, when mutated, they could potentiate or aggravate acquired hearing loss (drug-induced, noise-induced and age-related) and thus be considered as vulnerability genes affecting disease severity or onset. The gene encoding the mesencephalic astrocyte-derived neurotrophic factor (Manf)has been suggested to be such a deafness-modifying gene. MANF is an ER-resident protein and a promoter of ER homeostasis. MANF knock-out mice show increased expression of CHOP in OHCs leading to progressive OHC loss and increased hearing thresholds. Importantly, the results were strain-dependent such that mice strains presenting early-onset age-related hearing loss (C57BL/6 and CD-1) were predominantly affected (Herranen et al., 2020; Ikäheimo et al., 2021).

In the lab, we uncovered that disrupting proteostasis by knocking out the tRNA-modifying enzyme Elp3 was associated to profound deafness at hearing onset. Histological and biochemical analyses at various stages of development indicated that early proteotoxic stress could impact cochlear neuron survival as well as sensory cell differentiation and polarization processes. These findings point out the importance of proteostasis for the hearing sense and the dependency of cochlear tissue on efficient protein quality control systems to guarantee proper inner ear development and function.

7. Elongator complex – Elongator protein 3 (Elp3)

Elp3 is part of the Elongator complex, comprising six subunits (Elp1-6) (Otero et al., 1999) (Figure 30A). Elp3 is the **enzymatic subunit** housing a Lysine/histone acetyltransferase (KAT) domain and a radical S-adenosylmethionine (SAM) binding domain, but all of the 6 subunits are essential for the stability and functionality of the complex. It was initially reported to act as a transcription regulator through histone modification (Winkler et al., 2002; Wittschieben et al., 1999) and paternal genome demethylation (Okada et al., 2010). In parallel, it was shown to regulate neuronal migration in the developing cortex by acetylating microtubules (Creppe et al., 2009). During the last decade, accumulating evidence indicate that themain role of Elongator complex is to act as a tRNA-modifyer. It controls the addition of 5-methoxycarbonylmethyl and 5-carba-moylmethyl (mcm^5/ncm^5) modifications on the wobble Uridine 34 of 11 tRNA species (Figure 30B) (Huang et al., 2005; Johansson et al., 2008). This modification may be followed by the addition of a 2-thio group on three tRNAs (UUC, UUU and UUG anticodons with mcm5s2), allowing for increased flexibility towards non-standard *wobble* pairing. Thus, as a tRNA modifying enzyme, the major role of Elp3 relies in regulating translation speed and fidelity and the simultaneous protein folding (Grosjean et al., 2010; Johansson et al., 2008; Laguesse et al., 2015). Several studies have already shown that the loss of U34 modifications lead to a decrease in translation velocity and further to an impaired protein homeostasis in yeasts and nematodes (Nedialkova & Leidel, 2015) and mammals (Laguesse et al., 2015) due to the accumulation of misfolded proteins and protein aggregates. Today, the impact of Elp3 on codon-specific translation or global proteome health is thought to explain its multifaceted roles described previously. Indeed, many of the phenotypes initially reported upon Elp3 deficiency could be rescued by overexpressing specific tRNAs or could be recapitulated by disrupting proteostasis through chaperone depletion or protein degradation inhibitor treatments (Bauer & Hermand, 2012; Esberg et al., 2006; Freeman et al., 2019; Nedialkova & Leidel, 2015).

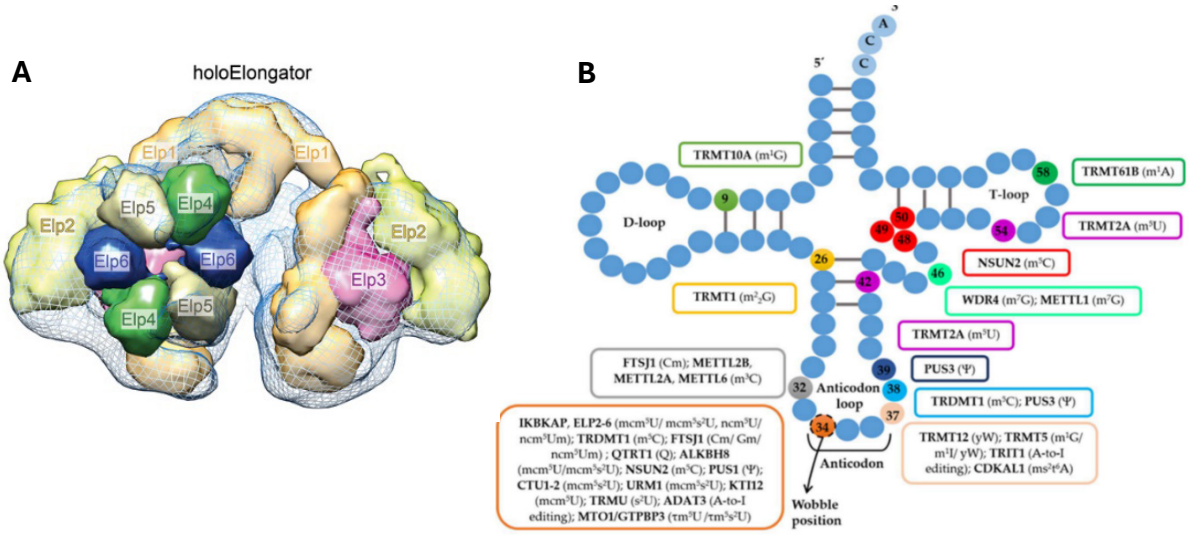

Figure 30. Structure of the Elongator complex and a tRNA with respective tRNA modifying enzymes. A) the Elongator complex is made of two copies of each of its 6 subunits which are all highly conserved among all eucaryotes. As well, it forms two subcomplexes, known as Elp123 and Elp456. Whereas Elp123 acts as a scaffold for the catalytic Elp3 subunit, Elp456 assembles asymmetrically to Elp123 and regulates tRNA binding (Dauden et al., 2017 + 2019). *From Dauden et al., 2017.* B) the structure of a tRNA with the positions colored that commonly undergo post-transcriptional modifications. The wobble Uridine at the position 34 (highlighted in orange) can be modified by a series of different tRNA-modifying enzymes, amongst them the Elongator complex (refers to IKBKAP(=Elp1),Elp2-6). The possible modifications induced by Elongator are: mcm^5, ncm^5, mcm^5s^2. *From Pereira et al., 2018.*

7.1 Implications of Elongator in pathologies

Impaired Elongator complex activity is associated with a defective protein homeostasis balance hence causing an accumulation of misfolded proteins and aggregates inducing neurodegenerative disorders.

Allele variants of Elongator subunits are commonly associated with neurological disorders including Familial Dysautonomia (Elp1), Cerebellar Ataxia (Elp6) and Intellectual Disability and Autism Spectrum Disorder (Elp2 + Elp4) that are characterized by neurodevelopmental defects and neurodegeneration.

In the case of Familial Dysautonomia, patients display a splice mutation in the Elp1 gene leading to a variable skipping of exon 2 and thus to tissue specific protein level reductions of ELP1 (Slaugenhaupt et al., 2001). The disease is characterized by peripheral neurodegeneration in the dorsal root ganglia (Pearson et al., 1978). Interestingly, in FD human olfactory ecto-mesenchymal stem cells an overactivity of the 26S proteasome could be observed suggesting a general problem of protein homeostasis (Hervé & Ibrahim, 2017).

Additionally, patients bearing biallelic variants in the Elp2 coding gene display Intellectual Disability as well as autistic features. In a mouse model carrying a patient-derived mutation of Elp2, the patient's clinical features including microcephaly could be recapitulated. This microcephaly is likely the

consequence of an impaired neuronal generation, myelinic loss and neuronal degeneration in the mutant mice. These phenotypes were shown to be associated with the loss of Elongator Complex ability to regulate tRNA modification and protein homeostasis (Kojic et al., 2021).

Mutations in the Elp4 gene alone have never been associated to a pathology, however Elp4/6 variants could be found in patients displaying developmental delays, epilepsy, intellectual disability and motor dysfunction. Patient-derived pathogenic variants of the Elp456 subcomplex *(Elp6L118W)* in mouse lines recapitulate the patients' phenotypes and lead to an impaired Elongator complex activity in regulating tRNA modifications. In parallel, the mutant mice presented a widespread degeneration of Purkinje Neurons in the cerebellum and an increased expression of ER-stress associated pro-apoptotic factors such as CHOP, suggesting a link between neurodegeneration and impaired proteostasis. This work provided evidence for an involvement of the Elp456 subcomplex in neurodevelopmental disorders (Gaik et al., 2022).

Mutations in the gene encoding Elp6 have been associated with Cerebellar Ataxia characterized by a substantial degeneration of the Purkinje neurons in the cerebellum. In a mouse model displaying a single missense point mutation in the Elp6 coding gene, called *wobbly* mouse, the Purkinje neurons undergo degeneration following the destabilization of the Elongator complex. These mutants display translational regulation defects, protein misfolding and the ultimate ER stress-mediated neuronal cell death (Kojic et al., 2018).

Lastly, variants of the Elp3 coding gene have been associated with an increased risk of developing Amyotrophic Lateral Sclerosis (ALS), which is characterized by the progressive degeneration of neurons in the motor cortex, as shown in a Human association study in 2009 (Simpson et al., 2009). Importantly, sporadic ALS patients show a decreased level of Elp3 mRNA expression in motor neurons that correlates with a reduced mcm^5s^2 modification of the U34. In vitro and in vivo studies showed that the reduction of Elp3 expression led to a reduction of the mcm^5s^2U modification and induced a general accumulation of protein aggregates. Further, it deteriorates the abundance of the insoluble form of the mutant human Superoxide Dismutase 1 protein (SOD1), but not of the wild-type human SOD1. Notably, the overexpression of the human Elp3 in vitro alleviates the amount of insoluble mutant SOD1, whereas the mcm^5s^2U modification was restored by 45.5% (Bento-Abreu et al., 2018). These studies could reinforce the importance of Elp3 in ALS as a disease-modifying factor by acting as a tRNA modifier and proteostasis regulator.

Very recently, a link between Alzheimer's disease (AD) and Elp3-related impaired proteostasis has been reported. More precisely, in Alzheimer patient's brain samples and mouse models of amyloid pathologies, reduced expression levels of Elp3 have been shown. As well, AD-mutant neuronal cells present reduced levels of Elp3 protein, tRNA hypomodifications and impaired protein homeostasis. The authors could show that it's the amyloid pathology that negatively regulates proteostasis by exposing WT cells to the secretome of mutant cells, which produced the same pattern of reduced Elp3 levels, tRNA hypomodifications and proteostasis impairments (Pereira et al., 2024).

7.2 Role of Elongator in brain development

Elp3 has been shown to be important during brain development at several levels. During cortical neurogenesis Elp3 controls the fate of cortical progenitors by ensuring proteostasis and negatively controlling the Unfolded Protein Response. During cortical neuron migration, Elp3 is likely to act through UPR-independent mechanisms by regulating cytoskeletal dynamics.

Laguesse and colleagues showed by using a conditional Elp3 Knock-Out in vivo model that UPR regulation contributes to normal cortical neurogenesis. More precisely, depleting Elp3 in cortical progenitors activates ER stress and UPR due to an impaired tRNA-U34 modification and a reduced translation velocity. The Apical Progenitors (APs), that in early cortical development generate neurons in a direct way through asymmetric division (direct neurogenesis), later generate neurons in an indirect way by giving first rise to Intermediate Progenitors (IPs) that themselves generate, in most cases, postmitotic neurons through symmetrical division. The activation of the UPR pathway in the early progenitors impairs the generation of Intermediate Progenitors and so impacts the indirect neurogenesis to favor the direct neuronal generation "pathway" leading to the formation of premature neurons accounting for a smaller cortex/microcephaly. The UPR activation seems to need a physiological (down-)regulation over time during corticogenesis to promote the indirect neurogenesis and so to allow the generation of neurons through IPs crucial for a normal cell fate acquisition and cortical development in the mammalian brain (Laguesse et al., 2015) (Figure 31).

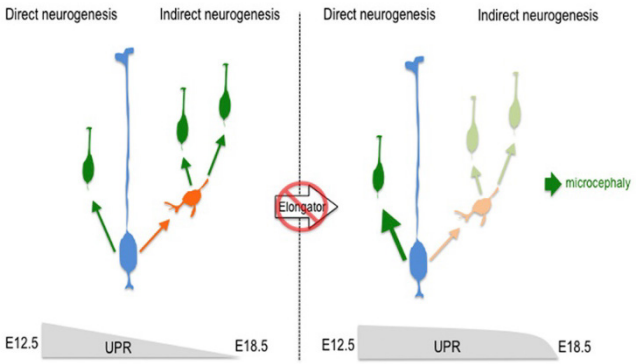

Figure 31. The role of Elp3 and UPR activity in cortical neurogenesis. During normal corticogenesis, UPR needs to be progressively downregulated to allow for an indirect neurogenesis, whereas the loss of Elp3 impacts UPR leading to a sustained activation favorizing the direct neurogenesis branch over the indirect and hence leading to a reduced overall formation of cortical neurons. *From Laguesse et al., 2015.*

Besides this, Tielens and colleagues proved that Elp3 is also implicated in the migration of cortical interneurons during mouse embryonic development. During this process, Elp3 regulates nucleokinesis and branching dynamics and plays a crucial role in regulating actomyosin forces. This happens mainly through the regulation of cofilin activity, one of the main enzymes responsible for actin-severing and thus controlling the balance of actin polymerization and severing (Tielens et al., 2016).

Further, a role of Elongator (and more specifically Elp1) in peripheral neurons has been shown in a mouse model for Familial dysautonomia. Conditional knockout of Elp1 led to a Casp3-mediated cell

death of sensory and sympathetic neurons and to impaired target tissue innervation, whereas the migration, differentiation and survival of their progenitors was not affected (George et al., 2013; Jackson et al., 2014).

7.3 Role of Elp3 in tumorigenesis

Several studies demonstrated that Elp3 promotes cancer growth, metastasis formation and resistance to targeted therapy by regulating U34-tRNA modification.

In the context of intestinal tumor, Elp3 has been reported to play a role in tumor initiation. It is dependent on Wnt signaling and itself promotes Sox9 translation which is needed to maintain a subpool of Dclk1+/Lgr5+ cancer stem cells in the intestinal epithelia. Hence, its depletion delays the tumor initiation together with a prolonged survival in a mouse model of intestinal tumor (Ladang et al., 2015).

In the PyMT breast cancer mouse model, Delaunay et al. demonstrated that Elp3 depletion significantly reduces breast cancer invasiveness and metastasis because of reduced levels of the oncoprotein DEK, which is enriched in codons requiring the mcm^5s^5 U34 tRNA modifications for decoding. Furthermore, reduced levels of DEK, an IRES trans-acting factor, lead to a decrease in the IRES-dependent translation of the proinvasive factor LEF1, hence interfering with cancer progression. This proves a functional link between tRNA modification and IRES-dependent translation of specific cancer-promoting proteins (Delaunay et al., 2016).

Human melanoma cells carrying the $BRAF^{V600E}$ mutation also require Elp3 for survival, as its depletion together with MAPK signaling inhibition is sufficient to induce melanoma cell death. Furthermore, U34-modifying enzymes like Elp3 contribute to the resistance of melanoma cells to anti-BRAF therapy by regulating the codon-specific translation of the HIF1a protein and thus promote glycolysis in those tumor cells (Rapino et al., 2018).

Those examples illustrate that, in the case of cancer, Elp3 plays a crucial role in influencing disease progression by regulating the translation of specific oncoproteins in a codon-dependent manner. Hence, targeting Elp3 to interfere with translational reprogramming is an attractive therapeutical approach to hinder invasion, metastasis formation, survival and targeted therapy resistance of different cancer types.

7.4 Role of Elp3 in the inner ear

Our laboratory highlighted the importance of Elp3 in the developing inner ear for neuronal survival and HC polarity. More precisely, depletion of Elp3 in the mouse inner ear resulted in the accumulation of misfolded proteins and protein aggregates in specific structures of the inner ear, such as the HCs and the SGNs, and resulted in deafness at hearing onset (Figure 32B).

The presence of aggregates at the apical surface of the HCs affected hair bundle polarity and ciliogenesis. Several polarity parameters such as the mean hair bundle angle, the bare zone surface, the medial zone surface and the kinocilium length at the surface of the inner and outer HCs were all significantly affected at Postnatal day 1. In parallel, the distribution of the intrinsic polarity proteins LGN, $G\alpha_{i3}$ and aPKC were no longer restricted to medio-lateral poles of HCs and covered larger areas at the apical surface of the epithelial sensory cells compared to WT mice. This phenotype can be attributed to the implication of Elp3 in regulating protein homeostasis as the treatment of whole mounted cochlear organs with the proteasome inhibitor MG-132 led to the same misdistribution of LGN and the presence of aggresomes at the apical surface of cochlear HCs. Importantly, LGN misdistribution can be rescued by treatment with the chemical chaperone 4-PBA, in both MG-132 treated cochlear organs and in Elp3cKO mice in vivo. Furthermore, the microtubular trafficking velocity is significantly affected at the HC apical surface of Elp3cKO mice and can be rescued by the treatment with 4-PBA. In the same manner, treatment of WT cochlear organs with MG-132 reduced the mean velocity which could be restored by 4-PBA as well. These results indicate that the presence of aggresome-like structures at the apical surface of HCs induced by the loss of Elp3 is responsible for the impaired microtubular trafficking speed resulting in a misdistribution of intrinsic polarity proteins and the malformation of the kinocilium leading to significant polarity defects (Freeman et al., 2019) (Figure 32A). In parallel, the presence of aggresomes in SGNs, close to their nucleus, resulted in an early apoptosis peaking between E13.5 and E14.5 and leading to a loss of 60% of SGNs up to E17.5. Of note, there is no further SGN loss in Elp3cKO animals from E17.5 onwards (Figure 32C+D). This loss of neurons could be related to an activation of the pro-apoptotic arm of UPR as Chop and Chac1 mRNA, two UPR pro-apoptotic factors, were significantly upregulated in E14 cochlear organs (Freeman et al., 2019). However, 4-PBA administration everyday starting from E9.5 was not sufficient to alleviate the load of misfolded proteins in the developing neurons and failed to rescue SGN survival at early embryonic stages.

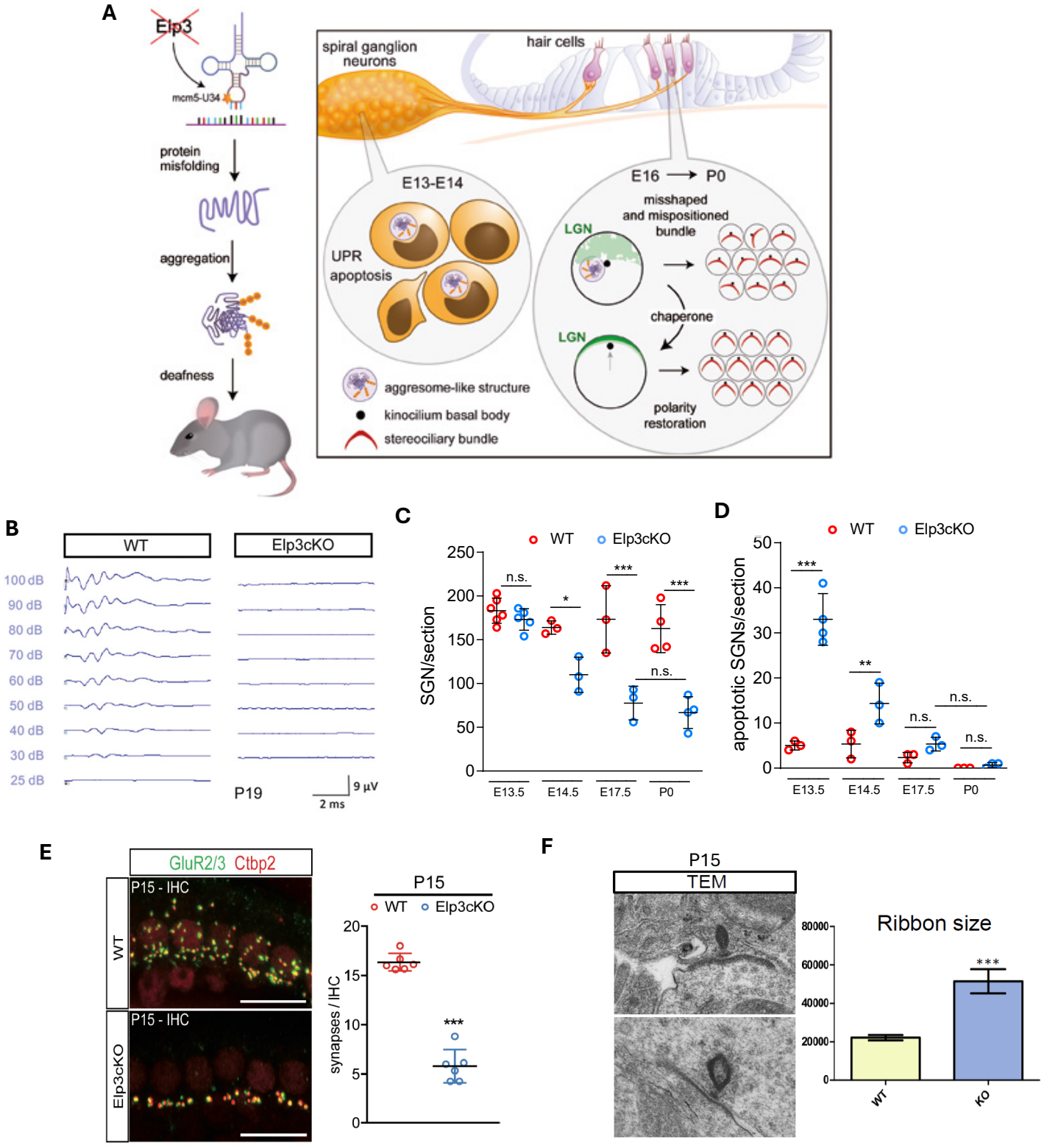

Figure 32 The role of Elp3 in HC polarity development and neuronal survival. A) Graphical abstract showing the phenotypical consequences of the depletion of Elp3 in the developing inner ear. At the level of the HCs, the presence of Aggresomes affected the correct ciliogenesis, HC polarity, the distribution of intrinsic polarity proteins (e.g. LGN) and the microtubular trafficking velocity. This phenotype could be rescued by the application of the chemical chaperone 4-PBA. At the level of the spiral ganglion neurons, the presence of Aggresome-like structures led to an ER stress-mediated apoptosis of SGNs at E14.5 and thus to a reduction of the SGN number by 60% at P0, likely causing the deafness phenotype of the mutant mice. B) Elp3cKO animals present profound deafness reflected by the absence of any auditory response up to 100 decibels. C+D) graph showing the number of SGNs and the number of apoptotic cells per section at different developmental timepoints. *For further details see Freeman et al., 2019.*

In line with those results, as the peripheral ending of bipolar auditory neurons make single synaptic contacts with their target cells, the drastic loss of SGNs before birth is accompanied with a 60% reduction in the number of ribbon synapses in neonatal Elp3-deficient IHCs. Intriguingly, the remaining presynaptic ribbons showed little size heterogeneity, and their mean size was increased compared to that of control littermates (unpublished data presented in Figure 32E+F). As larger ribbons are typical features of synapses established by SGN fibers belonging to the Ic subclass of SGNs, it is plausible that auditory neurons surviving to proteotoxic stress in Elp3-depleted cochlea predominantly belong to the high threshold/Low SR subtype. Although those Ic neurons are thought to be the most vulnerable SGN subtype towards noise-induced damage or aging, our results rather suggest that, during development, they could be particularly resistant to misfolded protein accumulation. Alternatively, these observations could indicate that neuronal differentiation programs are altered upon translational defects and/or Aggresome formation, causing a loss of neuronal diversity at mature stages.

Aim of the Study

A previous study conducted in our laboratory demonstrated that knocking out otic Elp3 gene, encoding a tRNA modifying enzyme that is essential to guarantee protein translation dynamics and fidelity, resulted in profound deafness at hearing onset due to cochlea development defects. Histological and biochemical analyses of Elp3-deficient inner ears revealed proteostasis disruption in the auditory cells during development, especially in the peripheral neurons present in the spiral ganglion and in the sensory HCs. In the absence of Elongator complex activity, differentiating HCs survive to misfolded protein accumulation but they display microtubular transport and polarity defects. In contrast, 60% of the Elp3-depleted SGNs undergo UPR-mediated apoptosis between E14.5 and E17.5. At birth, the remaining neuron fibers all faced large ribbons, which is a feature of the Ic subtype of SGNs. We thus wondered whether proteotoxic stress could be particularly deleterious to the developing Ia and Ib SGNs (subtype-specific apoptosis at the time of their emergence) or whether translational defects and misfolded/aggregated protein accumulation could skew otic neuron differentiation programs, causing neuronal diversity failure in the cochlea. In addition, we sought to decipher the mechanisms underlying cochlear innervation abnormalities by exploring cell intrinsic and target cell influences on selective survival or afferent identity acquisition of SGNs.

As the auditory neurons share common progenitors with the vestibular neurons, which are involved in conveying balance and spatial orientation information, we also assessed vestibular function and neuronal populations upon Elp3 invalidation. We first analyzed whether VGNs are subjected to aggresome formation and apoptosis during early embryonic stages and checked for neuronal identities and diversity in cristae and utricle at more mature stages.

Given the multitude of factors, genetic or environmental, that may compromise proteostasis during development, our findings could provide useful insights for congenital forms of hearing loss, which affect more than 1/1000 newborns.

It has been known for several decades that otic neurons present specific electrophysiological and morphological features that allow them to be divided into 3 subgroups. The emergence of transcriptomic studies finally enabled a division into three molecular clusters that largely matched the already defined morphological and physiological subgroups. These otic neurons have been shown to present a subtype-specific vulnerability, especially in case of aging and in response to noise-trauma. In our laboratory, we uncovered that disrupting proteostasis by knocking out Elp3 was associated with profound deafness due to cochlear developmental defects, with a crucial loss of spiral ganglion neurons and an increased Ribbon synapse size hinting for a subtype-specific vulnerability towards proteotoxic stress. In parallel, a prominent loss of vestibular neurons and Calyx-synapses has been observed, too, suggesting a similar subtype-specific loss in the vestibular counterpart.

In order to further unravel the role of proteostasis in neuronal diversification processes during inner ear development, we planned to use a mouse model in which Elp3 was invalidated in the whole inner ear including the Hair cells, supporting cells and spiral ganglion neurons. First, we aimed to determine the morphological and molecular features of the remaining neurons in our Knockout model to confirm our hypothesis of a subtype-specific loss. As well, we planned to use different invalidating procedures to determine the contribution of the neuronal and sensory compartment to the observed phenotype. Lastly, we tried to determine if the phenotype is related to the increased accumulation of misfolded proteins as a result of the Elp3 depletion, by performing rescue experiments using the chemical chaperone 4-PBA. Besides this, we also aimed to investigate the impact of Proteostasis on neuronal diversity in the vestibules, through morphological analysis of the synaptic innervation in the Cristae and Utricle.

Material and Methods

Mouse lines

The following mice were used: Foxg1$^{Cre/+}$ (Hebert *et al.*, 2000), Bhlhb5$^{Cre/+}$ Cdh23$^{G/G}$ (Ross *et al.*, 2010), Sox2Cre$^{ERT2/+}$ (Arnold *et al.*, 2011), Ngn1Cre$^{ERT2/+}$ (Koundakjian *et al.*, 2007), Elp3$^{Lox/Lox}$ (Laguesse *et al.*, 2015) and Rosa^{Tomato} mice. All mice are in a 129/SV genetic background.

The Elp3^{Lox} mice present an exon 2 flanked by two LoxP sites, which is deleted by the expression of the Cre Recombinase. The exon loss induces a frameshift that leads to Elp3 loss of function by generating a premature stop codon.

To deplete Elp3 in the whole inner ear tissue (Hair cells, supporting cells and spiral ganglion neurons), Foxg1$^{Cre/+}$;Elp3$^{Lox/+}$ males were crossed with Elp3$^{Lox/Lox}$ females to get Elp3cKO (Foxg1$^{Cre/+}$;Elp3$^{Lox/Lox}$). The phenotype of these animals was always compared to control littermates (Foxg1$^{+/+}$;Elp3$^{Lox/Lox}$ or Foxg1$^{+/+}$;Elp3$^{Lox/+}$).

To deplete Elp3 only in the spiral ganglion neurons in a time dependent manner, Ngn1$^{CreERT2/+}$;Elp3$^{Lox/Lox}$;Rosa^{Tomato} males were plugged with Elp3$^{Lox/Lox}$ females to get Elp3cKO (Ngn1$^{CreERT2/+}$;Elp3^{Lox}/Lox;Rosa^{Tomato}) and Tamoxifen was administered to activate the Cre^{ERT2} recombinase. Bhlhb5$^{Cre/+}$;Elp3$^{Lox/+}$ mice were used to avoid the usage of Tamoxifen and its toxic side effect.

To deplete Elp3 only in the otic sensory epithelium in a time dependent manner, Sox2$^{CreERT2/+}$;Elp3$^{Lox/Lox}$;Rosa^{Tomato} males were plugged with Elp3$^{Lox/Lox}$ females to get Elp3cKO (Sox2$^{CreERT2/+}$;Elp3$^{Lox/Lox}$;RosaTomato).

Rosa^{Tomato} was used as a reporter gene to follow the recombination efficiency of the inducible Cre Recombinase.

Genotyping

Genotyping was performed on a piece of tail. First, the piece of tissue was digested using 0.1 mg/mL Proteinase K (Promega, V3021) diluted in a TENS solution (100 mM Tris-HCl pH 8.2, 5 mM EDTA, 200 mM NaCl, 0.2% SDS) for 3h at 55°C, then DNA was precipitated using Isopropanol 100% followed by a centrifugation step of 15000 rpm for 10 min at 4°C. After removal of the supernatant, Ethanol 70% was added to wash the pellet and centrifuged again at the same settings. Finally, after removing the supernatant, the DNA was dissolved in 300 µL H_2O milliQ and stored at 4°C.

Next, PCR was performed using specific primers and programs, depending on the alleles to be detected. The PCR reactions were conducted on 1 µl of DNA in a final volume of 25 µl in a solution containing 0.2 µM of each primer, Green GoTaq Reaction Buffer 1x (Promega, M791) and 0.625 units of GoTaq polymerase (Promega, M784). To detect the PCR products, gel electrophoresis has been performed on a 1.5% agarose gel, containing MidoriGreen dye, for 20 min at 135 volts.

	Primers (5' -> 3')	Program	Product length
Elp3Lox	F: CGTGTTTGCTGCCATCACC R: GCACGATTGCCACATCATCC R : ATTCCTGCCCTGACTTCCCT	3 min at 94°C 20 sec at 94°C 20 sec at 56°C (35X) 30 sec at 72°C 5 min at 72°C	WT band: 172 bp Lox band: 459 bp recombined band: 320 bp
Foxg1Cre	F: GCCGCCCCCCGACGCCTGGGTGAT R1: TGGTGGTGGTGATGATGATGGTGATGCTGG R2: ATAATCGCAACATCTTCAGGTTCTGCGGG	3 min at 94°C 20 sec at 94°C 20 sec at 65°C (35X) 30 sec at 72°C 5 min at 72°C	WT band: 186 bp Cre band: 220 bp
Bhlhb5Cre	F: CCTGACTCTCCAGCCCAGGTG R1: ATCAGCGGGCTCGAAACAGC R2: GGCAACACCATTTTTTCTGACC	3 min at 94°C 20 sec at 94°C 30 sec at 58°C (35X) 50 sec at 72°C 3 min at 72°C	WT band: 241 bp Cre band: 780 bp
Ngn1Cre^{ERT2}	F: AGCCCATTCACTCCCTGAG R: ATCAACGTTTTCTTTTCGGA	3 min at 94°C 20 sec at 94°C 20 sec at 55°C (35X) 40 sec at 72°C 3 min at 72°C	Cre band: 527 bp
Rosa Tomato	F1: CTGTTCCTGTACGGCATGG F2: AAGGGAGCTGCAGTGGAGTA R1: GGCATTAAAGCAGCGTATCC R2: CCGAAAATCTGTGGGAAGTC	3 min at 94°C 20 sec at 94°C 20 sec at 58°C (35X) 30 sec at 72°C 3 min at 72°C	WT band: 297 bp Tomato band: 169 bp

Table 1: Primers and PCR programs used for different genes of interest.

RNAscope

For mRNA detection by RNAscope®, different Pretreatment protocols (Classical and Co-Detection) and different Detection Kits (V1 and V2, ACDBio #323100) have been applied depending on the developmental stage of the animals and the Antibody used in combination with the probes. The Table 2 summarizes the workflow for each stage studied as well as the specifications as soon as the protocol had to be adapted for particular reasons. Globally, the RNAscope consists of 4 major steps: Sample preparation (1), Pretreatment (2), RNAscope workflow (3) and Immunostaining (4).

1) Sample preparation:

To prepare the sections, samples were collected, fixed using Paraformaldehyde (PFA) 4%, rinsed 3x with Phosphate Buffered Saline (PBS) 1X and placed in successive baths of sucrose 10%-20%-30% for cryoprotection. In case mouse inner ears were collected from postnatal day 7 onwards, there was an additional step of decalcification using Ethylenediaminetetraacetic Acid (EDTA) 4% at 4°C for 1-2 days. Lastly, tissue samples were embedded in NEG-50 and sliced into 14-16 µm sections that were collected on SuperFrost Plus slides (ThermoScientific, J1830AMNZ).

2) Pretreatment

The classical Pretreatment was used if the primary Antibody shows no interference with the protease treatment (meaning the whole Immunostaining can be performed in *sequential* manner after the RNAscope workflow (3) (Figure 34A). The classical pretreatment consists in first baking the slides 30 min at 60°C and then post-fixing in fresh PFA 4% for 15 min at 4°C. The slides were then immersed in successive baths of Ethanol 50-70-100-100% for 5 min each time. After airdrying for 5 min at Room Temperature (RT), slides were covered with Hydrogen Peroxide (#322335) for 10 min at RT (this step is skipped for Detection Kit v1) before being treated with the RNAscope 1X Target Retrieval solution (#322000) for 5 min at 95°C in a beaker on a hot plate. At last, the slides were rinsed with distilled water and Ethanol 100% for 3 min and air dried at RT until further use.

The Co-Detection Pretreatment was used if the Protease treatment destroys the epitope normally recognized by the primary Antibody. In this case, the Primary Antibody had to be applied prior to the RNAscope workflow (3), called *Integrated* Immunostaining (Figure 34B). The Co-Detection Pretreatment consists in the same protocol than described above with the exception that a specific Co-Detection Target Retrieval Solution was used (#323166). After this step, slides were first rinsed with distilled water and further with a PBS-T solution (PBS + Tween 0.1%) 2 times for 2 min. Then, the tissue sections were incubated with the primary Antibody diluted in the Co-Detection Antibody Diluent (#323160) overnight (ON) at 4°C. After two rinsing steps with PBS-T, the slides were post-fixed with PFA 4% for 30 min at RT and rinsed again before completing the RNAscope workflow.

3) RNAscope workflow

For the RNAscope workflow Version 1 (V1), the tissue sections were first treated with Protease III (#322337) for 30 minutes, then the probes were hybridized for 2h followed by a series of signal amplifications (Amp 1-FL, 2-FL, 3-FL, 4-FL, #320851). The washing steps were performed using the Wash Buffer Reagent 1X (#310091) and all steps were carried out at 40°C in the HybEZ™ II Oven (#240200).

For the RNAscope workflow Version 2 (V2): Prior to hybridization, tissue sections were treated with Protease III (#322337) or Protease Plus (#322331) (durations for each stage are specified in Table 2), then the probes were hybridized for 2h followed by a series of amplification steps (#323110). The signal

of each channel was then revealed using a combination of FL v2 HRPs (-C1, -C2 or -C3) and TSA Vivid™ dyes (Tocris Bioscience, TSA Vivid Fluorophore Kit, #7523, 7526, 7527). The washing steps were performed using the Wash Buffer Reagent 1X (#310091). All steps were carried out at 40°C in the HybEZ™ II Oven.

4) Immunostaining

In case of Sequential Immunostaining (Figure 34A), the RNAscope workflow (3) was extended with an immunostaining to label the SGNs. First, the tissue sections were blocked and permeabilized using PBS containing Triton X-100 0.3% (Sigma Aldrich, #9002-93-1) and Donkey Serum 5% (Southern Biotech, #0030-01), Then, the samples were incubated with the primary Antibody in the blocking solution overnight at 4°C. After 3 rinsing steps with PBS, the samples were incubated with the secondary Antibody coupled to a fluorochrome and DAPI (#320858) in the blocking solution for 1h at RT. Finally, slides were mounted using the ProLong™ Gold Antifade Reagent (Invitrogen, P36934) mounting medium.

In case of Integrated Immunostaining (Figure 34B), the primary Antibody had already been applied at this point, so the RNAscope workflow (3) was followed with the incubation of the secondary Antibody for 30 min at RT before mounting as described before.

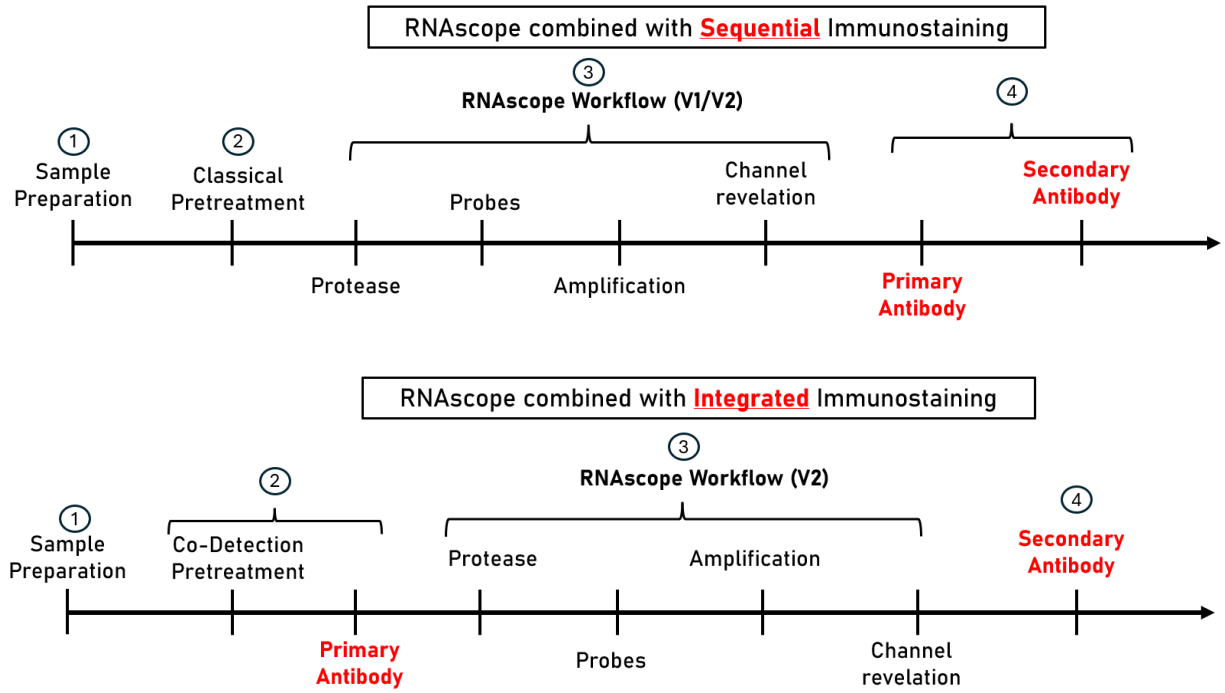

Figure 34. Workflow for Sequential and Integrated Immunostaining in combination with RNAscope. A) workflow for RNAscope combined with sequential Immunostaining. In this case, the Immunostaining is performed at the end of the RNAscope workflow. B) Workflow for RNAscope combined with an integrated Immunostaining.

	E14.5	E16.5	E18.5	P0	P0 (+4-PBA)	P15/22/35
1)Sample Preparation: Fixation time	ON at 4°C	8h at RT	ON at 4°C	ON at 4°C	ON at 4°C	ON at 4°C
2)Pre-treatment - Time in oven at 60°C	Classical ON	Classical ON	Classical ON	Classical 30 min	Co-Detection 30 min	Co-Detection ON
- Immunostaining -> Primary Antibody	Sequential X	Sequential X	Sequential X	Sequential X	Integrated Parv (1/300)	Integrated Parv (1/300)
3)RNAscope workflow	V2	V2	V2	V1	V2	V2
-Protease treatment	Plus, 15 min	III, 30 min	III, 30 min	III, 30 min	III, 10 min	III, 15 min
-Probes used	Lypd1 Tle4 Neurod1	Calb2 Lypd1	Calb2 Lypd1	Calb2 Lypd1	Calb2 Lypd1	Calb2 Lypd1 Grm8 Cacna1b
-Channel Revelation: Fluorophore dilution	1/1500-1/2000	1/2000	1/2000	/	1/2000	1/2000-5000
4)Immunostaining - Primary Antibody	Calb1 (1/500)	Calb1 (1/500)	Calb1 (1/500)	HuD (1/100)	X	X
- Secondary Antibody	Goat anti-Rb-594 (1/500)	Goat anti-Rb-594 (1/500)	Goat anti-Rb-555 (1/1000)	Donkey anti-Ms-488 (1/500)	Goat anti-Guinea Pig-488 (1/300)	Goat anti-Guinea Pig-488 (1/300)

Table 2: RNAscope protocol specifications for different stages.

Probe/Antibody	Name	Reference
Calb2-C3	Mus musculus Calbindin 2 (Calb2) mRNA	#313641
Lypd1-C1	Mus musculus Ly6/Plaur domain containing 1 (Lypd1) mRNA	#318361
Tle4-C2	Mus musculus transducing-like enhancer of split 4 (Tle4) mRNA	#417301
Neurod1-C1	Mus musculus neurogenic differentiation 1 (Neurod1) mRNA	#416871
Grm8	Mus musculus glutamate receptor, metabotropic 8 (Grm8) mRNA	#521491
Cacna1b	Mus musculus calcium channel, voltage-dependent, N type, alpha 1B subunit (Cacna1b) mRNA	#468811
Calb1	Rabbit anti-Calb1, Swant	CB38a
HuD	Mouse anti-HuD, Swant	sc-48421
Parv	Guinea Pig anti-Parvalbumin, Synaptic Systems	#195004
GP-488	Goat anti-Guinea Pig-488, 1/300, Invitrogen	A11073
Rb-594	Goat anti-rabbit IgG 594, Invitrogen	A11012
Rb-555	Donkey anti-rabbit IgG 555, Invitrogen	A31572
Ms-488	Donkey anti-mouse IgG 488, Invitrogen	A21202

Table 3: Probes, primary and secondary Antibodies used during RNAscope.

RNAscope quantification

For RNAscope performed at P0 with the Detection Kit version 1, the images were analyzed as followed: In CellProfiler, a pipeline had been created using the *RunCellPose* module (a generalist algorithm; Stringer et al., 2021) to automatically segment the neuronal body of SGNs based on the HuD staining within each image. Then, RNAscope dots were detected using the *IdentifyPrimaryObjects* module and finally the *RelateObjects* module was used to create a table comprising the number of dots in each channel per single neuron.

Further, a customized script was used to determine the proportion of single and double positive SGNs per image. More precisely, the threshold for a cell to be considered positive for a marker was set at 10% of the maximal dot count (determined for each litter separately) so that the same threshold is applied for WTs and KOs coming from the same litter. In addition, images from basal, middle and apical turn have been treated separately.

For RNAscope performed with the Multiplex Detection kit version 2, we had to perform a subjective quantification instead of the automatic one described above. More precisely, neuronal cells were detected based on Parvalbumin staining. Then, the threshold for the Calb2 marker has been set to 10 dots/cell for all images due to its high expression whereas the threshold for Lypd1 has been set to 3 dots/cell. Again, the proportion of double positive, double negative and single positive neurons has been calculated for all the markers used per image and per cochlear turn.

BaseScope®

Samples were collected, fixed overnight at 4°C using PFA 4%, rinsed 3 times with PBS 1X before being decalcified with EDTA 4% for 3-5 days at 4°C. Finally, inner ears were put in sucrose 30% for 1 day before being embedded in NEG-50 and further cut into 14 µm sections and placed on SuperFrost Plus slides.

Then, the slides were prepared according to the Co-Detection Pretreatment protocol in combination with a Parvalbumin (Guinea Pig, 1/300, Synaptic Systems, #195004) and RFP (Rabbit, 1/300, Rockland Immunochemicals, #600-401-379) Immunostaining. In particular, the slides were baked ON at 60°C in the oven to allow for better attachment of the tissue sections on the slides and to avoid detachment during pretreatment steps. Then, the slides are treated with Protease III during 15 min at 40°C before incubation with a probe targeting the exon 2 of the Elp3 gene (#1300821), which is deleted in Elp3cKO mice. For BaseScope validation, a positive (*Ppib*, #712351) and a negative control probe (*DapB*, #701021) was used. After 8 steps of signal amplification (Detection Kit, #323910), the BaseScope signal is finally revealed using a Fast RED solution (#322918-9) before being incubated with the secondary antibody (Goat anti-GuineaPig-647, 1/300, Invitrogen, #A11073) for 30 min at RT. The slides are finally mounted using Prolong Gold Antifade mounting medium as described before.

Ribbon Synapse Position Analysis

For synapse staining, inner ears were dissected and directly fixed for 1h with PFA 4% at RT. After decalcification with EDTA 4% for 1 day at 4°C, cochleae were dissected into three turns (base, mid, apex) and put on coverslips with Cell-Tak (Corning™, #10317081). Immunostaining was performed as followed: first, samples are blocked in a solution with PBS containing Triton X-100 0,5% and Goat Serum 10% for 1h at RT. Then, cochleae are incubated with the following primary antibodies in the blocking solution: Rabbit anti-Myo7A (1/500, Proteus, #25-6790) and Mouse anti-Ribeye (1/250, BD transduction, #612044) overnight at 4°C. For fluorescence labelling, Donkey anti-Rabbit-555 and Goat anti-Mouse-IgG1-647 secondary antibodies (all 1/1000, Invitrogen) diluted in PBST 0.3% with Goat Serum 1% were used. Images were taken either on an Olympus FV1000 confocal microscope or a Leica Stellaris 8 at 10X (for frequency mapping using the 'Measure Line' Tool/Plugin in imageJ; Mass Eye and Ear Institute, Boston) and 60X with 0.5 µm step size for analysis (similar frequency range were compared between WT and KO).

For Position analysis, images were analyzed using Imaris (Bitplane). More precisely, the 'Cell' Module was first used to segment the hair cells based on Myo7A staining, then to detect the Ribbon synapses based on Ribeye staining, and finally to attribute the synapses to each hair cell. Exclusion criteria for the hair cells are the following: 2 hair cells that are segmented as one, segmentations that go over the neighboring hair cell even partially, hair cells that are clipped along the border of the image, hair cells that have more than 20 or less than 3 synapses. Then, a XYZ reference frame is added individually to each hair cell that will further be analyzed. The reference frame is orientated such that the slicing plane Y goes from the back of the cuticular plate at the level of the kinocilium through the middle of the nucleus until the bottom of the hair cell which represents the center of the reference frame. The synapses that have a positive or negative Z value will therefore be considered "modiolar" or "pillar", respectively. The resulting data are subsequently computed using a customized script in R (version 4.2.2) to calculate the proportion of modiolar and pillar synapses per individual hair cell.

Hair bundle polarity measurements

Hair bundle angles were assessed based on the staining of Myo7A which labels the hair cell cytoplasm as well as the V-shaped stereociliary bundles. Images were taken at 60X with a 1.5 zoom at the basal region of the cochlea to generate maximal intensity projections. 10-15 Hair cells per row of each image, and one image per animal, was analyzed using the "Angle tool" in Fiji (version 1.53) to measure the deviation angle between the symmetry axis of the stereociliary bundle and the medio-lateral axis of the epithelium of each Hair bundle.

Cryosections

Fixed samples were immersed in sucrose 30% until they sink and localize at the bottom of the well. Then, the specimens were embedded in NEG-50 (Epredia™, 6502) using liquid nitrogen or carbo-ice before being stored at -80°C until sectioning on the Cryostat (Epredia™, CryoStar NX70) at 14-16 µm.

Immunostainings – Cochlea sections

WT and KO mice at 5 weeks of age were sacrificed to dissect inner ears in PBS. After poking a hole in the basal and apical turn, ears were fixed ON at 4°C using PFA 4%, decalcified with EDTA 4% for 4 days at RT, and cryoprotected for 1 day in sucrose 30%. Sections were prepared as described before. For Immunostainings, tissues were first blocked and permeabilized with a PBS solution containing Triton X-100 0.3% and Donkey Serum 10% (Jackson ImmunoResearch, #017-000-121) for 1h at RT. Then, sections were incubated with Primary Antibodies in the blocking solution over night at 4°C. The next day, after 3 washing steps with PBS 1X, fluorophore-coupled secondary antibodies (1/1000, Invitrogen) and DAPI (1/2500) were added in PBS containing Triton X-100 0.3% and Donkey Serum 1% during 1h at RT. Finally, slides were mounted with DAKO mounting medium (Agilent, S3023) and dried under a ventilator to be imaged the next day.

Antigen	Host	Brand, reference	Concentration used
Parvalbumin	Goat	Swant, PVG213	1/500
RFP	Rabbit	Rockland	1/500

Table 4: Antibodies used for Immunostainings on cryosections.

Immunostainings – Vestibule whole mounts

First, otic capsules were dissected from P15-22 mice, fixed for 1h at RT with PFA 4%, then the utricles and Cristae were removed and put in an Eppendorf to be further fixed for 30 min at RT. The Immunostaining was performed in the Eppendorfs. More precisely, permeabilization and blocking was performed using PBS containing Triton X-100 0.5% and Donkey Serum 10% for 2h at RT before incubation with the primary antibodies in the same permeabilization solution with Donkey Serum 5% ON at 4°C. After 3 rinsing steps with PBS for 5 min, secondary antibodies (1/1000, Invitrogen) were incubated with DAPI (1/2500) for 2h at RT. After 3 last rinsing steps, the cristae and utricular sensory epithelia were micro-dissected and put on coverslips coated with Cell-Tak (Corning™, #10317081) before being mounted on slides (Epredia, #AA00000112E01MNZ10).

Antigen	Host	Brand, reference	Concentration used
Neurofilament	Rat	Millipore, MAB5448	1/500
Oncomodulin	Rabbit	Swant, OMG4	1/250
Calb2 (Calretinin)	Goat	Swant, CG1	1/2500
Calb1 (Calbindin) D 28K	Rabbit	Swant, CB38a	1/500
TenascinC	Rabbit	Millipore, AB19013	1/500
Ribeye (Ctbp2)	Mouse	BD Transduction Laboratories, 612044	1/250
Myo7A	Rabbit	Proteus, 25-6790	1/500

Table 5: Antibodies used for Immunostainings on whole mounts.

Immunostainings – Vestibule sections

Time-mated pregnant females were sacrificed at embryonic day 13.5 (E13.5) or 14.5 (E14.5) to collect the embryos. Heads were fixed for 2h at RT before incubation in sucrose 30% for several hours at RT. Cryosections were prepared as described before.

For Immunolabeling, slides were first rinsed with PBS 3 times for 5 min. For Islet1 staining, an antigen demasking step was first performed. More precisely, DAKO antigen retrieval solution was prewarmed for 20 minutes at 95°C, then slides were placed on a hot plate and incubated with the retrieval solution for 10 min at 95°C, and finally re-rinsed 3 times with PBS 1X. Permeabilization and Blocking was performed for 1h at RT using PBS containing Triton X-100 0.3% and Donkey Serum 10%. The primary antibodies were incubated with the blocking solution overnight at 4°C. The next day, slides were rinsed 3 times with PBS for 5 min, incubated with the secondary antibodies (1/1000, Invitrogen) for 1h at RT in PBS Triton 0.3% and Donkey Serum 1%, before mounting on slides with DAPI, as described previously.

Antigen	Host	Brand, reference	Concentration used
Islet1	Rabbit	Genetex, GTX102807	1/500
cleaved Casp3	Rabbit	Promega, G7481	1/200
Tuj1	Mouse	Biolegend, 801202	1/500

Table 6: Antibodies used for Immunostainings on vestibule sections.

Proteostat staining

First, heads of E14.5 embryos were fixed for 3h at RT using Formaldehyde 4% and sections were prepared as described before.

For Proteostat® staining (Enzo, #ENZ-51023), sections were treated with a specific permeabilization solution (Assay Buffer 1X containing Triton X-100 0.5% and EDTA 3mM pH8) and Donkey Serum 5% for 30 min at 4°C. Then, slides were incubated with a primary antibody (Mouse anti-Tuj1, 1/500) diluted in the permeabilization solution and Donkey Serum 1% ON at 4°C. After 3 rinsing steps with PBS 1X, the Proteostat Detection Reagent combined with a Donkey anti-Mouse-647 (1/1000) secondary antibody and Hoechst had been put for 30 min at RT before mounting.

For Aggresome analysis, images comprising several plans of a vestibular ganglion were opened in ImageJ (Fiji). First, the channel for Proteostat staining was stacked using the *Sum Slices* function. Then, from this stack an Intensity threshold ("*Max Entropy*") was applied to create a binary image to count the Aggresomes within the vestibular ganglion based on Tuj1 staining. The number of Aggresomes was counted manually using the *Multi Point* tool.

4-PBA treatment

For rescue experiments, time-pregnant female mice were intraperitoneally injected daily, from E10.5 onwards, with the chemical chaperone 4-PBA (Sodium Phenylbutyrate, Sigma, #SML0309) dissolved in saline (NaCl 0.9%) at a concentration of 200mg/kg body weight. At P0, pups are first anesthetized in an ice water bath for 10-15 seconds before being injected intraperitoneally at the same dose, daily until P15. Control litters are injected with saline solution in the same way.

Tamoxifen treatment

Tamoxifen (Sigma, #T5648) was prepared according to the following protocol: 10 mg of Tamoxifen together with 5mg Progesterone (Sigma, P3972) are first dissolved in 100 µL ethanol 100% before adding Corn Oil to have a final volume of 1 mL. To ameliorate the dissolving, the solution is sonicated for 5 minutes. The Tamoxifen/Progesterone solution was injected in time-mated females at a dose of 1 mg per mouse of 20g body weight (100 µL) by intraperitoneal injection.

Vestibular behavioral analysis

To analyze the mice for vestibular behavioral defects, a set of different tests was applied. Briefly, the mice were placed in a 50*50cm cage and observed for 1 minute. For each test, the mice were ranked from 0 to 4 with 0 reflecting the absence of any abnormal behavior and 4 reflecting the most pronounced observed abnormal behavior. Circling was defined as movement of the mouse around its own axis. Retropulsion reflects backwards movement of the mouse. Head bobbing consisted of back-and-forth movement of the head in a repetitive way. The tail hanging test consists of hanging the mouse by its tail in the air. In the absence of any vestibular defect, the mouse tries to land on the closest object, however in case of vestibular defects it will try to grab its own tail by bending.

Auditory Brainstem recordings

For auditory brainstem recordings, mice were first anesthetized with an intraperitoneal injection of a mix of Ketamine 50mg/Kg and xylazine 10mg/Kg. Then, the mice are put on a heating pad to keep their body temperature at 37°C and Fucithalmic (CNK: 0674242) is applied on the eyes to keep them humid. During analysis, the mouse is placed in a soundproof chamber so that there is 10 cm between the mouse ear and the sound speaker and 30 cm from the opposite wall. Three Electrodes are placed on the head of the mouse: one at the level of the tragus (active), one between the right and left ear (reference) and one at the back of the external ear (ground). Click and frequency measurements are carried out with an MF1 Multifield magnetic speaker (TDT) and recordings are performed for 10 milliseconds.

Click sounds represent a mix of broad range sound frequencies, starting from 0 dB and going to 95 dB in 5 dB increments, with a stimulus duration of 0.1 milliseconds. Each measurement point is averaged 512 times for each sound intensity. The signal processing is performed by the BioSigRZ software.

Pure tone ABR represents stimulus delivered at 5 different frequencies (4-8-16-24-32 kHz) each time from 0 to 95 dB with 5 dB increments. The sound stimulus was sent for a duration of 2.5 milliseconds. Each measurement point was averaged 768 times, for each frequency and intensity level. Signals were processed by the BioSigRZ software.

For ABR analysis, the sound threshold was defined as the lowest intensity level at which peak I was clearly visible. The amplitude was defined as the difference between the top and the bottom point of each peak analyzed (I-V). The latency was defined as the time until the appearance of the top point of each peak analyzed (I-V). The final analysis was performed using a customized script in R by exporting CSV files from the BioSigRZ software.

Statistical Analysis

Statistical tests have been performed in GraphPad Prism™ software. Before applying a test, data have first been tested for normality. Then, parametric or non-parametric tests have been applied depending on the result. Details about the number of samples and the test applied are found in each figure legend. Significance is represented as followed:

*: p-value <0.05; **: p-value < 0.01; ***: p-value < 0.001; ****: p-value < 0.0001

Results

PART I – COCHLEA

1. Description of the remaining SGNs in Foxg1Cre Elp3cKO Model

1.1 Topological characteristics

As previously mentioned in the Introduction, our lab has already studied the role of Elp3 during inner ear development with the help of a mouse model in which Elp3 is depleted from E8.5 onwards by using a Cre Recombinase under the control of a *Foxg1* promoter. Foxg1 is expressed in the otic placode that gives rise to the otic vesicle und thus permits genetic recombination in most of the inner ear tissue, including the hair cells, supporting cells and spiral ganglion neurons. The recombination of exon 2 of the *Elp3* gene was confirmed by performing *in situ* hybridizations on tissue sections and the loss of Elp3, at the protein level, was confirmed by Western Blot on whole inner ear tissue samples (Freeman et al., 2019). In those $Foxg1^{Cre}Elp3^{Lox/Lox}$ mice (referred to as Elp3cKO from herein), a polarity defect is observed in OHCs in parallel to a loss of SGNs starting at E14.5 resulting in a 60% reduction at P0. Accordingly, there was a 60% reduction of Ribbon synapse number evidenced at P15 by GluR2/3 and Ctbp2/Ribeye staining (pre- and postsynaptic components). Interestingly, we could observe that Elp3cKO mice present larger ribbon mean size compared to control mice at P15, which is characteristic for the Ic subtype of SGNs.

As those preliminary results provide hints that the auditory neurons surviving to Epl3 depletion could all belong to the Ic subgroup of SGNs, we wanted to confirm this by analyzing the topographical mapping of their synaptic contacts at the level of the IHC. As described previously, Ic subtypes are known to innervate the modiolar side whereas the Ia subtypes innervate the pillar side of the IHC. Therefore, Immunostaining for Myo7A and Ctbp2/Ribeye has been performed on whole mounted cochlear tissue at P15, to label the HCs and the presynaptic component, respectively (Figure 35A). 3D reconstruction analyses using Imaris (Bitplane) enabled us to segment the HCs and to determine the relative position (modiolar-pillar) of each single synapse on their corresponding HC by tracing a reference system that passes through the central part of the nucleus and that divides the IHC in modiolar and pillar sides.

On Elp3WT cochlea ($Foxg1^{Cre/+}Elp3^{L/+}$ or $Foxg1^{+/+}Elp3^{L/L}$), the proportion of modiolar-pillar synapses per IHC was 50-50%, comparable to what has been described in the literature. In contrast, in Elp3cKO mice ($Foxg1^{Cre/+}Elp3^{L/L}$), modiolar synapses made out 86.67% and pillar synapses only 13.17% (Figure 35B). This phenotype is even better illustrated in a dot plot showing the position of each single synapse along the modiolar-pillar axis of the IHC (Figure 35D).

Thus, considering the loss of 50% of total synapses (Figure 35C), we can hypothesize that the pillar synapses are specifically lost in Elp3cKO mice (Figure 35E). These results suggest that the remaining neurons belong to the Ic subgroup of SGNs, based on the location where they innervate the IHC.

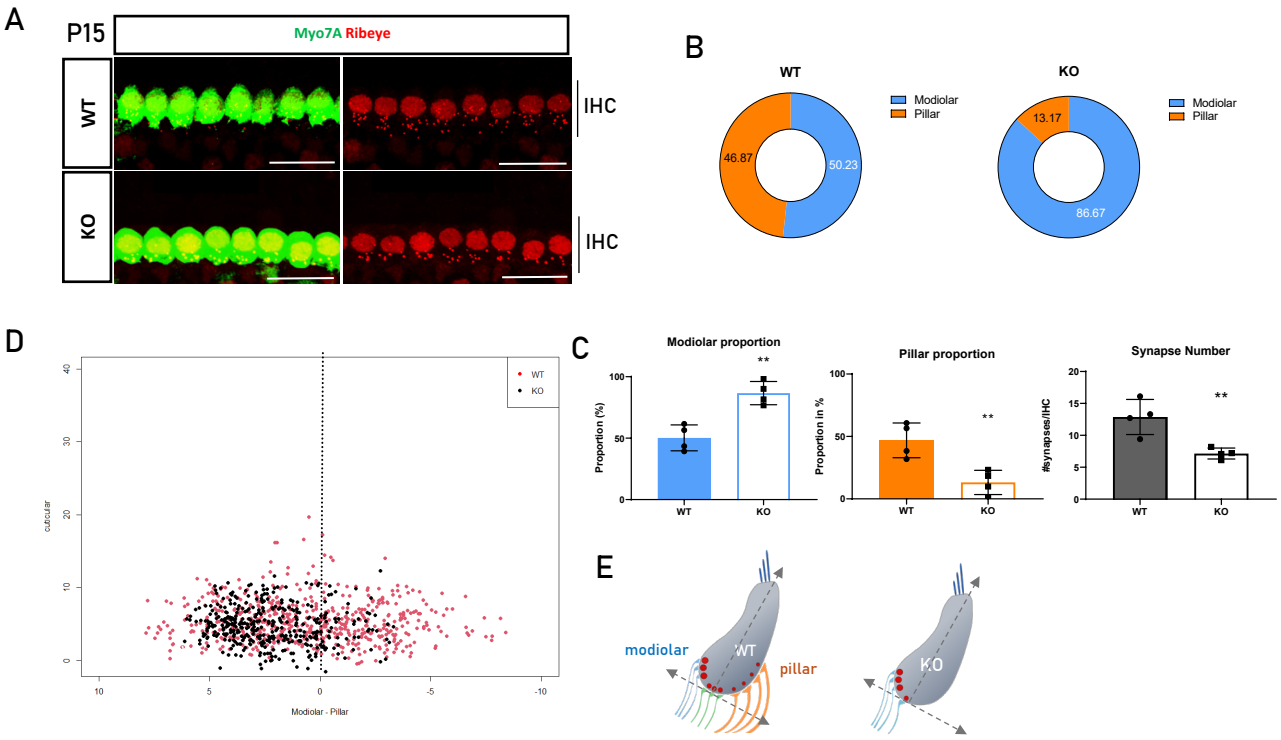

Figure 35. Synapse position analysis at P15. A) Immunostaining of WT and KO hair cells by Myo7A and of their presynaptic machineries by Ribeye. (Scale bar = 20 µm) B) 3D reconstruction analysis enabled calculation of Modiolar and Pillar proportions of synapses. Camembert graphs show a higher proportion of synapses located at the modiolar side of the *IHC*. C) Graph showing a significant increase in the modiolar proportion and a significant decrease in the pilar proportion at the same time than a significant reduction in synapse number. *(n=4 for WT and KO group; unpaired t-test; **p-value<0.01)* D) Scatterplot showing distribution of WT and KO synapses along the Modiolar-Pillar axis. E) Illustration of WT and KO Hair cell with remaining

1.2 Molecular characteristics

We wanted to confirm the identity of these surviving neurons at the molecular level by using the subtype specific markers Calb2 and Lypd1 that are well described markers of the Ia/Ib/Ic subtypes. According to the literature (Petitpré, 2018; Shrestha et al., 2018; S. Sun et al., 2018), Ia neurons express only Calb2, Ic neurons only Lypd1 and Ib neurons co-express Calb2 and Lypd1. Thus, we used a fluorescent *in situ* technique called RNAscope® that makes use of specific target probes to visualize the presence of mRNAs on any kind of tissue. Based on a signal amplification system, each mRNA molecule will be visualized as a single dot, but it has to be mentioned that highly expressed genes will show a cluster of signals requiring the usage of high-resolution confocal microscopes. RNAscope®

was carried out on WT and Elp3cKO inner ear sections at P15 and P0 in combination with Immunostainings for Parvalbumin or HuD to label the cytoplasm of all SGNs enabling the segmentation of single neurons.

At P15, on each WT section we could observe that the 3 types of SGNs are present at the apical, middle and basal turn of the cochlea. In addition, their relative proportions are comparable to those reported previously (Shrestha et al., 2018; S. Sun et al., 2018). However, Elp3cKO mice show a predominance of neurons expressing only Calb2 (putative Ia subtypes) in all of the three turns (Figure 36A). Quantifications by subjectively determining the subtype revealed a significant increase in the proportion of Calb2-only neurons and a significant decrease of the double-positive (Ib) and Lypd1-only cells (Ic) (Figure 36B). This was surprising as we expected a predominance of Ic-like (Lypd1-only cells) neurons based on the modiolar location and the larger volume of the remaining synapses.

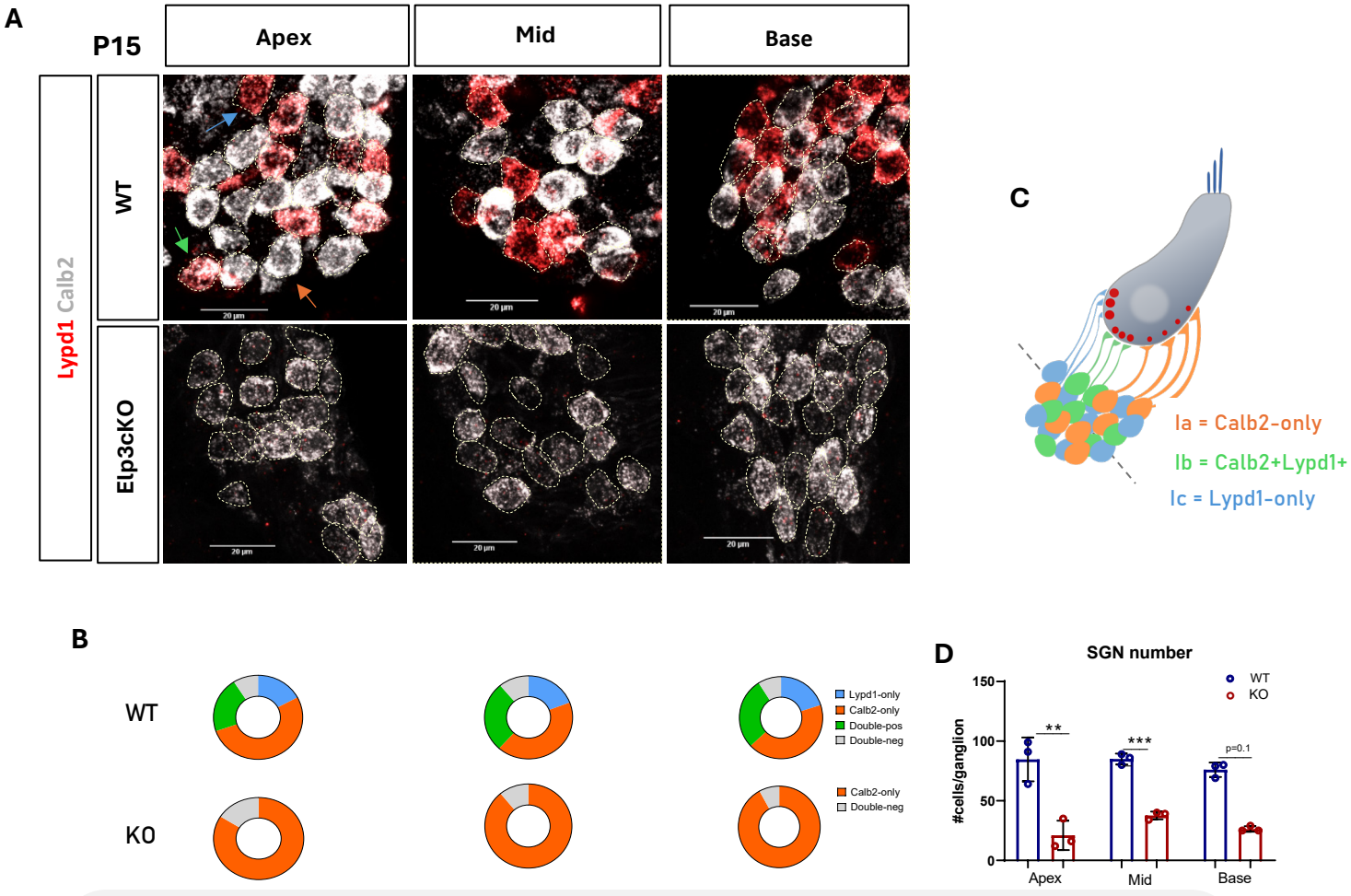

Figure 36. Postnatal SGN molecular pattern assessed by RNAscope. A) RNAscope was performed on inner ear tissue sections at P15 to determine the identity of the remaining neurons at the molecular level. Images are showing a representative region of the spiral ganglion. Probes against Calb2 (white) and Lypd1 (red) were used. B) At P15, the RNAscope expression pattern reveals the absence of Lypd1 expression in the KO SGNs in all three turns (Apex, Mid and Base). *(2-way ANOVA on dataset combined from P0, P7 and P15; n=5/4, 3/3, 3/3 for WT and KO, respectively)* C) Illustration of IHC innervated by the 3 subtypes (Ia=orange; Ib=green; Ic=blue) and the orientation of sectioning through the spiral ganglion for RNAscope analysis. D) Quantification of the number of SGNs per ganglion. *(n=3 for WT and KO; Unpaired t-test for Apex and Mid and Mann-Whitney test for Base; **p-value<0.01, ***p-value<0.001)*

As SGN identity should not be assumed based on a single marker, we used additional ones to validate our results. Here, we used Grm8, a metabotropic glutamate receptor expressed by the Ic subtype SGNs, and Cacna1b, a voltage gated calcium channel expressed by the Ia subtype. Thus, we performed RNAscope at P15 on cochlear sections together with an immunolabeling of Parvalbumin to segment individual SGNs.

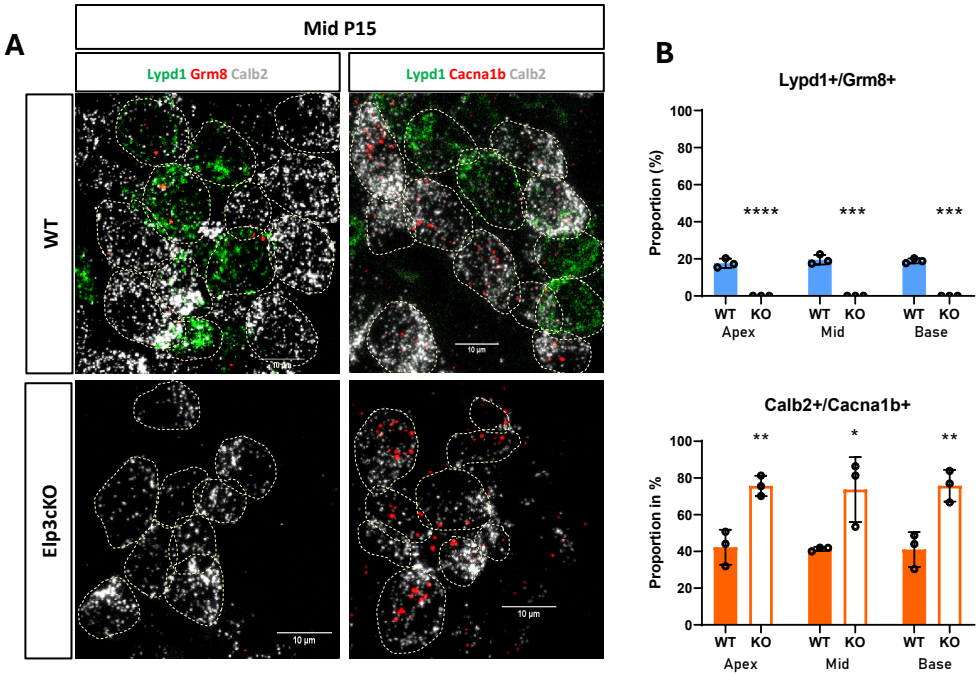

Figure 37. RNAscope using ion channel markers Grm8 and Cacna1b. Probes against Grm8 (Ic) and Cacna1b (Ia) together with the classical markers Calb2 and Lypd1 have been used to determine the proportion of the 3 subtypes. A) RNAscope experiments show an absence of Grm8-positive neurons and a predominance of Cacna1b-positive neurons. Silhouettes of individual neurons are traced based on cytoplasmic Parvalbumin staining. B) The proportion of Lypd1+/Grm8+ and Calb2+/Cacna1b+ in WT and Elp3KO animals has been calculated: Subjective quantifications have been performed in apex, mid and base and confirm the results observed with the RNAscope in all of the three turns. *(WT/KO n=3/3; unpaired t-test; *p-value<0.5, **p-value<0.01, ***p-value<0.001, ****p-value<0.0001)*

In control animals, neurons that are Lypd1-only also express Grm8 (red dots) and neurons that are Calb2-only are also positive for Cacna1b (red dots), confirming the specificity of those 2 markers for the Ic and Ia subtypes, respectively (Figure 37A, upper panel).

In contrast, KO animals completely lack Grm8-expressing cells and show a high proportion of Cacna1b-positive cells, confirming our previous results of the absence of Ic-like neurons and a predominance of Ia-like neurons (Figure 37A, lower panel). Subjective quantifications of the proportion of Lypd1+/Grm8+ and Calb2+/Cacna1b+ cells indicate significant differences between WT and KO cochlea regarding SGN diversity (Figure 37B).

1.3 Elp3cKO SGN diversification and fate consolidation

Because distinct SGN subtypes emerge during embryonic development and further consolidate during postnatal weeks, we next sought to analyze whether an abnormal distribution of the different SGN populations could already be evidenced in Elp3cKO at earlier time points. At P0, RNAscope® assay on control mice revealed the classical pattern of SGN heterogeneity at the apical, middle and basal turn, with subtype proportions comparable to what has been described previously (Shrestha et al., 2018). In Elp3cKO mice, we first observed a reduced staining for both probes Calb2 and Lypd1, suggesting lower levels of these transcripts, whereas the expression levels of the positive controls were similar between control and KO mice (Figure 38D). Furthermore, at the basal and middle cochlear turns we observed mostly Calb2-only neurons, similarly to what was noted at P15 (Figure 38A). However, the apical turn displays a predominance of Lypd1-only SGNs (putative Ic), as no Calb2 staining was visible. This is opposite to what we observed 2 weeks later after postnatal maturation. Quantifications using *CellProfiler* and a generalist algorithm (CellPose) to automatically segment neurons confirmed this pattern and showed a significant decrease in the proportion of Calb2-only neurons at the apex, while they are predominant in the other cochlear turns (Figure 38B).

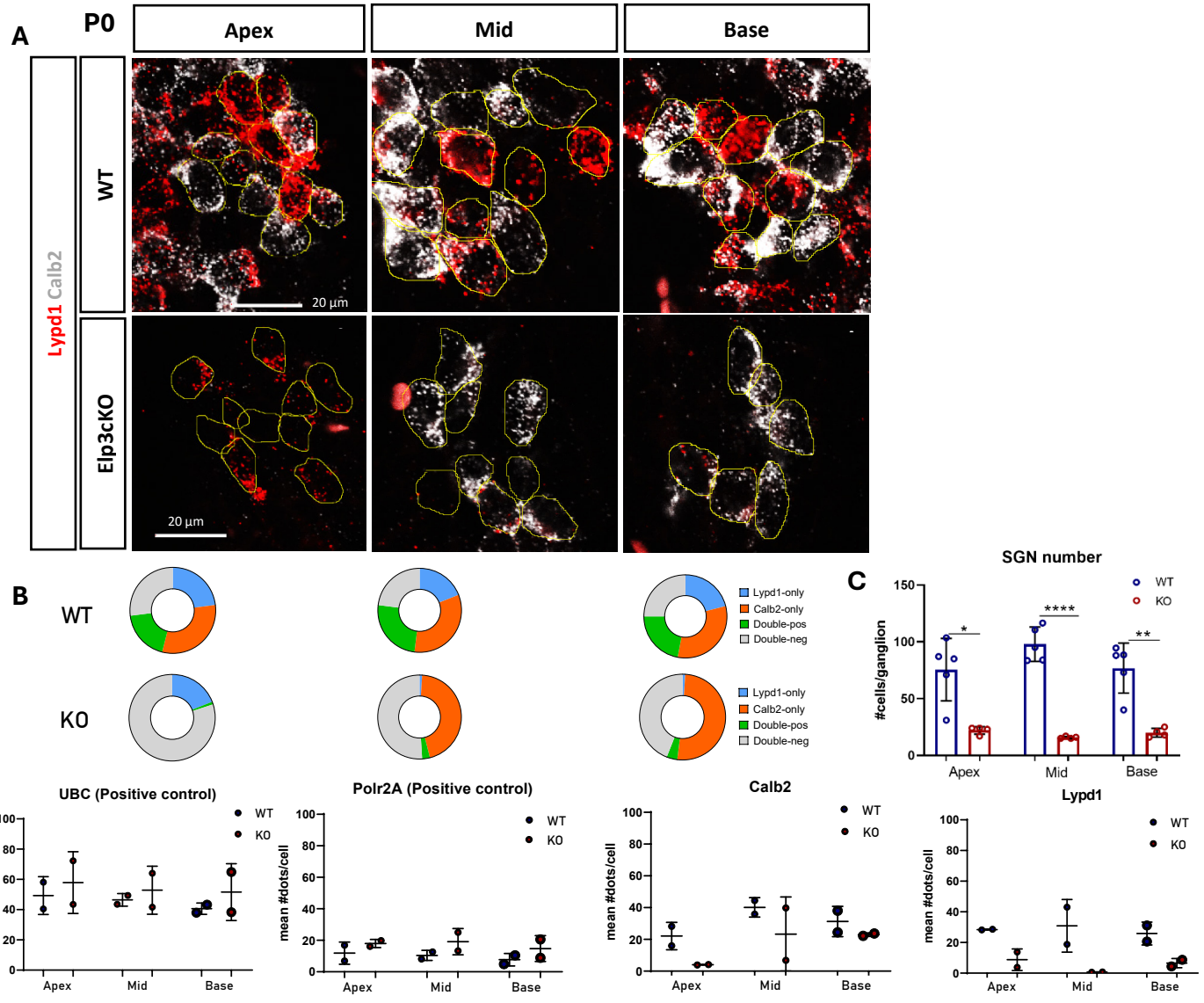

Figure 38 (previous page). Neonatal SGN molecular pattern assessed by RNAscope. A) RNAscope was performed on inner ear tissue sections at P0 to determine the identity of the remaining neurons at the molecular level. Images are showing a representative region of the spiral ganglion. Probes against Calb2 (white) and Lypd1 (red) were used. B) At P0, apical KO SGNs are predominantly Lypd1 positive whereas the basal and mid turn SGNs are predominantly Calb2 positive. *(n=5/4 for WT/KO condition, respectively; unpaired t-test).* C) Quantification of the number of SGNs per ganglion. *(n=5/4 for WT and KO; Unpaired t-test; *p-value<0.05, **p-value<0.01, ****p-value<0.0001).* D) mean number of dots per cell for positive control probes (UBC, high expression control gene; Polr2A, low expression control gene), Calb2 and Lypd1 in WT and Elp3cKOs. Data are from 4 animals (2 WTs, 2 KOs) from 2 different litters.

By performing RNAscope at E18.5 using the classical set of probes, Calb2 and Lypd1, we noticed that the absence of Calb2+ neurons in the apical part of the cochlea is also evidenced in WT spiral ganglion (Figure 39).

Indeed, the apex is populated by SGNs expressing exclusively Lypd1, whereas the Base and Mid turns in WTs already show the classical diversity pattern of neurons expressing Calb2 and/or Lypd1, similarly to P0 (Figure 39). We could thus hypothesize that this feature relates to the longitudinal gradient of differentiation/maturation from Base to Apex during normal SGN development. The emergence of distinct SGN clusters from Lypd1+ neurons in the apical region only occurs between E18.5 and P0 in normal conditions. Therefore, the persistence of apical Lypd1-only neurons in neonatal Elp3cKO (Figure 38) could reflect a delayed differentiation process upon proteotoxic stress conditions.

At E18.5, Elp3cKOs display similar patterns of SGN populations, when compared to controls (Figure 39A). Although the expression level of each marker is slightly reduced, likely reflecting a less healthier state due to the presence of misfolded proteins, Calb2 and/or Lypd1-expressing SGN populations are clearly present in the basal and middle turns. Hence, our results suggest that between E18.5 and P0, basal and mid turn Elp3cKO neurons switch towards Calb2-only neurons. The apical neurons remain Lypd1-only for a longer period but they also fail to consolidate into Ic neurons, as they switch towards a Calb2-only identity between P0 and P7 (data not shown). Alternatively to an identity switch, we could assume that Lypd1-expressing cells are lost by apoptosis between E18.5 and P0, however we showed previously that neuronal apoptosis peaks around E14.5 and progressively decreases up to E17.5, stage after which there is no further loss in the total SGN population (see Introduction Figure 27). The quantifications performed in the current study confirm the persistence of Elp3 cKO neurons at late embryonic stages. Indeed, the total number of SGNs doesn't change between E18.5 and P0 at any of the three turns (Figure 39B). Altogether our consistent findings indicating that SGN population remains stable from E18.5 onwards, combined with the loss of Lypd1-expressing cells between E18.5 and birth in the basal and mid-cochlear turns, prompt us to exclude the possibility of a subtype-specific loss and rather believe this occurs through a fate conversion of Ic into the Ia type.

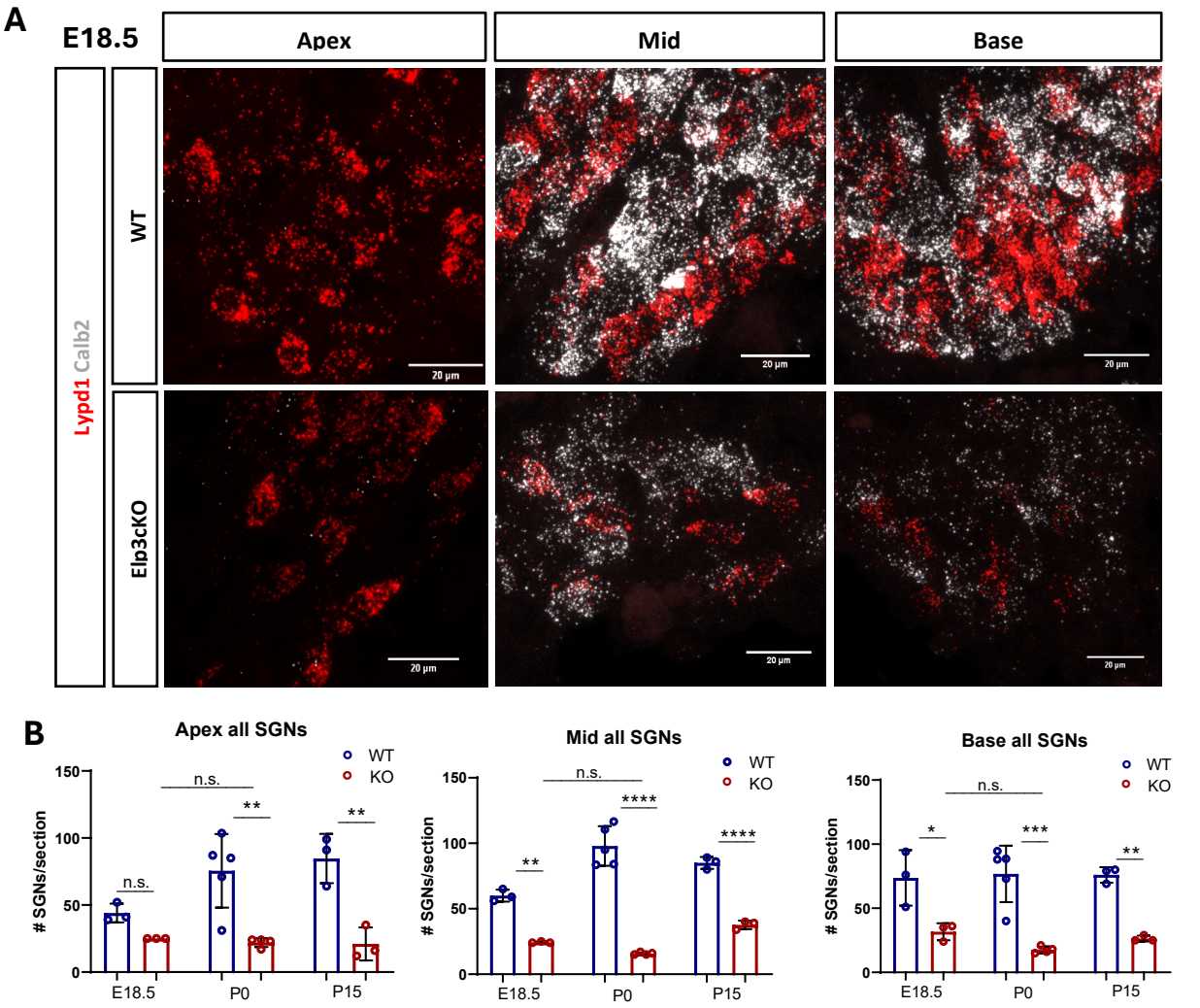

Figure 39. Prenatal molecular pattern described by RNAscope at E18.5. A) RNAscope has been performed on E18.5 tissue sections with the subtype specific probes Calb2 (white) and Lypd1 (red). Representative regions of the spiral ganglions of WTs and Elp3cKOs are shown. Experiment has been performed on 2 different animals coming from 2 different litters. B) number of total SGNs per section at E18.5, P0 and P15 at the apical, mid and basal turn. Note that there is no further SGN loss from E18.5 onwards. *(n=3-5 WT/KO, Two-way ANOVA, Tukey's multiple comparisons test; *p-value<0.05, **p-value<0.01, ***p-value<0.001, ****p-value<0.0001)*

The earlier stages of SGN diversification were reported to occur between E14.5 and E16. According to Sanders and Kelley, 2 SGN subclusters are already present at E14.5 in the developing spiral ganglion, one giving rise to the future Ia/II neurons and one giving rise to the future Ib/Ic subtypes. Therefore, we found it relevant to verify if those subclusters were already affected early during development, when apoptosis is occurring in KO ganglia. Indeed, a specific loss of the Ib/Ic SGN precursors would explain our phenotype later on. Therefore, we performed RNAscope® at E14.5 using probes targeting genes specifically expressed in the cluster Ia/II (Tle4) and Ib/Ic (Lypd1). Whereas Sanders identifies 2 clusters at E14 (future Ia/II and future Ib/Ic), Petitpré reports the emergence of the Ic subtype around E15-E16 showing high expression of Lypd1 compared to the intermediate Ia/Ib/II branch. Therefore, we performed RNAscope at E16.5 using a probe against Lypd1 and Calb2 to verify the presence of early Ic subtypes and intermediate Ia/Ib neurons, respectively.

The results showed that Tle4 and Lypd1 are both expressed by the spiral ganglion neurons in Elp3cKO mice at E14.5 (Figure 40A). Similarly to what is observed in control littermates, we found numerous neurons expressing exclusively Lypd1 and the others co-expressing both markers, the latter population presumably corresponding to less mature SGNs. Altogether, these results indicate that Lypd1-positive neurons have emerged during embryonic development of Elp3cKO cochleae. The presence, at E14 and E18, of SGNs destined to become Ic subtype rules out our hypothesis of the loss of one specific subcluster early during development. Accordingly, at E16.5 both Calb2 and Lypd1 are expressed in Elp3cKO SGNs, although at lower levels than in WT, confirming the presence of Ic neurons as well as intermediate Ia/Ib neurons (Figure 40B).

Altogether, our results confirm that during development, Elp3 invalidation does not induce the specific loss of a subtype or subcluster but likely causes a subtype identity switch of the remaining neurons towards a Calb2-only (Ia) identity in a base-to-apex gradient.

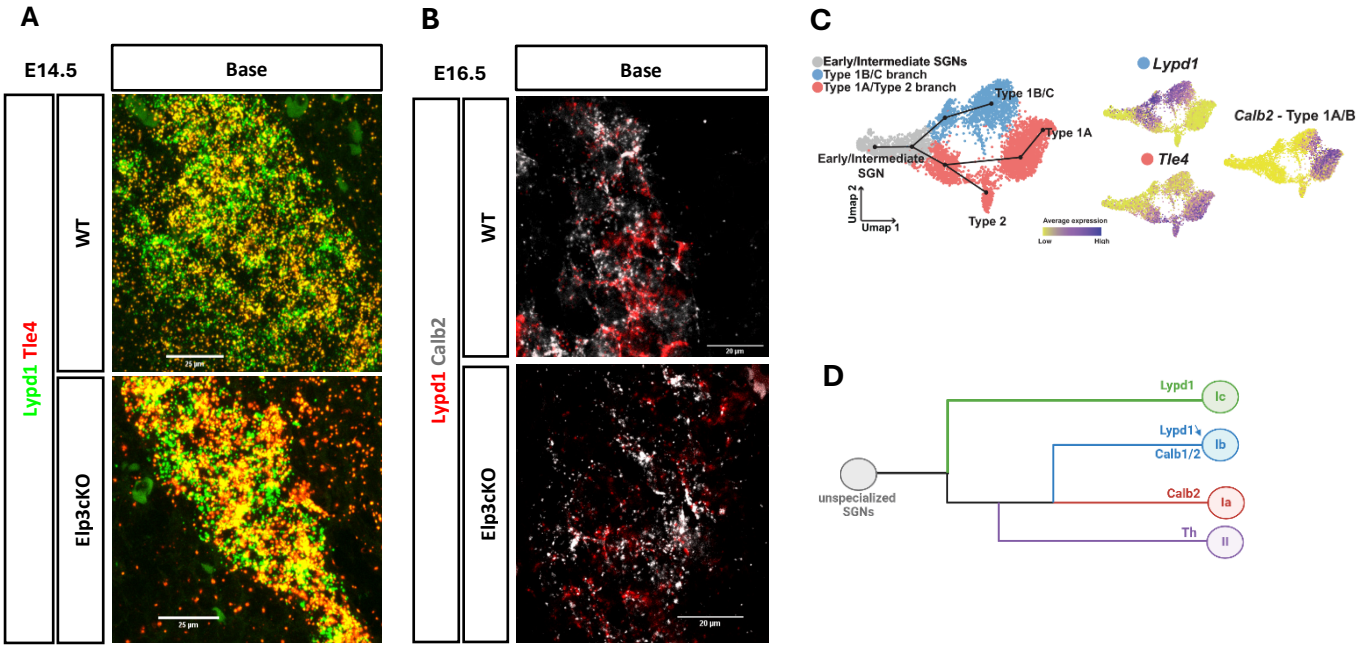

Figure 40. Prenatal molecular pattern described by RNAscope at E14.5 + E16.5. A) RNAscope on E14.5 WT and Elp3cKOs samples has been performed with probes against Lypd1 (green, Ib/Ic cluster) and Tle4 (red, Ia/II cluster). A representative image of the basal ganglion is shown as the presence of an apical and mid turn depends on the cutting orientation on the cryostat. B) RNAscope at E16.5 showing the expression pattern of Calb2 (white, Ia) and Lypd1 (red, Ic) within the SGNs of WT and Elp3cKO mice. Experiment has been performed on 2 different animals coming from 2 different litters. C) UMAP including slingshot trajectory showing the neuronal development over time and the corresponding cluster identities. Dataset combined from E14-16-18 and P1. From Sanders and Kelley, 2022. D) Simplified Scheme summarizing the diversification trajectory of the developing SGNs according to Petitpré et al. *Adapted from Petitpré 2022.*

In summary, our results show that Elp3KO neurons develop normally during embryonic stages, despite the significant apoptotic loss occurring between E14.5 and E17.5. Early diversification of SGNs is visible in Elp3-depleted neurons, as they diverge into distinct populations of intermediate neurons

at E14.5 and E16.5. Whether future Ic subtype emerges at E14.5 from a common differentiation branch for Ib/Ic SGNs (Tle4-/Lypd1+) (Sanders & Kelley, 2022), or whether Ic fate is the first to be selected along a unique trajectory at E16.5 (Calb2-/Lypd1+) (Petitpré et al., 2022), our results demonstrate that some Elp3cKO SGNs are committed to Ic lineage. Although Ic identity is defined during embryonic stages, changes occur postnatally upon fate consolidation. Indeed, abnormal distribution of SGN subtypes appear at P0 at the apical turn, with remaining SGNs still expressing exclusively Lypd1 (Ic-like) (Figure 41A), This presence of Lypd1-only SGNs in the apical turn is only transient during early neonatal period as they are no longer detected in P15 Elp3cKO spiral ganglions. From P0 to P15, this is changing into a complete predominance of Calb2-only (Figure 41A, lowest panel) and Cacna1b+/Grm8- cells, hinting for a subtype identity switch at the apical turn. In the basal as well as the middle turn, some Lypd1-only cells can be observed in Elp3cKO animals at E18.5 but they all turn Calb2-only at P0, suggesting that Ic SGNs seemed to have existed during embryonic stages and, similar to the apical SGNs but with some advance, have turned into Ia-like SGNs at birth (Figure 41B). Close to hearing onset (P15), the neurons surviving to Elp3-depletion are thus mostly Ia-like subtype, based on their molecular identity, however the topological characteristics of their peripheral processes are rather hinting to Ic-like neurons as they mainly innervate the modiolar side of the IHCs. This discrepancy between subtype specific markers and innervation profile is quite intriguing, as it suggests that Ia-like neurons are able to contact atypical IHC pole and face abnormally large ribbons.

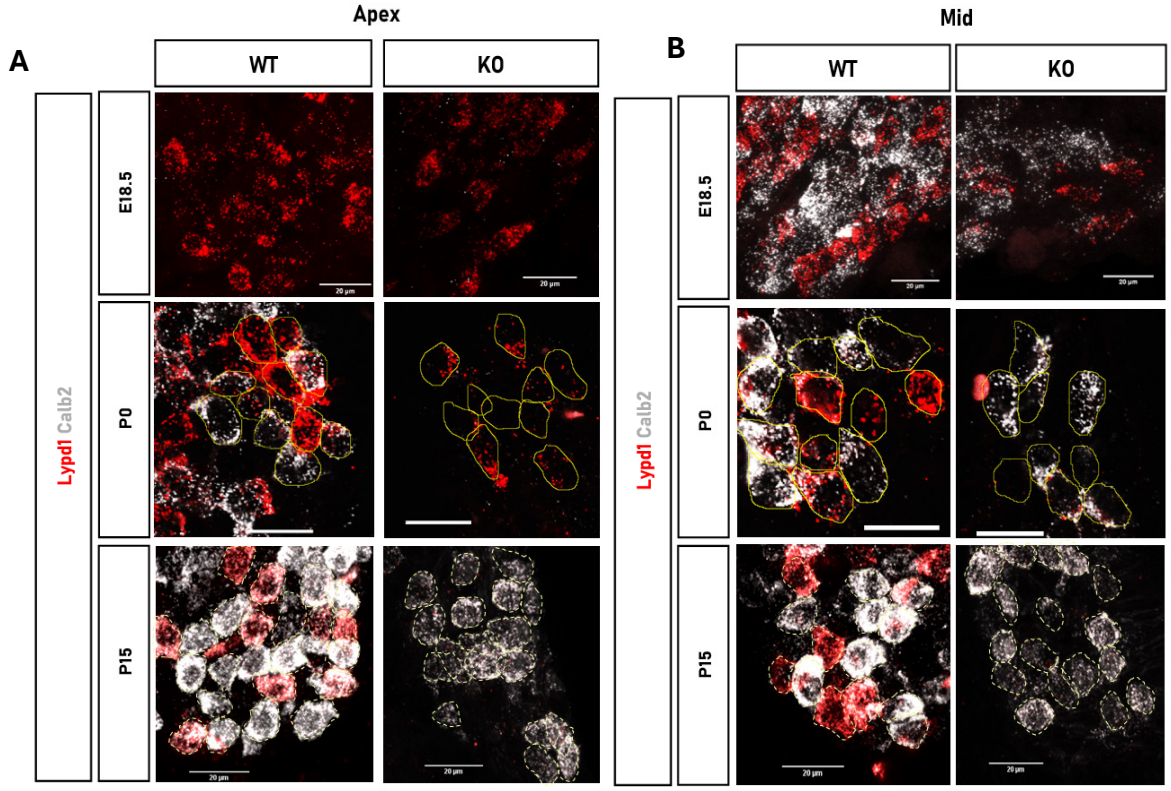

Figure 41. Evolution of subtype-specific marker expression between E18.5 and P15 in the Apex and Mid turn. A) At E18.5, all apical neurons express only Lypd1, in both WT and KO conditions. At P0, some WT Lypd1-positive neurons have become Calb2-positive, whereas KO neurons still remain Lypd1-postive before becoming all Calb2-positive at P15. B) At E18.5, some WT and KO neurons from the mid turn express Lypd1. At P0, WT neurons still express Lypd1 whereas all KO neurons have become Calb2-positive.

2. Determination of Cell autonomous or non-autonomous process

2.1 SGN cell death with Ngn1CreERT Mouse Model

Next, we sought to know if SGN loss and diversity failure upon Elp3 depletion is coming from intrinsic defects in the neuronal compartment (cell autonomous) or if it is influenced by the sensory compartment (cell non-autonomous). It has been shown in the literature that communication between IHCs and neurons during the early postnatal period by Glutamate release is crucial for their proper identity consolidation. For instance, Shrestha et al. showed that in absence of the vesicular Glutamate transporter Vglut3, characterized by the absence of synaptic neurotransmitter release into the synaptic cleft, the identity consolidation is impaired. This is reflected by a subtype proportion shift towards Ia SGNs occurring during the first postnatal week. Hence, we planned to verify if the phenotype in the Elp3cKO mice is influenced, even partially, by the sensory cells or if it is solely a result of Elp3 loss within the neuronal compartment.

To check for a cell autonomous phenotype, we first used a Tamoxifen inducible $Ngn1^{CreERT}$ mouse line. More precisely, this mouse line enables a specific recombination in the inner ear neurons of the vestibule and the cochlea, depending on the time point of Tamoxifen injection. To track the recombination efficiency, we made use of a Tomato reporter allele, which contains a floxed Stop codon upstream of the fluorescence gene. We injected Tamoxifen intraperitoneally in time mated females at E8.5 and E9.5 to label cochlear and vestibular neurons and sacrificed them at E13.5. We performed immunolabeling of cleaved caspase 3 to check for apoptosis in the spiral ganglion and verified the presence of Tomato signal to check the recombination efficiency (Figure 42A).

Immunostainings for cleaved caspase 3 (cCasp3) on tissue sections show a slight but significant increase in the number of apoptotic cells on KO sections (Figure 42C), whereas the size of the ganglion remains unchanged at this early stage (Figure 42B). This result suggests that Elp3 depletion in developing otic neurons is directly responsible of cell death and that neuronal apoptosis is thus a cell autonomous phenotype.

Unfortunately, the extent of SGN loss resulting from this early apoptosis as well as SGN diversity could not be monitored at later stages of development, as we experienced many technical problems with this mouse line and the usage of Tamoxifen leading to prenatal death and abortion of the pups. Therefore, we were obliged to switch to a Tamoxifen-independent mouse line, the $Bhlhb5^{Cre}$ mouse model (Ross et al., 2010).

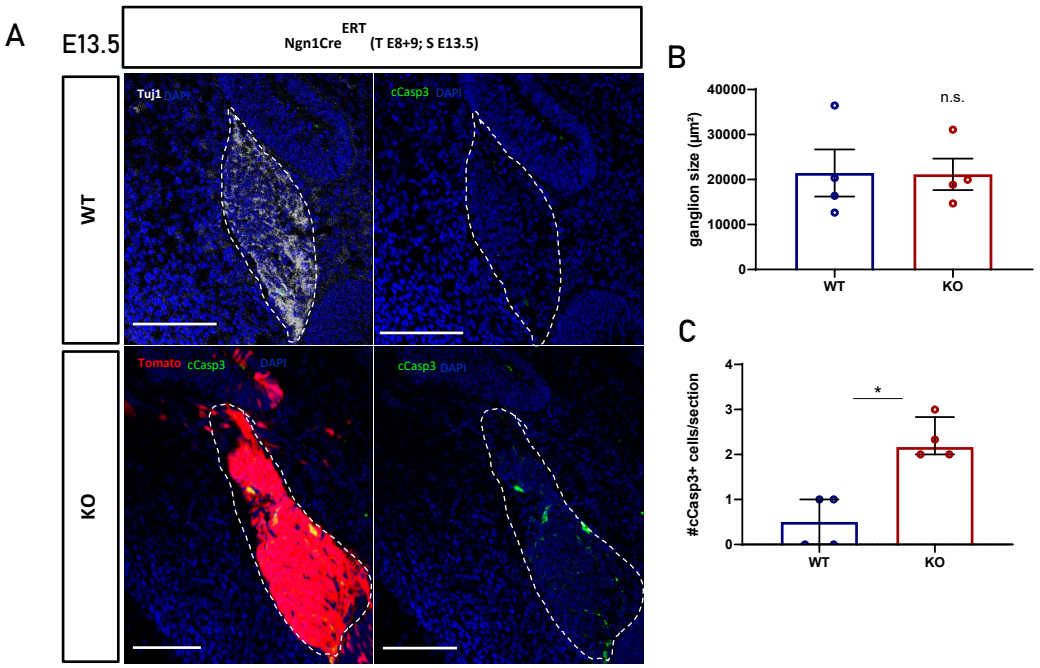

Figure 42. Immunostaining for cleaved Caspase3 in Ngn1CreERT Elp3cKO mice. (A) Immunostainings against cCasp3 showing more apoptotic cells in the KO ganglion compared to WT. (B+C) Quantifications confirm a significant increase of cCasp3 positive neurons (C) in the KO whereas the ganglion size remains stable (B). *(n=4 for both conditions; two-tailed Mann Whitney test; *p-value<0.05)*

2.2 Bhlhb5Cre Mouse Model

According to the literature, recombination by the Bhlhb5-Cre recombinase is induced from E9.5 onwards in the cochlear-vestibular ganglion, thus targeting specifically the spiral and vestibular ganglion neurons (Appler et al., 2013). Hence, by crossing Bhlhb5^{Cre} mice with Elp3$^{Lox/lox}$ mice we aimed to deplete Elp3 specifically in the otic neurons from an early time point on to study the effect of its loss on hearing, neuronal cell death and identity consolidation.

First, we performed Auditory Brainstem recordings (ABRs) to assess the hearing function of control and KO mice at 5 weeks of age. Click ABRs, which consist in sound stimulation covering a mix of different frequencies, show no significant difference regarding the auditory threshold between WT and Elp3cKO (Figure 43A). We also performed Pure Tone ABRs at 5 different frequencies: 4, 8, 16, 24 and 32 kHz, but no significant difference in the hearing sensitivity could be observed for any frequency tested (Figure 43B). As milder hearing impairments can be present despite a normal hearing threshold, we checked for the ABR peak I amplitude and latency, which reflect the activity and propagation speed of the cochlear nerve, respectively. A decreased peak I amplitude often speaks for a loss of ribbon synapses whereas an increased latency could speak for a myelinization defect. However, there was no significant difference neither for the amplitude nor the latency of peak I (Figure 43C+D).

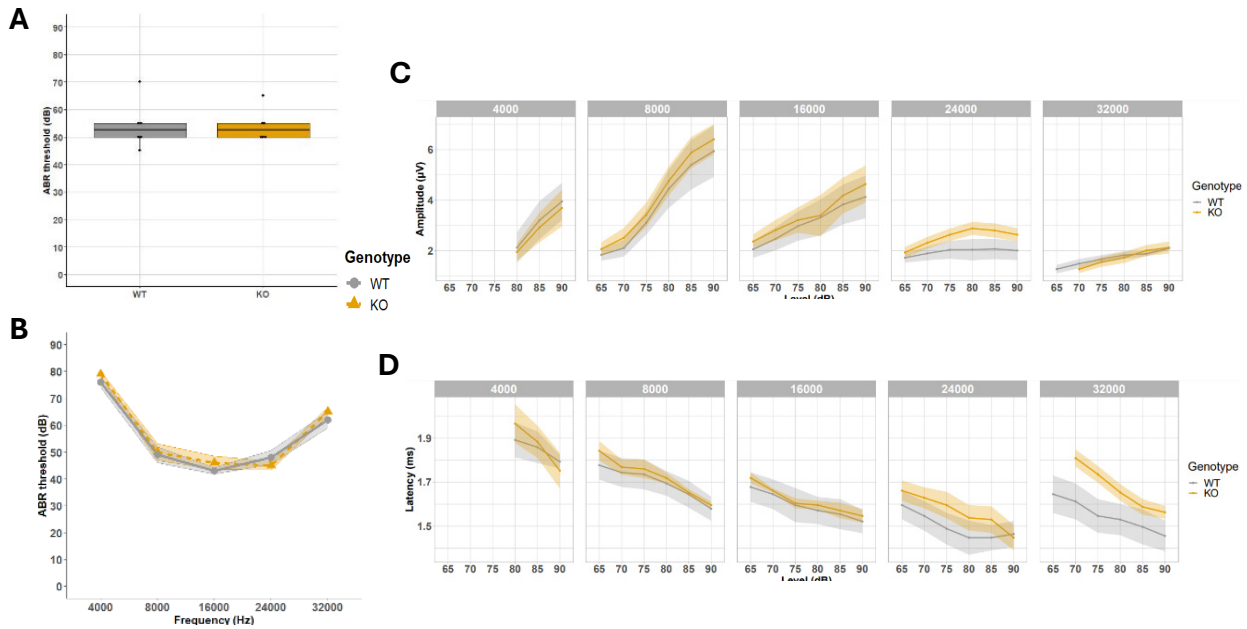

Figure 43. Bhlhb5Cre Elp3cKO mice at 5 weeks of age do not show hearing threshold, peak 1 amplitude or latency differences compared to control mice. Auditory Brainstem Recordings have been performed at 5 weeks of age. Thresholds of Click (A) and Pure Tone (B) ABRs are similar between WT and KO. Amplitudes (C) and latencies (D) of peak 1 are not different in KO mice compared to control. *(n=6/5 WT/KO respectively, from 2 independent litters; unpaired t-test)*

To study whether SGN differentiation into the three neuronal subtypes was affected by Elp3 invalidation we performed RNAscope with the subtype specific markers Calb2 and Lypd1 on control and KO animals at 5 weeks of age.

We subjectively determined the number of neurons expressing only Calb2 (Ia), only Lypd1 (Ic) and both Calb2 and Lypd1 (Ib). Our quantifications reveal normal proportions of the 3 subtypes in both WT and KO animals, at all of the three turns, indicating that there is no defect of neuronal diversity (Figure 44B). In parallel, there is no significant reduction in the number of SGNs per ganglion between WT and KO animals (Figure 44C).

Figure 44 (next page). Molecular pattern of SGNs in Bhlhb5Cre Elp3Lox mice of 5 weeks of age. A) RNAscope by using the specific markers Calb2 and Lypd1 has been performed at 5 weeks to determine the proportions of Ia, Ib and Ic subtypes. B) Quantifications show no difference regarding the molecular characteristics of the SGNs between WT and KO mice. *(n=3 for both conditions; Mann-Whitney test; p-value>0.05)* C) Assessment of the number of SGNs per ganglion of the three cochlear turns. *(n=3 for both conditions; Mann-Whitney test; p-value>0.05)*

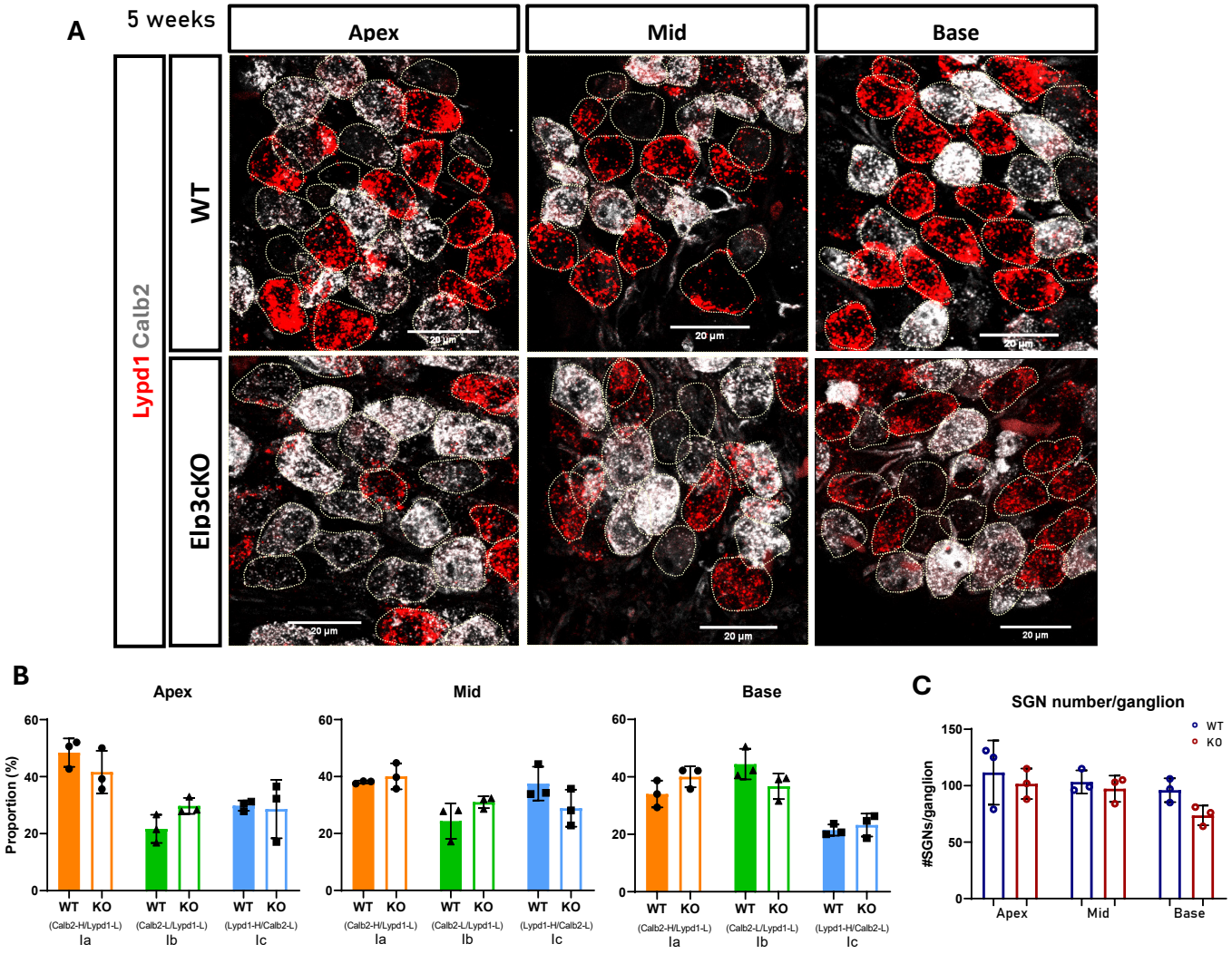

As the absence of a phenotype was quite intriguing to us, we verified if this could be due to a poor recombination efficiency. Therefore, we performed Immunostaining on tissue sections using an antibody against Parvalbumin to label all SGNs and against RFP to reinforce the Tomato signal arising from the reporter gene expression. In our control group, which usually displays no Cre allele, we decided to implement Bhlhb5$^{Cre/+}$ Elp3$^{Lox/+}$ Rosa$^{Tomato/+}$ heterozygous mice to be able to compare the recombination efficiency based on Tomato expression with our KO group. Indeed, we know from our previous experiments, performed on Foxg1^{Cre} colony, that heterozygous mice present no phenotype and can thus be considered as normal regarding SGN survival and differentiation.

We calculated the number of neurons per ganglion, but it was not affected in Elp3cKOs compared to controls confirming the absence of neuronal cell death (Figure 45A+B). Next, we calculated the percentage of neurons that are double-positive for Parvalbumin and RFP among all Parvalbumin-positive neurons to assess whether the recombination efficiency differs between control and KO animals. As shown in Figure 9, consistent recombination of the Cre reporter gene occurred in 60% to 80% in basal to apical SGNs, respectively, and this recombination is similar between WT and Elp3cKO animals (Figure 45 C).

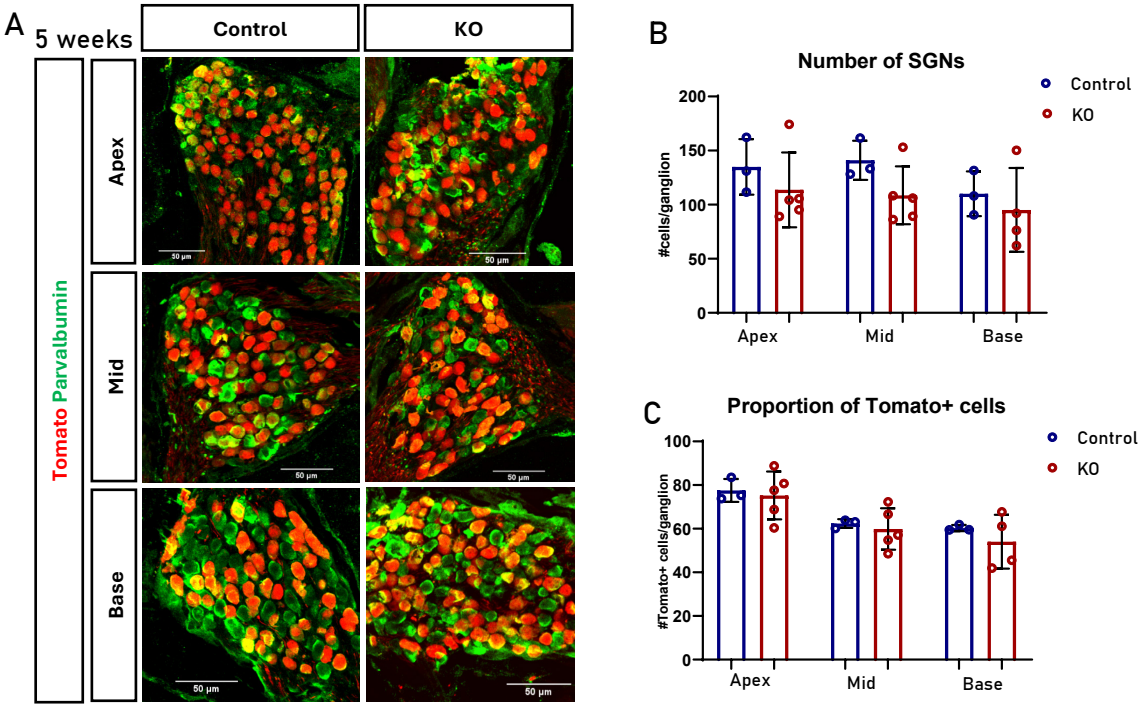

Figure 45. Tomato recombination and SGN number of Bhlhb5Cre Elp3Lox mice at 5 weeks of age. A+B) Immunostainings using anti-RFP and anti-Parvalbumin antibodies on tissue sections of 5 weeks old mice show similar number SGNs per ganglion. C) The recombination pattern within the spiral ganglion is similar in Control ($Bhlhb5^{Cre/+}Elp3^{L/+}Rosa^{Tom/+}$) and KO ($Bhlhb5^{Cre/+}\ Elp3^{L/L}Rosa^{Tom/+}$) mice. *(n=3/5 for Control/KO respectively; Mann-Whitney Test; p-value>0.05)*

Hence, these results suggest that Elp3-depleted SGNs developed normally in Bhlhb5Cre mouse model and that they were not subjected to early apoptosis, in contrast to what we found in the $Ngn1^{CreERT}$ mouse line. To further clarify this discrepancy between our 2 models, we investigated whether gene recombination, and thus Elp3 depletion, occurs at similar stages.

We verified if the genetic recombination starts at the expected time point, which according to the literature corresponds to E9.5. We therefore performed Immunostainings against Tuj1/Islet1 and Tomato to follow the recombination pattern of the reporter gene at E11.5 and E12.5. The results show that recombination occurs later than expected as Tomato expression in only visible in a few ganglionic neurons at E11.5 and E12.5 (Figure 46).

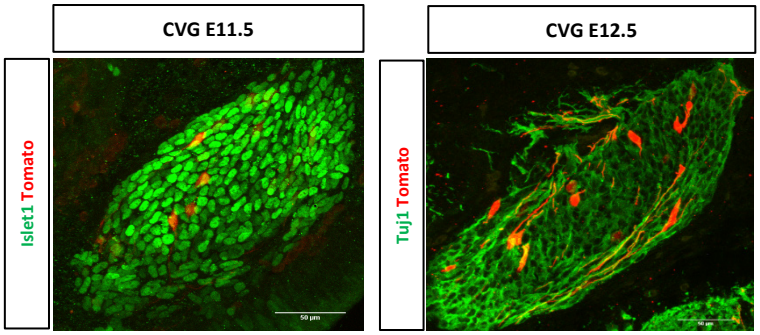

Those findings, strongly contrasting with those obtained previously in Ngn1Cre mouse lines made us suspicious about the experimental model. Even though Tomato reporter gene is expressed in more than 60% of SGNs of Bhlhb5Cre mice, thereby suggesting that Cre efficiently recombines the floxed Tomato locus, we needed to confirm that its activity also induces Elp3 gene invalidation. Of note, it has already been reported in the literature that the tdTomato reporter allele has a higher probability of being recombined due to the short distance between the two LoxP sites but also that the recombination of two different alleles in the same genomic locus happens independently (Bedolla et al., 2024; Dause & Kirby, 2020). To verify that Tomato expression correlates with Elp3 depletion, we used BaseScope®, an *in situ* hybridization technique, specifically adapted to detect short RNA sequences. We used a single Z pair probe targeting the exon 2 of Elp3, which should be deleted in our KO lines in case of effective recombination. We combined the BaseScope® with an Immunostaining for Parvalbumin and RFP to visualize respectively all SGNs and those in which Cre-mediated recombination occurred.

We quantified the number of dots per SGN on control and Elp3cKO sections of 5 weeks-old animals. The number of dots per SGNS is below 1, at all 3 turns, and it was similar in WT and Elp3cKO animals (Figure 47B). Moreover, the proportion of cells expressing no exon2-containing Elp3 transcript (0 dots) was not increased in KO animals compared with WT, whether they were quantified amongst all SGNs (Figure 47C) or within the Tomato+ population (Figure 47D).

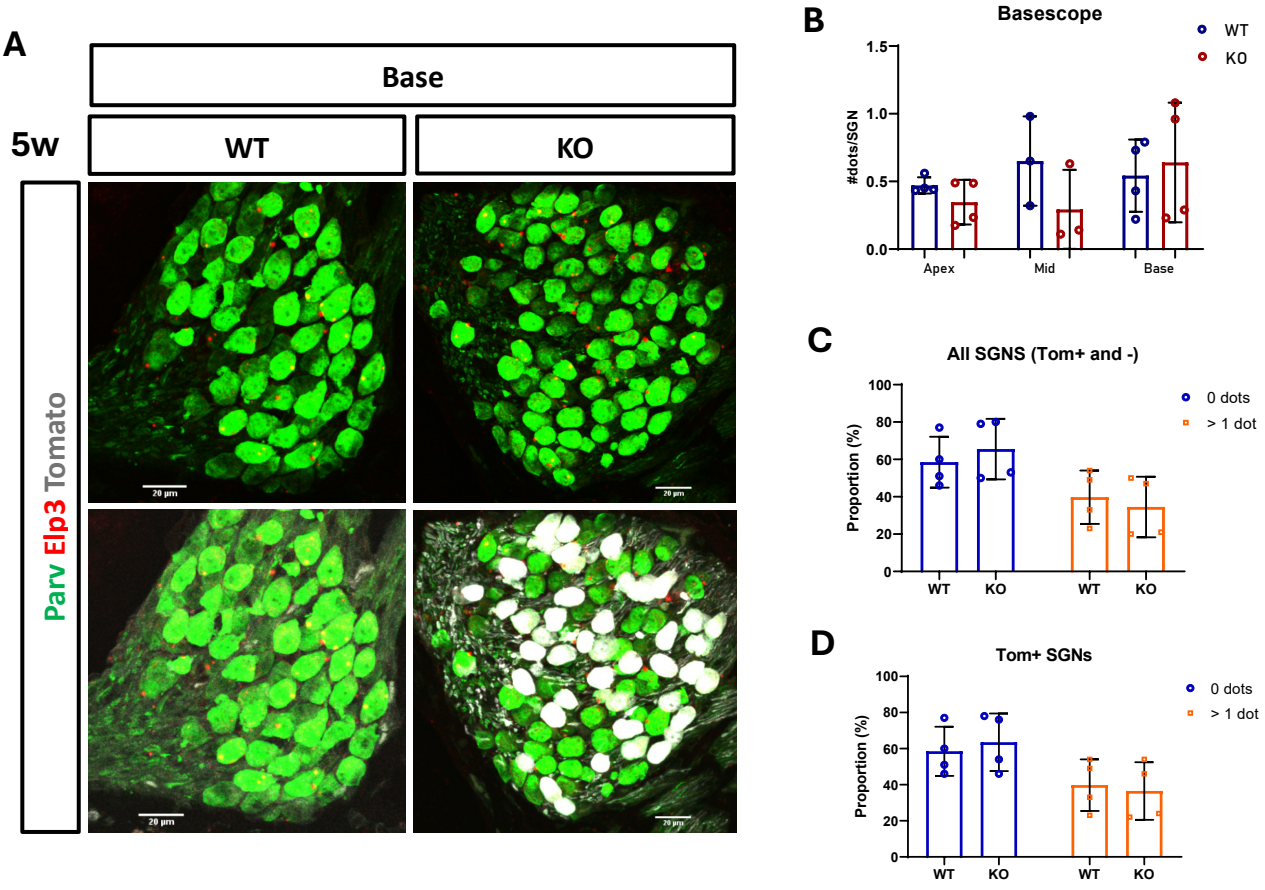

Figure 47 (previous page). Assessment of Elp3 recombination in Bhlhb5Cre Elp3Lox mice at 5 weeks of age. A) BaseScope using probes targeting exon 2 of the Elp3gene (red dots) in SGNs (stained in green by Parvalbumin), recombined (white) or not. B) Quantifications of the number of dots per SGN, C+D) and the proportion of SGNs containing 0 or more than 1 dot, in all KO SGNS (C) or only in Tom+ KO SGNs (D). (WT = Bhlhb5$^{-/-}$Elp3$^{L/+}$Rosa$^{Tomato/+}$; KO = Bhlhb5$^{Cre/-}$Elp3$^{L/L}$Rosa$^{Tomato/+}$) *(B: n=4 for WT and KO; two-tailed unpaired t-test. C+D: n=4 for WT and KO; ordinary two-way ANOVA)*

Regarding the low number of dots per neuron, we found it necessary to perform quality control experiments of the BaseScope technique. The use of positive *(Ppib)* and negative *(DapB)* control probes on our sections confirmed RNA integrity and probe specificity, respectively (Figure 48, left panels). In addition, exon 2 specific Elp3 signal is visible in Foxg1Cre WT animals but largely absent in neurons of Foxg1Cre Elp3cKO animals (Figure 48, right panels), confirming that the BaseScope is sensitive enough to distinguish WT from Elp3cKO genotypes.

Altogether, those results show that in our Bhlhb5Cre model there is no effective invalidation of the Elp3 gene despite the expression of the Tomato reporter gene. Consequently, we cannot conclude on a cell autonomous or cell non-autonomous phenotype based on this experimental model.

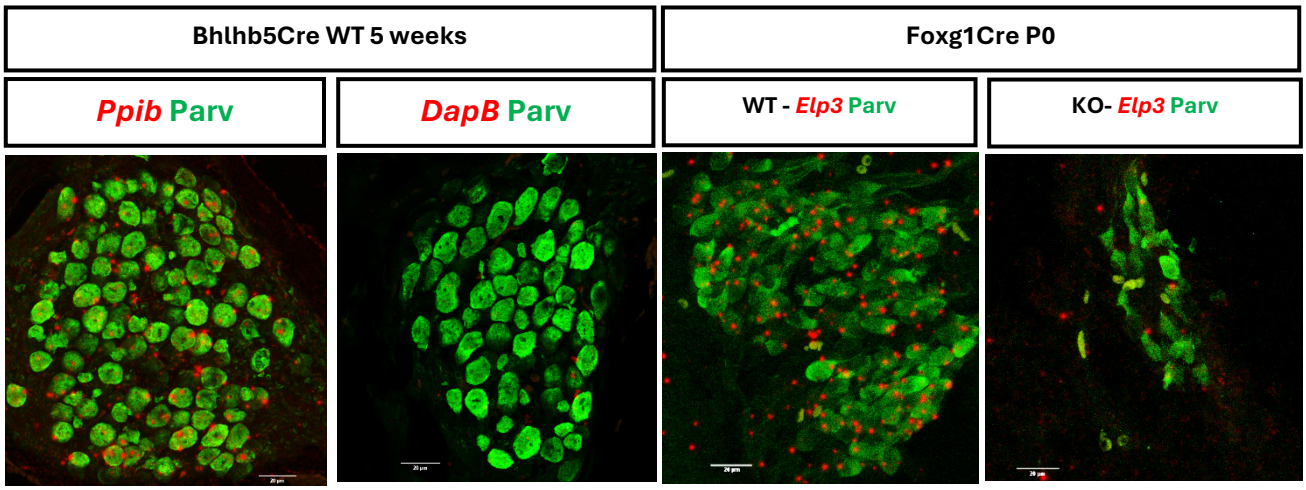

Figure 48. BaseScope control conditions. First 2 panels: BaseScope using either positive or negative control probe on Bhlhb5Cre WT slides from mice at 5 weeks of age. Notice the presence of BaseScope signal in the positive control and the absence of signal in negative control. ***Last 2 panels:*** BaseScope on Foxg1Cre mice at P0 using an Elp3 specific probe targeting Exon 2. Notice the presence of Elp3 signal in WTs and the absence of Elp3 signal in KOs.

3. SGN differentiation in Elp3KO cochlea upon chaperone treatment

3.1 SGN molecular pattern

To uncover the specific roles of neuronal loss versus HC polarity disruption in our Elp3KO phenotype, we turned to an alternative approach using the 4-PBA chaperone. Indeed, we previously demonstrated that the polarity defect at the level of HCs may be rescued by reducing the load of misfolded proteins

and protein aggregates through administration of the chemical chaperone, whereas neuronal survival was not ameliorated. To do this, we injected time mated females from E10.5 daily until E19.5 with saline or 4-PBA at a dose of 200 mg/kg body weight until birth and analyzed SGN subtype proportions by performing RNAscope® on tissue sections of P0 control and Elp3cKO animals.

Globally, the results from the saline injected WT and KO animals are comparable to those obtained previously (Figure 38) regarding the global reduction of the expression levels of the subtype specific markers Calb2 and Lypd1 and the predominance of Calb2-only neurons. Furthermore, the 4-PBA treatment had no effect in WT animals as the proportions of each subtype are identical to saline-injected WT animals. Next, the RNAscope results indicate that, although subtype-specific marker expression drastically increased after 4-PBA treatment in 2/4 samples (Figure 49A), the average proportion of Calb2-only cells (Ia) or Lpd1-only (Ic) cells does not change in KOs upon chaperone treatment (Figure 49B and D). In contrast, the proportion of double-positive (Ib) neurons, which is significantly decreased in saline-treated KOs , was partially rescued by 4-PBA treatment in the Base and Mid turn, but not in the Apex (Figure 49C). For double-negative cells (II), which are supernumerary in KO condition, their proportion was significantly decreased in basal turn after chaperone treatment (Figure 49E).

Overall, by alleviating proteotoxic stress during embryonic development of Elp3KO animals, 4-PBA treatment rescues the proportion of double-positive neurons but was not sufficient to restore the population of Lypd1-only SGNs at birth.

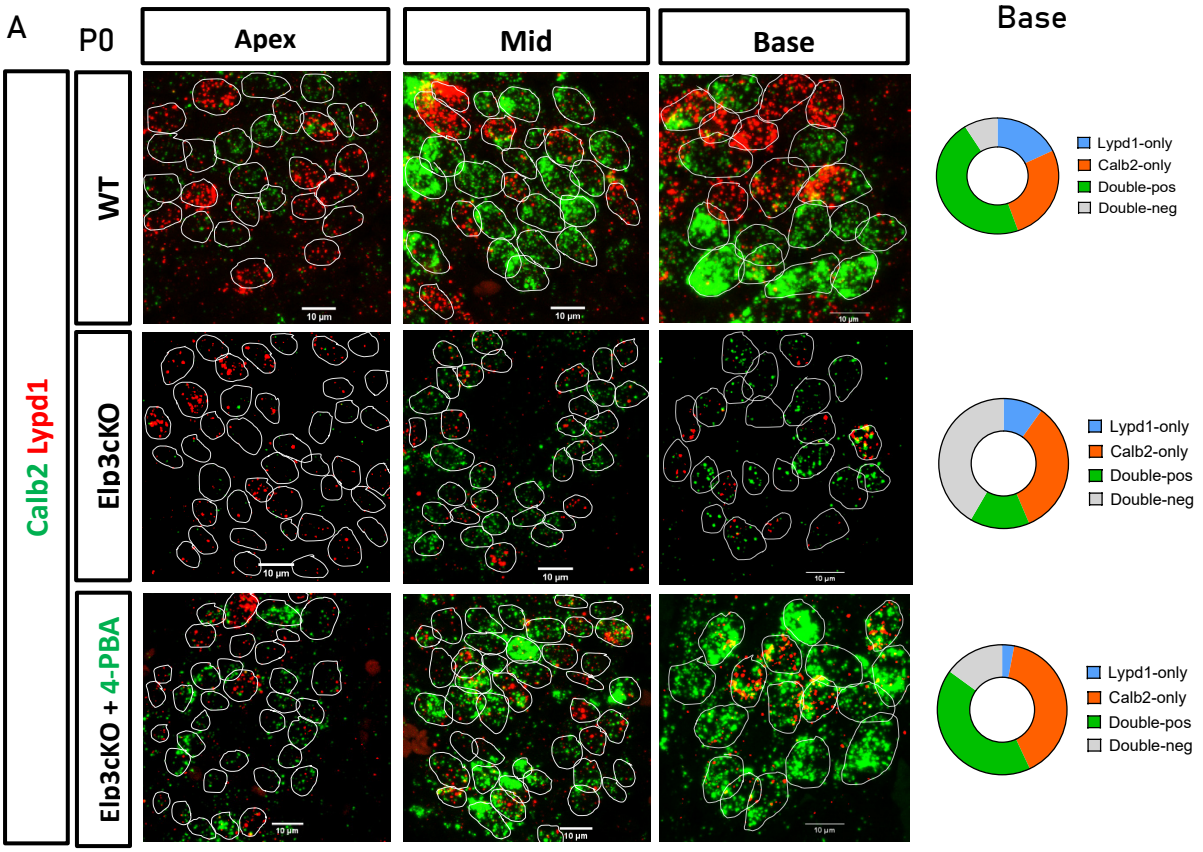

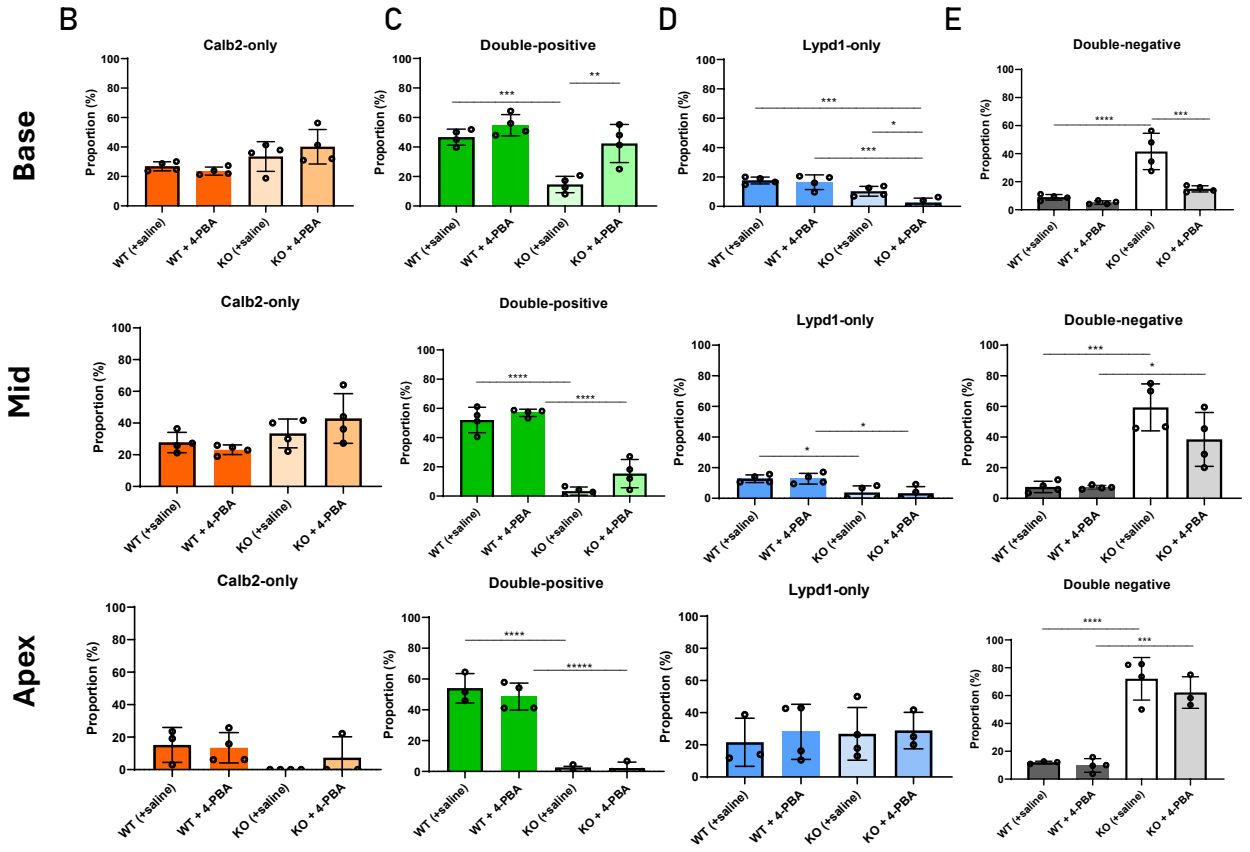

Figure 49. Molecular pattern in Foxg1Cre Elp3Lox mice treated with saline or 4-PBA at P0. A) RNAscope on P0 WT and Elp3cKO (saline or 4-PBA treated) samples with subtype specific markers Calb2 and Lypd1. Donut charts on the right side illustrate the relative proportions of each subgroup at the basal turn. B-E) Subjective quantifications of Ia (Calb2-only), Ib (Double-positive), Ic (Lypd1-only) and II (Double-negative) subtypes at the basal turn (upper row), middle turn (middle row) and apical turn (lowest row) show a partial restoration of the Double-positive and Double-negative subtypes in 4-PBA-treated KOs in the basal and the middle turn. *(n=4/4 for saline/4-PBA groups respectively; ordinary one-way ANOVA test; *p-value<0.05, **p-value<0.01, ***p-value<0.001, ****p-value<0.0001)*

To further investigate whether the population of double positive SGNs (Calb2+Lypd1+) corresponds to Ib neurons or whether co-expression of both markers could reflect some form of plasticity linked to a gradual switch of Ia towards Ic differentiation program, we repeated the experiment and analyzed SGN identities at hearing onset. Therefore, we continued the intraperitoneal injections daily until P15 at a dose of 200mg/kg bodyweight to perform RNAscope with the classical set of markers.

Figure 50 (next page). Molecular pattern in Foxg1Cre Elp3Lox mice treated with saline or 4-PBA at P15. A) RNAscope on P15 WT and Elp3cKO (saline or 4-PBA treated) samples with subtype specific markers Calb2 and Lypd1. B-E) Subjective quantifications of Ia (Calb2-only), Ib (Double-positive), Ic (Lypd1-only) and II (Double-negative) subtypes at the Base (upper row), Mid (middle row) and Apex (lowest row) show a significant loss of the Ib and Ic subtypes and a significant increase of the Ia subtype proportion in the KO and 4-PBA-treated KO animals, in all of the 3 turns. *(n=5/6 for saline/4-PBA groups respectively; ordinary one-way ANOVA test; *p-value<0.05, **p-value<0.01, ***p-value<0.001, ****p-value<0.0001)*

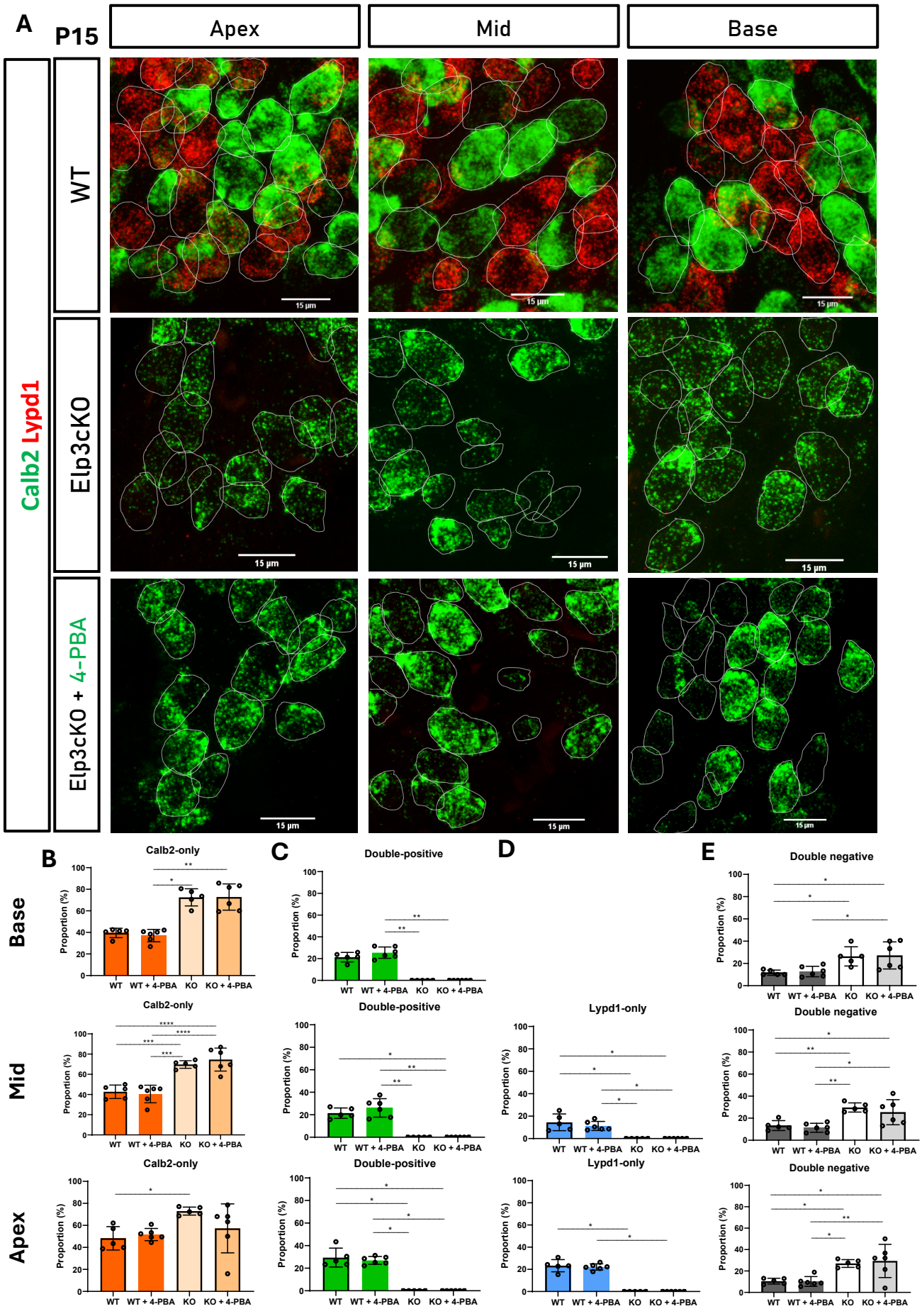
A
P15
Apex
Mid
Base
Calb2 Lypd1
WT
Elp3cKO
Elp3cKO + 4-PBA
15 µm
B
C
D
E
Base
Mid
Apex
Calb2-only
Double-positive
Lypd1-only
Double negative
Proportion (%)
WT
WT + 4-PBA
KO
KO + 4-PBA

The quantifications of the RNAscope results show that the proportion of Calb2-only neurons (Ia) is significantly increased in KOs but is not restored after embryonic and postnatal 4-PBA treatment (Figure 50B). In addition, the proportions of double-positive neurons (Ib) and Lypd1-only cells (Ic) are significantly reduced in KOs compared to controls but were not restored upon chaperone administration (Figure 50C-D). Lastly, the increased population of double-negative (II) neurons remained despite 4-PBA treatment (Figure 50E).

In summary, the results show that the rescue of double-positive and double-negative neurons at P0 is only transient and does not persist until P15. We speculate that 4-PBA treatment and thus alleviating proteostasis disruption is insufficient to restore normal SGN differentiation and subtype proportions.

3.2 SGN projection pattern

Although type Ia SGNs are still predominant in chaperone-treated Elp3KO, we wondered if HC polarity restoration by 4-PBA could have impacted the location at which their peripheral processes contact the target sensory cells. We assessed the synapse position gradient by performing Immunostaining using Myo7A and Ribeye Antibodies together with 3D reconstruction analysis using Imaris, as described before (Figure 51).

As shown previously (see Figure 35), the proportions of modiolar synapses and pillar synapses are respectively increased and decreased in Elp3cKOs compared to controls (Figure 51). However, the treatment with the chemical chaperone 4-PBA does not rescue the abolished modiolar-pillar gradient of synapses in Elp3cKO mice, nor the number of synapses per IHC (Figure 51B,C,D).

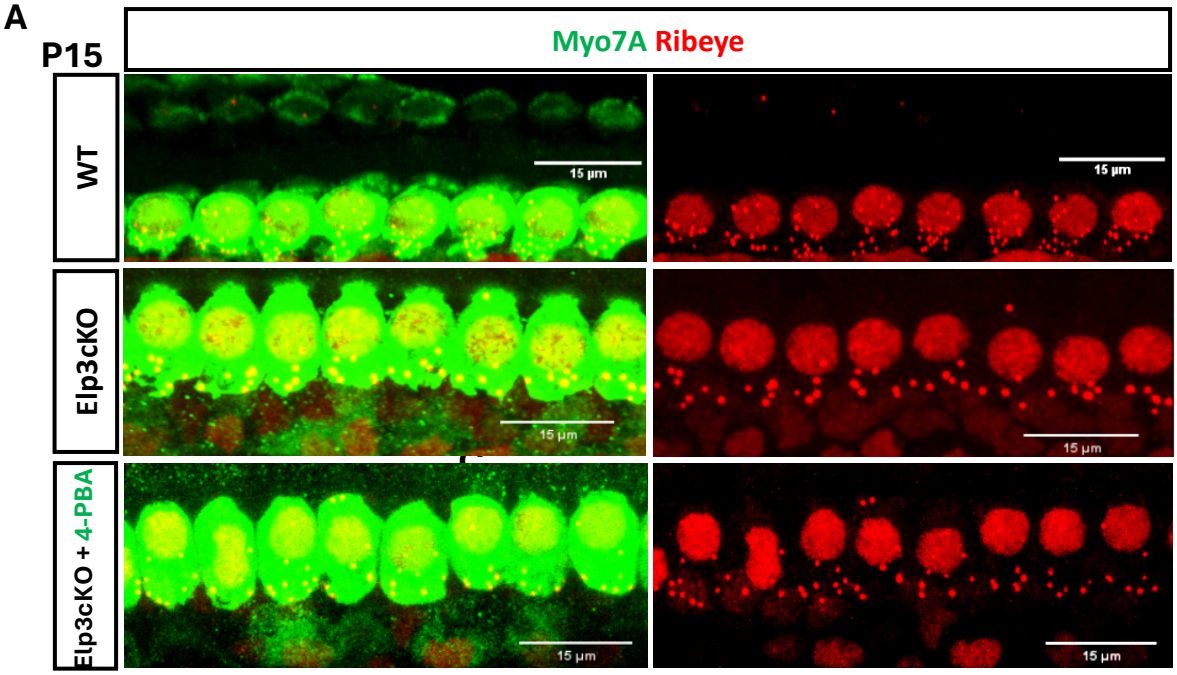

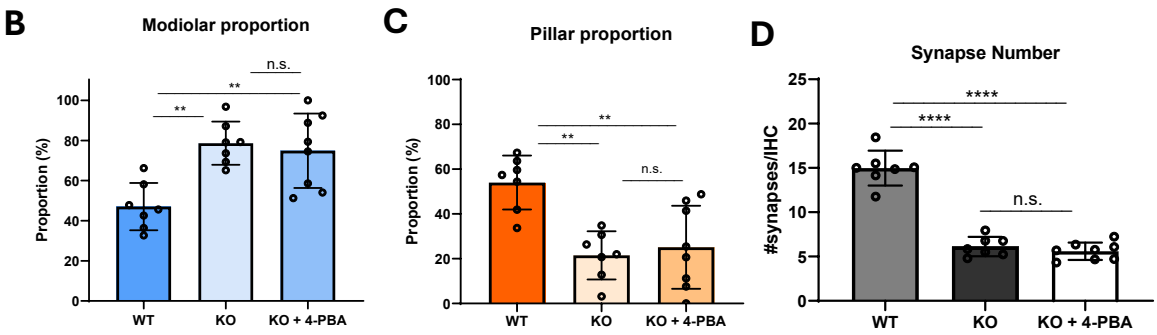

Figure 51. Morphological pattern in Foxg1Cre Elp3Lox mice at P15 treated with saline or 4-PBA. A) Immunostainings for the presynaptic marker Ribeye and Myo7A to enable for determination of the synapse position. B+C) quantification of the proportion of modiolar and pillar synapses in WT (+saline), KO (+saline) and KO (+4-PBA) mice. D) quantification of the number of synapses *(n=7/8 for saline/4-PBA groups respectively; ordinary one-way ANOVA test; **p-value<0.01)*

In summary, although 4-PBA treatment was shown to ameliorate HC polarity in Elp3KO cochlea, the chaperone was not able to rescue SGN neuronal diversity and synapse gradient, since most surviving SGNs still present Ia subtype molecular characteristics with abnormal projections towards the modiolar pole of target HCs.

PART II – VESTIBULE

1. Assessment of Vestibular function

In the absence of Elp3 expression in the inner ear, mice are profoundly deaf, but we also observed obvious signs of imbalance in our colony. In the literature, several behaviors have been described to provide insights into vestibular dysfunction. For instance, mice displaying vestibular defects tend to shake repetitively their head (head bobbing), circle around in their cage (circling), move backwards (retropulsion), or try to grab their tail when hanging freely in the air instead of extending limbs to reach the ground (Tail hanging test). We used those 4 tests to estimate the potential vestibular defects in two weeks-old Elp3cKO mice (P16).

For each test, a ranking system with 4 levels has been defined with "0" being normal and "4" being the highest level of abnormality observed in a defined time period. Each animal has been observed 3 times on different days, therefore an average score was attributed for each animal. Our observations indicate that only Elp3KO animals presented the "head bobbing" phenotype. The tail hanging test reveals that Elp3cKO mice often tended to crawl ventrally to grab their tail instead of extending to reach the ground, whereas control animals rarely showed this behavior. The retropulsion behavior could only be observed in KO mice but was rather rare. Lastly, each KO mice showed at least one circling behavior whereas it could only be observed in 2 control animals out of 7.

The results suggest that Elp3cKO mice suffer vestibular defects, especially circling that can be related to the Cristae and its role in angular orientational perception (Figure 52). To better understand the origin of these vestibular behavioral defects, we aimed to characterize the development of the vestibular ganglion neurons.

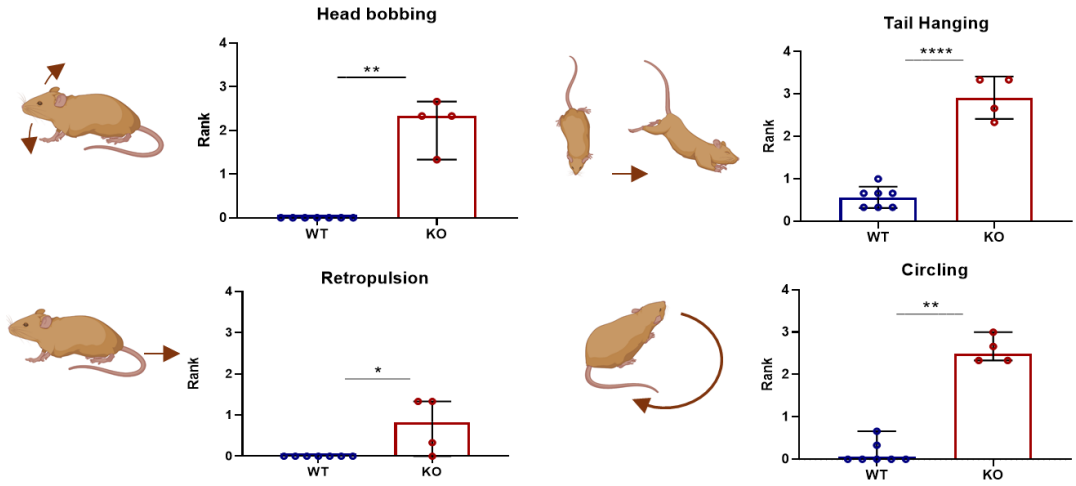

Figure 52. Behavioral analysis for vestibular defects at P15. 4 behavioral tests have been performed on WT and KO animals: head bobbing, tail hanging test, retropulsion test and circling (which can specifically be attributed to the vestibular function). KO mice show vestibular behavioral defects, especially circling behavior that can be attributed to the cristae function. *(n=7/4 for WT/KO group; non-parametric Mann Whitney test; *p-value<0.05, **p-value<0.01, ****p-value<0.0001)*

2. VGN development in Foxg1Cre Elp3cKO model

As we demonstrated a neuronal loss and diversity failure at the level of the cochlear ganglion, we were interested to know if a similar phenotype can be seen in the vestibule. Of note, VGNs and SGNs emerge from a common cluster, the cochleo-vestibular ganglion (CVG) present at E9.5, that divides into the 2 clusters at E11.5 (Sun et al., 2022). We thus made use of the Foxg1Cre mouse line enabling a recombination from E8.5-9 onwards in the CVG, as we can expect a similar depletion of Elp3 in the VG than in the SG.

First, we counted the number of VGNs per ganglion at E13.5 and P0 to assess for neuronal loss by performing Islet1 Immunostainings. Our quantifications indicated a normal development of VGNs until E13.5 (Figure 53A-left and 18B) but revealed a significant loss of neurons later on at P0 (Figure 53A-right and 18C). In parallel, whole mount immunostainings with antibodies against Myo7A (HCs) and Neurofilament revealed a strongly reduced innervation of the vestibular organs at P1 (Figure 53D).

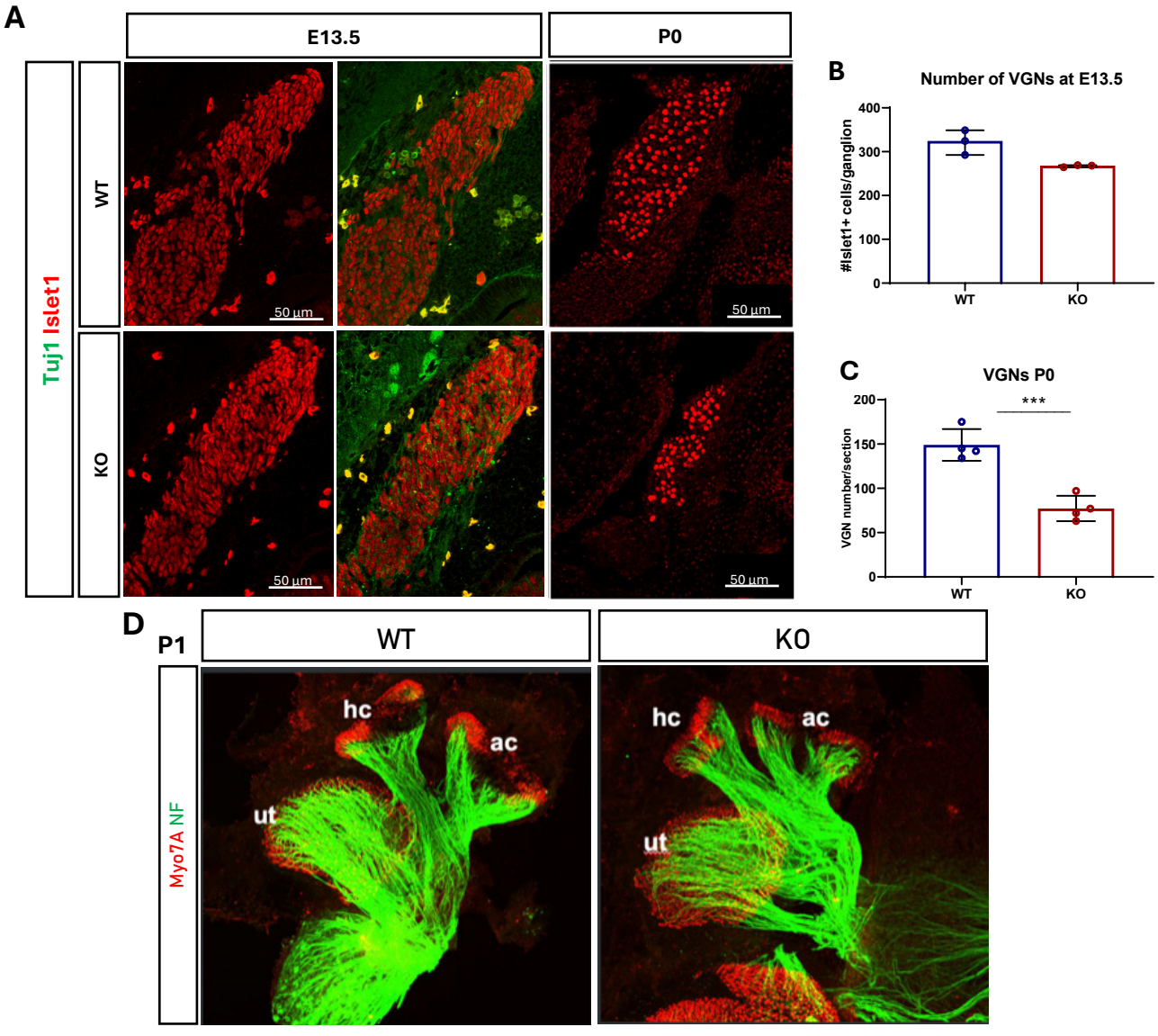

Figure 53 (previous page). Assessment of vestibular ganglion neuron (VGN) survival at E13.5 and P0. A) Tissue sections of control and KO animals at E13.5 and P0 have been stained with Islet1 (neuronal nuclear marker of VGNs) and Tuj1 (neuronal cytoplasmic marker). B) Graph showing no reduction of number of VGNs at E13.5. *(n=3 from 2 different litters; non-parametric Mann Whitney test; p-value=0.1).* C) Graph showing loss of 50% of VGNs at P0. *(n=4 WT/KO; unpaired t-test, ***p-value=0.0008)* D) Immunostaining with HC specific marker (Myo7A, red) and Neuron specific marker (NF, green) showing a strongly reduced innervation of the Utricle (ut), the horizontal cristae (hc) and anterior cristae (ac) at P1.

We then performed Cleaved Caspase3 staining on tissue sections at E13.5 and E14.5 to check whether, as in the cochlea, cells are dying by apoptosis at these early stages of development.

Our counting of cCasp3-positive VGN per section showed that there is no significant difference between WT and KO mice at E13.5 but that increased apoptosis is visible E14.5 (Figure 54), indicating that the beginning of neuronal loss is around E14.5.

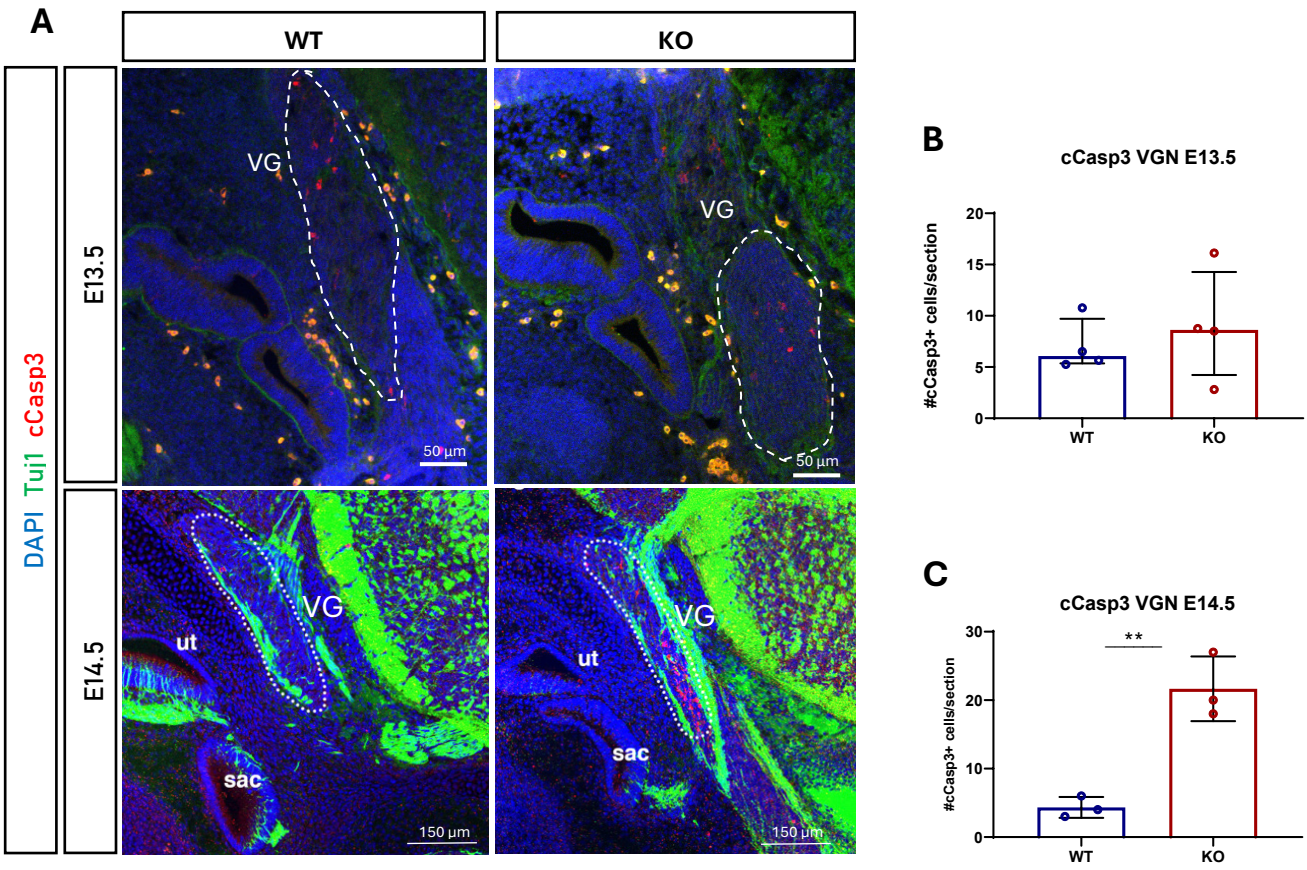

Figure 54. Assessment of apoptosis in vestibular ganglia at E13.5 and E14.5. A) Tissue of E13.5/14.5 WT and KO animals have been stained with the apoptotic marker cleaved Caspase 3 (cCasp3), the neuronal marker Tuj1 and DAPI. *VG=vestibular ganglion; ut=utricle; sac=saccule.* B) Graph showing equal levels of apoptotic neurons at E13.5 in WT and Elp3cKO. *(n=4 from 3 different litters; non-parametric Mann Whitney test; p-value=0.7).* C) Quantification of cCasp3+ cells per section showed increased number of apoptotic cells in VGN of Elp3KO animals at E14.5. *(n=3, unpaired t-test; **p-value=0.0038)*

Next, we wanted to verify that the loss of neurons is associated with the presence of Aggresome-like structures within the vestibular ganglion. Therefore, we performed Proteostat® staining on tissue sections of WT and KO heads at E14.5 and combined with Tuj1 staining to visualize the vestibular ganglion.

The figure below shows that at this stage there is a significant increase in the number of Aggresome-like structures per ganglion and per section in Elp3-depleted animals compared to controls (Figure 55A+B).

Altogether, these results show that in the vestibular ganglion, similar to the cochlea, there is a loss of VGNs at P0 induced by apoptosis starting at E14.5, likely resulting from the presence of Aggresomes at this time point. This loss of VGNs correlates with a reduced innervation of the vestibular organs (utricle, horizontal and anterior cristae) (Figure 53D).

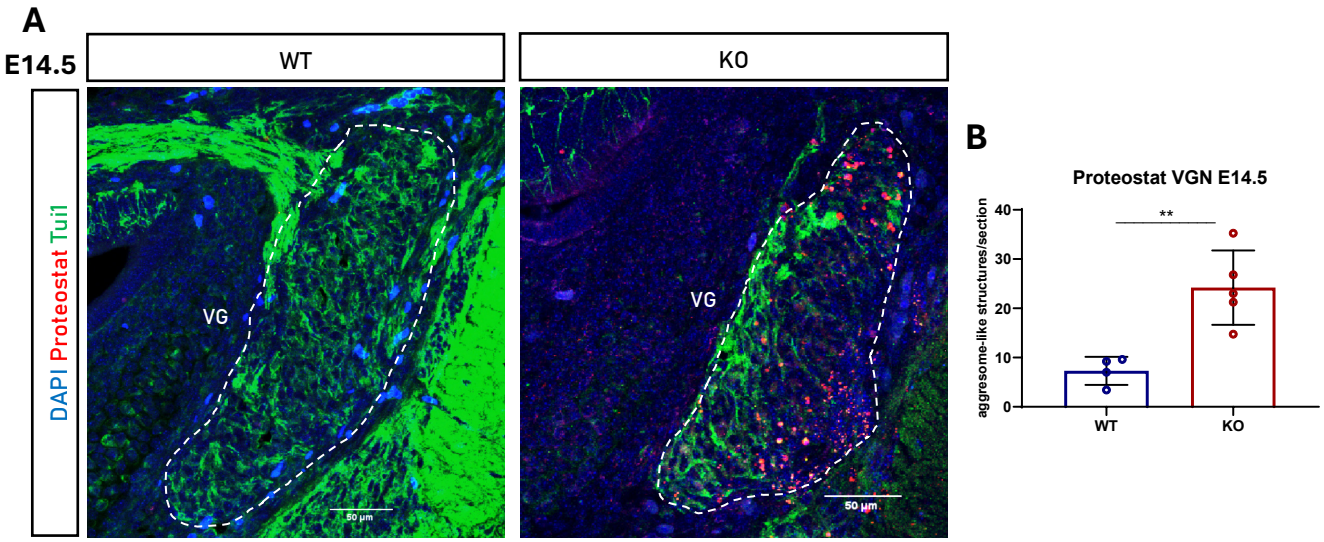

Figure 55. Aggresome staining in the vestibular ganglion at E14.5. A) Proteostat staining on tissue sections of the vestibular ganglion at E14.5 of control and KO animals. B) Quantification of the number of Aggresome-like structures per section shows a significant increase on KO samples. *(n=4/5 for WT/KO from 3 different litters, two-tailed unpaired t-test, p-value=0.0041). VG=vestibular ganglion.*

Lastly, we were able to explore whether VGN loss following embryonic apoptosis is a cell autonomous phenotype by making use of the Ngn1CreERT mouse line enabling a recombination only in the neuronal compartment without touching the sensory compartment. Tamoxifen-induced Elp3 depletion at E8.5 and E9.5, resulted in a slight but significantly increased number of cCasp3 positive cells per vestibular ganglion in KO compared to control mice (Figure 56).

This result indicates that neuronal cell death observed in the vestibule of Elp3-deficient mice is a cell autonomous process, which is likely to result from the accumulation of misfolded proteins and aggregates. Unfortunately, we could not further investigate the phenotype by quantifying and analyzing VGNs at postnatal stages using this experimental model, due to viability problems of the pups.

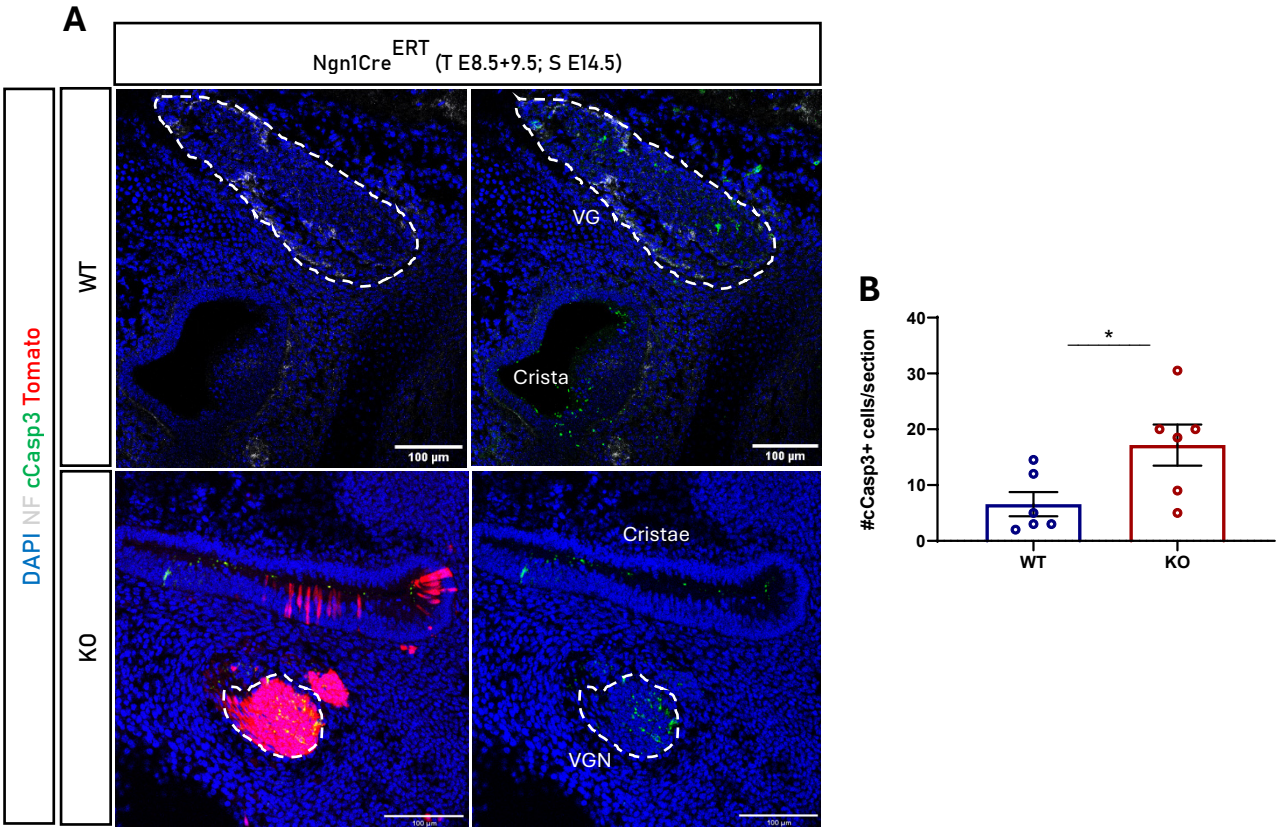

Figure 56. Determination of number of apoptotic cells at E14.5 in Ngn1Cre^{ERT2} WT and KO mice treated with Tamoxifen at E8.5 and E9.5. A) control and KO sections at E14.5 have been stained with cCasp3, NF and DAPI. Tomato is endogenously expressed. *VG=vestibular ganglion.* B) The number of apoptotic cells is significantly in VGNs of Elp3KO mice based on Immunostaining against cleaved Caspase3. *(n=6 for 4 different litters; unpaired t-test; *p-value= 0.0332)*

3. Description of the remaining neurons in Cristae

We then aimed to further characterize the remaining neurons innervating the utricle and cristae, the main organs responsible for balance sensation in case of linear and angular head movements, respectively. As we observed a loss of vestibular neuronal cell bodies at P0, we checked for the presence of Calyx synapses forming circular innervations around type I HCs, which are easily detectable in a top view of the sensory epithelium. To do this, we stained whole-mounted Cristae with an antibody directed against Myo7A and Neurofilament-H, to label respectively the HCs and the neurons including their synaptic terminals, respectively.

Performing 40x-zoomed images with several z-planes distanced by 0.5 µm, we could observe the presence of full Calyces in cristae of WT neonates (Figure 57A). Interestingly, in Elp3cKO animals these Calyx synapses were largely missing at birth throughout the sensory epithelia of the anterior,

horizontal and posterior cristae (Figure 57B). This result could indicate that calyx-forming neurons are specifically lost during Elp3KO development, however it could also point to a delayed synaptic development.

Hence, we checked if calyx synapses could be observed at later stages and our stainings indicate that calyces are present around type I HCs in P15 Elp3cKO cristae (Figure 57C). Although there is a tendency for a decreased number of total calyx synapses, this was no longer statistically different from controls, but the biological variance was high (Figure 57D).

We further analyzed them by discriminating between Calyces coming from Calyx-only neurons or from Dimorphic neurons. We combined Neurofilament staining (all Calyces) with Calb2, which labels specifically Calyx-only synapses, together with Oncomodulin to visualize central type I HCs (Figure 57D). We quantified the three kinds of neuronal populations at P15: the NF-positive Calyces surrounding Ocm-positive HCs (=Ocm+/NF+) correspond to the total number of Calyces, the NF-positive/Calb2-positive Calyces surrounding Ocm-positive HCs (=Calb2+/Ocm+/NF+) correspond to the Calyx-only synapses and the NF-positive/Calb2-negative Calyces surrounding Ocm-positive HCs (=Calb2-/Ocm+/NF+) correspond to the dimorphic Calyces.

Comparisons of the different VGN terminals only revealed a slight reduction in the number of Calyx-only synapses in the KOs but no difference regarding the number of Dimorphic synapses. At this stage, calyx synapses are thus partially restored but the relative proportion of those arising from calyx-only neurons is decreased (Figure 57E). Altogether, these results suggest a delayed maturation of vestibular neurons in Elp3-deficient cristae and an altered distribution of calyx-only versus dimorphic calyx endings. We can speculate that calyx-only neurons have been lost during embryonic stages, however it is also possible that cell death occurs for both VGN subtypes and that dimorphic neurons are able to compensate the loss of calyx synapses by forming additional branches to innervate extra type I HCs.

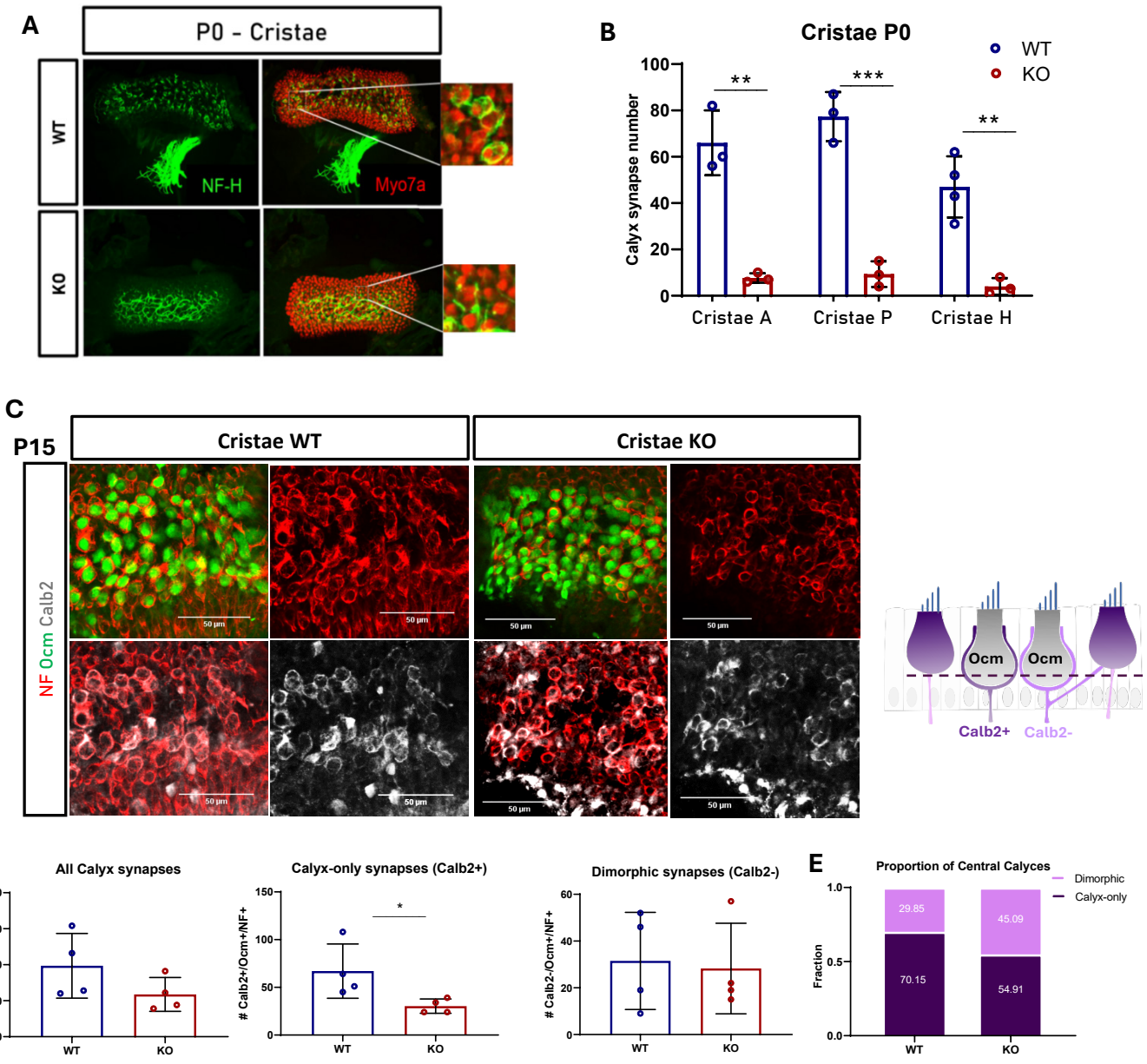

Figure 57. Evaluation of calyx synapse number in the Cristae at P0 and P15. A) Immunostaining showing Calyx synapses (Neurofilament, green) innervating HCs (Myo7A, red) in the horizontal Cristae of WT and KO mice. B) Graph showing reduced number of Calyx synapses in anterior, horizontal and posterior Cristae (AC, HC and PC, respectively) of Elp3KO animals. *(n=3 WT/KO; unpaired t-test; **p-value<0.01; ***p-value<0.0001).* C) Cristae whole mounted epithelia stained with NF (general neuronal marker), Ocm (HC type I marker) and Calb2 (Calyx-only marker). Illustration on the right show the level of the focal plane, at the level of the Calyx synapses. D) In Cristae at P15, number of Calyx-only synapses (Calb2-positive) is only slightly reduced whereas number of dimorphic Calyces (Calb2-negative) remains normal. *(n=4 from 2 different litters; Unpaired t-test; *p-value<0.05).* E) Proportion of Dimorphic and Calyx-only synapses among all Calyces in WT and KO animals.

To explain the abnormal cristae function, revealed by the circling phenotype, despite Calyx innervation recovery, we hypothesized that the signaling between the HCs type I and the restored Calyces could be dysfunctional due to an incomplete coupling between calyx terminal and HC type I. Therefore, we checked for the presence of TenascinC, an extracellular matrix (ECM) glycoprotein present in the synaptic cleft of functional Calyx synapses. Studies in rats exposed to the ototoxic compound IDPN

showed that vestibular dysfunctions correlate with calyx dismantlement following the loss of the junction protein CASPR1 and TenascinC (Sedó-Cabezón et al., 2015). To further investigate this, we performed TenascinC (TnC) staining together with Calb2 on whole mounted cristae epithelium at P15 and P20.

First, we had a closer look at the central region of control mice and observed that TnC is present in the Calb2-positive as well as Calb2-negative endings, indicating that ECM consolidates Calyces of both Calyx-only and Dimorphic neurons (Figure 58A). In contrast, Elp3cKO cristae show no TnC staining in the remaining Calb2-positive Calyces. Similarly, in the peripheral region that contains calyx synapses originating exclusively from dimorphic neurons (Calb2-negative), we also observed a massive reduction of TnC staining in KOs. This loss of synaptic ECM could be confirmed on P20 animals (Figure 58B).

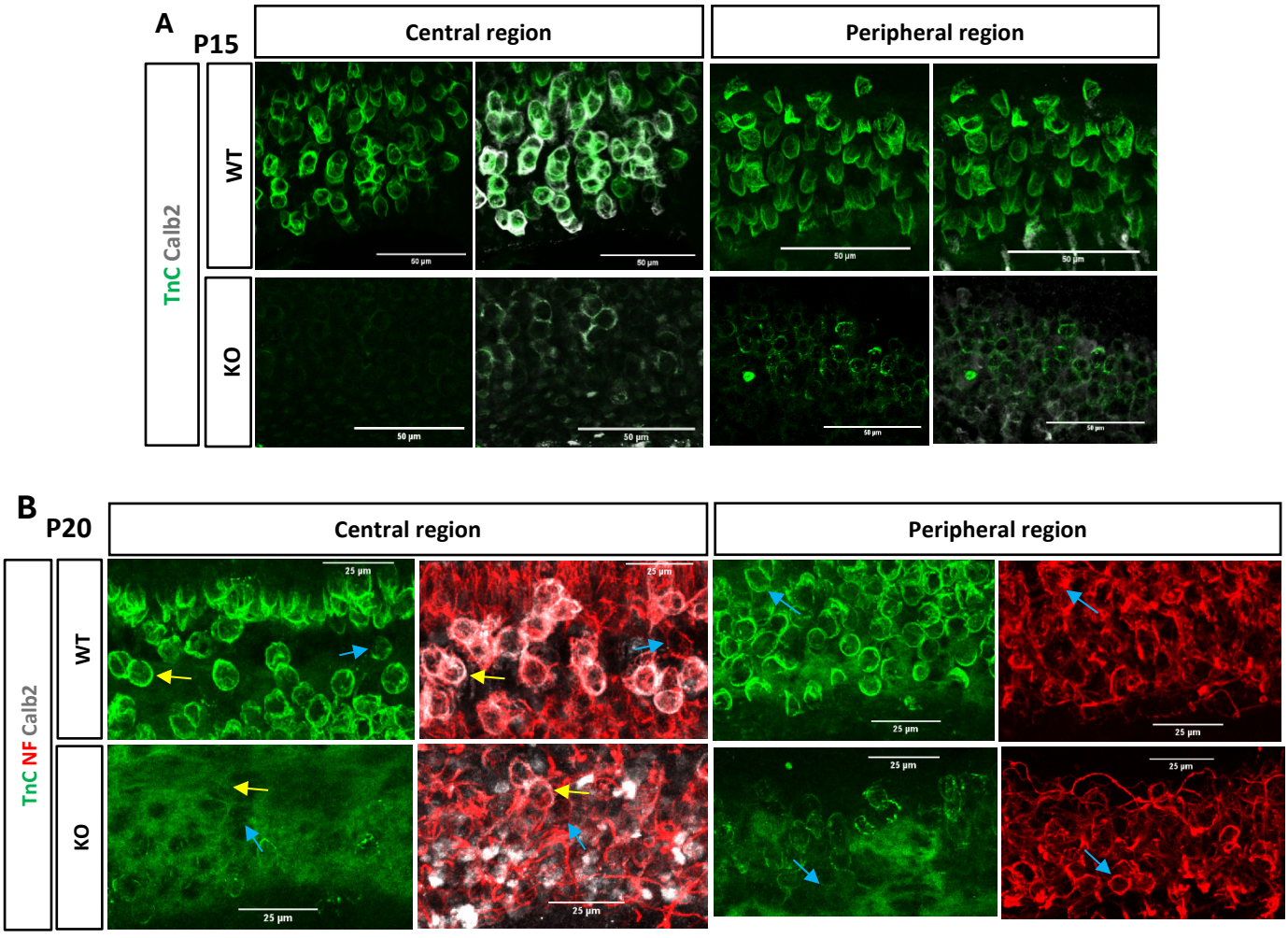

In rats exposed to vestibulotoxic IDPN, the loss of TenascinC in the Cristae was paralleled by the loss of ribbons, the presynaptic patches facing calyx terminals (Sedó-Cabezón et al., 2015). Therefore, we stained whole mounted cristae epithelia with antibodies against Ribeye and Calb2 to count the number of Ribbons per Calyceal innervation (Calb2+), in control and Elp3cKO mice (Figure 59A).

The results show that in KO animals compared to WTs the mean number of Ribbons is not statistically different, neither per Calyx-only afferent (Figure 59B), nor per Dimorphic Calyx (Figure 59C). Further experiments would be needed to verify if the number of postsynaptic patches is normal in KO animals or if the presynaptic and postsynaptic machineries are in close apposition, however the lack of TnC clearly suggests that calyx synapses are somehow abnormal. A reduced synaptic transmission between HCs and their calyceal terminals could thus explain the vestibular defects observed in the KO mice despite a restoration of the number of Calyx synapses.

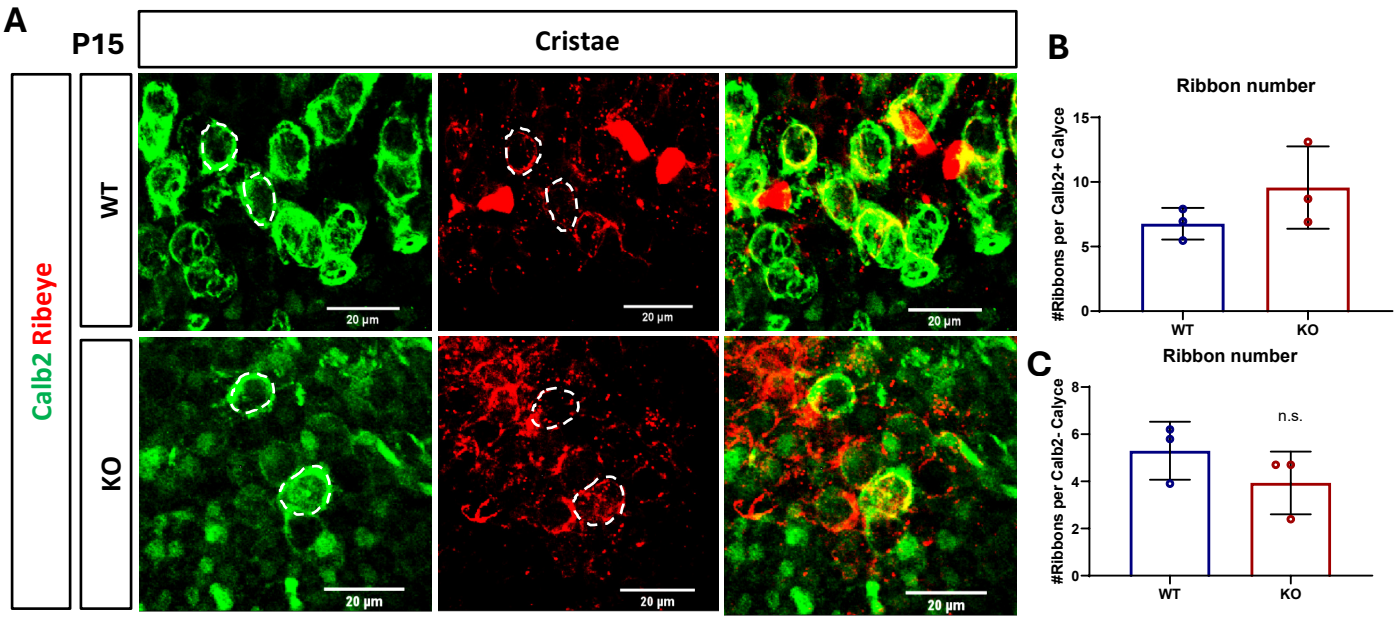

Figure 59. Counting of Ribbon synapse number in remaining Calyx-only synapses in horizontal Cristae at P15. A) Calb2 and Ribeye (presynaptic component) Immunostaining has been performed on control and KO cristae whole mounts at P15. B) The number of Ribbons per Calyx-only (Calb2+, white circle) synapse is similar in WT and Elp3cKO. *(n=3 for 3 different litters; unpaired t-test; p-value=0.2297).* C) The number of Ribbons per Dimorphic (Calb2-; yellow circle, based on NF staining not shown here) Calyx synapse is similar in WT and Elp3cKO. *(n=3 for 3 different litters; unpaired t-test; p-value=0.2609)*

4. Description of the remaining neurons in Utricles

Next, we sought to investigate the development of Calyx synapses within the macular epithelium. We focused on the utricle as its Calyx development over time has been well studied (see Warchol et al., 2019 and the introduction). Emergence of full Calyx synapses only starts around P0 in the utricle and

evolves over the first two postnatal weeks. Therefore, we performed our quantifications at P15 to evaluate the relative proportions of total Calyces (Ocm+/NF+), Calyx-only synapses (Calb2+/Ocm+/NF+) and Dimorphic Calyces (Calb2-/Ocm+/NF+).

Whereas ring-forming NF+ endings reveal numerous Calyx synapses (Calb2+ and Calb2-) surrounding Ocm+ HCs in the utricle of WT animals, only a few Calyces that are always Calb2-, are visible in KOs (Figure 60A). Our quantifications show that the total number of Calyx synapses is strongly reduced in Elp3cKO utricles, as well as the number of Calyx-only and dimorphic synapses (Figure 60B). Within the remaining calyx synapses, the proportion of Dimorphic Calyces largely predominates over Calyx-only synapses in Elp3cKO animals (Figure 60C).

To validate the loss of Calyx synapses, we analyzed 3-week-old vestibules and used another specific marker to distinguish Calyx-only from dimorphic synapses. Calb1 is known to be expressed in the same pattern as Calb2 and is additionally expressed in the cytoplasm of type I HCs leading to a positive staining of the HCs and their surrounding Calyces. Our quantifications were limited to the striolar region of the Utricle, as only synapses enwrapping Spp1-negative HCs were considered.

In control animals, we observe the presence of Calb1+ calyces surrounding Calb1+ HCs type I. These calyx-only synapses are easily identified since they appear as yellow rings in merged images (red NF signal overlapping the green Calb1 staining). In Elp3cKO animals, we can clearly see less Calyces, most of them displaying no Calb1 immunoreactivity (Figure 60D). Accordingly, the quantifications confirm the loss of Calyx synapses, as well as the significant reduction in the number of Calyx-only neurons and, to a lesser extent, of dimorphic neurons (Figure 60E).

To conclude, Elp3 depletion also affects neuronal survival and maturation in the vestibular portion of the inner ear, leading to balance function defects. Whereas Cristae innervation is delayed over the first 2 postnatal weeks and that only a slight reduction in the number of Calyx-only synapses was observed, we see a more drastic and persistent reduction of calyces in the utricle. In this vestibular organ, the loss of type I HC innervation seems to be associated with the combined loss of Calyx-only and Dimorphic afferents. Overall, the results do not underline a neuronal subtype-specific loss in the vestibule, but rather point out differential developmental processes or compensatory mechanisms between cristae and maculae.

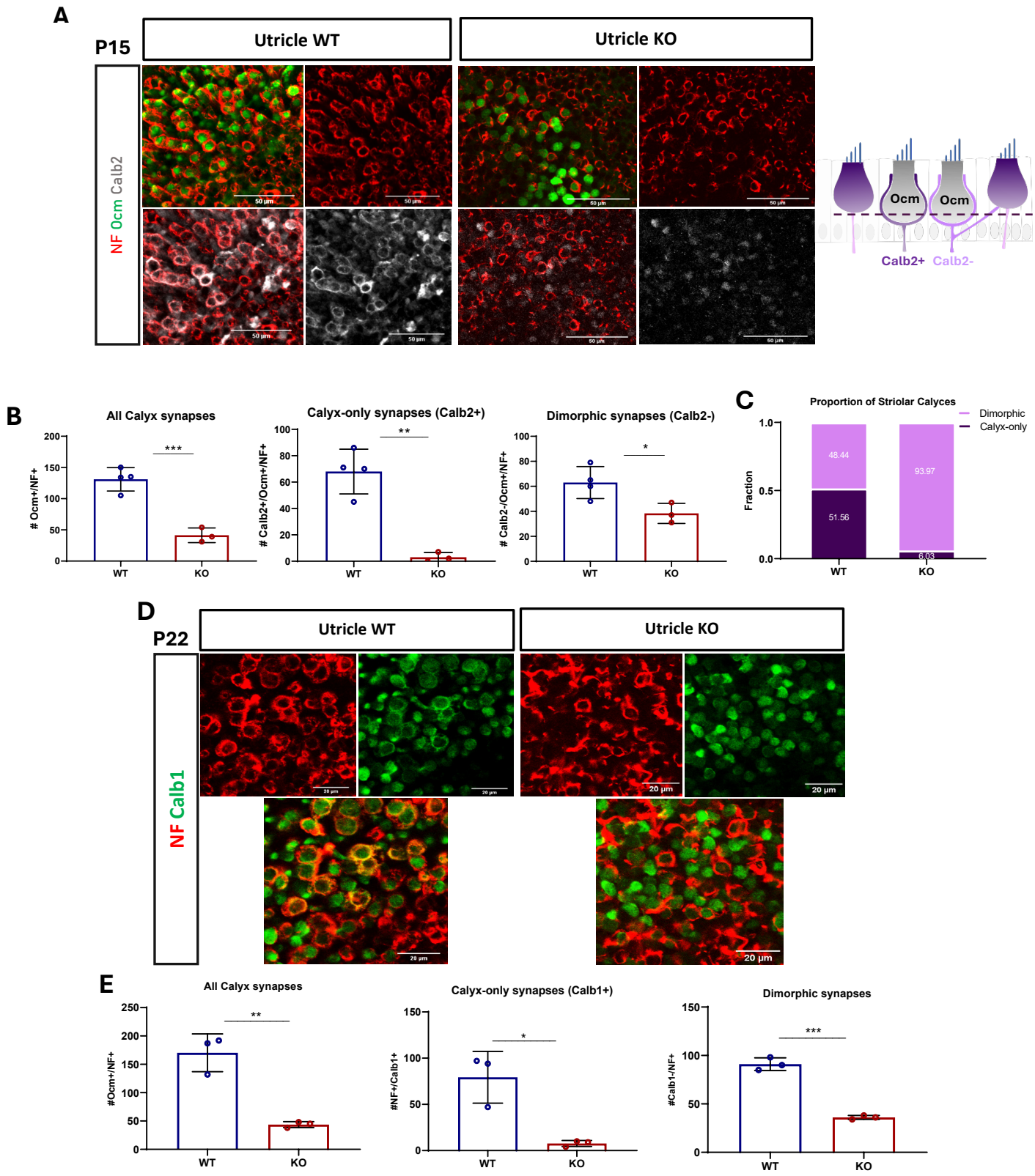

Figure 60. Counting of Calyx synapse number in Utricle at P15 and P22. A) Utricular whole mounted epithelia stained with NF (general neuronal marker), Ocm (HC type I marker) and Calb2 (Calyx-only marker). B) In Utricle at P15, both the number of Calyx-only and dimorphic synapses is strongly reduced. *(n=4 from 2 different litters; Unpaired t-test; *p-value<0.05, **p-value<0.01, ***p-value<0.001).* C) Proportion of Dimorphic and Calyx-only synapses among all Calyces in WT and KO animals. D) Utricular whole mounts stained with the Calyx-only specific marker Calb1 and the general neuronal marker NF. Calb1 labelling shows a positive staining in the Calyx synapses and the HCs type I in the WT and the absence of Calb1 signal in the KOs. E) Quantifications confirm the reduced number of Calyx synapses (Calyx-only and Dimorphic) in the Elp3cKOs. *(n=3 from 1 litter; Unpaired t-test; *p-value<0.05, **p-value<0.01, ***p-value<0.001).*

Discussion

PART I – COCHLEA

Our work demonstrates that Elp3 loss affects neuronal survival and differentiation in the whole inner ear and leads to functional defects of the hearing and balance senses. In both cochlear and vestibular portions, more than half of the neurons fail to survive during embryonic development and we showed that apoptosis is specifically induced around E14.5. We demonstrated that this otic neuronal apoptosis is cell-autonomous and we believe it is triggered by the accumulation of toxic protein aggregates as it is correlated with the presence of large aggregates of misfolded proteins within developing SGNs and VGNs. In addition, we also report that the absence of Elongator activity impairs postnatal maturation of the surviving otic neurons.

In the cochlea, the various SGN subtypes emerge normally but present altered differentiation programs after birth. The maturing Ib and Ic populations are progressively converted into SGNs expressing molecular features of the Ia subtype. Intriguingly, these Ia-like auditory neurons abnormally project to the modiolar side of IHC, where they face large ribbons. These topological and morphological characteristics of the auditory afferents are classically attributed to the Ic subtype, which is totally missing in mature Elp3cKO cochleae. Unfortunately, the lack of efficient and suitable experimental models prevented us from understanding whether skewed neuronal differentiation into Ia subtype or abnormal projection patterns could be linked to SGN intrinsic alterations or if it was instructed by the mispolarised target HCs. Furthermore, evidences that proteostasis disruption is responsible for this phenotype still remains to be provided as chaperone treatment failed to restore SGN diversity and pillar synapses.

In the vestibule, our findings demonstrate that the development of calyx-forming unit is impaired in cristae and utricle, however the phenotypes differ amongst those vestibular organs. In cristae, calyx synapse formation is delayed in Elp3-deficient animals and only a small reduction in the number of calyx arising from calyx-only neurons was observed at P15. Although the vast majority of type I HCs in the cristae are innervated by afferents, there are hints that those calyx synapses lack maturation processes as the ECM network that consolidates functional synapses is absent throughout the epithelia. Defective neurotransmission related to HC-calyx uncoupling is likely to explain the circling phenotype that was evidenced in 2 weeks-old Elp3KO mice. In the utricle, as far as we could go in development (P22), the majority of calyx synapses are missing in the sensory epithelium. We uncovered that synapses formed by calyx-only as well as dimorphic afferents were missing, suggesting that VGN from both subtypes are lost.

1. Skewed differentiation into Ia SGN and discrepancy between SGN topological and molecular characteristics

In the inner ear field, it has been known for several decades that otic neurons are characterized by specific electrophysiological characteristics, notably Ia subtypes having a low activation threshold and a high spontaneous discharge rate (SR), Ib subtypes a medium activation threshold and medium SR and Ic subtypes being low threshold and high SR fibers. Later, studies performed on cats have shown that the low threshold/high SR fibers preferentially innervate the pillar side of the IHC whereas the high threshold/low SR fibers innervate the modiolar side of the IHC. The emergence of scRNA sequencing and high throughput techniques revealed 3 subtypes of auditory neurons, displaying specific molecular signatures, which were assumed to correspond to the previously described fibers. This allowed the discovery of subtype-specific markers/tools enabling us to make a link between the molecular and morphological/physiological features. Using lineage tracing experiments, Lypd1-expressing neurons were shown to have high threshold/low SR characteristics whereas Calb2-expressing cells have a wider range of spontaneous discharge rate as they comprise Ia and Ib SGN subtypes. Altogether, those experiments demonstrate a strong correlation between morphological/physiological and molecular signature. Our findings that Elp3 depletion leads to skewed differentiation towards Ia-like SGNs, expressing Calb2 and Cacna1b, which at the same time display Ic characteristics based on the innervation location and the Ribbon size, are thus puzzling. We show that there is not a causal relationship between the molecular and topological characteristics of the SGN fibers but only a correlational, and that in specific non-physiological situations, discrepancies may exist between molecular and topological features.

In the literature, several mutants have been described to present SGN differentiation changes allowing for the predominance of Ia subtype. For instance, the depletion of the transcription factor Runx1 from the early neuronal population leads to a predominance of Ia subtypes based on their transcriptomic profile. As Runx1 is the major cell fate inducer of Ic type, its depletion even at postnatal stages, also allows the switch from Ic to Ia SGNs, indicating there is some form of plasticity even after neuronal identity acquisition. In their model, the supernumerary Ia fibers establish synaptic contacts on the modiolar side of HCs, however they retain the typical Ia features of facing small presynaptic ribbons, similar to WT pillar ribbons. The gradient of ribbon size, normally observed from modiolar to pillar side, is thus disrupted, as the remaining presynaptic Ribbons show a small size all along the basolateral side of the IHC. Similarly, the postsynaptic receptor GluA also shows a disrupted size gradient, with larger patches similar to WT pillar postsynaptic Glutamate receptors (Shrestha et al., 2023). The phenotype of Runx1KO SGNs thus contrasts with ours as the remaining SGNs in Elp3cKO, type Ia-like, all go to the wrong side of the target cell, forming large ribbons. There are 2 possible reasons for those difference. First, Runx1cKO mice do not suffer a loss of SGNs, therefore we hypothesize this is an important factor that contributes to the phenotype of an impaired modiolar-pillar proportion in our model. Second, the absence of Runx1 in their model only affects SGN

development, whereas Elp3 invalidation affects both the sensory and the neuronal compartments, meaning that the disrupted modiolar-pillar proportion could also be influenced by a defect within the HCs.

Depletion of Vglut3 from the inner hair cells also leads to the predominance of Ia subtype, but in this case, skewed differentiation is accompanied by SGN survival defects and a reduced number of neurons in the spiral ganglion (Seal et al., 2008). Impaired glutamate release affects HC-SGN communication during the prehearing period, which is thought to be instrumental for cell fate consolidation (Shrestha et al., 2018). Closer to our observations in Elp3KO mice, these mutants do not present an abolished ribbon size gradient along the modiolar-pillar axis, indicating that synaptic transmission does not affect the presynaptic heterogeneity of IHCs (Karagulyan & Moser, 2023). Overall, Elp3cKO, Runx1KO and Vglut3KO animals all show a skewed neuronal diversity with a predominance of Ia SGN subtypes. However, they all differ regarding the modiolar-pillar proportion of synapses and the synapse size gradient along the modiolar-pillar axis.

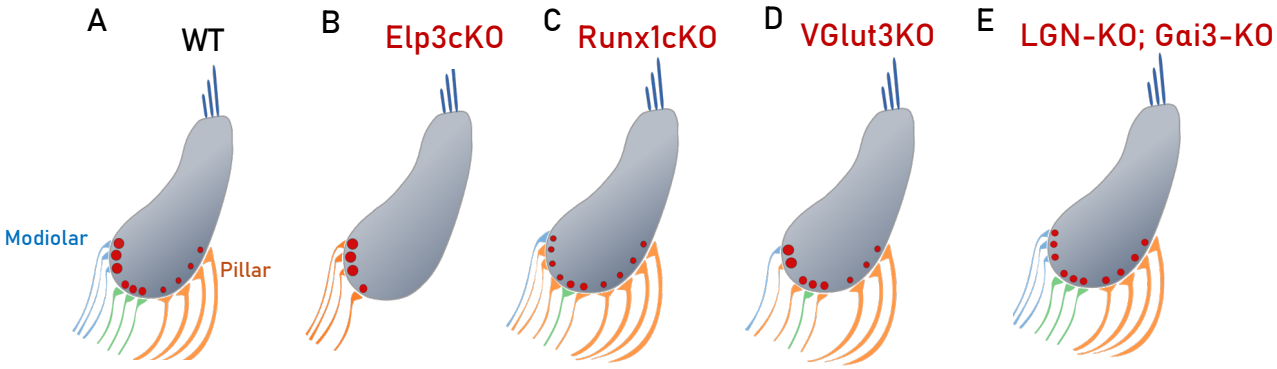

Figure 61. HC innervation and Ribbon synapse phenotypes in different mutants. A) WT mice show a 50/50 distribution of synapses on the modiolar and pillar side of the IHC. Ia SGNs (orange) innervate the pillar side, present larger postsynaptic density domains (PSDs) and face larger Ribbons, whereas Ic SGNs (blue) innervate the modiolar side, present smaller PSDs and face larger Ribbons. B) In Elp3KOs, we observed Ia-like SGNs innervating the modiolar side and facing larger Ribbons. C) Runx1KOs comprise predominantly Ia SGNs innervating pillar and modiolar side but facing smaller Ribbons with large PSDs. D) VGlut3KOs present mainly Ia SGNs with a small reduction in total SGNs (20%), but their modiolar-pillar gradient of synapse size is maintained. E) LGN and Gαi3 KOs have an abolishes modiolar-pillar gradient of synapse size.

Subtype-specific targeting of IHCs on their modiolar versus pillar poles is suggested to be governed by the combination of ligands and receptors involved in guidance and adhesion. The transcriptomic study in Petitpré 2022 identified several chemotropic signaling components/guidance factors that are highly expressed in all SGN subtypes but also some that are expressed in a subtype specific manner. CellPhoneDB analysis revealed several combinations of ligand/receptor pairs having a high score of cell-to-cell signaling between HCs and SGNs and thus potentially playing a crucial role in sensory epithelium innervation, among them the well-known Ephrin family. This raises questions concerning the final identity of the Elp3KO neurons that switched into Ia-like SGNs and whether they express the

full set of Ia genes involved in this process. Transcriptomic studies would help figuring out if some essential players in responding to pillar-specific cues could explain their mistargeting.

It is also possible that the establishment of synaptic contacts on the wrong side of target cells is linked to the birthdate of SGNs or the time at which they first contact HCs. For instance, if Ic subtype afferences emerge a little bit before Ib and Ia, they would go to the modiolar side if the concentration of common guidance cues is highest at this side, then the Ib would contact the IHC next to the Ic and the Ia would go for the pillar side. In our Elp3cKO cochlea, type Ic SGNs convert into Ia-like neurons after their initial targeting, and this could explain why peripheral processes are settled at the modiolar pole. Alternatively, mistargeting could be linked to the reduced number of fibers in Elp3KO cochleae. In the absence of other SGN subtypes, Ia-like SGNs could respond to the common cues that are enriched on the modiolar side, as there are no Ic and Ib SGNs occupying this area anymore.

Finally, the polarity defects exhibited at the apical surface of Elp3cKO HCs could reflect larger epithelial cell alterations affecting the compartmentalization of guidance and adhesion cues necessary for proper targeting. Indeed, a link between intrinsic polarity proteins (LGN, Gai3 and aPKC) and the position dependent Active Zone, as well as the synapse properties, has already been made previously (Jean et al., 2019). In this work, the authors showed that either the pharmacological inhibition of Gai signaling with PTXa or genetic ablation of Gai3 and LGN led to a collapse of the modiolar-pillar gradient of ribbon size as well as the modiolar-pillar gradient of maximal synaptic Ca2+ influx due to larger and more complex Ca2+ channel clusters. These studies suggest that mistargeting Elp3KO SGNs could be attributed to altered distribution of LGN and Gai3, however it cannot explain the phenotype of an increased Ribbon size associated with Ia-like afferents.

Overall, the cause of the SGN afferent and synapse phenotype has still to be elucidated and using SGN-specific and HC-specific mouse lines such as Islet1-Cre and Myo15Cre could help us answering this question.

1.1 Subcluster-independent loss of neurons during embryonic development

Based on the initial finding that the remaining SGNs at P15 show molecular Ia characteristics, we hypothesized that immature Ib and Ic subtypes have been lost during development in line with the results from Sanders and Kelley that described a first branching from the undifferentiated neurons into immature Ib/Ic and Ia/II subtypes. However, our RNAscope results could not recapitulate their findings at E14.5 as we could not observe an exclusive expression of Lypd1 (Ib/Ic) and Tle4 (Ia/II) in WT neurons as shown in their publication. In addition, their findings have to be taken with caution as a comprehensive validation of their scRNAseq results with an adequate number of markers seems to be missing. In contrast, our RNAscope results from E16.5 seem to be in line with the results from Petitpré et al. 2022 showing that Ic subtypes are the first to emerge from the undifferentiated neurons (and characterized by the expression of Lypd1) as they clearly show the presence of Lypd1-only

neurons in WT as well as KO mice. This supports our hypothesis of a cluster-independent loss of SGNs during early embryonic development and a subtype identity switch around birth.

1.2 Could Ia switch be a compensatory mechanism for auditory neuronal loss ?

Ia SGNs are known to contribute more than Ib or Ic SGNs to the compound action potential (CAP, measures directly the function of the cochlear nerve by placing an electrode close to the round window) threshold and amplitude of peak I due to their larger onset responses (Bourien et al., 2014), and thus a predominance of Ia subtypes without a loss of total SGNs is predicted to give an enhanced neuronal response. As such, Runx1 KO animals, with supernumerary Ia fibers, present an increased hearing sensitivity (Shrestha et al. 2023). However, it is more difficult to predict the contribution of a switch towards Ia SGNs on hearing function when 60% of the auditory neurons are lost, such as in Elp3KO mice. In case of ouabain treatments, low-SR fibers (Ic) have been shown to be highly sensitive but their loss leaves the CAP mainly unaffected (Bourien et al., 2014) whereas in case of noise-trauma it has been shown that the loss of low-SR connectivity led to a reduced suprathreshold peak I amplitude (Furman et al., 2013; Kujawa & Liberman, 2009). This discrepancy can be linked to the difference in SR cut-off defined by the authors. Whereas Bourier et al. included only the very low firing fibers in the low-SR group (<0.5 spikes/sec), in most of the noise-trauma or aging studies (Furman et al., 2013; Schmiedt et al., 1996) the authors set the cut-off much higher (18 spikes/sec) thus including also mid-SR fibers in this group. Thus, based on the results from Bourier et al., we cannot generalize that a loss of 60% of SGNs always leads to hearing impairment, it rather depends on the type of SGN which is lost that determines the impact on the hearing ability: e.g. they show that we can observe a loss of 60% of SGNs (low and mid SR fibers) and only encounter an impaired peak I amplitude, but in parallel a loss of 30% of SGNs (if it's the high-SR fibers) can be sufficient to impact the CAP threshold and peak I amplitude.

Nevertheless, we have not addressed the physiological properties of the Ia-like SGNs present in Elp3cKO animals. We cannot rule out that, despite their molecular identity, the remaining neurons would be physiologically closer to Ic subtypes. Of course, electrophysiological studies would be necessary to define if they are high or low threshold and high or low SR fibers, however we believe that the combined defects in neuronal and sensory cell compartments will prevent us from getting conclusive results on the properties of Ia-like neurons that populate Elp3cKO ganglion. In line with this, VGlut3KOs exhibiting neurotransmission defects present profound deafness evidenced at hearing onset (Seal et al., 2008) meaning that even if the subtype identity switch was supposed to compensate for the neuronal loss, this was not efficient enough.

2. Is the phenotype related to global proteostasis disruption or Elp3-specific protein mistranslation ?

As described in the introduction, Elp3 plays a crucial role in the biological function of cells, by acting as a tRNA-modifying enzyme. By adding mcm5 on the anticodon Uridine 34 of 11 tRNAs, Elongator complex facilitates the transport of those tRNAs to the ribosomal complex implicated in the translation of specific proteins. In parallel to this, Elp3 regulates the correct translation speed and fidelity, by ensuring the incorporation of the right tRNA and the smooth production of the amino acid chain allowing for an appropriate co-translational folding process. Impaired U34 modifications of tRNAs result in translation slow down, protein misfolding and accumulation of misfolded polypeptide chains that cluster into aggresome-like structures within the cell. These aggregates are toxic to cells, but they also prevent the affected proteins from being available to the pool of functional proteins.

In the nervous system, Elp3 is crucial to cortical neurogenesis and this is mainly underlined by its role in regulating protein homeostasis (Laguesse et al., 2015). Therefore, we hypothesized that the phenotype observed in the Elp3KOs within the inner ear also results from the proteostasis-regulating role of Elongator. However, 4-PBA chaperone treatment was not sufficient to restore neuronal diversity in the spiral ganglion. Noteworthy, we observed in 2 out of 4 animals an increased expression of the subtype specific markers Calb2 and Lypd1 at birth, suggesting that protein refolding offered some kind of amelioration of SGN health and differentiation process. Nonetheless, this was not sufficient to restore the normal proportions of the 3 SGN subtypes, as only the population of Double-positive neurons could be increased. In addition, this potential restoration could not be maintained throughout postnatal stages of maturation, as the results showed no difference between 4-PBA or saline-treated KOs at P15.

Of note, the variability in the outcome of 4-PBA administration to KOs was high at P15. While some animals showed a restoration of the modiolar-pillar proportion of synapses and a visible amelioration of the synapse size gradient, these effects could not be reproduced in other animals coming from different litters (and thus from different injected dams). This could suggest that 4-PBA has not been equally delivered across the litters, or that we should have tried higher concentrations, but the dose and the number of injections is similar to what has been done in other studies in the inner ear (B. Li et al., 2019) or in the brain (Jeanne et al., 2015; H. Li et al., 2018; Shimizu et al., 2014). Besides this, other chemical chaperones known to ameliorate protein misfolding could be tried in the future. An interesting candidate is TUDCA, as it has shown promising neuroprotective effects in recent preclinical and clinical studies to treat neurodegenerative diseases such as Alzheimer, Parkinson, Huntington and ALS and this mostly by alleviating ER stress and reducing UPR (reviewed in Khalaf et al., 2022; Kusaczuk, 2019). Of course, its other roles in reducing oxidative stress and protecting mitochondria could have contributed to its efficiency, but TUDCA treatment in $Cdh23^{erl/erl}$ mice was at least able to restore hearing loss and protected against ER stress-induced apoptosis of OHCs (Hu et al., 2015, 2016).

Alternatively, Elp3 could regulate cellular differentiation by ensuring the translation of specific target proteins in a codon-dependent manner. For instance, in the intestine Elp3 promotes tuft cell differentiation by regulating the codon-dependent translation of an mTorc1 inhibitor, which suppresses mTorc1 activity and ATF4 expression (Wathieu et al., 2024). Furthermore, Elp3 regulates macrophage polarization by mediating the translation of the mTORC2 activator Ric8b, in a codon-dependent manner (D. Chen et al., 2022).

One of the potential candidates for being a direct target of Elp3 involved in Ic subtype fate consolidation is Runx1, as the phenotype observed in Elp3KOs is partially comparable with the one in Runx1cKOs. Similarly, Neurod1 or Pou4f1 transcription factors, known to be involved in Ic SGNs development, could depend on Elongator activity to be properly synthesized and/or folded. Rapino et al. showed that the loss of U34-modifying enzymes, such as Elp3, leads to codon-dependent translation elongation defects, but if this leads to the aggregation of the target protein depends on the presence of specific hydrophilic motifs within the protein sequence. Proteins with a specific penta-hydrophilic amino acid pattern will aggregate upon codon-dependent translation defects and be subjected to degradation, thereby leading to reduced expression levels. The presence of hydrophilic motifs could provide an additional energetic barrier for the protein to exit the negatively charged ribosome tunnel and therefore represent a possible cause for protein misfolding and aggregation. Alternatively, the presence of charged/ampholytic hydrophilic motifs may affect protein phase behavior and liquid-liquid phase separation and thus trigger aggregation. Proteomic studies combined with transcriptomic studies would enable the identification of candidate proteins that are translationally downregulated upon the loss of Elp3, and in silico analyses could help uncovering whether their transcripts are enriched in Elp3-dependent codons and whether the candidate proteins comprise hydrophilic motifs.

A codon-bias in the transcriptional program of Ib/Ic SGN maturation compared to Ia neuronal trajectory would make them more dependent on Elp3 and would thus explain their failure to consolidate upon Elp3 deficiency. This suggests that the Ia identity is a *default* mode such that if the SGNs don't adopt a Ib/Ic fate, they will automatically switch to Ia fate. In the literature, similar cases of codon-biased translation of proteins in response to tRNA modification reprogramming have been reported in response to stress. In yeast for instance, in response to oxidative stress, the methyltransferase Trm4 mediates a codon-biased translation of proteins to better adapt to the cellular stress. In the absence of Trm4, the cells become hypersensitive to oxidative stress (Chan et al., 2012). Another example in mammalian peripheral neurons is the dependency in Elongator activity to mediate the codon-biased translation of DNA damage repair proteins. Accordingly, those genes are misregulated and DNA damage is increased in a model of Familial Dysautonomia, caused by mutations in the scaffolding subunit Elp1 (Goffena et al., 2018).

To gain further insight into the phenotype of neuronal diversity failure and uncover whether it is associated to proteotoxic stress induced by the accumulation of misfolded/aggregated proteins or if it is due to the hypotranslation of an Elp3-dependent differentiation factor, we tested alternative

experimental models. We tried to inject Tunicamycin, an ER stress inducer, during embryonic development, but this model was challenging. The compound exerted highly toxic effects during embryogenesis when used at high doses, preventing us getting viable embryos and pups for further analyses. Different doses and injection regimens were performed, however the highest concentrations allowing mice viability were not sufficient to observe canonical signs of proteotoxic stress and UPR in the cochlea. To replace the Elp3 model by another transgenic model, we could use an aggregation-prone mutant mouse line, such as SOD1 mutant, which is a model of ALS. Such proteins are known to sequester other proteins in aggresomes so that a general proteostasis disruption is induced, but nevertheless we would have to distinguish if the phenotype is due to the general accumulation of misfolded proteins or if it relates to the loss-of-function of the aggregation-prone mutant protein. A better alternative would be to use a mouse line modelling genetic mutations of Chaperones to induce general protein misfolding and aggresome formation. This could be the mouse line modelling a mutation in the Sil1 gene, encoding a nucleotide exchange factor for the ER chaperone BiP (main ER stress sensor) und thus playing an essential role as a co-chaperone. Mutations in this gene have been associated with the Marinesco-Sjögren syndrome (in 60% of the patients), a rare disease appearing during early infancy, which is characterized by cerebellar ataxia (due to Purkinje cell degeneration), cataracts, mental retardation and neuromuscular weakness. Interestingly, sensorineural hearing loss could be observed in two siblings presenting Marinesco-Sjögren syndrom (Newton, 1991) but a clearer link to the Sil1 mutation has not yet been demonstrated (Murillo-Bonilla et al., 2024).

PART II – VESTIBULE

3. Loss of Calyx-forming afferents in Elp3KO Cristae and utricle

Based on the preliminary results from the Elp3cKO vestibules, we observed that Calyx synapses are totally missing in whole mounted Cristae at P0. At this stage, Calyces are well present in control animals based on the Neurofilament staining that surrounds 60-80 type I HCS per Crista (Anterior, Posterior and Horizontal cristae). Later, when we checked the presence of Dimorphic and Calyx-only neurons at P15, a stage where synaptic connections are well mature, we observed no significant decrease for the dimorphic Calyces and only a slight decrease of the Calyx-only synapses. These findings may be interpreted as a delayed formation of calyx synapses in Elp3-deficient cristae, associated with the loss of calyx-only afferents.

However, an alternative interpretation is plausible: it is likely that dimorphic neurons are also lost during embryonic development, but they are able to compensate for the loss of calyces by extending additional branches to target extra type I HCs. Indeed, we believe that the neonatal calyces formed

around HCs in WT animals mainly arise from dimorphic afferents, since Dechesne et al. reported a temporal delay in Calb2-positive calyx-only synapse formation. Calyx-only terminals would thus be absent from the epithelium at birth and develop later on, during the first two postnatal weeks. This could suggest that the absence of calyces upon Elp3 depletion is consequent to the loss of dimorphic neurons during embryonic stages. Moreover, regarding the fact that dimorphic neurons make out the majority of the 3 VGN types within the adult sensory epithelium (central and peripheral region) whereas Calyx-only neurons only make out the minority of VGNs, we could speculate that the loss of Dimorphic neurons surely accounts for the loss of nearly 90% of calyx synapses at P0.

Restoration of calyx synapses happens in the first two postnatal weeks in the Elp3cKO Cristae and at this stage, missing calyces from calyx-only neurons was evidenced. As the neurons are normally postmitotic from E10, a mitotic proliferation of the VGNs can be excluded making it more likely that the remaining dimorphic neurons formed additional branches to innervate the remaining type I HCs. As this type of neuron has already the capacity to make numerous branches (20-30), this idea of a restoration of Calyx synapses by additional branching formation by the dimorphic neurons is not impossible. Additional experiments using Calb2 and NF staining to track each individual fiber in whole cristae organs would be necessary to support this hypothesis, however the high density of neuronal afferents in the vestibular organ and the high number of branches per fiber makes it quite challenging. Therefore, sparse labelling of the vestibular afferents would be necessary to track individual fibers (AAV viral transfections at low titrations expressing GFP could help).

Whereas in Cristae of Elp3cKO animals, we observed a partial restoration of Calyx synapses at P15, particularly from Dimorphic afferents, there was no restoration at all in the utricle at P15 and P22. In fact, the Calyx-only synapses (Calb2+) are more pronouncedly affected (with a nearly 90% reduction) than the dimorphic (50% reduction), which could give a hint that the Calb2+ VGNs innervating the utricle are preferentially lost during development compared to the dimorphic VGNs.

4. Calyx innervation restoration in the Cristae without a recuperation of Cristae-specific vestibular functions

One of the main questions is why the Elp3 mutant mice show a partial restoration of Calyx innervation in the Cristae, and in parallel presents circling behaviors, which can be attributed to a disturbed Cristae function. One of our hypotheses was that the transmission of the balance signal must be inefficient or incomplete between the HC and the Calyx synapses. We were able to show that TenascinC, an extracellular matrix junction protein present in the synaptic cleft and assuring the HC-Calyx junction, is strongly reduced within calyx synapses. Interestingly, disruption of this ECM network following ototoxic IDPN exposure is accompanied by a complete dismantlement of the calyx synapses

and an altered distribution of the pre and postsynaptic components Ribeye and PSD-95/GluA2, respectively. Interestingly, the authors showed that there might be a causal link between the vestibular dysfunctions and the loss of the junction proteins as well as the synapses by performing a washout period after the toxication phase. During this washout phase, the vestibular function could be reestablished and the junction proteins TenascinC and CASPR1 showed a near normal recovery. In addition, the Ribeye puncta per Calyx showed a better recovery than the post-synaptic puncta, and the toxic effect was stronger on PSD-95 than on GluA2 (Sedo et al., 2016). The role of TenascinC in synaptic coupling and function has already been demonstrated in the brain, as TnC mutant mice showed an increased inhibitory input in the dentate gyrus of the hippocampus of male mice (Jakovljević et al., 2024), and exposure to an enriched environment (EE) leads to an increase in the size of inhibitory synaptic terminals in TnC deficient mice (Stamenkovic et al., 2016), hinting that it plays a crucial role in fine-tuning excitation and inhibition in the brain.

Future experiments would be needed to verify that the lack of TnC in the calyx synapses impacts their structural organization and functionality. For instance, we would need to check by electron microscopy the architecture of the remaining Calyx synapses and study in further detail the presence of synaptic components as until now we were not able to study the colocalization of pre- and postsynaptic units.

Nevertheless, we still have to keep in mind that circling behavior can also be due to an imbalance of the forebrain dopamine system (Willis & Kennedy, 2004), which is a possibility not to be neglected in our model since Foxg1Cre enables a recombination in the forebrain during embryonic development (Hébert & McConnell, 2000). To exclude this possibility, Vestibular evoked potentials (VsEP, the vestibular pendant to ABRs) could be performed as they reflect the vestibular afferent nerve response. Briefly, a movement of the head of the animal is induced and the electrophysiological response is recorded giving a similar wave profile than ABRs with a first peak reflecting the vestibular afferent (peripheral) nerve response and the later peaks originating from the central nerves (whose exact sources within the brain is less well defined). However, it is less clear during recording from which end-organ (utricle, saccule or semicircular canals) the response originates from, it is generally assumed that it's mostly a response coming from the otolith organs with a potential contribution from the SCCs (reviewed in Brown et al., 2017). However, this would complicate the interpretation of the results as we observe different calyx innervation phenotypes in SCCs and utricles.

5. Clinical relevance and perspectives

Our team previously unveiled a link between proteostasis, cochlear development and hearing function. With this study, we report that vestibule integrity and balance function are similarly reliant on Elongator activity and on a healthy proteome during VGN development. To date, variants of genes encoding Elongator subunits have been associated with several neurodegenerative diseases

(reviewed in (Nguyen et al., 2010), and vestibular deficits were reported in patients suffering Familial Dysautonomia, a sensory and autonomic neuropathy caused by Elp1 mutation (Gutiérrez et al., 2018; Siggers et al., 1975). Affected patients present postural imbalance that worsens when placed in the dark or on uneven ground, which is a clinical sign of vestibular impairments (Kheradmand et al., 2016). Strikingly, histopathological studies performed on post-mortem inner ears demonstrate a significant loss of VGN in superior and inferior divisions of the vestibular nerve (N et al., 1978). To the best of our knowledge, hearing loss has never been associated to Familial Dysautonomia, however it should be noted that Elp1 causal mutation induces exon skipping and subsequent protein loss in a tissue-specific manner. Whether Elp1 mutation would impact alternative splicing and lead to Elongator loss of function in the cochlea remains unknown. In contrast, Elp3 gene is a disease-modifying gene affecting the risk, onset and severity of Amyotrophic Lateral Sclerosis, a disorder that has been linked to a few cases of sensorineural hearing loss (Philippou & Joubert, 2013).

Compromised proteostasis in developing otic neurons may arise from numerous factors, including genetic variations in protein quality control components (chaperones, protein translation and degradation systems, UPR, …), aggregation-prone mutants, viral infections (Isler et al., 2005; S. Liu et al., 2023) or ototoxic drugs such as cisplatin (Qu et al., 2023) and aminoglycosides (Oishi et al., 2015). It is thus likely that future studies will highlight some of those factors as newly described contributors to congenital hearing loss and vestibular disorders.

Conclusion and Perspectives

Whereas spiral ganglion neurons have long been known to present specific morphological and electrophysiological characteristics, only recently and thanks to the emergence of transcriptomic studies, they have been proven to show specific molecular signatures. This opened the door to new molecular tools to study the importance of each neuronal subtype in hearing function and their vulnerability towards external factors.

We could show that the depletion of Elp3 in the developing mouse inner ear affects neuronal survival and correct subtype specification resulting in complete deafness. By performing RNAscope with subtype specific markers at different developmental and postnatal stages, we were able to prove that spiral ganglion neurons do not show a subtype-specific vulnerability towards proteotoxic stress as until E18.5, Elp3-depleted SGN subtypes show normal expression patterns of the subtype specific markers. However, Ib and Ic subtypes start to change their molecular signature at birth by expressing Ia-specific markers in a base-to-apex gradient. Intriguingly, 3D reconstruction analysis demonstrated that these Ia-like SGNs abnormally innervate the modiolar side and face larger Ribbon synapses, a feature typical for Ic subtypes. This discrepancy of molecular and topological features has, to the best of our knowledge, not been described in this way in the literature. Transcriptomic and electrophysiological studies would be necessary to fully characterize the identity of the remaining SGNs, which remains technically highly challenging. Additionally, as we were not able to determine if the phenotype of mis-differentiated SGNs originates from the neuronal or HC compartment, future experiments are still necessary to unravel this.

Elp3 invalidation in the vestibular organs led to balance defects, a loss of vestibular ganglion neurons and Calyx-innervation defects that are more pronounced at the level of the maculae compared to the Cristae Ampullaris. In the Cristae, we evidence a moderate loss of Calyx-only synapses, suggesting a specific loss of the calyx-only afferents, however it remains possible that Dimorphic neurons are also affected but manage to compensate for their loss by forming supplementary branches. Transcriptomic studies would first be necessary to identify subtype specific markers that could help discriminating VGN nuclear bodies in order to characterize the proportional loss of these subtypes at the level of the vestibular ganglion. Additionally, lineage tracing studies or sparse labeling of individual neurons would help to prove for an increased branching of the Dimorphic neurons confirming a compensatory innervation process. Besides this, we showed that Elp3KO Cristae completely lack the ECM protein TenascinC suggesting a Calyx synapse uncoupling from HCs type I likely explaining the observed vestibular behavioral defects. In the utricle, we observed a major loss of Calyx-only synapses and a less pronounced loss of Dimorphic synapses, suggesting that VGNs from both Calyx-forming subtypes are affected.

References

Appler, J. M., Lu, C. C., Druckenbrod, N. R., Yu, W. M., Koundakjian, E. J., & Goodrich, L. V. (2013). Gata3 is a critical regulator of cochlear wiring. *Journal of Neuroscience*, *33*(8), 3679–3691. https://doi.org/10.1523/JNEUROSCI.4703-12.2013

Baker, T. G., Roy, S., Brandon, C. S., Kramarenko, I. K., Francis, S. P., Taleb, M., Marshall, K. M., Schwendener, R., Lee, F. S., & Cunningham, L. L. (2015). Heat shock protein-mediated protection against Cisplatin-induced hair cell death. *Journal of the Association for Research in Otolaryngology : JARO*, *16*(1), 67–80. https://doi.org/10.1007/S10162-014-0491-7

Barrionuevo, F., Naumann, A., Bagheri-Fam, S., Speth, V., Taketo, M. M., Scherer, G., & Neubüser, A. (2008). Sox9 is required for invagination of the otic placode in mice. *Developmental Biology*, *317*(1), 213–224. https://doi.org/10.1016/j.ydbio.2008.02.011

Bauer, F., & Hermand, D. (2012). A coordinated codon-dependent regulation of translation by Elongator. *Cell Cycle*, *11*(24), 4524. https://doi.org/10.4161/CC.22689

Bedolla, A. M., McKinsey, G. L., Ware, K., Santander, N., Arnold, T. D., & Luo, Y. (2024). A comparative evaluation of the strengths and potential caveats of the microglial inducible CreER mouse models. *Cell Reports*, *43*(1), 113660. https://doi.org/10.1016/J.CELREP.2023.113660

Bento-Abreu, A., Jager, G., Swinnen, B., Rué, L., Hendrickx, S., Jones, A., Staats, K. A., Taes, I., Eykens, C., Nonneman, A., Nuyts, R., Timmers, M., Silva, L., Chariot, A., Nguyen, L., Ravits, J., Lemmens, R., Cabooter, D., Van Den Bosch, L., … Robberecht, W. (2018). Elongator subunit 3 (ELP3) modifies ALS through tRNA modification. *Human Molecular Genetics*, *27*(7), 1276–1289. https://doi.org/10.1093/hmg/ddy043

Bermingham, N. A., Hassan, B. A., Price, S. D., Vollrath, M. A., Ben-Arie, N., Eatock, R. A., Bellen, H. J., Lysakowski, A., & Zoghbi, H. Y. (1999). Math 1: An essential gene for the generation of inner ear hair cells. *Science*, *284*(5421), 1837–1841. https://doi.org/10.1126/science.284.5421.1837

Bernard, P., Tang, P., Liu, S., Dewing, P., Harley, V. R., & Vilain, E. (2003). *Dimerization of SOX9 is required for chondrogenesis, but not for sex determination*. https://doi.org/10.1093/hmg/ddg182

Bird, J. E., Daudet, N., Warchol, M. E., & Gale, J. E. (2010). Supporting Cells Eliminate Dying Sensory Hair Cells to Maintain Epithelial Integrity in the Avian

Inner Ear. *Journal of Neuroscience*, *30*(37), 12545–12556. https://doi.org/10.1523/JNEUROSCI.3042-10.2010

Boettger, T., Hübner, C. A., Maier, H., Rust, M. B., Beck, F. X., & Jentsch, T. J. (2002). Deafness and renal tubular acidosis in mice lacking the K-Cl co-transporter Kcc4. *Nature*, *416*(6883), 874–878. https://doi.org/10.1038/416874a

Bonnet Wersinger, D., Benkafadar, N., Jagodzinska, J., Hamel, C., Tanizawa, Y., Lenaers, G., & Delettre, C. (2014). Impairment of visual function and retinal ER stress activation in Wfs1-deficient mice. *PloS One*, *9*(5). https://doi.org/10.1371/JOURNAL.PONE.0097222

Bourien, J., Tang, Y., Batrel, C., Huet, A., Lenoir, M., Ladrech, S., Desmadryl, G., Nouvian, R., Puel, J. L., & Wang, J. (2014). Contribution of auditory nerve fibers to compound action potential of the auditory nerve. *Journal of Neurophysiology*, *112*(5), 1025–1039. https://doi.org/10.1152/JN.00738.2013/ASSET/IMAGES/LARGE/Z9K01614253 50010.JPEG

Brehme, M., Voisine, C., Rolland, T., Wachi, S., Soper, J. H., Zhu, Y., Orton, K., Villella, A., Garza, D., Vidal, M., Ge, H., & Morimoto, R. I. (2014). A chaperome subnetwork safeguards proteostasis in aging and neurodegenerative disease. *Cell Reports*, *9*(3), 1135–1150. https://doi.org/10.1016/J.CELREP.2014.09.042

Brown, D. J., Pastras, C. J., & Curthoys, I. S. (2017). Electrophysiological measurements of peripheral vestibular function—A review of electrovestibulography. *Frontiers in Systems Neuroscience*, *11*, 262226. https://doi.org/10.3389/FNSYS.2017.00034/BIBTEX

Bucks, S. A., Cox, B. C., Vlosich, B. A., Manning, J. P., Nguyen, T. B., & Stone, J. S. (2017). Supporting cells remove and replace sensory receptor hair cells in a balance organ of adult mice. *ELife*, *6*. https://doi.org/10.7554/ELIFE.18128

Burns, J. C., Kelly, M. C., Hoa, M., Morell, R. J., & Kelley, M. W. (2015). Single-cell RNA-Seq resolves cellular complexity in sensory organs from the neonatal inner ear. *Nature Communications*, *6*, 8557. https://doi.org/10.1038/NCOMMS9557

Burns, J. C., On, D., Baker, W., Collado, M. S., & Corwin, J. T. (2012). Over half the hair cells in the mouse utricle first appear after birth, with significant numbers originating from early postnatal mitotic production in peripheral and striolar growth zones. *JARO - Journal of the Association for Research in Otolaryngology*, *13*(5), 609–627. https://doi.org/10.1007/S10162-012-0337-0/FIGURES/9

Carey, J. P., Fuchs, A. F., & Rubel, E. W. (1996). Hair cell regeneration and recovery of the vestibuloocular reflex in the avian vestibular system. *Journal of Neurophysiology*, *76*(5), 3301–3312. https://doi.org/10.1152/JN.1996.76.5.3301

Chan, C. T. Y., Pang, Y. L. J., Deng, W., Babu, I. R., Dyavaiah, M., Begley, T. J., & Dedon, P. C. (2012). Reprogramming of tRNA modifications controls the oxidative stress response by codon-biased translation of proteins. *Nature Communications*, *3*, 937. https://doi.org/10.1038/NCOMMS1938

Chen, D., Nemazanyy, I., Peulen, O., Shostak, K., Xu, X., Tang, S. C., Wathieu, C., Turchetto, S., Tielens, S., Nguyen, L., Close, P., Desmet, C., Klein, S., Florin, A., Büttner, R., Petrellis, G., Dewals, B., & Chariot, A. (2022). Elp3-mediated codon-dependent translation promotes mTORC2 activation and regulates macrophage polarization . *The EMBO Journal*, *41*(18). https://doi.org/10.15252/EMBJ.2021109353/SUPPL_FILE/EMBJ2021109353-SUP-00112-SDATAEV.ZIP

Chen, P., Johnson, J. E., Zoghbi, H. Y., & Segil, N. (2002). The role of Math1 in inner ear development: Uncoupling the establishment of the sensory primordium from hair cell fate determination. *Development*, *129*(10).

Chin, L., Olzmann, J., & Li, L. (2008). Aggresome Formation and Neurodegenerative Diseases: Therapeutic Implications. *Current Medicinal Chemistry*, *15*(1), 47. https://doi.org/10.2174/092986708783330692

Chou, C. C., Zhang, Y., Umoh, M. E., Vaughan, S. W., Lorenzini, I., Liu, F., Sayegh, M., Donlin-Asp, P. G., Chen, Y. H., Duong, D. M., Seyfried, N. T., Powers, M. A., Kukar, T., Hales, C. M., Gearing, M., Cairns, N. J., Boylan, K. B., Dickson, D. W., Rademakers, R., … Rossoll, W. (2018). TDP-43 pathology disrupts nuclear pore complexes and nucleocytoplasmic transport in ALS/FTD. *Nature Neuroscience*, *21*(2), 228–239. https://doi.org/10.1038/S41593-017-0047-3

Ciryam, P., Tartaglia, G. G., Morimoto, R. I., Dobson, C. M., & Vendruscolo, M. (2013). Widespread aggregation and neurodegenerative diseases are associated with supersaturated proteins. *Cell Reports*, *5*(3), 781–790. https://doi.org/10.1016/J.CELREP.2013.09.043

Copley, C. O., Duncan, J. S., Liu, C., Cheng, H., & Deans, M. R. (2013). Postnatal refinement of auditory hair cell planar polarity deficits occurs in the absence of Vangl2. *The Journal of Neuroscience : The Official Journal of the Society for Neuroscience*, *33*(35), 14001–14016. https://doi.org/10.1523/JNEUROSCI.1307-13.2013

Cortez, L., & Sim, V. (2014). The therapeutic potential of chemical chaperones in protein folding diseases. *Prion*, *8*(2), 197–202. https://doi.org/10.4161/PRI.28938

Costalupes, J. A., Young, E. D., & Gibson, D. J. (1984). Effects of continuous noise backgrounds on rate response of auditory nerve fibers in cat. *Https://Doi.Org/10.1152/Jn.1984.51.6.1326*, *51*(6), 1326–1344. https://doi.org/10.1152/JN.1984.51.6.1326

Creppe, C., Malinouskaya, L., Volvert, M. L., Gillard, M., Close, P., Malaise, O., Laguesse, S., Cornez, I., Rahmouni, S., Ormenese, S., Belachew, S., Malgrange, B., Chapelle, J. P., Siebenlist, U., Moonen, G., Chariot, A., & Nguyen, L. (2009). Elongator controls the migration and differentiation of cortical neurons through acetylation of alpha-tubulin. *Cell*, *136*(3), 551–564. https://doi.org/10.1016/J.CELL.2008.11.043

Curthoys, I. S., MacDougall, H. G., Vidal, P. P., & de Waele, C. (2017). Sustained and transient vestibular systems: A physiological basis for interpreting vestibular function. *Frontiers in Neurology*, *8*(MAR), 254700. https://doi.org/10.3389/FNEUR.2017.00117/BIBTEX

Dabdoub, A., Puligilla, C., Jones, J. M., Fritzsch, B., Cheah, K. S. E., Pevny, L. H., & Kelley, M. W. (2008). Sox2 signaling in prosensory domain specification and subsequent hair cell differentiation in the developing cochlea. *Proceedings of the National Academy of Sciences of the United States of America*, *105*(47), 18395–18401. https://doi.org/10.1073/pnas.0808175105

Daudet, N., Ariza-McNaughton, L., & Lewis, J. (2007). Notch signalling is needed to maintain, but not to initiate, the formation of prosensory patches in the chick inner ear. *Development*, *134*(12), 2369–2378. https://doi.org/10.1242/dev.001842

Dause, T. J., & Kirby, E. D. (2020). Poor Concordance of Floxed Sequence Recombination in Single Neural Stem Cells: Implications for Cell Autonomous Studies. *ENeuro*, *7*(2). https://doi.org/10.1523/ENEURO.0470-19.2020

Dechesne, C. J., Rabejac, D., & Desmadryl, G. (1994). Development of calretinin immunoreactivity in the mouse inner ear. *Journal of Comparative Neurology*, *346*(4), 517–529. https://doi.org/10.1002/CNE.903460405

Dechesne, C. J., Thomasset, M., Brehier, A., & Sans, A. (1988). Calbindin (CaBP 28 kDa) localization in the peripheral vestibular system of various vertebrates. *Hearing Research*, *33*(3), 273–278. https://doi.org/10.1016/0378-5955(88)90157-8

Delaunay, S., Rapino, F., Tharun, L., Zhou, Z., Heukamp, L., Termathe, M., Shostak, K., Klevernic, I., Florin, A., Desmecht, H., Desmet, C. J., Nguyen, L., Leidel, S. A., Willis, A. E., Büttner, R., Chariot, A., & Close, P. (2016). Elp3 links tRNA modification to IRES-dependent translation of LEF1 to sustain metastasis in breast cancer. *The Journal of Experimental Medicine*, *213*(11), 2503–2523. https://doi.org/10.1084/JEM.20160397

Desmadryl, G., & Dechesne, C. J. (1992). Calretinin immunoreactivity in chinchilla and guinea pig vestibular end organs characterizes the calyx unit subpopulation. *Experimental Brain Research*, *89*(1), 105–108. https://doi.org/10.1007/BF00229006

Eatock, R. A., Rusch, A., Lysakowski, A., & Saeki, M. (1998). Hair Cells in Mammalian Utricles. *Otolaryngology–Head and Neck Surgery*, *119*(3), 172–181. https://doi.org/10.1016/S0194-5998(98)70052-X

Eatock, R. A., & Songer, J. E. (2011). Vestibular hair cells and afferents: Two channels for head motion signals. *Annual Review of Neuroscience*, *34*(Volume 34, 2011), 501–534. https://doi.org/10.1146/ANNUREV-NEURO-061010-113710/CITE/REFWORKS

Elder, G. A., Friedrich, V. L., Kang, C., Bosco, P., Gourov, A., Tu, P. H., Zhang, B., Lee, V. M. Y., & Lazzarini, R. A. (1998). Requirement of heavy neurofilament subunit in the development of axons with large calibers. *Journal of Cell Biology*, *143*(1), 195–205. https://doi.org/10.1083/jcb.143.1.195

Esberg, A., Huang, B., Johansson, M. J. O., & Byström, A. S. (2006). Elevated levels of two tRNA species bypass the requirement for elongator complex in transcription and exocytosis. *Molecular Cell*, *24*(1), 139–148. https://doi.org/10.1016/J.MOLCEL.2006.07.031

Evsen, L., Sugahara, S., Uchikawa, M., Kondoh, H., & Wu, D. K. (2013). Progression of neurogenesis in the inner ear requires inhibition of Sox2 transcription by neurogenin1 and neurod1. *The Journal of Neuroscience : The Official Journal of the Society for Neuroscience*, *33*(9), 3879–3890. https://doi.org/10.1523/JNEUROSCI.4030-12.2013

Fedyukina, D. V., & Cavagnero, S. (2011). Protein folding at the exit tunnel. *Annual Review of Biophysics*, *40*(1), 337–359. https://doi.org/10.1146/ANNUREV-BIOPHYS-042910-155338

Fernandez, C., Goldberg, J. M., & Baird, R. A. (1990). The vestibular nerve of the chinchilla. III. Peripheral innervation patterns in the utricular macula. *Https://Doi.Org/10.1152/Jn.1990.63.4.767*, *63*(4), 767–780. https://doi.org/10.1152/JN.1990.63.4.767

Flores, E. N., Duggan, A., Madathany, T., Hogan, A. K., Márquez, F. G., Kumar, G., Seal, R. P., Edwards, R. H., Liberman, M. C., & García-Añoveros, J. (2015). A non-canonical pathway from cochlea to brain signals tissue-damaging noise. *Current Biology : CB*, *25*(5), 606–612. https://doi.org/10.1016/J.CUB.2015.01.009

Fonseca, S. G., Fukuma, M., Lipson, K. L., Nguyen, L. X., Allen, J. R., Oka, Y., & Urano, F. (2005). WFS1 is a novel component of the unfolded protein response and maintains homeostasis of the endoplasmic reticulum in pancreatic beta-cells. *The Journal of Biological Chemistry*, *280*(47), 39609–39615. https://doi.org/10.1074/JBC.M507426200

Forge, A., Li, L., Corwin, J. T., & Nevill, G. (1993). Ultrastructural evidence for hair cell regeneration in the mammalian inner ear. *Science (New York, N.Y.)*, *259*(5101), 1616–1619. https://doi.org/10.1126/SCIENCE.8456284

Freeman, S., Mateo Sánchez, S., Pouyo, R., Van Lerberghe, P., Hanon, K., Thelen, N., Thiry, M., Morelli, G., Van Hees, L., Laguesse, S., Chariot, A., Nguyen, L., Delacroix, L., & Malgrange, B. (2019). Proteostasis is essential during cochlear development for neuron survival and hair cell polarity. *EMBO Reports*, *20*(9), 1–20. https://doi.org/10.15252/embr.201847097

Fritzsch, B., Matei, V. A., Nichols, D. H., Bermingham, N., Jones, K., Beisel, K. W., & Wang, V. Y. (2005). Atoh1 null mice show directed afferent fiber growth to undifferentiated ear sensory epithelia followed by incomplete fiber retention. *Developmental Dynamics*, *233*(2), 570–583. https://doi.org/10.1002/DVDY.20370

Fujinami, Y., Mutai, H., Mizutari, K., Nakagawa, S., & Matsunaga, T. (2012). A Novel Animal Model of Hearing Loss Caused by Acute Endoplasmic Reticulum Stress in the Cochlea. *Journal of Pharmacological Sciences*, *118*(3), 363–372. https://doi.org/10.1254/JPHS.11227FP

Furman, A. C., Kujawa, S. G., & Charles Liberman, M. (2013). Noise-induced cochlear neuropathy is selective for fibers with low spontaneous rates. *Journal of Neurophysiology*, *110*(3), 577. https://doi.org/10.1152/JN.00164.2013

Gaik, M., Kojic, M., Stegeman, M. R., Öncü-Öner, T., Kościelniak, A., Jones, A., Mohamed, A., Chau, P. Y. S., Sharmin, S., Chramiec-Głąbik, A., Indyka, P., Rawski, M., Biela, A., Dobosz, D., Millar, A., Chau, V., Ünalp, A., Piper, M., Bellingham, M. C., … Glatt, S. (2022). Functional divergence of the two Elongator subcomplexes during neurodevelopment. *EMBO Molecular Medicine*, *14*(7). https://doi.org/10.15252/EMMM.202115608

Géléoc, G. S. G., Risner, J. R., & Holt, J. R. (2004). Developmental acquisition of voltage-dependent conductances and sensory signaling in hair cells of the embryonic mouse inner ear. *The Journal of Neuroscience : The Official Journal of the Society for Neuroscience*, *24*(49), 11148–11159. https://doi.org/10.1523/JNEUROSCI.2662-04.2004

George, L., Chaverra, M., Wolfe, L., Thorne, J., Close-Davis, M., Eibs, A., Riojas, V., Grindeland, A., Orr, M., Carlson, G. A., & Lefcort, F. (2013). Familial dysautonomia model reveals Ikbkap deletion causes apoptosis of Pax3+ progenitors and peripheral neurons. *Proceedings of the National Academy of Sciences of the United States of America*, *110*(46), 18698–18703. https://doi.org/10.1073/PNAS.1308596110/-/DCSUPPLEMENTAL/PNAS.201308596SI.PDF

Glowatzki, E., Cheng, N., Hiel, H., Yi, E., Tanaka, K., Ellis-Davies, G. C. R., Rothstein, J. D., & Bergles, D. E. (2006). The glutamate-aspartate transporter GLAST mediates glutamate uptake at inner hair cell afferent synapses in the mammalian cochlea. *The Journal of Neuroscience : The Official Journal of the Society for Neuroscience*, *26*(29), 7659–7664. https://doi.org/10.1523/JNEUROSCI.1545-06.2006

Glowatzki, E., & Fuchs, P. A. (2002). Transmitter release at the hair cell ribbon synapse. *Nature Neuroscience*, *5*(2), 147–154. https://doi.org/10.1038/NN796

Goffena, J., Lefcort, F., Zhang, Y., Lehrmann, E., Chaverra, M., Felig, J., Walters, J., Buksch, R., Becker, K. G., & George, L. (2018). Elongator and codon bias regulate protein levels in mammalian peripheral neurons. *Nature Communications*, *9*(1). https://doi.org/10.1038/S41467-018-03221-Z

Goldberg, J. M. (2000). Afferent diversity and the organization of central vestibular pathways. *Experimental Brain Research. Experimentelle Hirnforschung. Experimentation Cerebrale*, *130*(3), 277. https://doi.org/10.1007/S002210050033

Golub, J. S., Tong, L., Ngyuen, T. B., Hume, C. R., Palmiter, R. D., Rubel, E. W., & Stone, J. S. (2012). Hair Cell Replacement in Adult Mouse Utricles after Targeted Ablation of Hair Cells with Diphtheria Toxin. *The Journal of Neuroscience*, *32*(43), 15093. https://doi.org/10.1523/JNEUROSCI.1709-12.2012

González-Garrido, A., Pujol, R., López-Ramírez, O., Finkbeiner, C., Eatock, R. A., & Stone, J. S. (2021). The Differentiation Status of Hair Cells That Regenerate Naturally in the Vestibular Inner Ear of the Adult Mouse. *The Journal of*

Neuroscience, *41*(37), 7779. https://doi.org/10.1523/JNEUROSCI.3127-20.2021

Grimsley-Myers, C. M., Sipe, C. W., Géléoc, G. S. G., & Lu, X. (2009). The Small GTPase Rac1 Regulates Auditory Hair Cell Morphogenesis. *Journal of Neuroscience*, *29*(50), 15859–15869. https://doi.org/10.1523/JNEUROSCI.3998-09.2009

Groff, J. A., & Liberman, M. C. (2003). Modulation of cochlear afferent response by the lateral olivocochlear system: activation via electrical stimulation of the inferior colliculus. *Journal of Neurophysiology*, *90*(5), 3178–3200. https://doi.org/10.1152/JN.00537.2003

Grosjean, H., de Crécy-Lagard, V., & Marck, C. (2010). Deciphering synonymous codons in the three domains of life: Co-evolution with specific tRNA modification enzymes. *FEBS Letters*, *584*(2), 252–264. https://doi.org/10.1016/J.FEBSLET.2009.11.052

Gründer, S., Müller, A., & Peter Ruppersberg, J. (2001). Developmental and cellular expression pattern of epithelial sodium channel α, β and γ subunits in the inner ear of the rat. *European Journal of Neuroscience*, *13*(4), 641–648. https://doi.org/10.1046/j.1460-9568.2001.01426.x

Gubbay, J., Koopman, P., Collignon, J., Burgoyne, P., & Lovell-Badge, R. (1990). Normal structure and expression of Zfy genes in XY female mice mutant in Tdy. *Development*, *109*(3).

Guinan, J. J. (2010). Cochlear efferent innervation and function. *Current Opinion in Otolaryngology & Head and Neck Surgery*, *18*(5), 447–453. https://doi.org/10.1097/MOO.0B013E32833E05D6

Gutiérrez, J. V., Kaufmann, H., Palma, J. A., Mendoza-Santiesteban, C., Macefield, V. G., & Norcliffe-Kaufmann, L. (2018). Founder mutation in IKBKAP gene causes vestibular impairment in familial dysautonomia. *Clinical Neurophysiology : Official Journal of the International Federation of Clinical Neurophysiology*, *129*(2), 390–396. https://doi.org/10.1016/J.CLINPH.2017.11.010

Hartig, E. I., Day, M., Jarysta, A., & Tarchini, B. (2024). Proteins required for stereocilia elongation during mammalian hair cell development ensure precise and steady heights during adult life. *Proceedings of the National Academy of Sciences of the United States of America*, *121*(40), e2405455121. https://doi.org/10.1073/PNAS.2405455121/SUPPL_FILE/PNAS.2405455121.SAPP.PDF

Hartl, F. U., Bracher, A., & Hayer-Hartl, M. (2011). Molecular chaperones in protein folding and proteostasis. *Nature*, *475*(7356), 324–332. https://doi.org/10.1038/NATURE10317

Hartman, B. H., Reh, T. A., & Bermingham-McDonogh, O. (2010). Notch signaling specifies prosensory domains via lateral induction in the developing mammalian inner ear. *Proceedings of the National Academy of Sciences of the United States of America*, *107*(36), 15792–15797. https://doi.org/10.1073/pnas.1002827107

Hébert, J. M., & McConnell, S. K. (2000). Targeting of cre to the Foxg1 (BF-1) Locus Mediates loxP Recombination in the Telencephalon and Other Developing Head Structures. *Developmental Biology*, *222*(2), 296–306. https://doi.org/10.1006/DBIO.2000.9732

Herranen, A., Ikäheimo, K., Lankinen, T., Pakarinen, E., Fritzsch, B., Saarma, M., Lindahl, M., & Pirvola, U. (2020). Deficiency of the ER-stress-regulator MANF triggers progressive outer hair cell death and hearing loss. *Cell Death & Disease*, *11*(2). https://doi.org/10.1038/S41419-020-2286-6

Hervé, M., & Ibrahim, E. C. (2017). Proteasome inhibitors to alleviate aberrant IKBKAP mRNA splicing and low IKAP/hELP1 synthesis in familial dysautonomia. *Neurobiology of Disease*, *103*, 113–122. https://doi.org/10.1016/J.NBD.2017.04.009

Hoffman, L. F., Choy, K. R., Sultemeier, D. R., & Simmons, D. D. (2018). Oncomodulin Expression Reveals New Insights into the Cellular Organization of the Murine Utricle Striola. *Journal of the Association for Research in Otolaryngology : JARO*, *19*(1), 33–51. https://doi.org/10.1007/S10162-017-0652-6

Hu, J., Li, B., Apisa, L., Yu, H., Entenman, S., Xu, M., Stepanyan, R., Guan, B. J., Müller, U., Hatzoglou, M., & Zheng, Q. Y. (2016). ER stress inhibitor attenuates hearing loss and hair cell death in Cdh23erl/erl mutant mice. *Cell Death & Disease*, *7*(11). https://doi.org/10.1038/CDDIS.2016.386

Hu, J., Xu, M., Yuan, J., Li, B., Entenman, S., Yu, H., & Zheng, Q. Y. (2015). TAUROURSODEOXYCHOLIC ACID PREVENTS HEARING LOSS AND HAIR CELL DEATH IN Cdh23erl/erl MICE. *Neuroscience*, *316*, 311. https://doi.org/10.1016/J.NEUROSCIENCE.2015.12.050

Hua, Y., Ding, X., Wang, H., Gao, Y., Wang, F., Moser, T., & Wu, H. (2020). Electron microscopic reconstruction of neural circuitry in the cochlea. *BioRxiv*, *34*(1), 108551. https://doi.org/10.1101/2020.01.04.894816

Hua, Y., Ding, X., Wang, H., Wang, F., Lu, Y., Neef, J., Gao, Y., Moser, T., & Wu, H. (2021). Electron Microscopic Reconstruction of Neural Circuitry in the Cochlea. *Cell Reports*, *34*(1). https://doi.org/10.1016/J.CELREP.2020.108551

Huang, B., Johansson, M. J. O., & Byström, A. S. (2005). An early step in wobble uridine tRNA modification requires the Elongator complex. *RNA*, *11*(4), 424. https://doi.org/10.1261/RNA.7247705

Hullar, T. E., Della Santina, C. C., Hirvonen, T., Lasker, D. M., Carey, J. P., & Minor, L. B. (2005). Responses of irregularly discharging chinchilla semicircular canal vestibular-nerve afferents during high-frequency head rotations. *Journal of Neurophysiology*, *93*(5), 2777–2786. https://doi.org/10.1152/JN.01002.2004/ASSET/IMAGES/LARGE/Z9K0050545390007.JPEG

Hume, C. R., Bratt, D. L., & Oesterle, E. C. (2007). Expression of LHX3 and SOX2 during mouse inner ear development. *Gene Expression Patterns : GEP*, *7*(7), 798–807. https://doi.org/10.1016/J.MODGEP.2007.05.002

Iannitti, T., & Palmieri, B. (2011). Clinical and experimental applications of sodium phenylbutyrate. *Drugs in R&D*, *11*(3), 227–249. https://doi.org/10.2165/11591280-000000000-00000

Ikäheimo, K., Herranen, A., Iivanainen, V., Lankinen, T., Aarnisalo, A. A., Sivonen, V., Patel, K. A., Demir, K., Saarma, M., Lindahl, M., & Pirvola, U. (2021). MANF supports the inner hair cell synapse and the outer hair cell stereocilia bundle in the cochlea. *Life Science Alliance*, *5*(2). https://doi.org/10.26508/LSA.202101068

Ishihara, H., Takeda, S., Tamura, A., Takahashi, R., Yamaguchi, S., Takei, D., Yamada, T., Inoue, H., Soga, H., Katagiri, H., Tanizawa, Y., & Oka, Y. (2004). Disruption of the WFS1 gene in mice causes progressive beta-cell loss and impaired stimulus-secretion coupling in insulin secretion. *Human Molecular Genetics*, *13*(11), 1159–1170. https://doi.org/10.1093/HMG/DDH125

Isler, J. A., Skalet, A. H., & Alwine, J. C. (2005). Human Cytomegalovirus Infection Activates and Regulates the Unfolded Protein Response. *Journal of Virology*, *79*(11), 6890. https://doi.org/10.1128/JVI.79.11.6890-6899.2005

Jackson, M. Z., Gruner, K. A., Qin, C., & Tourtellotte, W. G. (2014). A neuron autonomous role for the familial dysautonomia gene ELP1 in sympathetic and sensory target tissue innervation. *Development (Cambridge, England)*, *141*(12), 2452–2461. https://doi.org/10.1242/DEV.107797

Jahan, I., Kersigo, J., Pan, N., & Fritzsch, B. (2010). Neurod1 regulates survival and formation of connections in mouse ear and brain. *Cell and Tissue Research*, *341*(1), 95–110. https://doi.org/10.1007/S00441-010-0984-6/FIGURES/9

Jakovljević, A., Stamenković, V., Poleksić, J., Hamad, M. I. K., Reiss, G., Jakovcevski, I., & Andjus, P. R. (2024). The Role of Tenascin-C on the Structural Plasticity of Perineuronal Nets and Synaptic Expression in the Hippocampus of Male Mice. *Biomolecules*, *14*(4), 508. https://doi.org/10.3390/BIOM14040508/S1

Jean, P., Özçete, Ö. D., Tarchini, B., & Moser, T. (2019). Intrinsic planar polarity mechanisms influence the position-dependent regulation of synapse properties in inner hair cells. *Proceedings of the National Academy of Sciences of the United States of America*, *116*(18), 9084–9093. https://doi.org/10.1073/PNAS.1818358116/SUPPL_FILE/PNAS.1818358116.SAPP.PDF

Jeanne, M., Jorgensen, J., & Gould, D. B. (2015). Molecular and Genetic Analysis of Collagen Type IV Mutant Mouse Models of Spontaneous Intracerebral Hemorrhage Identify Mechanisms for Stroke Prevention. *Circulation*, *131*(18), 1555. https://doi.org/10.1161/CIRCULATIONAHA.114.013395

Johansson, M. J. O., Esberg, A., Huang, B., Björk, G. R., & Byström, A. S. (2008). Eukaryotic Wobble Uridine Modifications Promote a Functionally Redundant Decoding System. *Molecular and Cellular Biology*, *28*(10), 3301. https://doi.org/10.1128/MCB.01542-07

Johnston, J. A., Ward, C. L., & Kopito, R. R. (1998). Aggresomes: a cellular response to misfolded proteins. *The Journal of Cell Biology*, *143*(7), 1883–1898. https://doi.org/10.1083/JCB.143.7.1883

Jones, T. A., & Nelson, R. C. (1992). Recovery of vestibular function following hair cell destruction by streptomycin. *Hearing Research*, *62*(2), 181–186. https://doi.org/10.1016/0378-5955(92)90184-O

Jørgensen, J. M., & Mathiesen, C. (1988). The avian inner ear - Continuous production of hair cells in vestibular sensory organs, but not in the auditory papilla. *Naturwissenschaften*, *75*(6), 319–320. https://doi.org/10.1007/BF00367330/METRICS

Kamachi, Y., Uchikawa, M., & Kondoh, H. (2000). Pairing SOX off: With partners in the regulation of embryonic development. In *Trends in Genetics* (Vol. 16, Issue 4, pp. 182–187). Trends Genet. https://doi.org/10.1016/S0168-9525(99)01955-1

Karagulyan, N., & Moser, T. (2023). Synaptic activity is not required for establishing heterogeneity of inner hair cell ribbon synapses. *Frontiers in Molecular Neuroscience*, *16*, 1248941. https://doi.org/10.3389/FNMOL.2023.1248941/FULL

Kaur, B., Bhat, A., Chakraborty, R., Adlakha, K., Sengupta, S., Roy, S., & Chakraborty, K. (2018). Proteomic profile of 4-PBA treated human neuronal cells during ER stress. *Molecular Omics*, *14*(1), 53–63. https://doi.org/10.1039/c7mo00114b

Kawamoto, K., Izumikawa, M., Beyer, L. A., Atkin, G. M., & Raphael, Y. (2009). Spontaneous hair cell regeneration in the mouse utricle following gentamicin ototoxicity. *Hearing Research*, *247*(1), 17. https://doi.org/10.1016/J.HEARES.2008.08.010

Kawase, T., Delgutte, B., & Liberman, M. C. (1993). Antimasking effects of the olivocochlear reflex. II. Enhancement of auditory-nerve response to masked tones. *Journal of Neurophysiology*, *70*(6), 2533–2549. https://doi.org/10.1152/JN.1993.70.6.2533

Kempfle, J. S., Turban, J. L., & Edge, A. S. B. (2016). Sox2 in the differentiation of cochlear progenitor cells. *Scientific Reports*, *6*. https://doi.org/10.1038/srep23293

Khalaf, K., Tornese, P., Cocco, A., & Albanese, A. (2022). Tauroursodeoxycholic acid: a potential therapeutic tool in neurodegenerative diseases. *Translational Neurodegeneration*, *11*(1), 33. https://doi.org/10.1186/S40035-022-00307-Z

Kheradmand, A., Colpak, A. I., & Zee, D. S. (2016). Eye movements in vestibular disorders. *Handbook of Clinical Neurology*, *137*, 103–117. https://doi.org/10.1016/B978-0-444-63437-5.00008-X

Kiernan, A. E., Pelling, A. L., Leung, K. K. H., Tang, A. S. P., Bell, D. M., Tease, C., Lovell-Badge, R., Steel, K. P., & Cheah, K. S. E. (2005). Sox2 is required for sensory organ development in the mammalian inner ear. *Nature*, *434*(7036), 1031–1035. https://doi.org/10.1038/nature03487

Kim, W. Y., Fritzsch, B., Serls, A., Bakel, L. A., Huang, E. J., Reichardt, L. F., Barth, D. S., & Lee, J. E. (2001). NeuroD-null mice are deaf due to a severe loss of the inner ear sensory neurons during development. *Development*, *128*(3), 417–426. https://doi.org/10.1242/DEV.128.3.417

Kojic, M., Gaik, M., Kiska, B., Salerno-Kochan, A., Hunt, S., Tedoldi, A., Mureev, S., Jones, A., Whittle, B., Genovesi, L. A., Adolphe, C., Brown, D. L., Stow, J. L., Alexandrov, K., Sah, P., Glatt, S., & Wainwright, B. J. (2018). Elongator

mutation in mice induces neurodegeneration and ataxia-like behavior. *Nature Communications*, *9*(1). https://doi.org/10.1038/S41467-018-05765-6

Kojic, M., Gawda, T., Gaik, M., Begg, A., Salerno-Kochan, A., Kurniawan, N. D., Jones, A., Drożdżyk, K., Kościelniak, A., Chramiec-Głąbik, A., Hediyeh-Zadeh, S., Kasherman, M., Shim, W. J., Sinniah, E., Genovesi, L. A., Abrahamsen, R. K., Fenger, C. D., Madsen, C. G., Cohen, J. S., … Wainwright, B. J. (2021). Elp2 mutations perturb the epitranscriptome and lead to a complex neurodevelopmental phenotype. *Nature Communications*, *12*(1), 19. https://doi.org/10.1038/S41467-021-22888-5

Koopman, P., Gubbay, J., Collignon, J., & Lovell-Badge, R. (1989). Zfy gene expression patterns are not compatible with a primary role in mouse sex determination. *Nature*, *342*(6252), 940–942. https://doi.org/10.1038/342940a0

Koundakjian, E. J., Appler, J. L., & Goodrich, L. V. (2007). Auditory neurons make stereotyped wiring decisions before maturation of their targets. *Journal of Neuroscience*, *27*(51), 14078–14088. https://doi.org/10.1523/JNEUROSCI.3765-07.2007

Kubota, K., Niinuma, Y., Kaneko, M., Okuma, Y., Sugai, M., Omura, T., Uesugi, M., Uehara, T., Hosoi, T., & Nomura, Y. (2006). Suppressive effects of 4-phenylbutyrate on the aggregation of Pael receptors and endoplasmic reticulum stress. *Journal of Neurochemistry*, *97*(5), 1259–1268. https://doi.org/10.1111/J.1471-4159.2006.03782.X

Kujawa, S. G., & Liberman, M. C. (1997). Conditioning-related protection from acoustic injury: effects of chronic deefferentation and sham surgery. *Journal of Neurophysiology*, *78*(6), 3095–3106. https://doi.org/10.1152/JN.1997.78.6.3095

Kujawa, S. G., & Liberman, M. C. (2009). Adding Insult to Injury: Cochlear Nerve Degeneration after “Temporary” Noise-Induced Hearing Loss. *The Journal of Neuroscience*, *29*(45), 14077. https://doi.org/10.1523/JNEUROSCI.2845-09.2009

Kusaczuk, M. (2019). Tauroursodeoxycholate—Bile Acid with Chaperoning Activity: Molecular and Cellular Effects and Therapeutic Perspectives. *Cells 2019, Vol. 8, Page 1471*, *8*(12), 1471. https://doi.org/10.3390/CELLS8121471

Ladang, A., Rapino, F., Heukamp, L. C., Tharun, L., Shostak, K., Hermand, D., Delaunay, S., Klevernic, I., Jiang, Z., Jacques, N., Jamart, D., Migeot, V., Florin, A., Göktuna, S., Malgrange, B., Sansom, O. J., Nguyen, L., Büttner, R., Close, P., & Chariot, A. (2015). Elp3 drives Wnt-dependent tumor initiation and

regeneration in the intestine. *Journal of Experimental Medicine*, *212*(12), 2057–2075. https://doi.org/10.1084/jem.20142288

Laguesse, S., Creppe, C., Nedialkova, D. D., Prévot, P. P., Borgs, L., Huysseune, S., Franco, B., Duysens, G., Krusy, N., Lee, G., Thelen, N., Thiry, M., Close, P., Chariot, A., Malgrange, B., Leidel, S. A., Godin, J. D., & Nguyen, L. (2015). A Dynamic Unfolded Protein Response Contributes to the Control of Cortical Neurogenesis. *Developmental Cell*, *35*(5), 553–567. https://doi.org/10.1016/j.devcel.2015.11.005

Lashuel, H. A., Hartley, D., Petre, B. M., Walz, T., & Lansbury, P. T. (2002). Neurodegenerative disease: amyloid pores from pathogenic mutations. *Nature*, *418*(6895), 291. https://doi.org/10.1038/418291A

Lee, M. P., & Waldhaus, J. (2022). In vitro and in vivo models: What have we learnt about inner ear regeneration and treatment for hearing loss? *Molecular and Cellular Neurosciences*, *120*, 103736. https://doi.org/10.1016/J.MCN.2022.103736

Leigh, P. N., Whitwell, H., Garofalo, O., Buller, J., Swash, M., Martin, J. E., Gallo, J. M., Weller, R. O., & Anderton, B. H. (1991). Ubiquitin-immunoreactive intraneuronal inclusions in amyotrophic lateral sclerosis. Morphology, distribution, and specificity. *Brain : A Journal of Neurology*, *114 (Pt 2)*(2), 775–788. https://doi.org/10.1093/BRAIN/114.2.775

Li, A., Xue, J., & Peterson, E. H. (2008). Architecture of the mouse utricle: Macular organization and hair bundle heights. *Journal of Neurophysiology*, *99*(2), 718–733. https://doi.org/10.1152/JN.00831.2007/ASSET/IMAGES/LARGE/Z9K0020886620010.JPEG

Li, B., Zheng, T., Yan, C., Wang, W., Zhang, J., Zhang, L., Hu, J., Zhang, L., Wan, Y., Zhang, M., & Zheng, Q. (2019). Chemical chaperone 4-phenylbutyrate prevents hearing loss and cochlear hair cell death in Cdh23erl/erl mutant mice. *Neuroreport*, *30*(3), 145. https://doi.org/10.1097/WNR.0000000000001173

Li, H., Wen, W., Xu, H., Wu, H., Xu, M., Frank, J. A., & Luo, J. (2018). 4-Phenylbutyric Acid Protects Ethanol-induced Damage in the Developing Mouse Brain. *Alcoholism, Clinical and Experimental Research*, *43*(1), 69. https://doi.org/10.1111/ACER.13918

Li, J., Rouse, S. L., Matthews, I. R., Park, Y., Eltawil, Y., Sherr, E. H., & Chan, D. K. (2024). Modulating the unfolded protein response with ISRIB mitigates

cisplatin ototoxicity. *Scientific Reports*, *14*(1), 22382. https://doi.org/10.1038/S41598-024-70561-W

Liberman, L. D., Wang, H., & Liberman, M. C. (2011). Opposing gradients of ribbon size and AMPA receptor expression underlie sensitivity differences among cochlear-nerve/hair-cell synapses. *The Journal of Neuroscience : The Official Journal of the Society for Neuroscience*, *31*(3), 801–808. https://doi.org/10.1523/JNEUROSCI.3389-10.2011

Liberman, M. C. (1980). Efferent synapses in the inner hair cell area of the cat cochlea: an electron microscopic study of serial sections. *Hearing Research*, *3*(3), 189–204. https://doi.org/10.1016/0378-5955(80)90046-5

Liberman, M. C. (1982). Single-neuron labeling in the cat auditory nerve. *Science (New York, N.Y.)*, *216*(4551), 1239–1241. https://doi.org/10.1126/SCIENCE.7079757

Liberman, M. C., & Brown, M. C. (1986). Physiology and anatomy of single olivocochlear neurons in the cat. *Hearing Research*, *24*(1), 17–36. https://doi.org/10.1016/0378-5955(86)90003-1

Liguori, L., Monticelli, M., Allocca, M., Mele, B. H., Lukas, J., Cubellis, M. V., & Andreotti, G. (2020). Pharmacological Chaperones: A Therapeutic Approach for Diseases Caused by Destabilizing Missense Mutations. *International Journal of Molecular Sciences*, *21*(2). https://doi.org/10.3390/IJMS21020489

Lim, D. J. (1986). Functional structure of the organ of Corti: a review. *Hearing Research*, *22*(1–3), 117–146. https://doi.org/10.1016/0378-5955(86)90089-4

Lin, V., Golub, J. S., Nguyen, T. B., Hume, C. R., Oesterle, E. C., & Stone, J. S. (2011). Inhibition Of Notch Activity Promotes Nonmitotic Regeneration of Hair Cells in the Adult Mouse Utricles. *Journal of Neuroscience*, *31*(43), 15329–15339. https://doi.org/10.1523/JNEUROSCI.2057-11.2011

Liu, M., Pereira, F. A., Price, S. D., Chu, M. J., Shope, C., Himes, D., Eatock, R. A., Brownell, W. E., Lysakowski, A., & Tsai, M. J. (2000). Essential role of BETA2/NeuroD1 in development of the vestibular and auditory systems. *Genes and Development*, *14*(22), 2839–2854. https://doi.org/10.1101/gad.840500

Liu, S., Heumüller, S. E., Hossinger, A., Müller, S. A., Buravlova, O., Lichtenthaler, S. F., Denner, P., & Vorberg, I. M. (2023). Reactivated endogenous retroviruses promote protein aggregate spreading. *Nature Communications 2023 14:1*, *14*(1), 1–19. https://doi.org/10.1038/s41467-023-40632-z

Locher, H., Frijns, J. H. M., van Iperen, L., de Groot, J. C. M. J., Huisman, M. A., & Chuva de Sousa Lopes, S. M. (2013). Neurosensory development and cell fate determination in the human cochlea. *Neural Development*, *8*(1). https://doi.org/10.1186/1749-8104-8-20

Lv, J., Wang, H., Cheng, X., Chen, Y., Wang, D., Zhang, L., Cao, Q., Tang, H., Hu, S., Gao, K., Xun, M., Wang, J., Wang, Z., Zhu, B., Cui, C., Gao, Z., Guo, L., Yu, S., Jiang, L., … Shu, Y. (2024). AAV1-hOTOF gene therapy for autosomal recessive deafness 9: a single-arm trial. *Lancet (London, England)*, *403*(10441), 2317–2325. https://doi.org/10.1016/S0140-6736(23)02874-X

Lyford-Pike, S., Vogelheim, C., Chu, E., Della Santina, C. C., & Carey, J. P. (2007). Gentamicin is Primarily Localized in Vestibular Type I Hair Cells after Intratympanic Administration. *Journal of the Association for Research in Otolaryngology 2007 8:4*, *8*(4), 497–508. https://doi.org/10.1007/S10162-007-0093-8

Ma, Q., Anderson, D. J., & Fritzsch, B. (2000). Neurogenin 1 null mutant ears develop fewer, morphologically normal hair cells in smaller sensory epithelia devoid of innervation. *JARO - Journal of the Association for Research in Otolaryngology*, *1*(2), 129–143. https://doi.org/10.1007/S101620010017/METRICS

Ma, Q., Chen, Z., del Barco Barrantes, I., de la Pompa, J. L., & Anderson, D. J. (1998). neurogenin1 is essential for the determination of neuronal precursors for proximal cranial sensory ganglia. *Neuron*, *20*(3), 469–482. https://doi.org/10.1016/s0896-6273(00)80988-5

Mackowetzky, K., Yoon, K. H., Mackowetzky, E. J., & Waskiewicz, A. J. (2021). Development and evolution of the vestibular apparatuses of the inner ear. *Journal of Anatomy*, *239*(4), 801–828. https://doi.org/10.1111/JOA.13459

Mak, A. C. Y., Szeto, I. Y. Y., Fritzsch, B., & Cheah, K. S. E. (2009). Differential and overlapping expression pattern of SOX2 and SOX9 in inner ear development. *Gene Expression Patterns*, *9*(6), 444–453. https://doi.org/10.1016/j.gep.2009.04.003

Mansour, S., Offiah, A. C., McDowall, S., Sim, P., Tolmie, J., & Hall, C. (2002). The phenotype of survivors of campomelic dysplasia. *Journal of Medical Genetics*, *39*(8), 597–602. https://doi.org/10.1136/jmg.39.8.597

Marciniak, S. J., Chambers, J. E., & Ron, D. (2022). Pharmacological targeting of endoplasmic reticulum stress in disease. *Nature Reviews. Drug Discovery*, *21*(2), 115–140. https://doi.org/10.1038/S41573-021-00320-3

McInturff, S., Burns, J. C., & Kelley, M. W. (2018). Characterization of spatial and temporal development of Type I and Type II hair cells in the mouse utricle using new cell-type-specific markers. *Biology Open*, *7*(11). https://doi.org/10.1242/BIO.038083

Mikitsh, J. L., & Chacko, A. M. (2014). Pathways for small molecule delivery to the central nervous system across the blood-brain barrier. *Perspectives in Medicinal Chemistry*, *6*(6), 11–24. https://doi.org/10.4137/PMC.S13384

Mikuriya, T., Sugahara, K., Sugimoto, K., Fujimoto, M., Takemoto, T., Hashimoto, M., Hirose, Y., Shimogori, H., Hayashida, N., Inouye, S., Nakai, A., & Yamashita, H. (2008). Attenuation of progressive hearing loss in a model of age-related hearing loss by a heat shock protein inducer, geranylgeranylacetone. *Brain Research*, *1212*, 9–17. https://doi.org/10.1016/j.brainres.2008.03.031

Milanesi, L., Sheynis, T., Xue, W. F., Orlova, E. V., Hellewell, A. L., Jelinek, R., Hewitt, E. W., Radford, S. E., & Saibil, H. R. (2012). Direct three-dimensional visualization of membrane disruption by amyloid fibrils. *Proceedings of the National Academy of Sciences of the United States of America*, *109*(50), 20455–20460. https://doi.org/10.1073/PNAS.1206325109

Mitsuda, T., Omi, T., Tanimukai, H., Sakagami, Y., Tagami, S., Okochi, M., Kudo, T., & Takeda, M. (2011). Sigma-1Rs are upregulated via PERK/eIF2α/ATF4 pathway and execute protective function in ER stress. *Biochemical and Biophysical Research Communications*, *415*(3), 519–525. https://doi.org/10.1016/J.BBRC.2011.10.113

Monzack, E. L., May, L. A., Roy, S., Gale, J. E., & Cunningham, L. L. (2015). Live imaging the phagocytic activity of inner ear supporting cells in response to hair cell death. *Cell Death & Differentiation 2015 22:12*, *22*(12), 1995–2005. https://doi.org/10.1038/cdd.2015.48

Morsli, H., Choo, D., Ryan, A., Johnson, R., & Wu, D. K. (1998). Development of the mouse inner ear and origin of its sensory organs. *Journal of Neuroscience*, *18*(9), 3327–3335. https://doi.org/10.1523/jneurosci.18-09-03327.1998

Murillo-Bonilla, L. M., Zermeño-Póhls, F., Reyes-Morales, S., Escamilla-Garza, J. M., & José Méndez, J. (2024). Marinesco-Sjögren Syndrome. *Archivos de Neurociencias*, *6*(1), 33–35. https://doi.org/10.1212/wnl.35.3.415

N, T., HK, S., M, S., & JF, D. (1978). Familial dysautonomia (Riley-Day syndrome). Temporal bone findings and otolaryngological manifestations. *The Annals of Otology, Rhinology & Laryngology. Supplement*, *87*(1 Pt 3 Suppl 46), 287. https://doi.org/10.1177/00034894780871S201

Nedialkova, D. D., & Leidel, S. A. (2015). Optimization of Codon Translation Rates via tRNA Modifications Maintains Proteome Integrity. *Cell*, *161*(7), 1606–1618. https://doi.org/10.1016/j.cell.2015.05.022

Neves, J., Parada, C., Chamizo, M., & Giráldez, F. (2011). Jagged 1 regulates the restriction of Sox2 expression in the developing chicken inner ear: a mechanism for sensory organ specification. *Development (Cambridge, England)*, *138*(4), 735–744. https://doi.org/10.1242/dev.060657

Neves, J., Vachkov, I., & Giraldez, F. (2013). Sox2 regulation of hair cell development: incoherence makes sense. *Hearing Research*, *297*, 20–29. https://doi.org/10.1016/j.heares.2012.11.003

Newton, V. E. (1991). Sensorineural hearing loss and the Marinesco-Sjögren syndrome. *The Journal of Laryngology and Otology*, *105*(3), 210–212. https://doi.org/10.1017/S0022215100115385

Nguyen, L., Humbert, S., Saudou, F., & Chariot, A. (2010). Elongator - an emerging role in neurological disorders. *Trends in Molecular Medicine*, *16*(1), 1–6. https://doi.org/10.1016/J.MOLMED.2009.11.002

Oesterle, E. C., Campbell, S., Taylor, R. R., Forge, A., & Hume, C. R. (2008). Sox2 and JAGGED1 expression in normal and drug-damaged adult mouse inner ear. *Journal of the Association for Research in Otolaryngology : JARO*, *9*(1), 65–89. https://doi.org/10.1007/S10162-007-0106-7

Oishi, N., Duscha, S., Boukari, H., Meyer, M., Xie, J., Wei, G., Schrepfer, T., Roschitzki, B., Boettger, E. C., & Schacht, J. (2015). XBP1 mitigates aminoglycoside-induced endoplasmic reticulum stress and neuronal cell death. *Cell Death and Disease*, *6*(5), 1–11. https://doi.org/10.1038/cddis.2015.108

Okada, Y., Yamagata, K., Hong, K., Wakayama, T., & Zhang, Y. (2010). A role for elongator in zygotic paternal genome demethylation. *Nature*, *463*(7280), 554. https://doi.org/10.1038/NATURE08732

Olsson, C., Jansson, H., & Swenson, J. (2016). The Role of Trehalose for the Stabilization of Proteins. *The Journal of Physical Chemistry. B*, *120*(20), 4723–4731. https://doi.org/10.1021/ACS.JPCB.6B02517

Olzscha, H., Schermann, S. M., Woerner, A. C., Pinkert, S., Hecht, M. H., Tartaglia, G. G., Vendruscolo, M., Hayer-Hartl, M., Hartl, F. U., & Vabulas, R. M. (2011). Amyloid-like aggregates sequester numerous metastable proteins with essential cellular functions. *Cell*, *144*(1), 67–78. https://doi.org/10.1016/J.CELL.2010.11.050

Otero, G., Fellows, J., Yang, L., De Bizemont, T., Dirac, A. M. G., Gustafsson, C. M., Erdjument-Bromage, H., Tempst, P., & Svejstrup, J. Q. (1999). Elongator, a multisubunit component of a novel RNA polymerase II holoenzyme for transcriptional elongation. *Molecular Cell*, *3*(1), 109–118. https://doi.org/10.1016/S1097-2765(00)80179-3

Paganoni, S., Macklin, E. A., Hendrix, S., Berry, J. D., Elliott, M. A., Maiser, S., Karam, C., Caress, J. B., Owegi, M. A., Quick, A., Wymer, J., Goutman, S. A., Heitzman, D., Heiman-Patterson, T., Jackson, C. E., Quinn, C., Rothstein, J. D., Kasarskis, E. J., Katz, J., … Cudkowicz, M. E. (2020). Trial of Sodium Phenylbutyrate-Taurursodiol for Amyotrophic Lateral Sclerosis. *The New England Journal of Medicine*, *383*(10), 919–930. https://doi.org/10.1056/NEJMOA1916945

Pan, N., Jahan, I., Kersigo, J., Kopecky, B., Santi, P., Johnson, S., Schmitz, H., & Fritzsch, B. (2011). Conditional deletion of Atoh1 using Pax2-Cre results in viable mice without differentiated cochlear hair cells that have lost most of the organ of Corti. *Hearing Research*, *275*(1–2), 66–80. https://doi.org/10.1016/J.HEARES.2010.12.002

Park, S. H., Kukushkin, Y., Gupta, R., Chen, T., Konagai, A., Hipp, M. S., Hayer-Hartl, M., & Hartl, F. U. (2013). PolyQ proteins interfere with nuclear degradation of cytosolic proteins by sequestering the Sis1p chaperone. *Cell*, *154*(1), 134–145. https://doi.org/10.1016/J.CELL.2013.06.003

Pearson, J., Pytel, B. A., Grover-Johnson, N., Axelrod, F., & Dancis, J. (1978). Quantitative studies of dorsal root ganglia and neuropathologic observations on spinal cords in familial dysautonomia. *Journal of the Neurological Sciences*, *35*(1), 77–92. https://doi.org/10.1016/0022-510X(78)90103-X

Pechmann, S., & Frydman, J. (2013). Evolutionary conservation of codon optimality reveals hidden signatures of cotranslational folding. *Nature Structural and Molecular Biology*, *20*(2), 237–243. https://doi.org/10.1038/nsmb.2466

Pereira, M., Ribeiro, D. R., Berg, M., Tsai, A. P., Dong, C., Nho, K., Kaiser, S., Moutinho, M., & Soares, A. R. (2024). Amyloid pathology reduces ELP3 expression and tRNA modifications leading to impaired proteostasis. *Biochimica et Biophysica Acta. Molecular Basis of Disease*, *1870*(1). https://doi.org/10.1016/J.BBADIS.2023.166857

Perlmutter, D. H. (2002). Chemical chaperones: a pharmacological strategy for disorders of protein folding and trafficking. *Pediatric Research*, *52*(6), 832–836. https://doi.org/10.1203/00006450-200212000-00004

Petitpré, C. (2018). *Neuronal heterogeneity and stereotyped connectivity in the auditory afferent system*.

Petitpré, C., Faure, L., Uhl, P., Fontanet, P., Filova, I., Pavlinkova, G., Adameyko, I., Hadjab, S., & Lallemend, F. (2022). Single-cell RNA-sequencing analysis of the developing mouse inner ear identifies molecular logic of auditory neuron diversification. *Nature Communications*, *13*(1), 3878. https://doi.org/10.1038/S41467-022-31580-1

Philippou, E., & Joubert, K. (2013). The audiological profile and perceptions of hearing loss in individuals with amyotrophic lateral sclerosis. *Amyotrophic Lateral Sclerosis: Symptoms, Treatment and Prognosis*, 1–56.

Prins, T. J., Myers, Z. A., Saldate, J. J., & Hoffman, L. F. (2020). Calbindin expression in adult vestibular epithelia. *Journal of Comparative Physiology A: Neuroethology, Sensory, Neural, and Behavioral Physiology*, *206*(4), 623–637. https://doi.org/10.1007/S00359-020-01418-6/FIGURES/4

Pujol, R., Pickett, S. B., Nguyen, T. B., & Stone, J. S. (2014). Large basolateral processes on type II hair cells comprise a novel processing unit in mammalian vestibular organs. *The Journal of Comparative Neurology*, *522*(14), 3141. https://doi.org/10.1002/CNE.23625

Pujols, J., Peña-Díaz, S., Pallarès, I., & Ventura, S. (2020). Chemical Chaperones as Novel Drugs for Parkinson's Disease. *Trends in Molecular Medicine*, *26*(4), 408–421. https://doi.org/10.1016/J.MOLMED.2020.01.005

Puligilla, C., & Kelley, M. W. (2017). Dual role for Sox2 in specification of sensory competence and regulation of Atoh1 function HHS Public Access. *Dev Neurobiol*, *77*(1), 3–13. https://doi.org/10.1002/dneu.22401

Qi, J., Tan, F., Zhang, L., Lu, L., Zhang, S., Zhai, Y., Lu, Y., Qian, X., Dong, W. X., Zhou, Y., Zhang, Z., Yang, X., Jiang, L., Yu, C., Liu, J., Chen, T., Wu, L., Tan, C., Sun, S., … Chai, R. (2024). AAV-Mediated Gene Therapy Restores Hearing in Patients with DFNB9 Deafness. *Advanced Science (Weinheim, Baden-Wurttemberg, Germany)*, *11*(11). https://doi.org/10.1002/ADVS.202306788

Qu, Y., Zong, S., Wang, Z., Du, P., Wen, Y., Li, H., Wu, N., & Xiao, H. (2023). The PERK/ATF4/CHOP signaling branch of the unfolded protein response mediates cisplatin-induced ototoxicity in hair cells. *Drug and Chemical Toxicology*, *46*(2), 369–379. https://doi.org/10.1080/01480545.2022.2039181

Raft, S., Koundakjian, E. J., Quinones, H., Jayasena, C. S., Goodrich, L. V., Johnson, J. E., Segil, N., & Groves, A. K. (2007). Cross-regulation of Ngn1 and Math1 coordinates the production of neurons and sensory hair cells during inner ear

development. *Development*, *134*(24), 4405–4415. https://doi.org/10.1242/DEV.009118

Rajan, R. (1988). Effect of electrical stimulation of the crossed olivocochlear bundle on temporary threshold shifts in auditory sensitivity. I. Dependence on electrical stimulation parameters. *Journal of Neurophysiology*, *60*(2), 549–568. https://doi.org/10.1152/JN.1988.60.2.549

Ranjan, N., & Rodnina, M. V. (2017). Thio-Modification of tRNA at the Wobble Position as Regulator of the Kinetics of Decoding and Translocation on the Ribosome. *Journal of the American Chemical Society*, *139*(16), 5857–5864. https://doi.org/10.1021/JACS.7B00727

Rapino, F., Delaunay, S., Rambow, F., Zhou, Z., Tharun, L., De Tullio, P., Sin, O., Shostak, K., Schmitz, S., Piepers, J., Ghesquière, B., Karim, L., Charloteaux, B., Jamart, D., Florin, A., Lambert, C., Rorive, A., Jerusalem, G., Leucci, E., … Close, P. (2018). Codon-specific translation reprogramming promotes resistance to targeted therapy. *Nature 2018 558:7711*, *558*(7711), 605–609. https://doi.org/10.1038/s41586-018-0243-7

Ross, S. E., Mardinly, A. R., McCord, A. E., Zurawski, J., Cohen, S., Jung, C., Hu, L., Mok, S. I., Shah, A., Savner, E. M., Tolias, C., Corfas, R., Chen, S., Inquimbert, P., Xu, Y., McInnes, R. R., Rice, F. L., Corfas, G., Ma, Q., … Greenberg, M. E. (2010). Loss of inhibitory interneurons in the dorsal spinal cord and elevated itch in Bhlhb5 mutant mice. *Neuron*, *65*(6), 886–898. https://doi.org/10.1016/J.NEURON.2010.02.025

Rouse, S. L., Matthews, I. R., Li, J., Sherr, E. H., & Chan, D. K. (2020). Integrated stress response inhibition provides sex-dependent protection against noise-induced cochlear synaptopathy. *Scientific Reports*, *10*(1). https://doi.org/10.1038/S41598-020-75058-W

Ruben, R. J. (1967). Development of the inner ear of the mouse: a radioautographic study of terminal mitoses. *Acta Oto-Laryngologica*.

Rudy, B., & McBain, C. J. (2001). Kv3 channels: voltage-gated K+ channels designed for high-frequency repetitive firing. *Trends in Neurosciences*, *24*(9), 517–526. https://doi.org/10.1016/S0166-2236(00)01892-0

Rüsch, A., & Eatock, R. A. (1996). A delayed rectifier conductance in type I hair cells of the mouse utricle. *Journal of Neurophysiology*, *76*(2), 995–1004. https://doi.org/10.1152/JN.1996.76.2.995

Russell, I. J., & Murugasu, E. (1997). Medial efferent inhibition suppresses basilar membrane responses to near characteristic frequency tones of moderate to

high intensities. *The Journal of the Acoustical Society of America*, *102*(3), 1734–1738. https://doi.org/10.1121/1.420083

Sadeghi, S. G., Chacron, M. J., Taylor, M. C., & Cullen, K. E. (2007). Neural variability, detection thresholds, and information transmission in the vestibular system. *Journal of Neuroscience*, *27*(4), 771–781. https://doi.org/10.1523/JNEUROSCI.4690-06.2007

Saint-Germain, N., Lee, Y. H., Zhang, Y., Sargent, T. D., & Saint-Jeannet, J. P. (2004). Specification of the otic placode depends on Sox9 function in Xenopus. *Development*, *131*(8), 1755–1763. https://doi.org/10.1242/dev.01066

Sanders, T. R., & Kelley, M. W. (2022). Specification of neuronal subtypes in the spiral ganglion begins prior to birth in the mouse. *Proceedings of the National Academy of Sciences*, *119*(48), e2203935119. https://doi.org/10.1073/PNAS.2203935119

Savarirayan, R., Robertson, S. P., Bankier, A., & Rogers, J. G. (2003). Variable Expression of Campomelic Dysplasia in a Father and his 46, XY Daughter. *Pediatric Pathology & Molecular Medicine*, *22*(1), 37–46. https://doi.org/10.1080/pdp.22.1.37.46

Schmiedt, R. A., Mills, J. H., & Boettcher, F. A. (1996). Age-related loss of activity of auditory-nerve fibers. *Https://Doi.Org/10.1152/Jn.1996.76.4.2799*, *76*(4), 2799–2803. https://doi.org/10.1152/JN.1996.76.4.2799

Seal, R. P., Akil, O., Yi, E., Weber, C. M., Grant, L., Yoo, J., Clause, A., Kandler, K., Noebels, J. L., Glowatzki, E., Lustig, L. R., & Edwards, R. H. (2008). Sensorineural Deafness and Seizures in Mice Lacking Vesicular Glutamate Transporter 3. *Neuron*, *57*(2), 263. https://doi.org/10.1016/J.NEURON.2007.11.032

Sedo, L., Jedynak, P., Boadas-vaello, P., Llorens, J., Sedo, L., Jedynak, P., Boadas-vaello, P., & Llorens, J. (2016). Erratum: Transient alteration of the vestibular calyceal junction and synapse in response to chronic ototoxic insult in rats (Dis. Model. Mech. (2016) 8 (1323-1337)). *DMM Disease Models and Mechanisms*, *9*(7), 821. https://doi.org/10.1242/dmm.026278

Sedó-Cabezón, L., Jedynak, P., Boadas-Vaello, P., & Llorens, J. (2015). Transient alteration of the vestibular calyceal junction and synapse in response to chronic ototoxic insult in rats. *DMM Disease Models and Mechanisms*, *8*(10), 1323–1337. https://doi.org/10.1242/DMM.021436/-/DC1

Severinsen, S. V., Sørensen, M. S., Kirkegaard, M., & Nyengaard, J. R. (2010). Stereological estimation of total cell numbers in the young human utricular

macula. *Acta Oto-Laryngologica*, *130*(7), 773–779. https://doi.org/10.3109/00016480903397694

Shimizu, D., Ishitsuka, Y., Miyata, K., Tomishima, Y., Kondo, Y., Irikura, M., Iwawaki, T., Oike, Y., & Irie, T. (2014). Protection afforded by pre- or post-treatment with 4-phenylbutyrate against liver injury induced by acetaminophen overdose in mice. *Pharmacological Research*, *87*, 26–41. https://doi.org/10.1016/J.PHRS.2014.06.003

Shrestha, B. R., Chia, C., Wu, L., Kujawa, S. G., Liberman, M. C., & Goodrich, L. V. (2018). Sensory Neuron Diversity in the Inner Ear Is Shaped by Activity. *Cell*, *174*(5), 1229-1246.e17. https://doi.org/10.1016/j.cell.2018.07.007

Shrestha, B. R., Wu, L., & Goodrich, L. V. (2023). Runx1 controls auditory sensory neuron diversity in mice. *Developmental Cell*, *58*(4), 306-319.e5. https://doi.org/10.1016/j.devcel.2023.01.008

Siebald, C., Vincent, P. F. Y., Bottom, R. T., Sun, S., Reijntjes, D. O. J., Manca, M., Glowatzki, E., & Müller, U. (2023). Molecular signatures define subtypes of auditory afferents with distinct peripheral projection patterns and physiological properties. *Proceedings of the National Academy of Sciences of the United States of America*, *120*(31). https://doi.org/10.1073/PNAS.2217033120

Siggers, D. C., Haciska, D. T., & McKusick, V. A. (1975). Vestibular dysfunction in familial dysautonomia. The Riley-Day syndrome. *Archives of Disease in Childhood*, *50*(11), 890–893. https://doi.org/10.1136/ADC.50.11.890

Simmons, D. D., Tong, B., Schrader, A. D., & Hornak, A. J. (2010). Oncomodulin identifies different hair cell types in the mammalian inner ear. *Journal of Comparative Neurology*, *518*(18), 3785–3802. https://doi.org/10.1002/CNE.22424

Simpson, C. L., Lemmens, R., Miskiewicz, K., Broom, W. J., Hansen, V. K., van Vught, P. W. J., Landers, J. E., Sapp, P., van Den Bosch, L., Knight, J., Neale, B. M., Turner, M. R., Veldink, J. H., Ophoff, R. A., Tripathi, V. B., Beleza, A., Shah, M. N., Proitsi, P., Van Hoecke, A., … Al-Chalabi, A. (2009). Variants of the elongator protein 3 (ELP3) gene are associated with motor neuron degeneration. *Human Molecular Genetics*, *18*(3), 472. https://doi.org/10.1093/HMG/DDN375

Slaugenhaupt, S. A., Blumenfeld, A., Gill, S. P., Leyne, M., Mull, J., Cuajungco, M. P., Liebert, C. B., Chadwick, B., Idelson, M., Reznik, L., Robbins, C. M., Makalowska, I., Brownstein, M. J., Slaugenhaupt, S. A., Scheidereit, C., Maayan, C., Axelrod, F. B., & Gusella, J. F. (2001). Tissue-specific expression

of a splicing mutation in the IKBKAP gene causes familial dysautonomia. *American Journal of Human Genetics*, *68*(3), 598–605. https://doi.org/10.1086/318810

Smith-Cortinez, N., Tan, A. K., Stokroos, R. J., Versnel, H., & Straatman, L. V. (2023). Regeneration of Hair Cells from Endogenous Otic Progenitors in the Adult Mammalian Cochlea: Understanding Its Origins and Future Directions. *International Journal of Molecular Sciences*, *24*(9). https://doi.org/10.3390/IJMS24097840

Stamenkovic, V., Stamenkovic, S., Jaworski, T., Gawlak, M., Jovanovic, M., Jakovcevski, I., Wilczynski, G. M., Kaczmarek, L., Schachner, M., Radenovic, L., & Andjus, P. R. (2016). The extracellular matrix glycoprotein tenascin-C and matrix metalloproteinases modify cerebellar structural plasticity by exposure to an enriched environment. *Brain Structure and Function 2016 222:1*, *222*(1), 393–415. https://doi.org/10.1007/S00429-016-1224-Y

Steevens, A. R., Sookiasian, D. L., Glatzer, J. C., & Kiernan, A. E. (2017). SOX2 is required for inner ear neurogenesis. *Scientific Reports*, *7*(1). https://doi.org/10.1038/s41598-017-04315-2

Stringer, C., Wang, T., Michaelos, M., & Pachitariu, M. (2021). Cellpose: a generalist algorithm for cellular segmentation. *Nature Methods*, *18*(1), 100–106. https://doi.org/10.1038/s41592-020-01018-x

Sun, S., Babola, T., Pregernig, G., So, K. S., Nguyen, M., Su, S. S. M., Palermo, A. T., Bergles, D. E., Burns, J. C., & Müller, U. (2018). Hair Cell Mechanotransduction Regulates Spontaneous Activity and Spiral Ganglion Subtype Specification in the Auditory System. *Cell*, *174*(5), 1247-1263.e15. https://doi.org/10.1016/j.cell.2018.07.008

Sun, Y., Wang, L., Li, C., Wei, W., Correspondence, Z. L., Zhu, T., Wu, B., Wang, G., Luo, Z., & Liu, Z. (2022). Single-cell transcriptomic landscapes of the otic neuronal lineage at multiple early embryonic ages. *Cell Reports*, *38*(12), 110542. https://doi.org/10.1016/J.CELREP.2022.110542

Suzuki, T. (2021). The expanding world of tRNA modifications and their disease relevance. *Nature Reviews Molecular Cell Biology 2021 22:6*, *22*(6), 375–392. https://doi.org/10.1038/s41580-021-00342-0

Szeto, I. Y. Y., Chu, D. K. H., Chen, P., Chu, K. C., Au, T. Y. K., Leung, K. K. H., Huang, Y. H., Wynn, S. L., Mak, A. C. Y., Chan, Y. S., Chan, W. Y., Jauch, R., Fritzsch, B., Sham, M. H., Lovell-Badge, R., & Cheah, K. S. E. (2022). SOX9 and SOX10 control fluid homeostasis in the inner ear for hearing through independent and cooperative mechanisms. *Proceedings of the National*

Academy of Sciences of the United States of America, *119*(46). https://doi.org/10.1073/PNAS.2122121119

Tadenev, A. L. D., Akturk, A., Devanney, N., Mathur, P. D., Clark, A. M., Yang, J., & Tarchini, B. (2019). GPSM2-GNAI Specifies the Tallest Stereocilia and Defines Hair Bundle Row Identity. *Current Biology*, *29*(6), 921-934.e4. https://doi.org/10.1016/J.CUB.2019.01.051/ATTACHMENT/76E1BC29-F635-4E86-BB83-206D31894A7C/MMC2.PDF

Tarchini, B., Jolicoeur, C., & Cayouette, M. (2013). A Molecular Blueprint at the Apical Surface Establishes Planar Asymmetry in Cochlear Hair Cells. *Developmental Cell*, *27*(1), 88–102. https://doi.org/10.1016/J.DEVCEL.2013.09.011/ATTACHMENT/4B5F3A51-E3C5-4F69-A980-5230750AA282/MMC1.PDF

Taylor, J. P., Tanaka, F., Robitschek, J., Sandoval, C. M., Taye, A., Markovic-Plese, S., & Fischbeck, K. H. (2003). Aggresomes protect cells by enhancing the degradation of toxic polyglutamine-containing protein. *Human Molecular Genetics*, *12*(7), 749–757. https://doi.org/10.1093/HMG/DDG074

Taylor, R. R., Filia, A., Paredes, U., Asai, Y., Holt, J. R., Lovett, M., & Forge, A. (2018). Regenerating hair cells in vestibular sensory epithelia from humans. *ELife*, *7*. https://doi.org/10.7554/ELIFE.34817

Tielens, S., Huysseune, S., Godin, J. D., Chariot, A., Malgrange, B., & Nguyen, L. (2016). Elongator controls cortical interneuron migration by regulating actomyosin dynamics. *Cell Research*, *26*(10), 1131–1148. https://doi.org/10.1038/CR.2016.112

Tokita, N., Chandra Sekhar, H. K., Daly, J. F., Becker, M. H., & Aleksic, S. (1979). The Campomelic Syndrome: Temporal Bone Histopathologic Features and Otolaryngologic Manifestations. *Archives of Otolaryngology*, *105*(8), 449–454. https://doi.org/10.1001/archotol.1979.00790200011003

Tritsch, N. X., & Bergles, D. E. (2010). Developmental regulation of spontaneous activity in the Mammalian cochlea. *The Journal of Neuroscience : The Official Journal of the Society for Neuroscience*, *30*(4), 1539–1550. https://doi.org/10.1523/JNEUROSCI.3875-09.2010

Tritsch, N. X., Yi, E., Gale, J. E., Glowatzki, E., & Bergles, D. E. (2007). The origin of spontaneous activity in the developing auditory system. *Nature*, *450*(7166), 50–55. https://doi.org/10.1038/nature06233

Tsue, T. T., Watling, D. L., Weisleder, P., Coltrera, M. D., & Rubel, E. W. (1994). Identification of hair cell progenitors and intermitotic migration of their nuclei

in the normal and regenerating avian inner ear. *Journal of Neuroscience*, *14*(1), 140–152. https://doi.org/10.1523/JNEUROSCI.14-01-00140.1994

Tu, Y., Fan, G., Sun, H., Cai, X., & Kong, W. (2019). Endoplasmic reticulum stress is involved in spiral ganglion neuron apoptosis following chronic kanamycin-induced deafness. *Bioscience Reports*, *39*(2). https://doi.org/10.1042/BSR20181749

Veithen, M., Huyghe, A., Van Den Ackerveken, P., Fukada, S. I., Kokubo, H., Breuskin, I., Nguyen, L., Delacroix, L., & Malgrange, B. (2023). Sox9 Inhibits Cochlear Hair Cell Fate by Upregulating Hey1 and HeyL Antagonists of Atoh1. *Cells*, *12*(17). https://doi.org/10.3390/cells12172148

Wang, W., Sun, Y., Chen, S., Zhou, X., Wu, X., Kong, W., & Kong, W. (2015). Impaired unfolded protein response in the degeneration of cochlea cells in a mouse model of age-related hearing loss. *Experimental Gerontology*, *70*, 61–70. https://doi.org/10.1016/j.exger.2015.07.003

Warchol, M. E., Massoodnia, R., Pujol, R., Cox, B. C., & Stone, J. S. (2019). Development of hair cell phenotype and calyx nerve terminals in the neonatal mouse utricle. *The Journal of Comparative Neurology*, *527*(11), 1913. https://doi.org/10.1002/CNE.24658

Wathieu, C., Lavergne, A., Xu, X., Rolot, M., Nemazanyy, I., Shostak, K., El Hachem, N., Maurizy, C., Leemans, C., Close, P., Nguyen, L., Desmet, C., Tielens, S., Dewals, B. G., & Chariot, A. (2024). Loss of Elp3 blocks intestinal tuft cell differentiation via an mTORC1-Atf4 axis. *The EMBO Journal*. https://doi.org/10.1038/S44318-024-00184-4/SUPPL_FILE/44318_2024_184_MOESM15_ESM.PDF

Weisz, C. J. C., Glowatzki, E., & Fuchs, P. A. (2014). Excitability of type II cochlear afferents. *The Journal of Neuroscience : The Official Journal of the Society for Neuroscience*, *34*(6), 2365–2373. https://doi.org/10.1523/JNEUROSCI.3428-13.2014

Willis, G. L., & Kennedy, G. A. (2004). The implementation of acute versus chronic animal models for treatment discovery in Parkinson's disease. *Reviews in the Neurosciences*, *15*(1), 75–87. https://doi.org/10.1515/REVNEURO.2004.15.1.75

Winkler, G. S., Kristjuhan, A., Erdjument-Bromage, H., Tempst, P., & Svejstrup, J. Q. (2002). Elongator is a histone H3 and H4 acetyltransferase important for normal histone acetylation levels in vivo. *Proceedings of the National Academy of Sciences of the United States of America*, *99*(6), 3517–3522. https://doi.org/10.1073/PNAS.022042899

Wittschieben, B., Otero, G., De Bizemont, T., Fellows, J., Erdjument-Bromage, H., Ohba, R., Li, Y., Allis, C. D., Tempst, P., & Svejstrup, J. Q. (1999). A novel histone acetyltransferase is an integral subunit of elongating RNA polymerase II holoenzyme. *Molecular Cell*, *4*(1), 123–128. https://doi.org/10.1016/S1097-2765(00)80194-X

Woerner, A. C., Frottin, F., Hornburg, D., Feng, L. R., Meissner, F., Patra, M., Tatzelt, J., Mann, M., Winklhofer, K. F., Hartl, F. U., & Hipp, M. S. (2016). Cytoplasmic protein aggregates interfere with nucleocytoplasmic transport of protein and RNA. *Science (New York, N.Y.)*, *351*(6269), 173–176. https://doi.org/10.1126/SCIENCE.AAD2033

Wu, J. S., Young, E. D., & Glowatzki, E. (2016). Maturation of Spontaneous Firing Properties after Hearing Onset in Rat Auditory Nerve Fibers: Spontaneous Rates, Refractoriness, and Interfiber Correlations. *Journal of Neuroscience*, *36*(41), 10584–10597. https://doi.org/10.1523/JNEUROSCI.1187-16.2016

Xia, K., Ma, H., Xiong, H., Pan, Q., Huang, L., Wang, D., & Zhang, Z. (2010). Trafficking abnormality and ER stress underlie functional deficiency of hearing impairment-associated connexin-31 mutants. *Protein & Cell*, *1*(10), 935–943. https://doi.org/10.1007/S13238-010-0118-7

Xue, Q., Li, C., Chen, J., Guo, H., Li, D., & Wu, X. (2016). The Protective effect of the endoplasmic reticulum stress-related factors BiP/GRP78 and CHOP/Gadd153 on noise-induced hearing loss in guinea pigs. *Noise & Health*, *18*(84), 247–255. https://doi.org/10.4103/1463-1741.192481

Yamada, T., Ishihara, H., Tamura, A., Takahashi, R., Yamaguchi, S., Takei, D., Tokita, A., Satake, C., Tashiro, F., Katagiri, H., Aburatani, H., Miyazaki, J. I., & Oka, Y. (2006). WFS1-deficiency increases endoplasmic reticulum stress, impairs cell cycle progression and triggers the apoptotic pathway specifically in pancreatic beta-cells. *Human Molecular Genetics*, *15*(10), 1600–1609. https://doi.org/10.1093/HMG/DDL081

Yamashita, D., Sun, G. wei, Cui, Y., Mita, S., Otsuki, N., Kanzaki, S., Nibu, K. I., Ogawa, K., & Matsunaga, T. (2015). Neuroprotective effects of cutamesine, a ligand of the sigma-1 receptor chaperone, against noise-induced hearing loss. *Journal of Neuroscience Research*, *93*(5), 788–795. https://doi.org/10.1002/JNR.23543

Yin, Y., Liberman, L. D., Maison, S. F., & Liberman, M. C. (2014). Olivocochlear innervation maintains the normal modiolar-pillar and habenular-cuticular gradients in cochlear synaptic morphology. *JARO - Journal of the Association*

for Research in Otolaryngology, *15*(4), 571–583. https://doi.org/10.1007/S10162-014-0462-Z/FIGURES/9

Yu, A., Shibata, Y., Shah, B., Calamini, B., Lo, D. C., & Morimoto, R. I. (2014). Protein aggregation can inhibit clathrin-mediated endocytosis by chaperone competition. *Proceedings of the National Academy of Sciences of the United States of America*, *111*(15). https://doi.org/10.1073/PNAS.1321811111/-/DCSUPPLEMENTAL/PNAS.201321811SI.PDF

Zeng, S., Ni, W., Jiang, H., You, D., Wang, J., Lu, X., Liu, L., Yu, H., Wu, J., Chen, F., Li, H., Wang, Y., Chen, Y., & Li, W. (2020). Toxic Effects of 3,3'-Iminodipropionitrile on Vestibular System in Adult C57BL/6J Mice In Vivo. *Neural Plasticity*, *2020*. https://doi.org/10.1155/2020/1823454

Zhang, Y. J., Gendron, T. F., Grima, J. C., Sasaguri, H., Jansen-West, K., Xu, Y. F., Katzman, R. B., Gass, J., Murray, M. E., Shinohara, M., Lin, W. L., Garrett, A., Stankowski, J. N., Daughrity, L., Tong, J., Perkerson, E. A., Yue, M., Chew, J., Castanedes-Casey, M., … Petrucelli, L. (2016). C9ORF72 poly(GA) aggregates sequester and impair HR23 and nucleocytoplasmic transport proteins. *Nature Neuroscience*, *19*(5), 668–677. https://doi.org/10.1038/NN.4272

Zheng, J. L., & Gao, W. Q. (2000). Overexpression of Math1 induces robust production of extra hair cells in postnatal rat inner ears. *Nature Neuroscience*, *3*(6), 580–586. https://doi.org/10.1038/75753

Zheng, J., Shen, W., He, D. Z. Z., Long, K. B., Madison, L. D., & Dallos, P. (2000). Prestin is the motor protein of cochlear outer hair cells. *Nature*, *405*(6783), 149–155. https://doi.org/10.1038/35012009

Xue Qiuhong, Chen Jia, Gong Shusheng, He Jian, Xie Jing und Chen Xiaolin

. (2009). Role of caspase 12 in apoptosis of cochlea induced by intense noise in guinea pigs, *44*(02), 154–159. https://doi.org/10.3760/CMA.J.ISSN.1673-0860.2009.02.018

Appendix

I contributed to this work as it was the research project I conducted for my Master Thesis (from February until July 2020) in Brigitte Malgrange's lab under the supervision of Laurence Delacroix.

cells

MDPI

Article

Sox9 Inhibits Cochlear Hair Cell Fate by Upregulating Hey1 and HeyL Antagonists of Atoh1

Mona Veithen [1,†], Aurélia Huyghe [1,†], Priscilla Van Den Ackerveken [1], So-ichiro Fukada [2], Hiroki Kokubo [3], Ingrid Breuskin [1], Laurent Nguyen [4], Laurence Delacroix [1,‡] and Brigitte Malgrange [1,*,‡]

1 Laboratory of Developmental Neurobiology, GIGA-Neurosciences, University of Liege, 4000 Liege, Belgium; mona.veithen@uliege.be (M.V.); aurelia.huyghe@lyon.unicancer.fr (A.H.); p.vandenackerveken@outlook.be (P.V.D.A.); ingrid.breuskin@gustaveroussy.fr (I.B.); ldelacroix@uliege.be (L.D.)
2 Laboratory of Stem Cell Regeneration and Adaptation, Graduate School of Pharmaceutical Sciences, Osaka University, Osaka 565-0871, Japan; fukada@phs.osaka-u.ac.jp
3 Graduate School of Biomedical and Health Sciences, 1-2-3 Kasumi, Minamiku, Hiroshima 734-8551, Japan; hkokubo@hiroshima-u.ac.jp
4 Laboratory of Molecular Regulation of Neurogenesis, GIGA-Neurosciences, University of Liege, 4000 Liege, Belgium; lnguyen@uliege.be
* Correspondence: bmalgrange@uliege.be
† These authors contributed equally to this work.
‡ These authors jointly supervised this work.

Abstract: It is widely accepted that cell fate determination in the cochlea is tightly controlled by different transcription factors (TFs) that remain to be fully defined. Here, we show that Sox9, initially expressed in the entire sensory epithelium of the cochlea, progressively disappears from differentiating hair cells (HCs) and is finally restricted to supporting cells (SCs). By performing ex vivo electroporation of E13.5–E14.5 cochleae, we demonstrate that maintenance of Sox9 expression in the progenitors committed to HC fate blocks their differentiation, even if co-expressed with Atoh1, a transcription factor necessary and sufficient to form HC. Sox9 inhibits Atoh1 transcriptional activity by upregulating Hey1 and HeyL antagonists, and genetic ablation of these genes induces extra HCs along the cochlea. Although Sox9 suppression from sensory progenitors ex vivo leads to a modest increase in the number of HCs, it is not sufficient in vivo to induce supernumerary HC production in an inducible Sox9 knockout model. Taken together, these data show that Sox9 is downregulated from nascent HCs to allow the unfolding of their differentiation program. This may be critical for future strategies to promote fully mature HC formation in regeneration approaches.

Keywords: Sox9; cochlea; organ of Corti; transfection; differentiation; development

Citation: Veithen, M.; Huyghe, A.; Van Den Ackerveken, P.; Fukada, S.-i.; Kokubo, H.; Breuskin, I.; Nguyen, L.; Delacroix, L.; Malgrange, B. Sox9 Inhibits Cochlear Hair Cell Fate by Upregulating Hey1 and HeyL Antagonists of Atoh1. *Cells* **2023**, *12*, 2148. https://doi.org/10.3390/cells12172148

Academic Editor: Lon J. van Winkle

Received: 1 August 2023
Revised: 23 August 2023
Accepted: 24 August 2023
Published: 25 August 2023

1. Introduction

The mammalian cochlea has a specialized sensory epithelium, the organ of Corti, which is involved in sound perception. Cochlear sensory epithelium morphogenesis is a highly complex and stereotyped process that gives rise to a specific mosaic pattern of hair cells (HCs) and supporting cells (SCs). In mice, the development of the organ of Corti from the otocyst can be divided in two phases [1]. Starting around embryonic stage 12.5 (E12.5), the first step specifies a prosensory area within the ventral part of the developing otocyst. During the second phase, beginning at E14.5–E15.5 at the base of the cochlea, the HCs and their accompanying SCs differentiate from common progenitor cells within the prosensory epithelial domain.

Prosensory progenitors exit the cell cycle around E12.5 and form a post-mitotic zone of non-proliferating cells [2]. In contrast to fish and birds, mature cells of the mammalian organ of Corti do not contribute to cellular regeneration after injury, as they cannot re-enter the cell cycle. Unsurprisingly, hair cell loss in the adult mammalian auditory system is irreversible

and is a leading cause of permanent hearing loss. Therefore, defining the transcriptional programs that pattern the cochlea and specify HC and SC fate from progenitors will likely contribute to establishing new strategies for treating neurosensory deafness [3,4].

Previously, several studies have brought to light the mechanisms contributing to cochlear terminal cell differentiation (after E14.5), and major players, such as the transcription factor (TF) Atoh1 and the Notch signaling pathway, have been identified. The proneural basic helix–loop–helix (bHLH) *Atoh1* gene has been identified as the earliest specific gene required for HC differentiation. Deletion of *Atoh1* leads to a complete absence of HCs, whereas Atoh1 overexpression induces ectopic HCs in both sensory and non-sensory regions of the cochlea [5–7]. Differentiating HCs express Delta1 and Jagged2 ligands [8,9], which signal to Notch-expressing neighboring SCs to inhibit them from acquiring HC fate, in a process named lateral inhibition [10]. Conditional deletion of either *Jagged2* or *Delta1* in the cochlea leads to an overproduction of HCs, via a fate switch of SCs [11,12]. Upon activation through ligand binding, the Notch receptor is cleaved and its intracellular domain (NICD) associates with RBP-Jκ in the nucleus to transactivate target genes [13], including the Hairy Enhancer of Split (Hes) family members, Hes1 and Hes5. In the cochlea, these transcriptional repressors act as critical regulators of cell fate by inhibiting *Atoh1* transcription [14], and deletion of either of these genes induces supernumerary HCs in the cochlea [15].

Sox9, a high-mobility group (HMG) box TF, is expressed during embryonic development in several tissues including chondrocytes, lung, pancreas, heart, the central nervous system, and the inner ear [16–18]. Typically, Sox9 is essential during early stages of development to maintain a progenitor cell pool, while, at later stages of organogenesis, it plays a role in terminal cell differentiation [19–21]. In humans, mutations of *Sox9* are associated with inherited genetic birth defects, including campomelic dysplasia (CD), an autosomal dominant disease characterized by skeleton malformation, XY sex reversal, and a high neonatal lethality rate [22]. Surviving patients often suffer sensorineural hearing loss associated with a malformation of the inner ear canals [22–24]. Because Sox9 is one of the first specific markers of the otic placode, various studies have focused on the early functions of Sox9 in the inner ear. In Xenopus [25,26] and Zebrafish [27], loss of *Sox9* results in the failure of the otic placode and vesicle development, while in mice, it is required for placode invagination [28].

Given the known role of Sox9 in cell fate specification in multiple organs [29] and its expression in the mammalian cochlea [18], we investigated the contribution of Sox9 to mouse cochlear differentiation. Gain of function experiments revealed that Sox9 prevents HC differentiation by reducing Atoh1 activity. This effect was mediated by upregulating Hey1 and HeyL factors, which in turn inhibit Atoh1 transactivation potential. Altogether, our data support that Sox9 is a regulator of cell fate in the sensory epithelium of the organ of Corti.

2. Materials and Methods

2.1. Mouse Strains and Tamoxifen Treatment

Hey1$^{+/-}$, HeyL$^{+/-}$ [30], Sox9^{eGFP} [31], Sox2^{CreERT2} [32], Sox9$^{lox/lox}$ [33], and wild-type NMRI or BALB/c mice (Animal Facility of the University of Liège) were used. A Cre-inducible R26R^{EYFP} responder strain [34] was also incorporated into the breeding scheme to monitor the extent of Cre-mediated recombination.

Mice were time-mated, and conception was confirmed by the presence of a vaginal plug, which was considered as day 0.5 (E0.5). The day of birth was regarded as P0. All experimental procedures and protocols were reviewed and approved by the Institutional Animal Care and Use Ethics Committee of the University of Liège (Belgium). The "Guide for the Care and Use of Laboratory Animals", prepared by the Institute of Laboratory Animal Resources, National Research Council, and published by the National Academy Press, was followed carefully as well as European and local legislation.

Tamoxifen was dissolved at 30 mg/mL in a sunflower oil/ethanol mixture (9:1) and administered to time-pregnant mice orally (100 µL) and by intraperitoneal injection (100 µL) for 2 consecutive days (E12.5–E13.5).

2.2. Plasmid Constructions

Plasmids encoding specific shRNAs were constructed by cloning synthesized oligonucleotides into pCA-b-EGFPm5 silencer 3 vector [35] with the following targeting sequences: 5′-CAGACTCACATCTCTCCTAAT-3′ (shRNA-Sox9#1), 5′-CTCCACCTTCACTTACATGAA-3′ (shRNA-Sox9#2), 5′-AGACCGAATCAATAACAGTTT-3′ (shRNA-Hey1) and 5′-GCTGTTGA CTTCCGGAGTAT-3′ (shRNA-HeyL). A control shRNA vector was generated by cloning a sequence with no significant homology to any known gene sequence from a mouse: 5′-TACGCGCATAAGATTAGGG-3′.

Expression plasmids were constructed by cloning Atoh1, Sox9, Hey1, and HeyL coding sequences into the bicistronic pCAGGS-IRES-GFP vector. Using Expand™ high-fidelity PCR system (Merck Life Science BV, Hoeilaart, Belgium), we generated Sox9 coding sequence corresponding to amino acids 1–304 and cloned it in the same plasmid to generate a DN-Sox9 expression vector.

Luciferase reporters controlled by Atoh1 (7EBox-Luc) and Sox9 binding sites (called pCol2a1-Luc in this paper) as well as those driven by promoters of *Sox9* (pSox9-luc), *Hey1* (−604/+87pHey1-Luc), and *HeyL* (1168/+288pHeyL-Luc) were described previously [36–40]. Additional reporter vectors were created by inserting shorter promoter fragments into the pLUC reporter construct. Inserts were generated by high-fidelity PCR amplification using forward primers containing NheI site and reverse primers containing XhoI site (Supplementary Materials Table S3), except for pHey1 (−50/+3), which was synthesized (IDT, Leuven, Belgium). All constructs were verified by sequencing.

2.3. Cell Culture and Transfection

Immortalized organ of Corti cells derived from the mouse at E13.5, UB/OC-1 cells [41], were obtained from Pr. Matthew Holley (Department of Biomedical Science, Sheffield, UK) and cultured in MEM (Lonza, Basel, Switzerland) supplemented with 10% fetal bovine serum (Lonza) and 50 U/mL γ-Interferon (Sigma) in a humidified 5% CO_2 atmosphere at 33 °C. HEK293 cells were maintained in DMEM medium supplemented with 10% FBS in a humidified 5% CO_2 atmosphere at 37 °C.

Cells were transfected in 24-well plates with a total of 500 ng DNA and 1–1.5 µL of Lipofectamine 2000 reagent (Invitrogen, Carlsbad, CA, USA) 48 h before experimentation.

Validated endoribonuclease-prepared siRNA for silencing *Hey1* (N°EMU044841 directed against the exon 5 of mouse Hey1) and *HeyL* (N°SASI_Mm01_00137911) genes were purchased from Merck Life Science BV (Hoeilaart, Belgium). In transfection experiments combining DNA plasmids and siRNAs, the cells were first transfected with 20 nM siRNA using Lipofectamine 2000 and further transfected two days later with 20 nM siRNA and 500 ng DNA.

2.4. Western Blot

Cells were lysed on ice in a solution containing 50 mM Tris HCl, pH7.4, 1% Triton X-100, 150 mM NaCl, 10 mM NaF, 1 mM Na3VO4, and protease inhibitors (Protease Inhibitor Cocktail Tablets, Roche). Protein concentration was assessed using the Bradford method. Protein lysates (30 µg) were separated by 10% SDS-polyacrylamide gel electrophoresis and transferred onto PVDF membranes (Millipore, Burlington, MA, USA). Non-specific binding was blocked with 5% dried fat-free milk in TTBS (50 mM Tris-HCl pH 7.4, 150 mM NaCl, 0.1% Tween 20) for 1 h at room temperature and subsequently incubated overnight at 4 °C with the following primary antibodies: rabbit polyclonal antibody to Sox9 (1:1000, Santacruz, Santa Cruz, CA, USA) and mouse monoclonal antibody to β-actin (1:5000, clone AC-15, Sigma Aldrich). After washing steps in TTBS, membranes were incubated with the appropriate horseradish peroxidase-conjugated secondary antibody (1/5000, AbCam,

Cambridge, UK) for 2 h at room temperature. Protein expression was detected by enhanced chemiluminescence (ECL, GE Healthcare, Chicago, IL, USA).

2.5. RT-qPCR

Total RNA from UB/OC1 cells or dissected cochleae was extracted using TriPure Isolation Reagent (Roche) with a DNase I (Roche) step according to the manufacturer's instructions. cDNA was prepared from 1 µg of RNA using the RevertAid H Minus First Strand cDNA Synthesis Kit (Fisher scientific BVBA, Brussels, Belgium) and used for qPCR in a LightCycler 480 (Roche, Machelen, Belgium). Expression levels were normalized to the expression of *glyceraldehyde-3-phosphate dehydrogenase* (GAPDH). All amplifications were performed in duplicate, and at least three biological replicates were performed. PCR primer sequences that were used are listed in Supplementary Table S2.

2.6. Luciferase Assay

UB/OC1 or HEK293 cells (5×10^4 cells/well in 24-well plates) were transfected using 200 ng reporter vector (Firefly Luciferase), 10 ng pRL-SV (Renilla Luciferase control vector, Promega, Madison, WI, USA), and 300 ng expression vectors (when necessary). The total amount of DNA was kept constant by adding the control pCAGGS plasmid. Cell lysates were assayed for luciferase activity two days post-transfection using the Promega Dual Luciferase kit and a Berthold LB 960 microplate luminometer. Firefly Luciferase activity was reported to Renilla Luciferase activity to normalize for the differences in transfection efficiencies. Each experiment was repeated at least three times, and each measurement was performed in duplicates.

2.7. Organotypic Cochlear Cultures

2.7.1. Tissue Isolation and Culture

Cochleae of stage E13.5 or E14.5 were collected in PBS (Lonza). Each organ of Corti was freed from surrounding tissues and explanted intact onto the surface of a sterile membrane (Millicell®, Millipore) in DMEM (Gibco, Billings, MT, USA) containing N1 supplement (Invitrogen), glucose 0.15%, penicillin (100 U/mL), and insulin (5 µg/mL). Cultures were maintained in a 5% CO_2-humidified incubator at 37 °C.

2.7.2. Electroporation

Cochlear ducts were injected with a 2 µg/µL DNA solution in 0.5% Fast Green (Sigma) and placed in a Sonidel electroporation chamber (CUY520P5). A total of 8 electrical pulses were applied at 30 V (50 ms duration) at 800 ms intervals using a square wave electroporation system (ECM-830 BTX, San Diego, CA, USA). Cochleae were dissected after electroporation and cultured on Millicell® for 6 days to allow terminal cell differentiation. The culture medium was replaced after the first 3 days.

2.8. Immunohistochemistry

For immunohistological analysis, heads were fixed with 4% paraformaldehyde (Sigma-Aldrich, Burlington, MA, USA) for 4–6 h at 4 °C. After three PBS rinses, the fixed heads were immersed in 20% sucrose in PBS overnight at 4 °C. Tissues were frozen, embedded in 7.5% gelatin/15% sucrose in PBS, then sectioned at 12 µm, mounted on SuperFrost® slides, and stored at −80 °C. Sections were washed three times with PBS and blocked for 1 h with 0.25% gelatin and 0.1% Triton X100 (Sigma-Aldrich) in PBS at room temperature. For cochlear explants, the tissues were fixed in 4% paraformaldehyde for 10 min at room temperature, washed in PBS, and then directly processed for blocking. Antigens were unmasked, when necessary, by incubating samples in an antigen retrieval solution (Dako) for 15 min at 95 °C, followed by slow cooling back to room temperature before blocking. Primary antibodies were incubated overnight at 4 °C in the same blocking solution. The following primary antibodies were used in various combinations: Myosin 6 (Myo6, rabbit, 1:250, Santa Cruz); Parvalbumin (mouse, 1:250, Sigma-Aldrich); Prox1 (rabbit, 1:500, Mil-

lipore); Sox2 (goat, 1:200, Santa Cruz); Sox9 (rabbit, 1:100, Millipore or gift from Brigitte Boizet); and GFP (chicken, 1:500, Aves Labs). Samples were subsequently washed three times in PBS and incubated for 45 min at room temperature in a blocking solution containing a secondary antibody (1:1000) conjugated to FITC-, RRX-, or Cy5 fluorophores (Jackson Immunoresearch Laboratories, West Grove, PA, USA). After three rinses in PBS, preparations were mounted in Vectashield containing DAPI (Hard Set Mounting Medium, Vector Laboratories, Burlingame, CA, USA) and examined with a confocal microscope (NIKON A1, Brussels, Belgium).

2.9. Quantification of HC Fate in Cultured Explants

Immunostained explants were analyzed with a NIKONA1 confocal microscope, with a 60× magnification, and images were taken at different focal planes spanning the depth of the sensory epithelium (hair cells and underlying supporting cells). Except for the apical region of the explant, all GFP-positive cells residing in the region comprising the hair cells and the supporting cells displaying strong Sox2 labelling (from inner phalangeal cells to Deiters cells) were considered for further analysis. Using the cell counter tool in ImageJ software (version 1.51h), cells expressing Myo6 and no or low Sox2 were considered as hair cells, and their proportion within all GFP-positive cells was determined manually for each explant. Ectopic HCs, which are only induced upon Atoh1 transfection, were determined by analyzing GFP-positive cells that are present in Kölliker's organ, the region located at the medial side of inner HCs. All data were collected from a minimum of 5 explants (see Supplementary Materials Table S1), from 2–3 independent cultures, and the results are expressed as the percentage mean ± SEM.

2.10. Supernumerary HC Counts

Whole-mount cochlear samples from newborn mice were dissected, immunostained for HC marker Myo6, and imaged with a NIKONA1 confocal microscope. Extra HCs were quantified all along the cochlea except for the most apical part. The length of the sensory epithelium submitted to analysis was measured using ImageJ software, and the results are expressed as the mean ± SEM of the number of supernumerary HCs per mm of cochlea (more than $n = 4$ for each group).

2.11. In Situ Hybridization

E14.5, E17.5, or P0 heads were fixed in 4% paraformaldehyde in PBS overnight at 4 °C, sunk in 20% sucrose in PBS overnight at 4 °C, and embedded in 7.5% gelatin with 15% sucrose in PBS. Cochlear explants were fixed in 4% paraformaldehyde for 4 h at room temperature and washed in PBS before ISH. ISH was performed on 12 µm thick transverse sections of the head or entire cochleae using digoxigenin-labelled riboprobes, as previously described [42]. Plasmids containing full-length mouse Hey1 and HeyL cDNAs were provided by Manfred Gessler.

2.12. Statistical Analysis

Statistical analyses were carried out using the unpaired Student's *t*-test for pairwise comparisons or a one-way ANOVA followed by Tukey's post hoc test using GraphPad Prism 8 (GraphPad Software, Boston, MA, USA) for all the other studies. The results are presented as mean ± SEM and were considered significant when $p < 0.05$. The number of biological replicates relevant for individual experiments are stated in the Results section or Supplementary Table S1.

3. Results

3.1. Analysis of Sox9 Expression Pattern in the Developing Mouse Cochlea

Previous analyses have shown that Sox9 is expressed at E8.5 in the nascent otic placode and at E9.5 in the entire otic vesicle [18,28]. We performed in situ hybridization on E13.5 cochlear sections to extend this analysis to later developmental stages. We found

that Sox9 mRNA is highly expressed in the otic epithelium throughout the cochlear duct and in the otic capsule (Figure 1A). Consistent with published results by Mak et al. [18], Sox9 protein was detected by immunohistochemistry in the entire cochlear epithelium (Figure 1B). This pattern of expression was further confirmed in the developing cochleae of a transgenic mouse line in which GFP expression is under the control of the Sox9 regulatory sequences [31] (Figure 1C, $Sox9^{EGFP}$). Between E14.5 and E18.5, Sox2-positive progenitor cells are subjected to a baso-apical wave of differentiation generating the HC and their surrounding SC [1]. At E16.5, Sox9 immunoreactivity was lost specifically in some Sox2-expressing cells that likely correspond to differentiating HC in the basal turn of the cochlea. At the same time, it was still detected in all prosensory cells of the apical turn (compare Figure 1G–I to Figure 1D–F). Finally, Sox9 remains absent from Myo6-positive HC at P0 and is restricted to the SC in the organ of Corti (Figure 1J–L).

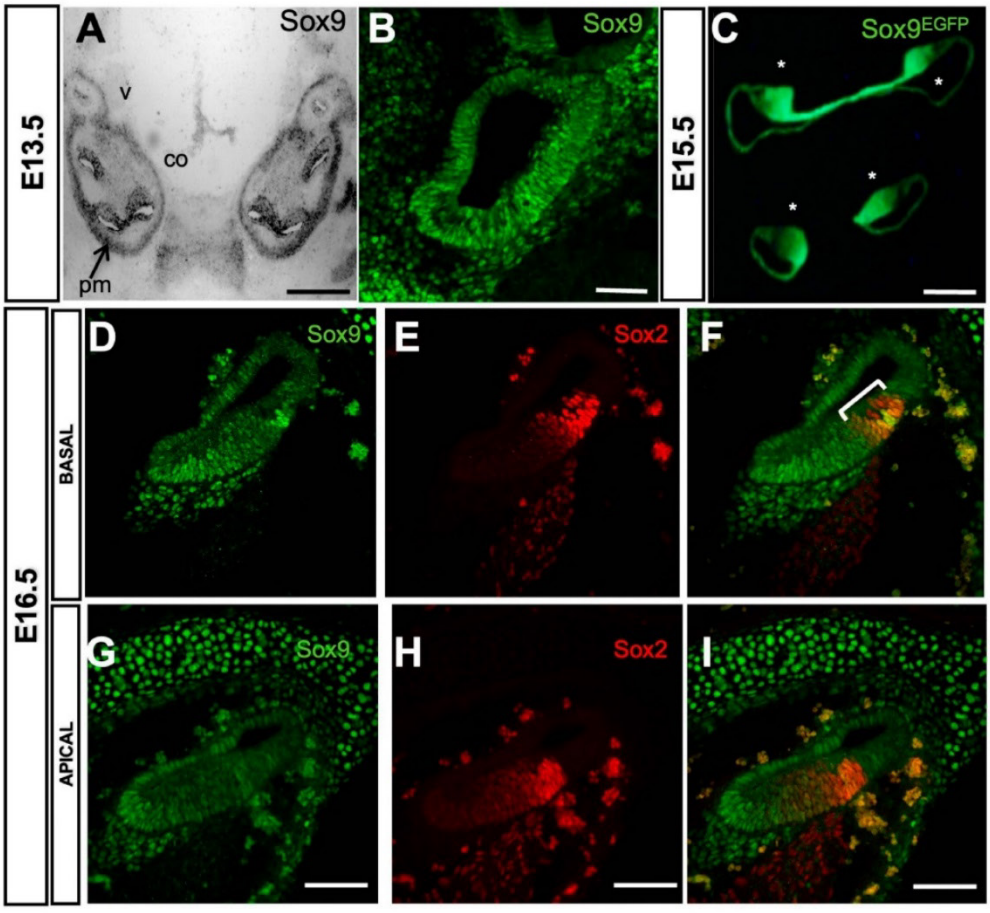

Figure 1. *Cont.*

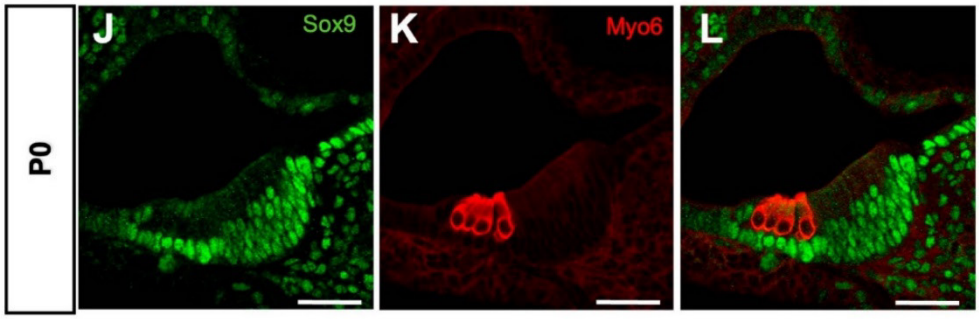

Figure 1. Sox9 expression in the developing cochlea. (**A**,**B**) In situ hybridization (**A**) and immunostainings (**B**) directed against Sox9 in E13.5 mouse inner ear. Sox9 is broadly expressed in the otic capsule and in the cochlear duct epithelium at the transcript and protein levels. (**C**) Cross-section from Sox9EGFP mouse at E15.5 reveals strong Sox9 expression within the cochlear duct (asterisks indicate individual turns of the coiled cochlea). (**D**–**I**) Immunostainings of Sox9 (green) and Sox2 (red) through basal (**D**–**F**) and apical (**G**–**I**) turns of E16.5 cochlea. Sox9 is absent from HCs at the base ((**D**,**F**), differentiating OHCs are indicated by a bracket) but is still detected in future HCs at the apex (**G**,**I**), while Sox2 is present in these cells for both areas (**E**,**F**,**H**,**I**). Sox9 is highly expressed in the surrounding mesenchyme. (**J**–**L**) Representative cross-section through the mid-basal turn of P0 cochlea labeled for Sox9 (green) and Myo6 (red). Sox9 is absent from Myo6-positive HCs and highly expressed in the neighboring SCs. Scale bars: (**A**,**C**) 100 µm, (**B**,**D**–**L**) 50 µm.

3.2. Sox9 Inhibits Cochlear Hair Cell Fate Ex Vivo

We next sought to characterize the functional significance of Sox9 downregulation from the nascent HC population of the developing cochlea. We performed Sox9 gain-of-function experiments to test whether we could change cell fate in the E14.5 organs of Corti. Six days after electroporation, when terminal differentiation was complete, cultured explants were immunolabelled with HC and SC markers. In the sensory epithelium, 28.5 ± 2.15% of cells transfected with the control GFP plasmid became fully differentiated HCs and were positive for Myo6 or Parvalbumin (Figure 2B,C,P and Supplementary Figure S1A,B). In contrast, Sox9-GFP electroporated cells rarely expressed Myo6 or Parvalbumin (1.52% ± 1.13, Figure 2D–G,P and Supplementary Figure S1C–F). Within the HC layer, some of these Myo6-negative Sox9 transfected cells still showed weak staining for Sox2 (Supplementary Figure S1E–H, white arrows), similar to that observed in the neighboring non-transfected HCs. However, for most of them, Sox2 was absent from the nucleus (Supplementary Figure S1E–H, yellow arrowheads). These cells did not express SC-specific markers Prox1 or p27, indicating that HC fate was inhibited but not at the profit of a switch towards SC fate. Within the SC layer, transfected cells do not seem to be affected by Sox9 overexpression, as they expressed normal levels of Prox1, Sox2, or p27 (Figure 2I–K and Supplementary Figure S1M–P).

To further study the role of Sox9 in cochlear cell fate and patterning, we performed loss-of-function experiments. Two shRNAs targeting different regions of Sox9 transcript were tested in UB/OC1 cells, which derive from a murine otocyst and are classically used as a model for organ of Corti cell differentiation [41]. We transfected them in an otocyst-derived UB/OC1 cell line to establish their efficacy and performed a Western blot for Sox9 48 h later. Both shRNAs efficiently reduced the expression of Sox9 (Supplementary Figure S2A). We then performed a knockdown of Sox9 by electroporating these shRNAs in E13.5 cochlear explants and analyzed the phenotype of transfected cells after 6 days in vitro (DIV). A modest increase in the proportion of Myo6-GFP-positive cells was observed in the presence of both Sox9 shRNAs (Figure 2M–O and Supplementary Table S1), revealing the formation of extra HCs.

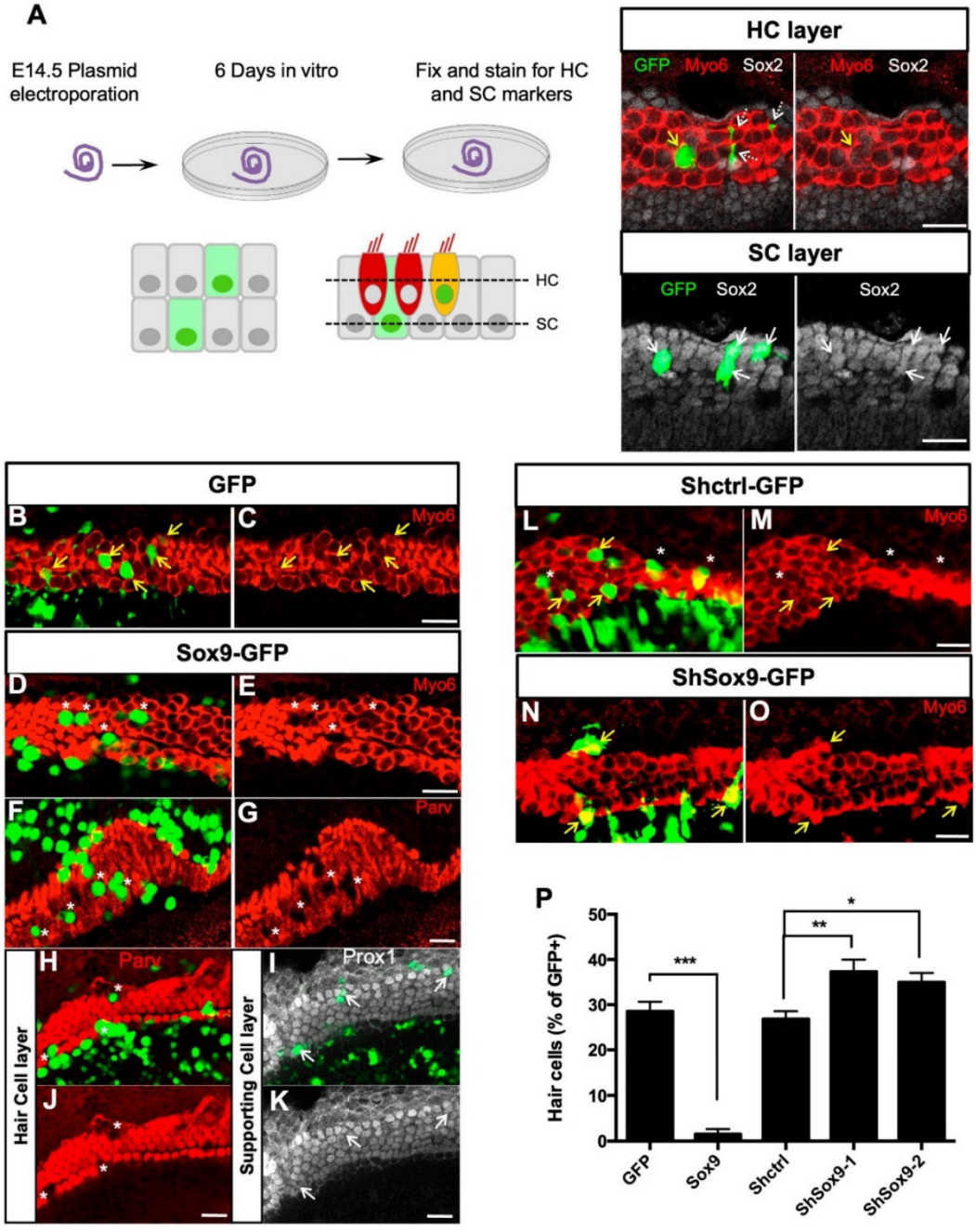

Figure 2. Modulation of Sox9 expression affects HC differentiation. (**A**) Experimental design: E14.5 cochleae were electroporated with GFP-expressing plasmids and further cultured for 6 DIV before fixation and immunohistochemical analysis of HC and SC markers. The total number of GFP-positive cells was evaluated throughout the depth of the sensory epithelium, in the HC and SC layers. In this representative result, only 1/5 GFP+ transfected cell has developed into a Myo6+ HC (indicated by a

yellow arrow) and 4/5 have adopted an SC fate (white arrows). Cochlear explants were electroporated at E14.5 with GFP (**B**,**C**) or Sox9-GFP (**D**–**G**) and further cultured for 6 DIV. Yellow arrows = Transfected cells in the sensory epithelium. Cells overexpressing Sox9 within the HC layer rarely express Myo6 (**E**) or Parv (**G**), indicating that they do not develop as HCs (white asterisks). (**H**–**K**) Confocal images taken at the level of HCs (**H**,**J**) or SCs (**I**–**K**) after electroporating Sox9-GFP (white asteriks = transfected cells within the sensory epithelium). While Sox9 overexpression prevents the formation of GFP+Parv+ HCs, it does not affect the number of SCs (GFP+Prox1+) beneath the sensory cells (indicated by white arrows). (**L**–**O**) E13.5 cochleae electroporated with Shctrl (**L**–**M**) or ShSox9-GFP (**N**–**O**) and cultured for 6DIV. Sox9 knockdown increased the population of GFP+Myo6+ HCs (yellow arrows) at the expense of those developing as SCs (white asterisks). (**P**) Quantification of (**A**–**N**) the percentage of Parv+ or Myo6+ cells among the GFP+ cell population was analyzed within the sensory region of each explant. Data are expressed as mean ± SEM (6–10 cochlear explants per condition from 3 independent experiments). * = $p < 0.05$, ** = $p < 0.01$ and *** = $p < 0.001$. Scale bars (**A**–**N**): 25 µm.

Altogether, these results suggest that Sox9 inhibits HC differentiation from progenitors and that the correct cell patterning in the organ of Corti requires the downregulation of Sox9 in nascent HCs.

3.3. Sox9 Inhibits Atoh1 Activity

The specification of HCs requires the transcriptional factor of Atoh1 [5,7,8]. Atoh1 expression is first detected at a low level in progenitor cells of the organ of Corti, before cell differentiation, and then further upregulated in differentiating HCs [43–45]. Because we showed that modulating Sox9 expression in situ interferes with HC differentiation, we investigated the impact of Sox9 overexpression on Atoh1 function. Ex vivo electroporations of Atoh1-GFP alone or combined with Sox9 in E14.5 cochlear explants were performed and subsequently analyzed after 6 DIV. Consistent with a previous report [7], most Atoh1-GFP-transfected cells expressed the HC marker Parvalbumin within the organ of Corti (86.42% ± 3.65, Figure 3A,B,E). Interestingly, the number of transfected cells adopting HC fate was drastically reduced upon co-transfection with Sox9-GFP (10.25%± 3.17, Figure 3C–E), indicating that Sox9 is able to counteract Atoh1-mediated HC induction. Noteworthy is that Atoh1 transfection in cells residing in Kölliker's organ gave rise to ectopic HCs. Indeed, the vast majority of GFP-positive cells located on the medial side of the HC region expressed Parvalbumin (Figure 3A,B) and KO. The ability of Atoh1 to induce HC fate outside the organ of Corti was also impaired by the presence of Sox9-GFP, as many cotransfected cells lack the Parvalbumin marker (Figure 3C,D, white arrows). Sox9 could act by inhibiting Atoh1 DNA binding or transactivation of specific target genes, thus blocking the initiation of the HC developmental program. Therefore, we monitored Atoh1 transcriptional activity by performing in vitro reporter assays using a multimerized Atoh1 responsive element (seven repeats of Ebox; see Figure 3F) upstream of the luciferase coding sequence [14]. This analysis was performed in the UB/OC1 cell line. When Sox9 was co-transfected with Atoh1, the reporter activity was significantly reduced dose-dependently, while it had no effect in the absence of Atoh1 (Figure 3H). These results indicate that Sox9 interferes with the transcriptional activity of Atoh1.

To decipher whether the effect of Sox9 involves the upregulation of Atoh1 modulators, we decided to block Sox9 transcriptional activity by using a dominant negative form of Sox9 (DN-Sox9). This mutant lacking the C-terminal transactivation domain represses the Sox9-dependent activation of one of its main targets, i.e., the Col2a1 promoter (Supplementary Figure S2B) [46]. In the Atoh1 reporter assay (Figure 3H), DN-Sox9 suppressed, in a dose-dependent manner, the inhibitory effect of Sox9 on Atoh1. Accordingly, DN-Sox9 also suppresses, dose-dependently, the inhibitory effect of Sox9 on HC fate when co-electroporated with Sox9 in cochlear explants (Supplementary Figure S2C–I).

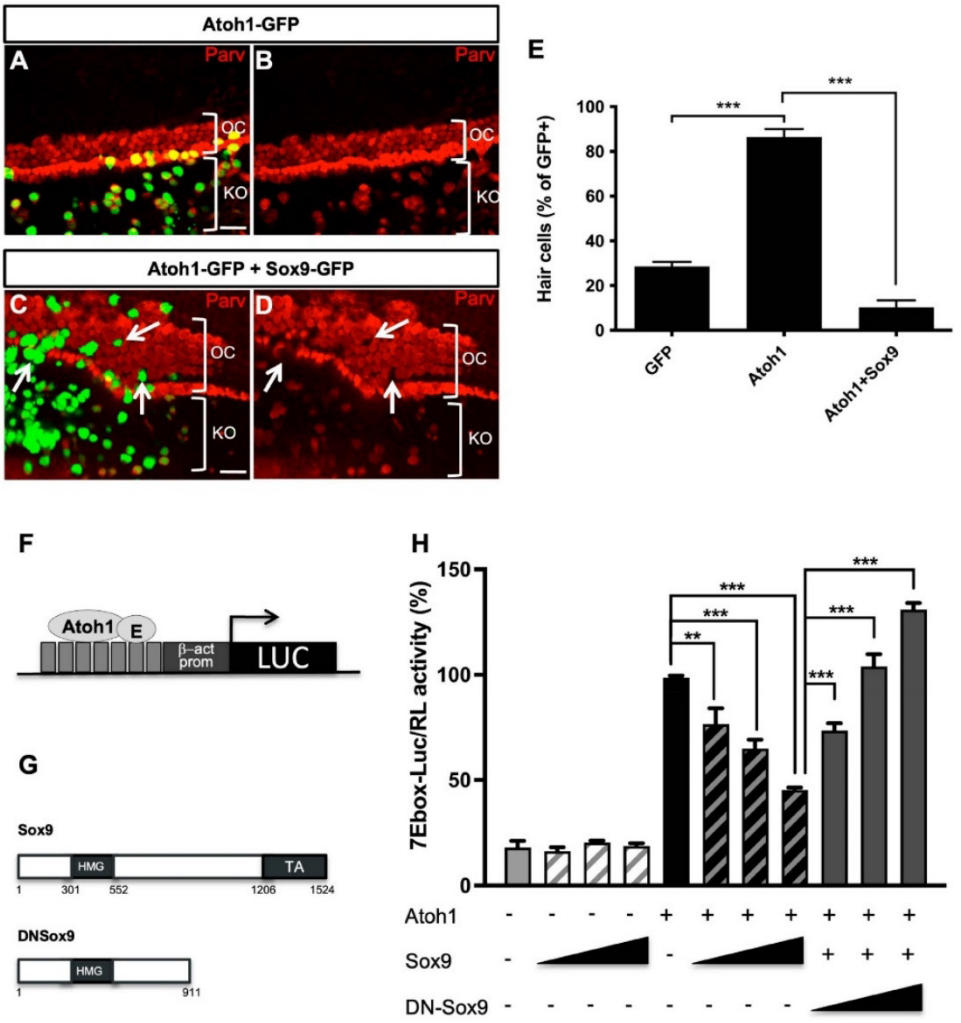

Figure 3. Sox9 inhibits Atoh1 activity. (**A**–**D**) Parvalbumin (Parv) immunostainings of cochlear explants cultured for 6 days after electroporation with Atoh1-GFP alone (**A**,**B**) or in combination with Sox9-GFP (C-D). While most of the cells expressing Atoh1-GFP develop as Parv+ HCs, even in Kölliker's organ (KO), outside the organ of Corti (OC), most cells expressing Atoh1 together with Sox9-GFP fail to express HC marker. Scale bars (**A**–**D**): 25 µm (**E**) Quantifications of (**A**–**D**). The percentage of GFP+Parv+ cells, within the organ of Corti, was evaluated for each explant. Data are presented as mean ± SEM (6–12 cochlear explants per condition from 3 independent experiments). (**F**,**G**) Schematic representation of luciferase reporter controlled by Atoh1 and Sox9 constructs (**H**) Luciferase assays of UB/OC1 cells transfected with Atoh1-responsive reporter (7Ebox-Luc) and control GFP, Atoh1-GFP, Sox9-GFP, or DNSox9-GFP expressing vectors. The firefly luciferase activity of the reporter constructs in transfected cells was normalized to the Renilla luciferase activity of the control construct (pRL-SV). Data are presented as a percentage of Atoh1 relative activity from three independent experiments. Atoh1 efficiently activates transcription from E-box-containing promoters, but this is dose-dependently inhibited by the presence of Sox9. The use of a dominant negative form of Sox9 protein (DN-Sox9), lacking the transactivation domain, suppresses Sox9 effect on Atoh1. ** = $p < 0.01$ and *** = $p < 0.001$.

Collectively, these results indicate that Sox9 activates the transcription of genes that inhibit Atoh1 transactivation potential and HC induction.

3.4. Sox9 Activates Hey1 and HeyL Gene Expression

To identify Sox9 target genes acting as Atoh1 putative antagonists, we examined the role of Hes/Hey and Id proteins, two families of negative regulators of bHLH proteins [47]. Interestingly, some of these factors are implicated in cochlear differentiation [48,49]. We transfected a Sox9 expression plasmid in UB/OC1 cells (an otic cell line) and measured the relative mRNA expression level of Hes1, Hes5, Hey1, Hey2, HeyL, and Id1-3 by RT-qPCR. Transcripts for all genes were detected at low levels in basal conditions except for Hes5, which was not detected. We found that the expression of Hey1 and HeyL was strongly enhanced by Sox9 overexpression in the otic cell line (Figure 4A), and this was prevented by co-transfecting the dominant negative DN-Sox9 (Supplementary Figure S2J).

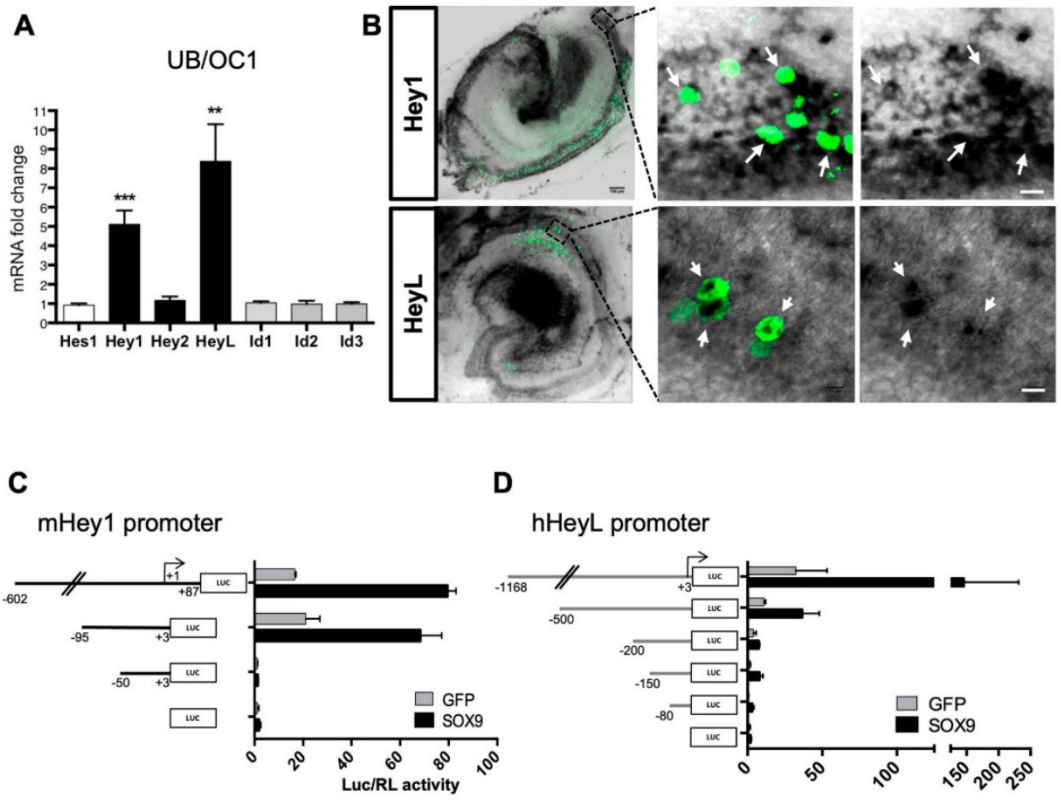

Figure 4. Sox9 upregulates Hey1 and HeyL factors. (**A**) RT-qPCR was performed in UB/OC1 cells transfected with control-GFP or Sox9-GFP plasmids. The expression level was normalized over GAPDH transcript level and reported to control-GFP condition (mean ± SD from 3 individual experiments). (**B**) E14.5 cochleae were electroporated with Sox9-GFP and cultured for 6 DIV. Hey1 and HeyL in situ hybridization were performed before anti-GFP staining. Scale bars left panels: 100 µm, right panels: 10 µm. White arrows indicated transfected cells (**C**,**D**) Luciferase reporter vectors containing fragments from Hey1 (**C**) or HeyL (**D**) promoters as well as controlling empty pLUC4 vectors were transfected in UB/OC1 cells with Renilla control (RL) vector and either GFP or Sox9-GFP plasmid. Data are presented as the normalized Luc/RL ratio reported to control conditions (mean ± SEM from 3 individual experiments). ** = $p < 0.01$ and *** = $p < 0.001$.

We next performed in situ hybridization analyses at E14.5, E16.5, and P1 to examine the spatio-temporal expression patterns of Hey1 and HeyL in developing organs of Corti (Supplementary Figure S3). These data revealed that Hey1 and HeyL expression profiles were consistent with the Sox9 expression pattern and Atoh1 modulation in the developing organ of Corti. Indeed, as HC differentiation arises in the murine organ of Corti, between E14.5 and E16.5, the expression of Hey1 and HeyL is progressively restricted to future SCs, in agreement with previously published data [49,50].

To confirm Sox9 regulation of Hey1 and HeyL expression in the cochlea, we first electroporated Sox9 in the E14.5 organ of Corti explants and performed in situ hybridization to detect Hey1 and HeyL expression after 6 DIV. Hey1 and HeyL mRNAs were specifically detected along the length of the sensory epithelium, and GFP-positive cells, overexpressing Sox9, showed increased Hey1 and HeyL expression levels (Figure 4B).

We also performed luciferase assays in UB/OC1 cells to study the effect of Sox9 on Hey1 and HeyL promoter reporters. The murine Hey1 promoter fragment (ranging from −602 to +87 positions, relative to transcription start site TSS) showed increased transcriptional activity upon Sox9 expression in UB/OC1 cells (Figure 4C). This Sox9-dependent increase was also observed for a shorter promoter spanning −95/+3, whereas it was lost on a −50/+3 fragment. These results indicated that the Hey1 promoter includes a Sox9 responsive element located between 90 and 50 bp upstream of the TSS. Sox9 also activated the HeyL promoter when a minimum of 200 bp upstream of the TSS was used (Figure 4D). This response was reduced progressively as promoter fragments were shortened to 150 and 80 bp. These in vitro experiments revealed that Hey1 and HeyL promoters respond to Sox9 through sequences located within their proximal region.

Altogether, these results demonstrate that Hey1 and HeyL are Sox9 target genes activated in the cochlea and suggest that these factors mediate the inhibitory effect of overexpressed Sox9 on Atoh1 protein and HC differentiation.

3.5. Overexpression of Hey1 and HeyL Prevents Hair Cell Differentiation

We next assessed whether Hey1 and HeyL could modulate cell fate in the organ of Corti. Firstly, we electroporated Hey1- and HeyL-expression plasmids in the E14.5 organ of Corti explants and harvested them after 6 DIV. Within the HC layer, the majority of cells transfected by Hey1 or HeyL did not express Myo6, indicating that these Hey factors strongly inhibited HC differentiation (Figure 5A–G, and Supplementary Table S1). This outcome resembled the effects observed upon Sox9 overexpression. We next examined whether homozygous deletion of Hey1 and HeyL genes leads to a modification of HC number in the developing mouse cochlea. At birth, cochleae from single Hey1 or HeyL knock-out embryos displayed a few extra HCs in the organ of Corti, a phenotype almost never detected in wild-type littermates (Figure 5H–N). The number of supernumerary HCs was further increased when Hey1 and HeyL were absent (Figure 5M,N). Together, these results indicate that both Hey1 and HeyL prevent HC fate acquisition and contribute to the development of a highly ordered mosaic in the organ of Corti.

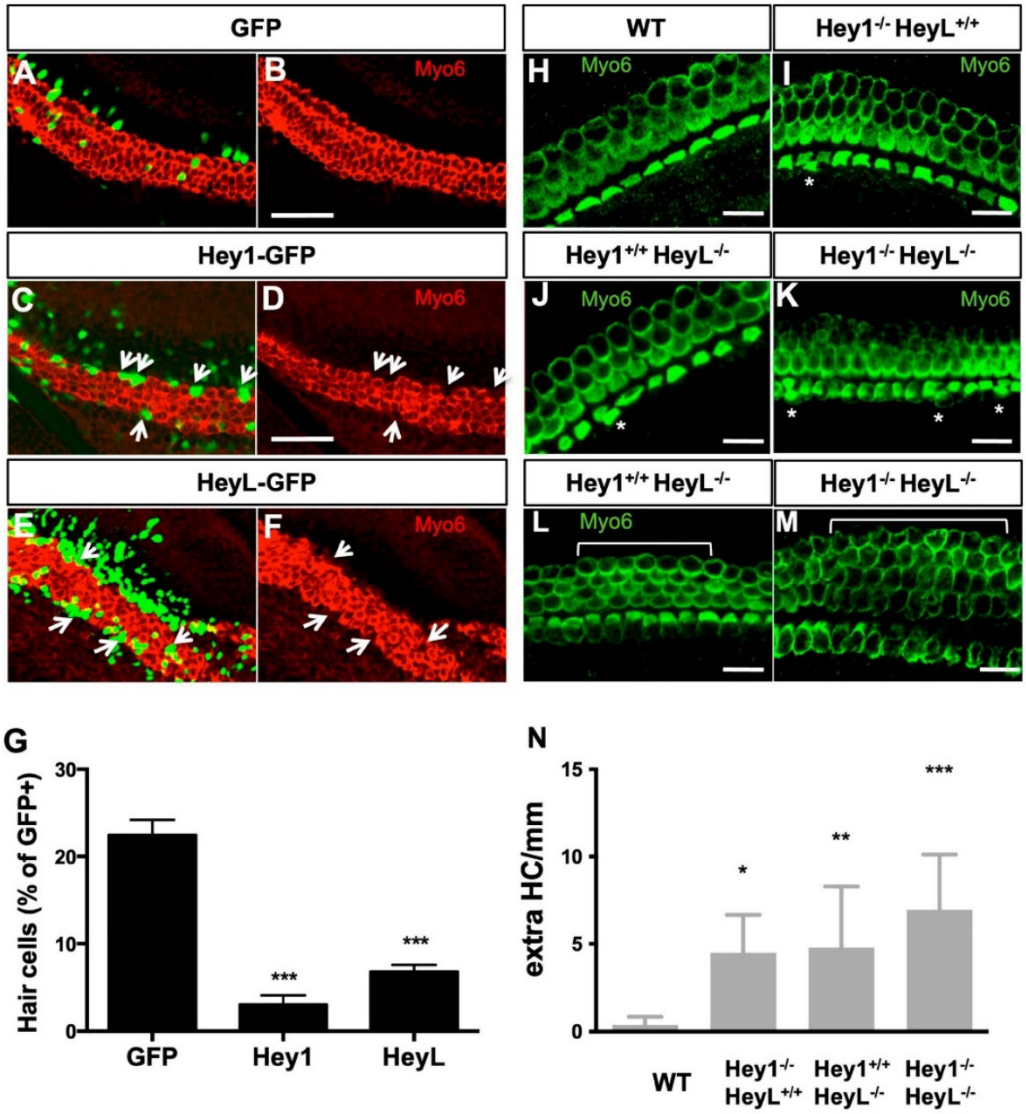

Figure 5. Hey1 and HeyL inhibit hair cell fate. (**A**–**F**) Myo6 immunostainings after electroporating GFP (**A**,**B**), Hey1-GFP (**C**,**D**), or HeyL-GFP (**E**,**F**) in E14.5 cochleae and culturing them for 6 days. Transfected cells overexpressing Hey factors often lack Myo6 staining (arrows), indicating that HC differentiation is blocked by Hey1 and HeyL. (**G**) Quantifications of (**A**–**F**). The percentage of transfected cells developing as HCs was evaluated for each explant. Data are presented as mean ± SEM (6–12 cochlear explants per condition from 3 independent experiments). (**H**–**M**) Myo6 immunolabeling of E18.5 whole-mounted cochleae from wild-type (**H**), Hey1$^{-/-}$ (**I**), HeyL$^{-/-}$ (**J**,**L**), or double knock-out animals (**K**,**M**). In the absence of Hey factors, extra HCs are formed in the organ of Corti (indicated by asterisks for IHC and bracket for OHC). (**N**) Quantifications of supernumerary HCs. The number of extra HCs per mm of cochlea was evaluated for wild-type animals (n = 10) or mice lacking expression from Hey1 (n = 5), HeyL (n = 4), or both genes (n = 4). Data are presented as mean ± SEM. * = $p < 0.05$, ** = $p < 0.01$ and *** = $p < 0.001$. The scale bar is 50 µm in (**A**–**F**) and 25 µm in (**G**–**J**).

3.6. Sox9 Inhibition of Atoh1 Partially Relies on Hey1 and HeyL Upregulation

We next investigated whether Hey1 and HeyL were required downstream of Sox9 to inhibit Atoh1 activity. We tested this hypothesis by co-transfecting the 7Ebox-Luc reporter, Sox9- and Atoh1-expressing vectors in UB/OC1 cells with or without endoribonuclease-prepared siRNAs targeting Hey1 andHeyL. After 48 h, we assessed the Atoh1-induced luciferase reporter activity (Figure 6A). Our results showed that preventing Hey1 and HeyL expression reduced the inhibitory effect of Sox9 on Atoh1 activity. To confirm these results in the cochlea, we co-electroporated Sox9-GFP plasmid and shRNA directed against Hey1 and HeyL in E14.5 explants. After 6 days in culture, down-regulation of endogenous Hey1 and HeyL significantly reduced the ability of Sox9 to inhibit HC fate (Figure 6B,C, percentage of GFP+Myo6+ cells for Shctrl: 24.26% ± 1.33, Sox9-GFP+Shctrl: 2.13% ± 0.79, and Sox9-GFP+ShHey1/L: 7.79% ± 1.61). Notably, the percentage of HCs amongst GFP-positive cells was still reduced compared to controls, suggesting that Hey1 and HeyL are not the only mediators of Sox9 inhibitory action on HC differentiation.

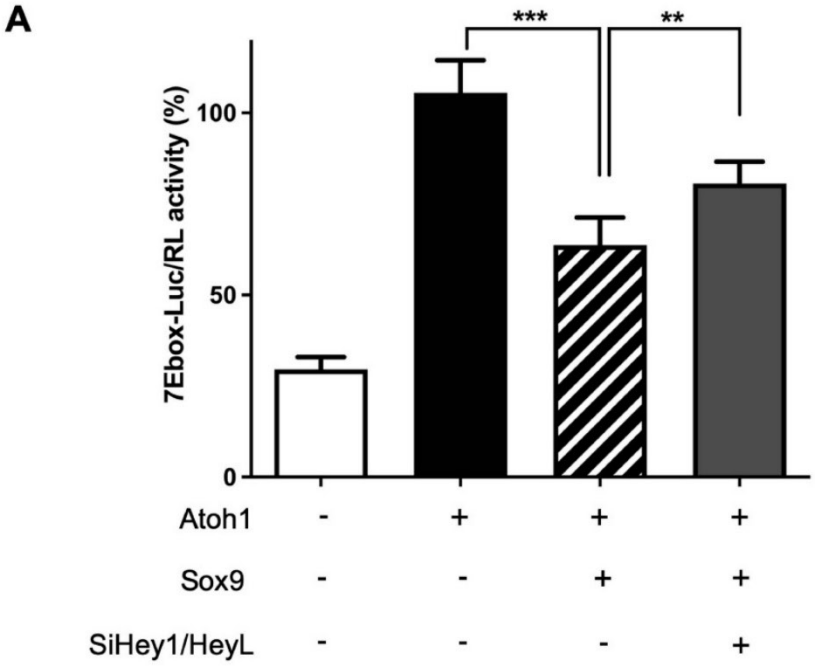

Figure 6. *Cont.*

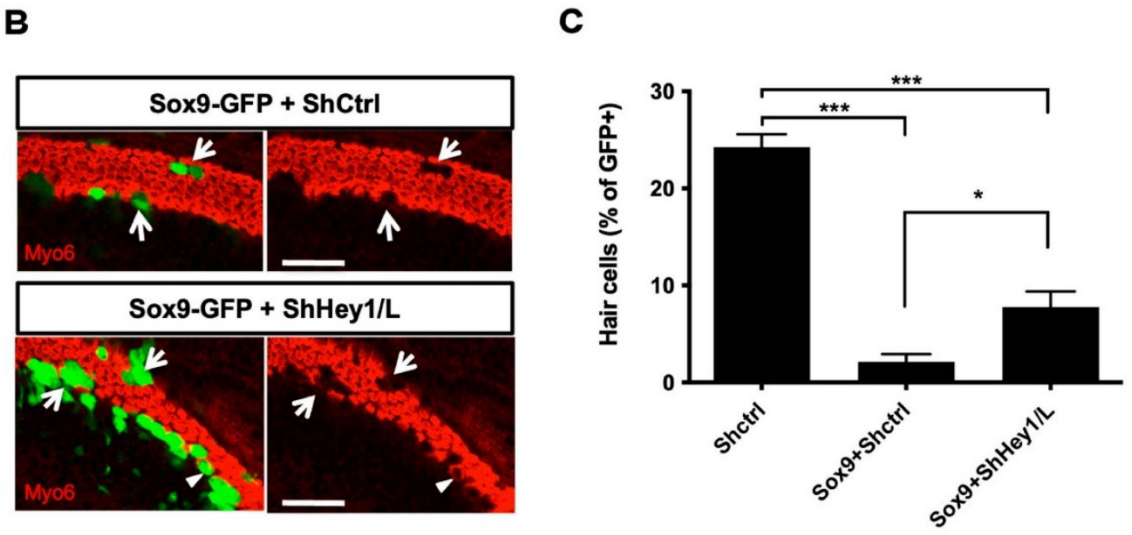

Figure 6. Hey1 and HeyL participate in Sox9 inhibition of Atoh1 activity and inhibition of hair cell fate. (**A**) Luciferase assays of UB/OC1 cells transfected with Atoh1-responsive reporter (7Ebox-Luc), Sox9-GFP vector and siRNA control or directed against Hey1 and HeyL. Data are presented as percentages of Atoh1 relative activity from three independent experiments. When Hey1 and/or HeyL upregulation is prevented by the use of specific siRNAs, Sox9 effect on Atoh1 function is abolished. (**B**) E14.5 cochleae were electroporated with Sox9-expression plasmid together with shRNA-control or shRNA-Hey1/HeyL and further cultured for 6 DIV. While none of the Sox9-transfected cells express Myo6 HC marker (arrows), some of the cells transfected with Sox9 in combination with shHey1 and shHeyL were able to fully differentiate into HCs (arrowhead). (**C**) The percentage of transfected cells (GFP+) that differentiate into hair cell is presented as the mean ± SEM for 8 individual explants within 3 experiments. Scale bar is 50 µm. * = $p < 0.05$, ** = $p < 0.01$ and *** = $p < 0.001$.

3.7. Sox9 Loss Leads to Supernumerary HCs but Not upon Sox2 Hypomorphism

To study cochlear cell patterning upon depletion of Sox9 in vivo, we crossed $Sox9^{lox/lox}$ mice with $Sox2^{CreERT2/+}$ and $R26R^{EYFP}$ mice. The activity of the Cre recombinase, expressed in the prosensory Sox2-positive cells, was induced by tamoxifen administration at E12.5 and E13.5 prior to terminal cell differentiation and was monitored by visualization of the YFP reporter (Figure 7A). As reported previously, the presence of the Cre allele, substituting the Sox2 gene in the $Sox2^{CreERT2/+}$ mouse line, leads to Sox2 hypomorphism [51], which is accompanied by some overproduction of HCs within the sensory epithelium (Figure 7A,B; compare $Sox2^{+/+}$ and $Sox2^{CreERT2/+}$ animals). We thus analyzed cochlear patterning in tamoxifen-treated littermates of all genotypes but found no effect of Sox9 loss upon Sox2 deficiency. The inhibitory action of Sox9 on Atoh1 and HC differentiation may be masked or prevented [52], as Sox2 was also shown to antagonize Atoh1 function [53]. It is also conceivable that Sox2 hypomorphism leads to gene expression changes of additional developmental regulators that compensate for the loss of Sox9 in the $Sox2^{CreERT2/+}$ mouse model.

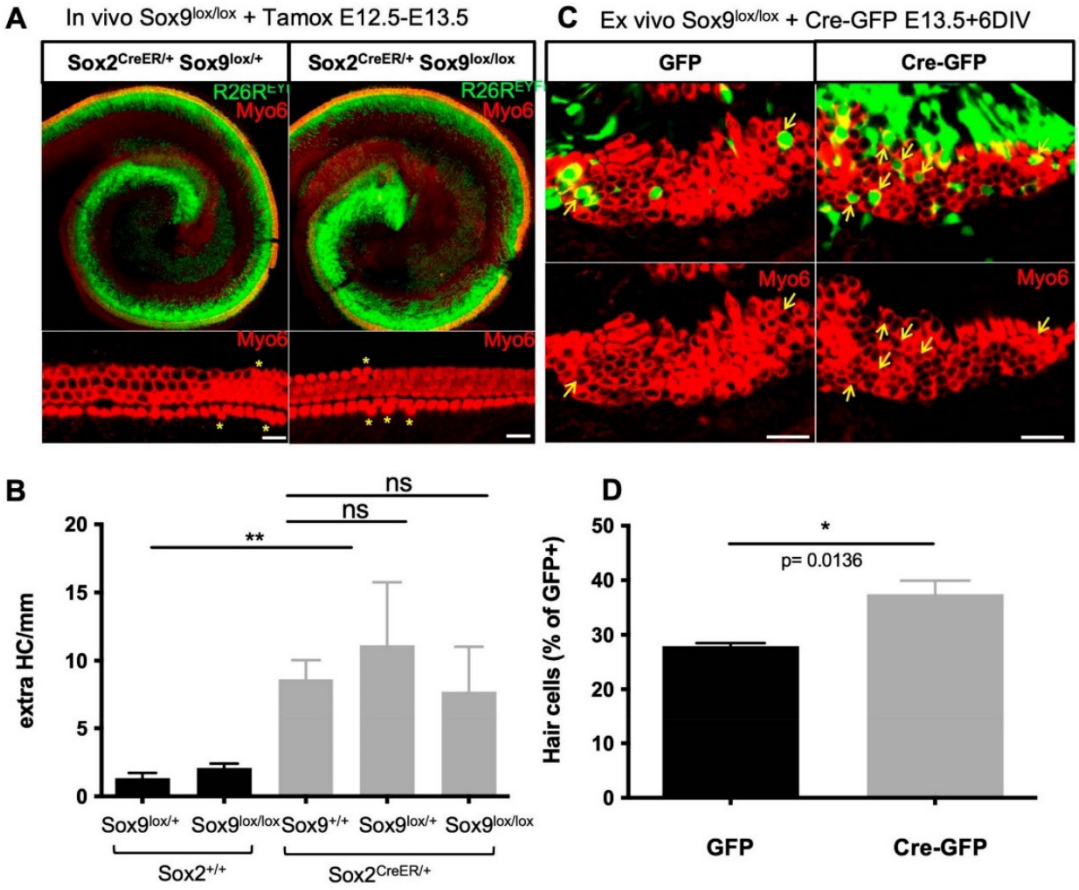

Figure 7. Sox9 loss in prosensory cells leads to some extra HCs ex vivo but not in Sox2CreERT2/+ Sox9Lox/Lox mice in vivo. (**A**) Myo6 immunostainings of whole-mounted P0 cochlea from Sox2CreERT2/+; R26REYFP; Sox9lox/+ (Het) or Sox2CreERT2/+; R26REYFP; Sox9lox/lox (KO) mice injected with tamoxifen at day E12.5 and E13.5. Supernumerary HCs (asterisks) were detected in both genotypes regardless of Sox9 gene status. (**B**) The number of extra HCs was quantified along the entire length of the cochlea and normalized to the cochlear length for all littermates, whether they express the inducible Cre from the Sox2 allele or not (mean ± SD, n = 3–6 animals per genotype). Sox2 hypomorphism induces extra HCs, which is not further increased by Sox9 invalidation. (**C**) Myo6 immunostainings after electroporating GFP or Cre-GFP in E13.5 Sox9Lox/Lox cochleae and further cultured for 6 days. An increased proportion of GFP+ cells developing into HCs (arrows) was seen in Cre-transfected cochleae, indicating that HC differentiation is promoted by Sox9 suppression. (**D**) Quantifications of the percentage of GFP+ cells developing as HCs. Data are presented as mean ± SEM (5–8 cochlear explants per condition from 2 independent experiments). * = $p < 0.05$ and ** = $p < 0.01$. Scale bars: 25 µm.

As the ex vivo knockdown of Sox9 by shRNA promoted the occurrence of supernumerary HCs, we sought to use the $Sox9^{lox/lox}$ model to confirm these findings. The inner ears were electroporated at E13.5 with a Cre-GFP plasmid to delete Sox9, and the proportion of transfected cells that differentiated into HCs was evaluated and compared to GFP-transfected controls. Again, HC fate was significantly promoted in Sox9-depleted cells (Figure 7C,D), indicating that Sox9 fine-tunes the transcriptional program during sensory cell development in the cochlea.

4. Discussion

Hearing depends on sound wave detection by the mechanosensory HCs in the cochlea. These cells are highly vulnerable to environmental insults as they are lost following noise or ototoxic drug exposure. In mammals, these cells cannot regenerate, or with poor efficiency and only during the perinatal development period [54]. For many years, researchers have been investigating strategies to promote HC regeneration to replace damaged or lost auditory cells. Because HCs and SCs share common precursors, deciphering the mechanisms that regulate cell fate decisions and early differentiation during inner ear development is necessary to enable attempts to promote HC regeneration.

In this study, we report a novel requirement for Sox9 in fine-tuning the organ of Corti cell patterning. We show that dynamic changes in Sox9 expression during cochlear development are required for terminal HC differentiation from the prosensory cells. We show that Sox9 acts as an inhibitor of Atoh1, the primary inducer of HC development. Its expression must be turned off specifically in cells committed to HC fate to ensure proper differentiation into mature sensory cells.

4.1. Sox9 Cell Fate Determiner Is an Inhibitor of Atoh1 in the Cochlea

Atoh1 has been identified as the earliest gene necessary and sufficient for HC development. Its absence results in a complete loss of HCs [5], while its expression is sufficient to induce ectopic HCs [52]. Our results indicate that overexpression of Sox9 in the cochlear prosensory progenitors prevents Atoh1 from inducing HC differentiation and is associated with reduced Atoh1 transcriptional activity. Indeed, in the presence of Sox9, the ability of Atoh1 to activate transcription from Ebox-containing regulatory regions is strongly reduced. As Atoh1 also relies on Ebox enhancers for its regulation [55], the transcription factor is part of a positive feedback loop reinforcing its own expression. As such, expression of Sox9 in nascent HCs reduces Atoh1 transcriptional activity and consequently downregulates Atoh1 and its downstream target genes, thereby preventing the HC differentiation program.

Importantly, blockade of HC differentiation by Sox9 did not result in their conversion towards an SC fate. This contradicts the prevailing view that SC differentiation occurs as a default mode ref. Although SC formation has been extensively studied, and despite the advances in their molecular profile provided by single-cell transcriptomic studies throughout developmental stages, specific regulators of SC fate still need to be identified.

Sox9 overexpression in developing HCs precludes the execution of Atoh1 transcriptional program, but it is not clear what is the outcome of these cells. Previous studies in the nervous system suggest that Sox9 could be an epithelial–mesenchymal transition (EMT) modulator [56,57]. Thus, Sox9-overexpressing nascent HCs could mis-differentiate into a mesoderm-like phenotype.

4.2. Functional Redundancy for Sox Factors in the Differentiating Organ of Corti?

Previous reports have suggested similar roles for Sox2, which is also initially expressed in all prosensory cells before becoming restricted to SCs, and that was shown to antagonize Atoh1 function [53]. However, Sox2 is retained in nascent HCs already devoid of Sox9 and is progressively downregulated later on [8,15,18,58]. Expression analyses in human cochleae confirm that Sox9 downregulation coincides with HC differentiation and occurs several weeks before the downregulation of Sox2 [59]. Moreover, Sox2 seems to exert opposite effects during terminal cell differentiation in the developing organ of Corti. It was also shown to increase the transcription of Atoh1, favoring HC differentiation when transfected with Eya1/Six1 factors [60]. Similarly, Sox2 can induce Atoh1 and form ectopic HCs in the chick [61].

Altogether, both Sox2 and Sox9 are involved in the intricate regulatory networks that control cell differentiation within the organ of Corti, but they seem to have distinct functions.

4.3. Hey1 and HeyL Are Downstream Effectors of Sox9

Our data indicate that Sox9 regulates cochlear cell differentiation in a Hey1/HeyL-dependent manner. Interestingly, mice lacking both Hey1 and HeyL have an increased number of HCs. However, this relatively mild effect may be due to a possible compensatory effect by other members of the Hes/Hey gene family. Indeed, Hes1, Hes5, or Hey2 have overlapping patterns of expression within the cochlear epithelium, and genetic inactivation of these genes also leads to moderately increased numbers of HCs [15,50,62]. A graded increase in the numbers of HCs is induced by the loss of multiple members of the Hes family, but even in triple mutants, the observed phenotypic defects are not substantial [49]. Intriguingly, Sox9 upregulates Hey1 and HeyL proteins that are known to be direct targets of Notch signaling [50]. The co-existence of two pathways for Hes/Hey factor activation during cochlear differentiation allows cells to respond appropriately to specific environmental cues and ensures robustness in regulating cell fate decisions.

Altogether, these multiple ways to inhibit Atoh1 in cells destined for an SC fate likely reflect the biological importance of a tightly controlled expression and activity to ensure correct cell patterning in the cochlear epithelium. The multiplicity of Atoh1 inhibitors could also explain why depleting Sox9 from progenitor cells in vivo was insufficient to induce Atoh1 expression and HC differentiation.

Hes/Hey factors could inhibit Atoh1 function by two mechanisms [63]. First, these bHLH proteins could act by competing with Atoh1 for dimerization partners that are essential for Atoh1 function. The activity of Atoh1 relies on its interaction with E proteins to bind E boxes present in the promoter of target genes. Since Hes/Hey factors were also shown to interact with these proteins, the upregulation of Hey1 and HeyL could lead to the sequestration of Atoh1 partner, thereby limiting the number of active Atoh1 transcriptional complexes. Second, Hes/Hey factors could compete with Atoh1 for DNA binding. Indeed, Hey1 and HeyL bind preferentially to E boxes, and their upregulation would result in increased occupancy of Atoh1 target promoters. Moreover, Hes/Hey factors could also exert a direct repressive effect on Atoh1 target genes since they were shown to recruit transcriptional repressors like histone deacetylases.

5. Conclusions

Here we report a role for Sox9 during cell patterning in the developing mammalian organ of Corti. These data imply that Sox9 mutation leads to a modification of the sensorineural epithelium by affecting the integrity of the Atoh1 pathway and may contribute to the hearing loss seen in a subset of patients with campomelic dysplasia (OMIN No. 114290). In a recent study, it was observed that heterozygous mice carrying the Y440X mutation in the Sox9 gene, which results in the truncation of the C-terminal transactivation domain of Sox9, exhibited neurosensory deafness [64]. However, it appears to be associated with the endolymphatic sac and the stria vascularis. Whether the development of the organ of Corti is unaffected remains to be demonstrated.

In mammals, genetic and/or environmental insults to the cochlea lead to hearing loss, often due to permanent loss or dysfunction of the organ of Corti. Thus, manipulating Sox9 expression or activity may be an important pathway when designing therapies to treat deafness caused by loss or dysfunction of HCs and/or SCs.

Supplementary Materials: The following supporting information can be downloaded at: https://www.mdpi.com/article/10.3390/cells12172148/s1, Figure S1: Sox9 overexpression blocks HC differentiation but does not interfere with SC development; Figure S2: Sox9 is efficiently downregulated or inactivated by specific shRNA or DN-Sox9; Figure S3: Hey1 and HeyL expression pattern in the developing cochlea; Table S1: Hair cell fate in electroporation experiments; Table S2: Primer sequences used in RT-qPCR; Table S3: Primer sequences used for promoter cloning into pLUC reporter construct.

Author Contributions: Conceptualization, B.M. and L.D. Methodology, B.M., L.D. and A.H.; Validation, B.M., L.D. and A.H.; Formal Analysis, M.V., A.H. and L.D.; Investigation, M.V., I.B., A.H. and P.V.D.A.; Resources, S.-i.F., H.K. and L.N.; Writing—Original Draft Preparation, B.M. and L.D.; Writing—Review and Editing, B.M., L.N. and L.D.; Visualization, A.H., B.M. and L.D.; Supervision, B.M. and L.D.; Project Administration, B.M.; Funding Acquisition, B.M. All authors have read and agreed to the published version of the manuscript.

Funding: This research was funded by grants from the F.R.S.-F.N.R.S. (R.FNRS.4549), the Fonds Léon Frédéricq, the Fondation Médicale Reine Elisabeth and the Belgian Science Policy (IAP-VII network P7/7).

Institutional Review Board Statement: The study was conducted according to the guidelines of the Declaration of Helsinki and approved by the Ethics Committee of the University of Liège (protocol N°1883 approved on 19 February 2020).

Informed Consent Statement: Not applicable.

Data Availability Statement: Not applicable.

Acknowledgments: We thank the following for generous gifts of reagents and cells: Matt Holley for the UB/OC-1 cells, Dagmar Wilhelm for the Sox9-Luc vector, Kris Kintner for the NICD expression vector, Manfred Gessler for the Hey1-Luc and HeyL-Luc vectors, Kageyama for the 7EBOX-Luc plasmid, Véronique Lefebvre for the Col2a1-Luc vector, Brigitte Boizet for the Sox9 antibody, Andreas Schedl (University of Nice, France), Patrick Jacquemin, and Frederic Lemaigre (UCL, Louvain, Belgium) for Sox9fl/fl mouse line, and Scott T. Magness (University of North Carolina, Chapel hill, USA) for Sox9-GFP mice. We thank Patricia Ernst, Alexandra Pieltain, and Pierre-Bernard Vanlerberghe for technical assistance, and the GIGA technology platforms (GIGA-Research Centre, University of Liege) for help with imaging and animal husbandry. L.N. and B.M. are Research Directors of the F.R.S.-F.N.R.S.

Conflicts of Interest: The authors declare no conflict of interest.

References

1. Kelley, M.W. Regulation of cell fate in the sensory epithelia of the inner ear. *Nat. Rev. Neurosci.* **2006**, *7*, 837–849. [CrossRef] [PubMed]
2. Chen, P.; Segil, N. p27(Kip1) links cell proliferation to morphogenesis in the developing organ of Corti. *Development* **1999**, *126*, 1581–1590. [CrossRef] [PubMed]
3. Chen, Y.; Zhang, S.; Chai, R.; Li, H. Hair Cell Regeneration. In *Hearing Loss: Mechanisms, Prevention and Cure*; Advances in Experimental Medicine and Biology; Springer: Singapore, 2019; Volume 1130, pp. 1–16. [CrossRef]
4. Atkinson, P.J.; Huarcaya Najarro, E.; Sayyid, Z.N.; Cheng, A.G. Sensory hair cell development and regeneration: Similarities and differences. *Development* **2015**, *142*, 1561–1571. [CrossRef] [PubMed]
5. Bermingham, N.A.; Hassan, B.A.; Price, S.D.; Vollrath, M.A.; Ben-Arie, N.; Eatock, R.A.; Bellen, H.J.; Lysakowski, A.; Zoghbi, H.Y. Math1: An essential gene for the generation of inner ear hair cells. *Science* **1999**, *284*, 1837–1841. [CrossRef]
6. Chen, P.; Johnson, J.E.; Zoghbi, H.Y.; Segil, N. The role of Math1 in inner ear development: Uncoupling the establishment of the sensory primordium from hair cell fate determination. *Development* **2002**, *129*, 2495–2505. [CrossRef]
7. Zheng, J.L.; Gao, W.Q. Overexpression of Math1 induces robust production of extra hair cells in postnatal rat inner ears. *Nat. Neurosci.* **2000**, *3*, 580–586. [CrossRef]
8. Lanford, P.J.; Shailam, R.; Norton, C.R.; Gridley, T.; Kelley, M.W. Expression of Math1 and HES5 in the cochleae of wildtype and Jag2 mutant mice. *J. Assoc. Res. Otolaryngol.* **2000**, *1*, 161–171. [CrossRef]
9. Morrison, A.; Hodgetts, C.; Gossler, A.; Hrabe de Angelis, M.; Lewis, J. Expression of Delta1 and Serrate1 (Jagged1) in the mouse inner ear. *Mech. Dev.* **1999**, *84*, 169–172. [CrossRef]
10. Lanford, P.J.; Lan, Y.; Jiang, R.; Lindsell, C.; Weinmaster, G.; Gridley, T.; Kelley, M.W. Notch signalling pathway mediates hair cell development in mammalian cochlea. *Nat. Genet.* **1999**, *21*, 289–292. [CrossRef]
11. Brooker, R.; Hozumi, K.; Lewis, J. Notch ligands with contrasting functions: Jagged1 and Delta1 in the mouse inner ear. *Development* **2006**, *133*, 1277–1286. [CrossRef]
12. Kiernan, A.E.; Cordes, R.; Kopan, R.; Gossler, A.; Gridley, T. The Notch ligands DLL1 and JAG2 act synergistically to regulate hair cell development in the mammalian inner ear. *Development* **2005**, *132*, 4353–4362. [CrossRef] [PubMed]
13. Artavanis-Tsakonas, S.; Rand, M.D.; Lake, R.J. Notch signaling: Cell fate control and signal integration in development. *Science* **1999**, *284*, 770–776. [CrossRef] [PubMed]

14. Akazawa, C.; Ishibashi, M.; Shimizu, C.; Nakanishi, S.; Kageyama, R. A mammalian helix-loop-helix factor structurally related to the product of Drosophila proneural gene atonal is a positive transcriptional regulator expressed in the developing nervous system. *J. Biol. Chem.* **1995**, *270*, 8730–8738. [CrossRef] [PubMed]
15. Zine, A.; Aubert, A.; Qiu, J.; Therianos, S.; Guillemot, F.; Kageyama, R.; de Ribaupierre, F. Hes1 and Hes5 activities are required for the normal development of the hair cells in the mammalian inner ear. *J. Neurosci.* **2001**, *21*, 4712–4720. [CrossRef]
16. Dy, P.; Wang, W.; Bhattaram, P.; Wang, Q.; Wang, L.; Ballock, R.T.; Lefebvre, V. Sox9 directs hypertrophic maturation and blocks osteoblast differentiation of growth plate chondrocytes. *Dev. Cell* **2012**, *22*, 597–609. [CrossRef] [PubMed]
17. Bagheri-Fam, S.; Barrionuevo, F.; Dohrmann, U.; Gunther, T.; Schule, R.; Kemler, R.; Mallo, M.; Kanzler, B.; Scherer, G. Long-range upstream and downstream enhancers control distinct subsets of the complex spatiotemporal Sox9 expression pattern. *Dev. Biol.* **2006**, *291*, 382–397. [CrossRef]
18. Mak, A.C.; Szeto, I.Y.; Fritzsch, B.; Cheah, K.S. Differential and overlapping expression pattern of SOX2 and SOX9 in inner ear development. *Gene Expr. Patterns—GEP* **2009**, *9*, 444–453. [CrossRef]
19. Seymour, P.A.; Freude, K.K.; Tran, M.N.; Mayes, E.E.; Jensen, J.; Kist, R.; Scherer, G.; Sander, M. SOX9 is required for maintenance of the pancreatic progenitor cell pool. *Proc. Natl. Acad. Sci. USA* **2007**, *104*, 1865–1870. [CrossRef]
20. Stolt, C.C.; Lommes, P.; Sock, E.; Chaboissier, M.C.; Schedl, A.; Wegner, M. The Sox9 transcription factor determines glial fate choice in the developing spinal cord. *Genes. Dev.* **2003**, *17*, 1677–1689. [CrossRef]
21. Pritchett, J.; Athwal, V.; Roberts, N.; Hanley, N.A.; Hanley, K.P. Understanding the role of SOX9 in acquired diseases: Lessons from development. *Trends Mol. Med.* **2011**, *17*, 166–174. [CrossRef]
22. Mansour, S.; Offiah, A.C.; McDowall, S.; Sim, P.; Tolmie, J.; Hall, C. The phenotype of survivors of campomelic dysplasia. *J. Med. Genet.* **2002**, *39*, 597–602. [CrossRef] [PubMed]
23. Tokita, N.; Chandra-Sekhar, H.K.; Daly, J.F.; Becker, M.H.; Aleksic, S. The Campomelic syndrome. Temporal bone histopathologic features and otolaryngologic manifestations. *Arch. Otolaryngol.* **1979**, *105*, 449–454. [CrossRef]
24. Savarirayan, R.; Robertson, S.P.; Bankier, A.; Rogers, J.G. Variable expression of campomelic dysplasia in a father and his 46, XY daughter. *Pediatr. Pathol. Mol. Med.* **2003**, *22*, 37–46. [CrossRef] [PubMed]
25. Saint-Germain, N.; Lee, Y.H.; Zhang, Y.; Sargent, T.D.; Saint-Jeannet, J.P. Specification of the otic placode depends on Sox9 function in Xenopus. *Development* **2004**, *131*, 1755–1763. [CrossRef] [PubMed]
26. Taylor, K.M.; Labonne, C. SoxE factors function equivalently during neural crest and inner ear development and their activity is regulated by SUMOylation. *Dev. Cell* **2005**, *9*, 593–603. [CrossRef]
27. Yan, Y.L.; Willoughby, J.; Liu, D.; Crump, J.G.; Wilson, C.; Miller, C.T.; Singer, A.; Kimmel, C.; Westerfield, M.; Postlethwait, J.H. A pair of Sox: Distinct and overlapping functions of zebrafish sox9 co-orthologs in craniofacial and pectoral fin development. *Development* **2005**, *132*, 1069–1083. [CrossRef]
28. Barrionuevo, F.; Naumann, A.; Bagheri-Fam, S.; Speth, V.; Taketo, M.M.; Scherer, G.; Neubuser, A. Sox9 is required for invagination of the otic placode in mice. *Dev. Biol.* **2008**, *317*, 213–224. [CrossRef]
29. Jo, A.; Denduluri, S.; Zhang, B.; Wang, Z.; Yin, L.; Yan, Z.; Kang, R.; Shi, L.L.; Mok, J.; Lee, M.J.; et al. The versatile functions of Sox9 in development, stem cells, and human diseases. *Genes. Dis.* **2014**, *1*, 149–161. [CrossRef]
30. Fukada, S.; Yamaguchi, M.; Kokubo, H.; Ogawa, R.; Uezumi, A.; Yoneda, T.; Matev, M.M.; Motohashi, N.; Ito, T.; Zolkiewska, A.; et al. Hesr1 and Hesr3 are essential to generate undifferentiated quiescent satellite cells and to maintain satellite cell numbers. *Development* **2011**, *138*, 4609–4619. [CrossRef]
31. Formeister, E.J.; Sionas, A.L.; Lorance, D.K.; Barkley, C.L.; Lee, G.H.; Magness, S.T. Distinct SOX9 levels differentially mark stem/progenitor populations and enteroendocrine cells of the small intestine epithelium. *Am. J. Physiology. Gastrointest. Liver Physiol.* **2009**, *296*, G1108–G1118. [CrossRef]
32. Arnold, K.; Sarkar, A.; Yram, M.A.; Polo, J.M.; Bronson, R.; Sengupta, S.; Seandel, M.; Geijsen, N.; Hochedlinger, K. Sox2(+) adult stem and progenitor cells are important for tissue regeneration and survival of mice. *Cell Stem Cell* **2011**, *9*, 317–329. [CrossRef]
33. Kist, R.; Schrewe, H.; Balling, R.; Scherer, G. Conditional inactivation of Sox9: A mouse model for campomelic dysplasia. *Genesis* **2002**, *32*, 121–123. [CrossRef] [PubMed]
34. Srinivas, S.; Watanabe, T.; Lin, C.S.; William, C.M.; Tanabe, Y.; Jessell, T.M.; Costantini, F. Cre reporter strains produced by targeted insertion of EYFP and ECFP into the ROSA26 locus. *BMC Dev. Biol.* **2001**, *1*, 4. [CrossRef] [PubMed]
35. Creppe, C.; Malinouskaya, L.; Volvert, M.L.; Gillard, M.; Close, P.; Malaise, O.; Laguesse, S.; Cornez, I.; Rahmouni, S.; Ormenese, S.; et al. Elongator controls the migration and differentiation of cortical neurons through acetylation of alpha-tubulin. *Cell* **2009**, *136*, 551–564. [CrossRef] [PubMed]
36. Flora, A.; Garcia, J.J.; Thaller, C.; Zoghbi, H.Y. The E-protein Tcf4 interacts with Math1 to regulate differentiation of a specific subset of neuronal progenitors. *Proc. Natl. Acad. Sci. USA* **2007**, *104*, 15382–15387. [CrossRef]
37. Wilhelm, D.; Hiramatsu, R.; Mizusaki, H.; Widjaja, L.; Combes, A.N.; Kanai, Y.; Koopman, P. SOX9 regulates prostaglandin D synthase gene transcription in vivo to ensure testis development. *J. Biol. Chem.* **2007**, *282*, 10553–10560. [CrossRef]
38. Lefebvre, V.; Zhou, G.; Mukhopadhyay, K.; Smith, C.N.; Zhang, Z.; Eberspaecher, H.; Zhou, X.; Sinha, S.; Maity, S.N.; de Crombrugghe, B. An 18-base-pair sequence in the mouse proalpha1(II) collagen gene is sufficient for expression in cartilage and binds nuclear proteins that are selectively expressed in chondrocytes. *Mol. Cell. Biol.* **1996**, *16*, 4512–4523. [CrossRef] [PubMed]
39. Maier, M.M.; Gessler, M. Comparative analysis of the human and mouse Hey1 promoter: Hey genes are new Notch target genes. *Biochem. Biophys. Res. Commun.* **2000**, *275*, 652–660. [CrossRef]

40. Kanai, Y.; Koopman, P. Structural and functional characterization of the mouse Sox9 promoter: Implications for campomelic dysplasia. *Hum. Mol. Genet.* **1999**, *8*, 691–696. [CrossRef]
41. Rivolta, M.N.; Grix, N.; Lawlor, P.; Ashmore, J.F.; Jagger, D.J.; Holley, M.C. Auditory hair cell precursors immortalized from the mammalian inner ear. *Proc. Biol. Sci.* **1998**, *265*, 1595–1603. [CrossRef]
42. Breuskin, I.; Bodson, M.; Thelen, N.; Thiry, M.; Borgs, L.; Nguyen, L.; Stolt, C.; Wegner, M.; Lefebvre, P.P.; Malgrange, B. Glial but not neuronal development in the cochleo-vestibular ganglion requires Sox10. *J. Neurochem.* **2010**, *114*, 1827–1839. [CrossRef] [PubMed]
43. Matei, V.; Pauley, S.; Kaing, S.; Rowitch, D.; Beisel, K.W.; Morris, K.; Feng, F.; Jones, K.; Lee, J.; Fritzsch, B. Smaller inner ear sensory epithelia in Neurog 1 null mice are related to earlier hair cell cycle exit. *Dev. Dyn.* **2005**, *234*, 633–650. [CrossRef] [PubMed]
44. Woods, C.; Montcouquiol, M.; Kelley, M.W. Math1 regulates development of the sensory epithelium in the mammalian cochlea. *Nat. Neurosci.* **2004**, *7*, 1310–1318. [CrossRef]
45. Yang, H.; Xie, X.; Deng, M.; Chen, X.; Gan, L. Generation and characterization of Atoh1-Cre knock-in mouse line. *Genesis* **2010**, *48*, 407–413. [CrossRef] [PubMed]
46. Lefebvre, V.; Huang, W.; Harley, V.R.; Goodfellow, P.N.; de Crombrugghe, B. SOX9 is a potent activator of the chondrocyte-specific enhancer of the pro alpha1(II) collagen gene. *Mol. Cell Biol.* **1997**, *17*, 2336–2346. [CrossRef]
47. Kageyama, R.; Nakanishi, S. Helix-loop-helix factors in growth and differentiation of the vertebrate nervous system. *Curr. Opin. Genet. Dev.* **1997**, *7*, 659–665. [CrossRef]
48. Jones, J.M.; Montcouquiol, M.; Dabdoub, A.; Woods, C.; Kelley, M.W. Inhibitors of differentiation and DNA binding (Ids) regulate Math1 and hair cell formation during the development of the organ of Corti. *J. Neurosci. Off. J. Soc. Neurosci.* **2006**, *26*, 550–558. [CrossRef]
49. Tateya, T.; Imayoshi, I.; Tateya, I.; Ito, J.; Kageyama, R. Cooperative functions of Hes/Hey genes in auditory hair cell and supporting cell development. *Dev. Biol.* **2011**, *352*, 329–340. [CrossRef]
50. Doetzlhofer, A.; Basch, M.L.; Ohyama, T.; Gessler, M.; Groves, A.K.; Segil, N. Hey2 regulation by FGF provides a Notch-independent mechanism for maintaining pillar cell fate in the organ of Corti. *Dev. Cell* **2009**, *16*, 58–69. [CrossRef]
51. Atkinson, P.J.; Dong, Y.; Gu, S.; Liu, W.; Najarro, E.H.; Udagawa, T.; Cheng, A.G. Sox2 haploinsufficiency primes regeneration and Wnt responsiveness in the mouse cochlea. *J. Clin. Invest.* **2018**, *128*, 1641–1656. [CrossRef]
52. Yang, J.; Bouvron, S.; Lv, P.; Chi, F.; Yamoah, E.N. Functional features of trans-differentiated hair cells mediated by Atoh1 reveals a primordial mechanism. *J. Neurosci.* **2012**, *32*, 3712–3725. [CrossRef] [PubMed]
53. Dabdoub, A.; Puligilla, C.; Jones, J.M.; Fritzsch, B.; Cheah, K.S.; Pevny, L.H.; Kelley, M.W. Sox2 signaling in prosensory domain specification and subsequent hair cell differentiation in the developing cochlea. *Proc. Natl. Acad. Sci. USA* **2008**, *105*, 18396–18401. [CrossRef]
54. Cox, B.C.; Chai, R.; Lenoir, A.; Liu, Z.; Zhang, L.; Nguyen, D.H.; Chalasani, K.; Steigelman, K.A.; Fang, J.; Rubel, E.W.; et al. Spontaneous hair cell regeneration in the neonatal mouse cochlea in vivo. *Development* **2014**, *141*, 816–829. [CrossRef]
55. Helms, A.W.; Abney, A.L.; Ben-Arie, N.; Zoghbi, H.Y.; Johnson, J.E. Autoregulation and multiple enhancers control Math1 expression in the developing nervous system. *Development* **2000**, *127*, 1185–1196. [CrossRef] [PubMed]
56. Akiyama, H.; Chaboissier, M.C.; Behringer, R.R.; Rowitch, D.H.; Schedl, A.; Epstein, J.A.; de Crombrugghe, B. Essential role of Sox9 in the pathway that controls formation of cardiac valves and septa. *Proc. Natl. Acad. Sci. USA* **2004**, *101*, 6502–6507. [CrossRef] [PubMed]
57. Cheung, M.; Chaboissier, M.C.; Mynett, A.; Hirst, E.; Schedl, A.; Briscoe, J. The transcriptional control of trunk neural crest induction, survival, and delamination. *Dev. Cell* **2005**, *8*, 179–192. [CrossRef] [PubMed]
58. Bermingham-McDonogh, O.; Oesterle, E.C.; Stone, J.S.; Hume, C.R.; Huynh, H.M.; Hayashi, T. Expression of Prox1 during mouse cochlear development. *J. Comp. Neurol.* **2006**, *496*, 172–186. [CrossRef]
59. Locher, H.; Frijns, J.H.; van Iperen, L.; de Groot, J.C.; Huisman, M.A.; Chuva de Sousa Lopes, S.M. Neurosensory development and cell fate determination in the human cochlea. *Neural Dev.* **2013**, *8*, 20. [CrossRef]
60. Ahmed, M.; Wong, E.Y.; Sun, J.; Xu, J.; Wang, F.; Xu, P.X. Eya1-Six1 interaction is sufficient to induce hair cell fate in the cochlea by activating Atoh1 expression in cooperation with Sox2. *Dev. Cell* **2012**, *22*, 377–390. [CrossRef]
61. Neves, J.; Uchikawa, M.; Bigas, A.; Giraldez, F. The prosensory function of Sox2 in the chicken inner ear relies on the direct regulation of Atoh1. *PLoS ONE* **2012**, *7*, e30871. [CrossRef]
62. Li, S.; Mark, S.; Radde-Gallwitz, K.; Schlisner, R.; Chin, M.T.; Chen, P. Hey2 functions in parallel with Hes1 and Hes5 for mammalian auditory sensory organ development. *BMC Dev. Biol.* **2008**, *8*, 20. [CrossRef] [PubMed]
63. Fischer, A.; Gessler, M. Delta-Notch--and then? Protein interactions and proposed modes of repression by Hes and Hey bHLH factors. *Nucleic Acids Res.* **2007**, *35*, 4583–4596. [CrossRef] [PubMed]
64. Szeto, I.Y.Y.; Chu, D.K.H.; Chen, P.; Chu, K.C.; Au, T.Y.K.; Leung, K.K.H.; Huang, Y.H.; Wynn, S.L.; Mak, A.C.Y.; Chan, Y.S.; et al. SOX9 and SOX10 control fluid homeostasis in the inner ear for hearing through independent and cooperative mechanisms. *Proc. Natl. Acad. Sci. USA* **2022**, *119*, e2122121119. [CrossRef] [PubMed]